

EFFECT OF SOIL CONSOLIDATION ON SOIL-LINING INTERACTION IN TUNNELS

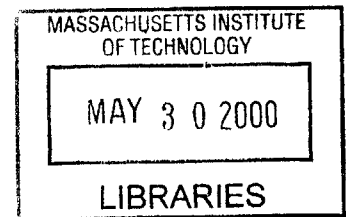
By

Alexios Leonidas Liakos

ENG

B.S., Civil Engineering (1998)

National Technical University of Athens



SUBMITTED TO THE DEPARTMENT OF
CIVIL AND ENVIRONMENTAL ENGINEERING
IN PARTIAL FULFILLMENT OF THE REQUIREMENTS FOR THE DEGREE OF
MASTER OF SCIENCE IN CIVIL AND ENVIRONMENTAL ENGINEERING

at the

MASSACHUSETTS INSTITUTE OF TECHNOLOGY

June 2000

© 2000 Massachusetts Institute of Technology
All rights reserved

Signature Author.....
Department of Civil and Environmental Engineering
May 19, 2000

Certified by.....
Herbert H. Einstein
Professor of Civil and Environmental Engineering
Thesis Supervisor

Certified by.....
Dr. Varya Nasri
Visiting Scientist, Massachusetts Institute of Technology
Thesis Co-Supervisor

Accepted by.....
Daniele Veneziano
Chairman, Departmental Committee on Graduate Studies

EFFECT OF SOIL CONSOLIDATION ON SOIL-LINING INTERACTION IN TUNNELS

by

Alexios Leonidas Liakos

Submitted to the Department of Civil and Environmental Engineering on
May 19, 2000, in partial fulfillment of the requirements for the degree of
Master of Science in Civil and Environmental Engineering

ABSTRACT

Most of the solutions developed for the prediction of a tunnel behavior refer to short-term conditions. However, when an excavation is performed in a saturated medium, the behavior of the surrounding ground is time dependent. Any change in the stress field requires a certain amount of time for the consolidation to take place.

In this thesis, a finite element analysis method is used to determine the ground liner interaction incorporating the effect of consolidation and the three-dimensional behavior near the face of a circular tunnel excavation. The analysis is based on the assumption of a linear elastic ground. Two-dimensional and three-dimensional models are used for the simulation of the construction (excavation and support) process.

Initially, an axisymmetric model is used for the simulation of a staged excavation of a tunnel. The behavior of the liner is examined in both dry and wet conditions to determine the effect of consolidation on the development of stresses and displacements. An increase in the liner stresses is observed when the consolidation is taken into account.

In the second part a 2d and a 3d model are used to examine the effect of the initial stress field on the tunnel behavior. When two principal stresses are equal, the stresses in the ground are greater with the axisymmetric model than with the 3d one. When the initial stress field is uniform in all three principal directions, the stresses in the ground are greater when the 3d model is used. Thus, when the axisymmetric model is used, the stresses around the tunnel are underestimated for a uniform stress field and overestimated when two principal stresses are equal.

In the last part, two 2d models namely an axisymmetric and a plane strain model are combined to take into account both the effect of the distance from the face at which the liner is placed and the effect of consolidation. For a permeability of $K=10^{-7}$ m/sec, the tangential stress in the liner, at the springline of the tunnel is increased by 10% compared to that in dry conditions. A decrease in the permeability to $K=10^{-9}$ m/sec, results in an increase of tangential stress by almost 100%.

Thesis Supervisor: Prof. Herbert H. Einstein

Title: Professor of Civil and Environmental Engineering

Acknowledgements

I would like first to acknowledge the continuous help and support from my thesis supervisor Professor Herbert H.Einstein. With his insights and suggestions he made this thesis a challenging experience, never hesitating to share his ideas and his endless supply of enthusiasm.

I also want to thank my thesis co-supervisor and friend Dr. Verrya Nasri for his tireless support and encouragement towards the completion of my work and most important for his friendship.

I thank all my friends from the Geotechnical group at MIT; Jorge, Martin, Dimitri, Attasit "Pong", Kurt, Catalina, Karim, Christoph and Federico. Their friendship was very valuable.

I thank my family who supported me in this challenging part of my life, and for giving me strength to continue.

I want also to thank Katerina for her support, encouragement and mainly for her patience during these two years. Thank you for being there for me.

to my family

Table of Contents

Chapter 1 – Introduction.....	13
1.1. Thesis outline.....	14
Chapter 2 – Elastic Stresses around a Tunnel	
2.1. Introduction.....	16
2.2. Elastic Analysis of a Circular Opening.....	16
2.2.1. In-situ Stresses and Strains.....	17
2.2.2. Plane Strain Equations.....	20
2.2.3. Stresses around a Tunnel in a pre-stressed Medium (Pender,1980)	23
2.3. Change of Stresses with Tunnel advance.....	25
Chapter 3 – Elastic Consolidation around a Tunnel	
3.1. Introduction.....	26
3.2. Consolidation Theories.....	27
3.2.1 General assumptions.....	27
3.2.2 Assumptions used in the Finite Element Analysis.....	28
3.3. Elastic Consolidation around a deep circular tunnel (Carter & Booker, 1982).....	28
Chapter 4 – Application of Numerical Methods in Tunnel Engineering	
4.1. Introduction.....	34
4.2. Applicability of Numerical Methods.....	35
4.3. Numerical Methods – Description and Comparison.....	36
4.3.1. Modeling with Finite Elements.....	37
4.4. Mathematical Formulation.....	41
Chapter 5 – Modeling a Tunnel Excavation	
5.1. Introduction.....	44
5.2. Modeling the Ground Subsurface.....	44
5.3. Simulation of Tunnel Advance.....	45
5.3.1. Change of Equilibrium during Construction.....	46
5.4. Effect of Water and Consolidation.....	47
5.5. 2d and 3d Analysis of a Tunnel Excavation.....	48
Chapter 6 – Two Dimensional Modeling of a Tunnel Excavation	
6.1. Introduction.....	54
6.2. Problem Description.....	55
6.2.1. Ground Behavior.....	56
6.2.2. Tunnel geometry.....	56
6.2.3. Staged Excavation.....	57

6.2.4. Consolidation during Excavation.....	58
6.5. Numerical Simulation of the Excavation.....	59
6.5.1. Numerical Code.....	59
6.5.2. Building the Model.....	59
6.5.2.1. Simulation Steps.....	60
6.5.3. Time Stepping during Consolidation.....	63
6.6. Analysis of Results.....	65
6.6.1. Displacement at the liner.....	65

Chapter 7 – Three Dimensional Modeling of a Tunnel Excavation

7.1. Introduction.....	78
7.2. Analysis Description.....	78
7.2.1. Staged Excavation.....	79
7.2.2. Stress Variation.....	79
7.3. Numerical Simulation of the excavation.....	80
7.3.1. Building the model.....	80
7.3.2. Simulation Steps.....	81
7.4. Analysis of the results.....	83
7.4.1. Effect of K_0 variation in a 3d model	83
7.4.2. Comparison of 3d axisymmetric model.....	88

Chapter 8 – Combination of axisymmetric and plane strain model

8.1. Introduction.....	92
8.2. Description of the analysis.....	92
8.2.1. Axisymmetric model.....	92
8.2.2. Plane Strain Model.....	93
8.2.3. Combination of axisymmetric – plane strain models.....	94
8.3. Ground properties and tunnel geometry.....	97
8.3.1. Effect of Consolidation.....	98
8.4. Numerical Simulation of the excavation.....	98
8.4.1. Building the model.....	98
8.4.2. Simulation Steps.....	100
8.5. Analysis of results.....	101
8.5.1. Displacement of the crown along the tunnel axis.....	101
8.5.2. Stresses in the liner.....	103

Chapter 9 – Conclusions

9.1. Summary.....	106
9.2. Conclusions.....	107
9.2.1 Effect of Consolidation.....	107
9.2.2. Effect of initial Stress Field.....	107
9.3.2. Combination of 2d Models.....	108
9.4 Further Recommendations.....	108

References..... 109

Appendix I..... 117

Appendix II..... 118

Appendix III..... 123

Appendix IV..... 158

Appendix IVa..... 159

Appendix IVb..... 185

Appendix IVc..... 210

List of figures

Figure	Page
2.1 Coordinate System.....	18
2.2 Strain Components in polar coordinates (Obert & Duvall).....	20
4.1 Common Numerical Methods used in Engineering.....	36
4.2 Examples of 2-D mesh.....	38
4.3. 3-D mesh formed by solid elements.....	38
4.4 Node and face numbering for generalized plain strain elements (Source: Abaqus Theory Manual).....	39
4.5 Numbering of Integration points for output results in plain strain elements (Source: Abaqus Theory Manual).....	39
4.6 Numbering of nodes and faces in solid elements (Source: Abaqus Theory Manual).....	40
5.1. Load transfer in three-dimensional model (Source: Underground Structures, 1989).....	46
5.2 Three-dimensional character of a tunnel excavation (Source: Underground Structures, 1989).....	48
5.3 a) 3d model with different principal stresses in all three directions b) axisymmetric 2d model with two principal stresses being equal	49
5.4 Effect of in-situ stresses on tunnel deformation and tangential stresses on a tunnel lining (Chen & Lin 1997).....	50
5.5 Coefficients of horizontal stresses used in the analysis.....	51
5.6 Axis Symmetric model with rotation to simulate a 3d problem.....	52
6.1 Axisymmetric model of a full advance excavation with three different unsupported lengths examined.....	55
6.2 Simulation of the excavation.....	58
6.3 Axisymmetric model used in the analysis.....	60
6.4 Definition of initial stress field.....	61
6.5 Excavation sequence during the analysis.....	63

6.6	Location of the reference point for the calculation of the displacement of the lining.....	65
6.7	Displacement in z direction for reference point 2 in dry ground	66
6.8	Displacement in z direction, for reference point 2 in fully saturated ground	67
6.9	Displacement in z direction, for reference point 2 in dry and fully saturated ground ($l_u=2m$).....	68
6.10	Displacement in z direction, for reference point 1 in dry ground.....	69
6.11	Displacement in z direction, for reference point 1 in fully saturated ground	70
6.12	Displacement in z direction, for reference point 1 in dry and fully saturated ground	70
6.13	Location of the reference point for the calculation of the radial stress acting on the lining.....	71
6.14	Radial Stress S11 in z direction in dry ground (reference element 1)..	72
6.15	Radial Stress S11 in z direction in fully saturated ground (reference element 1).....	72
6.16	Comparison of radial stresses in z direction in dry and fully saturated ground, for $l_u=2m$ – (reference element 1).....	73
6.17	Location of the reference points for the calculation of the pore pressures above the lining.....	74
6.18	Dissipation of pore pressures with time, above the lining with unsupported tunnel length $l_u=1m$	75
6.19	Dissipation of pore pressures with time, above the lining with unsupported tunnel length $l_u=2m$	75
6.20	Dissipation of pore pressures with time, above the lining with unsupported tunnel length $l_u=3m$	76
6.21	Dissipation of pore pressures with time, above the lining with variation of the unsupported tunnel length l_u ...	77
7.1	Tunnel Cross Section.....	79
7.2	Horizontal stresses applied in the analysis.....	80

7.3	Mesh of the three-dimensional model simulating the excavation of a tunnel.....	81
7.4	Reference points and elements used for the interpretation of results....	83
7.5	Tunnel deformation for $K_0=0.1$ and $K_0=0.5$	84
7.6	Radial convergence in crown (reference point c - figure 7.4).....	85
7.7	Radial convergence at springline (reference point e - figure 7.4).....	85
7.8	Radial stress (direction 3 – Figure 7.4) in the crown of the tunnel (reference element 1 - figure 7.4).....	87
7.9	Radial stress (direction 3 – Figure 7.4) in the crown (reference element 2 - figure 7.4).....	87
7.10	Comparative graph of radial displacements in the crown for the axisymmetric model and the 3d model (reference point c - figure 7.4)	88
7.11	Comparative graph of radial stresses at crown, for the axisymmetric and the 3d models (reference element 1 - figure 7.4)	91
7.12	Comparative graph of radial stresses at crown, for the axisymmetric and the 3d models (reference element 2 - figure 7.4).....	91
8.1	2d models used in this analysis: axisymmetric model (a) and plane Strain (b).....	93
8.2	Variation of the displacements at the crown of the tunnel close the face of excavation, for dry and wet conditions.....	95
8.3	Stress field around the tunnel applied on the liner after a reduction of the initial stress field.....	96
8.4	Axisymmetric model of an excavated unlined tunnel.....	99
8.5	Plane strain model of an excavated tunnel with a liner in place.....	99
8.6	Variation of radial displacements with permeability at the crown and along the tunnel axis place.....	102
8.7	Reference points for the stress calculation.....	104
8.8	Variation of tangential stresses at intrados and extrados of liner.....	105

Notation

Chapter 2

r : tunnel radius

A-F: constants

γ : unit weight of soil

ϵ_r : radial strain

ϵ_θ : circumferential strain

$\epsilon_{\theta 1}$: circumferential strain due to the radial displacement

$\epsilon_{\theta 2}$: circumferential strain due to the radial displacement

θ : angular coordinate

ν : Poisson's ratio

r : radial coordinate

σ_v : vertical normal stress

σ_h : horizontal normal stress

σ_r : radial normal stress

σ_θ : circumferential normal stress

$\tau_{r\theta}$: shearing stress

u : radial displacement

u : circumferential displacement

Chapter 3

e_r, e_θ : radial and circumferential strains

e_v : volume strain

E_v : Fourier coefficient of volume strain

G : elastic shear modulus

K_0 : coefficient of earth pressure at rest

p_0 : in situ pore water pressure

p : excess pore pressure

r_0 : radius of tunnel

s : Laplace transform variable
 t : time since tunnel cutting
 u_r, u_θ : radial and circumferential displacements
 U_r, U_θ : Fourier Coefficients of displacement
 $S_{rr}, S_{\theta\theta}, S_{r\theta}$: Fourier Coefficients of stress
 γ_w : unit weight of water
 θ : circumferential coordinate
 λ : Lamé constant for soil skeleton
 ν : Poisson's ratio for soil skeleton
 $\sigma_{rr}, \sigma_{\theta\theta}, \sigma_{r\theta}$: stress components
 ϕ : deformation function
 Φ : Fourier Coefficient of ϕ

Chapter 1

Introduction

In tunnel engineering, the behavior of the ground mass is a major consideration during the design phase. The mechanical behavior of a tunnel during excavation is affected by several parameters, which control the interaction between the ground and the support that is installed. Such parameters are the tunnel geometry, the subsurface conditions, and the stages in which the excavation is performed. An accurate estimation of these parameters and a comprehensive description of the tunnel behavior are necessary for a successful design.

The excavation and the subsequent placement of the different means of support generate a new state of equilibrium mobilizing the strength of the surrounding ground. Depending on the prevailing conditions around the tunnel, this change may occur during the construction phase or may continue for a period of time.

Usually during the excavation through saturated ground, a lining is placed at the tunnel periphery to control the deformations that occur. This lining does not only provide support against ground deformations but also keeps the water out of the excavated area.

A significant number of analytical and empirical solutions have been developed for the analysis of ground liner interaction. These solutions make approximations and can predict the ground behavior with very few input parameters. In these earlier investigations the ground was considered to be a single-phase material, so the solutions developed were referring to short-term conditions and not long term. When the excavation of the tunnel is performed in a saturated medium, the behavior of the surrounding ground will be time dependent. Since the movement of water throughout the ground mass is not

instantaneous, any change in the stress field will require a certain time to have an effect on displacements and liner stresses.

Analytical solutions model the behavior of an infinitely long cylindrical tunnel but they are not capable of representing the real conditions during the excavation. The excavation stages and the stress field close to the face of the excavation are two major issues that have to be taken into consideration. Since the interaction of the tunnel and the surrounding ground is a three-dimensional problem, especially close to the face of excavation, a more complex method must be used.

The purpose of this thesis is to examine the effect of ground consolidation on ground liner interaction. A finite element analysis is performed using Abaqus (Abaqus Standard, V5.7). Different scenarios of tunnel excavation are examined. A comparison of two-dimensional and three-dimensional finite element models is also performed, to show the importance of the three-dimensional character of tunnel excavation and how it affects the results.

1.1 Thesis Outline

Chapter 2 describes a solution from the theory of elasticity, for the calculation of the stresses and displacements around a circular opening. A short reference is also made to the effect of the change of the stress field on the strength of the surrounding ground and the plastic deformations that might occur.

In Chapter 3 the basic assumptions of consolidation theory are described. The theories of Terzaghi and Biot are extended for the application of consolidation theory around a circular tunnel (Carter & Booker, 1982). A method of analysis is presented for the consolidation of linear elastic ground due to the excavation of a deep lying circular tunnel.

Chapter 4 is a short introduction to the numerical methods for solving engineering problems. The finite element method is described with reference to the creation of two-dimensional and three-dimensional models.

Chapter 5 describes in more detail the application of the finite element method in tunnel engineering. Basic difficulties during modeling are also mentioned. The two types of models, the 2d and the 3d model, that are going to be used in later chapters are compared. The limitations of the 2d model to simulate the three dimensional character of a tunnel excavation, as well as the advantages of the 3d models are also described.

In the following chapters, the excavation of a deep circular tunnel is simulated. Specifically, in Chapter 6, an axisymmetric model is used for the simulation of the staged excavation of an underground opening. The results from the excavation in dry and wet conditions are compared to show the effect of consolidation on the distribution of the stresses and displacements in the tunnel liner. In the same analysis different excavation scenarios are examined.

In Chapter 7 the excavation is simulated with a three-dimensional model. The excavation of the tunnel is performed in dry ground. The results from this analysis are compared with those obtained from a 2d axisymmetric model. The purpose in this chapter is mainly to examine the limitations of the 2d model compared to the 3d one, such as the inability to simulate a non-uniform initial stress field.

Chapter 8 examines the combination of two separate 2d models, an axisymmetric and a plane strain model, for the simulation of tunnel excavation. The purpose of this analysis is to use simple 2d models, to take into account the effect of the distance from the face of the excavation at which the liner is placed and the effect of consolidation on the liner. A comparison of the results of this analysis with those obtained from the more complex 3d model can show if a 3d model can be replicated to some extent by a combination of 2d models with an acceptable accuracy.

Chapter 2

Elastic Stresses around a Tunnel

2.1 Introduction

The ground where a tunnel is to be excavated can be considered either as a continuum or a discontinuum. Average values of physical properties of the material (stress, density, etc) can be used in physical models in order to define the mechanical behavior of the material.

When the ground is approximated by a continuum, there is an opportunity for the investigation of the tunnel behavior with theories of continuum mechanics. Hence elastic analysis methods with a short reference to elasto-plastic effects will be discussed in this chapter.

2.2 Elastic Analysis of a Circular Opening

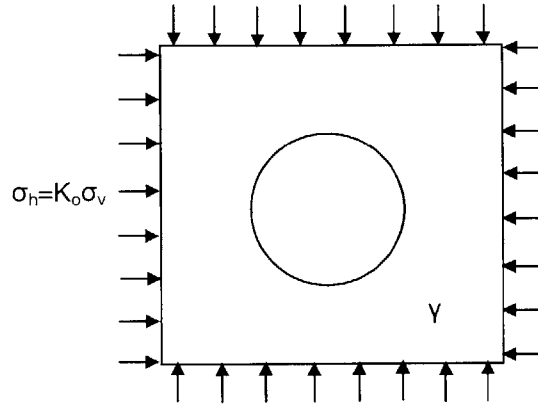
One of the aspects of great concern during the design of tunnels embedded in soil is the tunnel stability and its behavior during and after excavation. The basis of the analysis is the understanding of distribution and development of stresses and displacements induced around the tunnel. Theory of elasticity is widely used to define the stress field around an excavation.

Although in most cases the ground where a tunnel is excavated is not truly elastic and the tunnel's cross section is not always circular, the simplicity of elastic solutions can offer a preliminary insight into the significance of various parameters (Muir-Wood 1975, Curtis 1976).

2.2.1 In-situ Stresses and Strains

Let us consider a deep tunnel¹. Prior to the excavation of the tunnel and before the removal of the ground the stress field can be represented by the total stresses σ_v and σ_H in the vertical and horizontal axes respectively. The relation between the horizontal and the vertical normal stress is the following:

$$\sigma_H = K_o \cdot \sigma_v \quad (1)$$



The in situ stresses in polar coordinates, before the excavation of an opening, are given by the following equations:

$$\sigma_r = \frac{1}{2}(\sigma_v + \sigma_H) - \frac{1}{2}(\sigma_v - \sigma_H)\cos 2\theta \quad (3)$$

$$\sigma_\theta = \frac{1}{2}(\sigma_v + \sigma_H) + \frac{1}{2}(\sigma_v - \sigma_H)\cos 2\theta \quad (4)$$

$$\tau_{r\theta} = \frac{1}{2}(\sigma_v - \sigma_H)\sin 2\theta \quad (5)$$

¹ A tunnel is regarded deep when the free surface does not significantly affect the stress distribution around the excavation. This depth is large, usually several tunnel diameters, when compared to the tunnel radius.

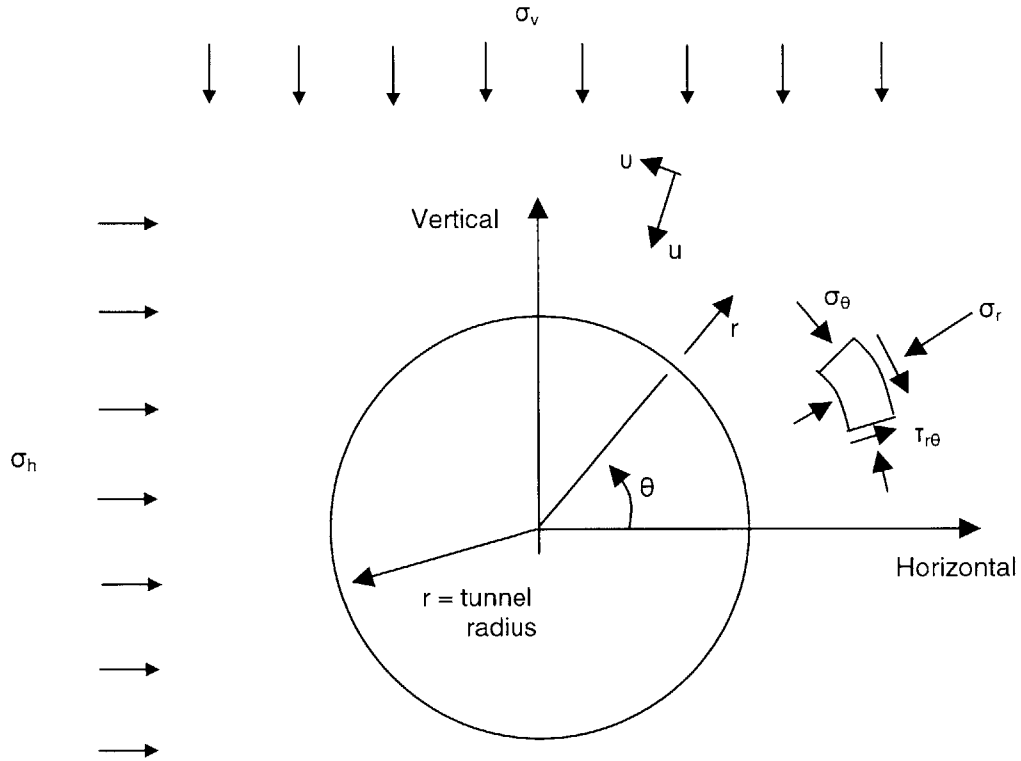


Figure 2.1 Coordinate System

To solve the elastic problem of a circular hole, we assume the following Airy stress function (Timoshenko and Goodier, 1970) (5)

$$\Phi = A \cdot \log r + Br^2 + \{Cr^2 + Dr^2 + Er^{-2} + F\} \cos 2\theta \quad (6)$$

where A, B, ..., F are constants

The stress components can be obtained from the following equations in terms of an Airy stress function Φ :

$$\sigma_r = \frac{1}{r} \frac{\partial \Phi}{\partial r} + \frac{1}{r^2} \frac{\partial^2 \Phi}{\partial \theta^2} = \frac{A}{r^2} + 2B + \{ 2C - 6Er^{-4} - 4Fr^{-2} \} \cos 2\theta \quad (7)$$

$$\sigma_\theta = \frac{\partial^2 \Phi}{\partial r^2} = -\frac{A}{r^2} + 2B + \{ 2C + 12Dr^2 + 6Er^{-4} \} \cos 2\theta \quad (8)$$

$$\tau_{r\theta} = \frac{1}{r^2} \frac{\partial \Phi}{\partial \theta} - \frac{1}{r} \frac{\partial^2 \Phi}{\partial r \partial \theta} = \{ 2C + Dr^2 - 6Er^{-4} - 2Fr^{-2} \} \sin 2\theta \quad (9)$$

The constants A, B, ..., F can be evaluated considering the stress conditions for $r=\alpha$ and for $r=\infty$:

$$(\sigma_r)_{r=\infty} = \frac{1}{2}(\sigma_v + \sigma_H) + \frac{1}{2}(\sigma_v - \sigma_H) \cos 2\theta \quad (10)$$

$$(\tau_{r\theta})_{r=\infty} = -\frac{1}{2}(\sigma_v - \sigma_H) \sin 2\theta \quad (11)$$

$$(\sigma_r)_{r=\alpha} = (\tau_{r\theta})_{r=\alpha} = 0 \quad (12)$$

Using the last equations, the constants A, B, ..., F can be calculated.

The substitution of the constants in the equations (7), (8) and (9) give the equations for the stress components in an infinite plate of a circular hole, with an applied stress σ_v and σ_H (Obert and Duvall, 1967).

$$\sigma_r = \frac{1}{2}(\sigma_v + \sigma_H) \left(1 - \frac{\alpha^2}{r^2} \right) + \frac{1}{2}(\sigma_H - \sigma_v) \left(1 + \frac{3\alpha^4}{r^4} - \frac{4\alpha^2}{r^2} \right) \cos 2\theta \quad (13)$$

$$\sigma_\theta = \frac{1}{2}(\sigma_v + \sigma_H) \left(1 + \frac{\alpha^2}{r^2} \right) - \frac{1}{2}(\sigma_H - \sigma_v) \left(1 + \frac{3\alpha^4}{r^4} \right) \cos 2\theta \quad (14)$$

$$\tau_{r\theta} = -\frac{1}{2}(\sigma_H - \sigma_v) \left(1 - \frac{3\alpha^4}{r^4} + \frac{2\alpha^2}{r^2} \right) \sin 2\theta \quad (15)$$

The last equations give the state of stress around a circular opening at any point, referring to polar coordinates, where the stresses σ_v and σ_H are applied after the tunnel has been excavated.

2.2.2 Plane Strain Equations

If we consider a point in the medium at distance r , with a displacement u at the radial direction and displacement v in the tangential direction, then the strain relations can be determined by the following equations:

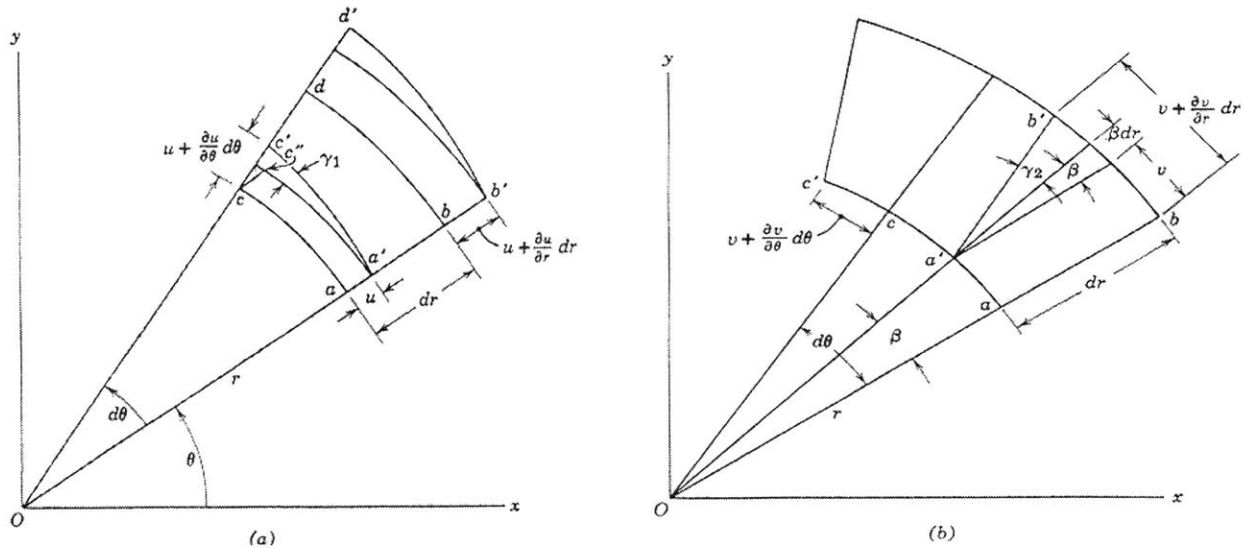


Figure 2.2 Strain Components in polar coordinates (Obert & Duvall)

$$\epsilon_r = \frac{\alpha' b' - \alpha b}{\alpha b} = \frac{u + \frac{\partial u}{\partial r} dr - u}{dr} \Rightarrow \epsilon_r = \frac{\partial u}{\partial r} \quad (16)$$

where,

u: radial displacement

r: radial coordinates

ϵ_r : radial strain

In a similar way, the tangential strain can be defined by the radial and the tangential displacements:

$$\epsilon_{\theta 1} = \frac{(r + u)d\theta - rd\theta}{rd\theta} = \frac{u}{r} \quad (17)$$

$$\epsilon_{\theta 2} = \frac{u + \frac{\partial u}{\partial \theta} \cdot d\theta - u}{rd\theta} = \frac{1}{r} \frac{\partial u}{\partial \theta} \quad (18)$$

With substitution of (15) and (16) in (14):

$$\epsilon_{\theta} = \epsilon_{\theta 1} + \epsilon_{\theta 2} = \frac{u}{r} + \frac{1}{r} \frac{\partial u}{\partial \theta} \quad (19)$$

where,

$\epsilon_{\theta 1}$: tangential strain due to the radial displacement

$\epsilon_{\theta 2}$: tangential strain due to the tangential displacement

Under the assumption of plane strain, the stress in the longitudinal direction is:

$$\sigma_v = \nu(\sigma_r + \sigma_{\theta}) \quad (20)$$

The stress-strain relations for plane strain conditions are:

$$\varepsilon_r = \frac{1}{E} (1-\nu)^2 \sigma_r - \nu(1+\nu) \sigma_\theta \Rightarrow \frac{\partial u}{\partial r} = \frac{1}{E} [(1-\nu^2) \sigma_r - \nu(1+\nu) \sigma_\theta] \quad (21)$$

$$\varepsilon_\theta = \frac{1}{E} (1-\nu)^2 \sigma_\theta - \nu(1+\nu) \sigma_r \Rightarrow \frac{u}{r} + \frac{1}{r} \frac{\partial u}{\partial \theta} = \frac{1}{E} [(1-\nu^2) \sigma_\theta - \nu(1+\nu) \sigma_r] \quad (22)$$

Under plane strain conditions, the radial and tangential displacements around a circular opening, can be calculated with integration of the last equations.

The equations for the radial and the tangential displacements are the following:

$$u = \frac{1-\nu^2}{E} \left[\left(\frac{\sigma_v + \sigma_h}{2} \right) \left(r + \frac{\alpha^2}{r} \right) + \left(\frac{\sigma_h - \sigma_v}{2} \right) \left(r - \frac{\alpha^4}{r^3} + \frac{4\alpha^2}{r} \right) \cos 2\theta \right] - \frac{\nu(1+\nu)}{E} \left[\left(\frac{\sigma_v + \sigma_h}{2} \right) \left(r - \frac{\alpha^2}{r} \right) + \left(\frac{\sigma_h - \sigma_v}{2} \right) \left(r - \frac{\alpha^4}{r^3} \right) \cos 2\theta \right] \quad (23)$$

$$u = \frac{1-\nu^2}{E} \left[- \left(\frac{\sigma_h - \sigma_v}{2} \right) \left(r + \frac{2\alpha^2}{r} + \frac{\alpha^4}{r^3} \right) \sin 2\theta \right] - \frac{\nu(1+\nu)}{E} \left[\left(\frac{\sigma_h - \sigma_v}{2} \right) \left(r - \frac{2\alpha^2}{r} + \frac{\alpha^4}{r^3} \right) \sin 2\theta \right] \quad (24)$$

At the tunnel perimeter, the displacements are:

$$u = \frac{1-\nu^2}{E} [\alpha(\sigma_v + \sigma_h) + 2\alpha(\sigma_h - \sigma_v) \cos 2\theta] \quad (25)$$

$$u = - \frac{1-\nu^2}{E} [- 2\alpha(\sigma_h - \sigma_v) \sin 2\theta] \quad (26)$$

2.2.3 Stresses around a Tunnel in a pre-stressed Medium (Pender, 1980)

Using the previous equations we are able to calculate the stresses in polar coordinates, at a point (equations (3), (4) and (5)), and around a tunnel that is excavated before the stresses σ_v and σ_h are applied at the medium. Although this solution does not approach the real excavation sequence (since it refers to a tunnel where the change in the stress medium occurs before its excavation), it is shown with the following equations that the state of stress is the same when the tunnel is excavated before or after the state of stress is changed.

When the tunnel is excavated, the radial and the shear stresses given by the equations (3) and (5) are relieved at the tunnel periphery. This change in stress gradually diminishes as the distance from the tunnel periphery is increasing. This gradual change in the stresses, while moving away from the tunnel is the reason for the generation of displacements around the excavation.

In equations (7), (8) and (9), the stress components were expressed in terms of an Airy stress function Φ . Considering this incremental change in stress, the constants A,B,...F can be calculated from the following conditions.

When the distance from the center of the tunnel , $r \rightarrow \infty$:

$$\Delta\sigma_r = \Delta\sigma_\theta = \Delta\tau_{r\theta} = 0 \quad (27)$$

At the periphery of the tunnel:

$$\Delta\sigma_r = -\frac{1}{2}(\sigma_v + \sigma_h) + \frac{1}{2}(\sigma_v - \sigma_h)\cos 2\theta \quad (28)$$

$$\Delta\tau_{r\theta} = -\frac{1}{2}(\sigma_v - \sigma_h)\sin 2\theta \quad (29)$$

The incremental stresses are:

$$\Delta\sigma_r = \frac{1}{2}(\sigma_v + \sigma_h)\left(\frac{\alpha^2}{r^2}\right) + \frac{1}{2}(\sigma_h - \sigma_v)\left(\frac{3\alpha^4}{r^4} - \frac{4\alpha^2}{r^2}\right)\cos 2\theta \quad (30)$$

$$\Delta\sigma_\theta = \frac{1}{2}(\sigma_v + \sigma_h)\left(\frac{\alpha^2}{r^2}\right) - \frac{1}{2}(\sigma_h - \sigma_v)\left(\frac{3\alpha^4}{r^4}\right)\cos 2\theta \quad (31)$$

$$\Delta\tau_{r\theta} = \frac{1}{2}(\sigma_h - \sigma_v)\left(\frac{3\alpha^4}{r^4} - \frac{2\alpha^2}{r^2}\right)\sin 2\theta \quad (32)$$

The equations for the radial and the tangential displacements are the following:

$$u = \frac{1+\nu}{E} \left[\left(\frac{\sigma_v + \sigma_h}{2} \right) \left(\frac{\alpha^2}{r} \right) + \left(\frac{\sigma_h - \sigma_v}{2} \right) \left((1-\nu) \frac{4\alpha^2}{r} - \frac{\alpha^4}{r^3} \right) \cos 2\theta \right] \quad (33)$$

$$v = \frac{1+\nu}{E} \left[- \left(\frac{\sigma_h - \sigma_v}{2} \right) \left((1-2\nu) \frac{2\alpha^2}{r} + \frac{\alpha^4}{r^3} \right) \sin 2\theta \right] \quad (34)$$

When $r=\alpha$ the displacements are:

$$u = \frac{1+\nu}{2E} \alpha \left[(\sigma_v + \sigma_h) + (3-4\nu)(\sigma_h - \sigma_v) \cos 2\theta \right] \quad (25)$$

$$v = \frac{1+\nu}{2E} (3-4\nu) \alpha (\sigma_v + \sigma_h) \sin 2\theta \quad (26)$$

2.3 Change of Stresses with Tunnel Advance

The initial stress field before the excavation of a circular tunnel is often considered uniform when the tunnel is located at considerable depth. The vertical stress around the opening is equal to the unit weight of the mass multiplied by the depth of the tunnel. The horizontal stress can be defined through the vertical stresses with the use of the coefficient of horizontal stresses.

Observing the equations that define the stresses around an unlined tunnel, there is a decrease of the radial stress σ_r close to the tunnel periphery (zero value at the boundary of the excavation), while the tangential stress σ_θ reaches a maximum value equal to $2\sigma_v$ (when $\sigma_v = \sigma_h$).

When moving away from the tunnel periphery, both the radial and the axial stresses approach the initial stresses before the excavation of the tunnel. At certain distance from the tunnel the stress field is not affected by the tunnel excavation. Depending on the depth of the excavation and the properties of the ground material, the combination of stresses can be such that the material will deform beyond its elastic limit. This will gradually extend inward to the mass leading to the creation of a plastic zone. In this zone permanent deformations are created. At some distance the combination of stresses will not satisfy the yield criterion. Beyond this point which defines the end of the plastic zone around the tunnel, the material will be in an elastic state.

Chapter 3

Elastic Consolidation around a Tunnel

3.1 Introduction

In this chapter the theory of consolidation is described and how it applies in practical problems such as the excavation of a tunnel. Consolidation of a ground mass occurs when due to applied loads there is a change in the volume of the ground while at the same time there is a fluid flow.

When the ground material is fully saturated (pores are completely filled with liquid), it can be considered a two-phase system; A system with a solid phase and a liquid phase. The liquid phase, often called pore phase, is considered incompressible.

Part of the load is transmitted to the skeleton of the ground and part to the pore fluid. With rapid loading the initial volume of the system does not change. With time, the pore fluid will start to flow causing a change in the volume of the ground. These deformations are time-dependent, and continue until equilibrium is reached (dissipation of pore pressures).

When a tunnel is excavated in a fully saturated ground, the following two types of time dependent behavior occur in the surrounding ground. The first is due to the intrinsic rate dependent characteristics of the materials, such as the creep deformation or stress relaxation. The second is caused by the movement of the pore water due to pore water pressure dissipating into the surrounding ground and also into the tunnel opening. The following pages are focused on the second type of time dependent behavior of the surrounding ground, i.e. consolidation

3.2 Consolidation Theories

The theory was developed originally from Terzaghi (1925) for the one-dimensional case, and extended to a more general theory for the three-dimensional case by Biot (1941).

3.2.1 General Assumptions

The assumptions made for the three-dimensional consolidation refer both to the behavior of the ground, as well as to the flow of the fluid through the pores of the ground. The ground is considered a two-phase material. The following assumptions are divided below into different categories as they were mentioned by Terzaghi and Biot.

Load deformation behavior of the ground

- (a) Stresses are transmitted to the ground by the effective stresses of the ground skeleton and to the pore pressures of the fluid according to Terzaghi's effective stress principle.
- (b) The deformation of the ground occurs in small increments.

Nature of soil:

- (c) The pores are completely filled with fluid
- (d) Both the pore fluid and the ground particles are incompressible but the ground skeleton itself is compressible

Material properties of both phases

- (g) The relation between the fluid velocity and the pore pressure gradients is linear (Darcy's law)
- (h) Small strains and effective stresses are related linearly (elastic and isotropic relation)
- (i) The material properties can vary throughout the geometry of the problem but cannot vary with time

Boundary Conditions

- (j) Flow is allowed in all three principal directions.
- (k) Stresses and deformations vary in all three principal directions in the ground.

Boundary conditions are specified with loads and displacements.

For the 1-D consolidation theory, Terzaghi used the assumptions (a), (b), (c), (d), (f), (g) and (h). Assumptions (j) and (k) were applied to one dimension. Material properties (g) and (h) cannot vary with depth and the specified boundary conditions must remain constant with time.

3.2.2 Assumptions used in the Finite Element Analysis

The finite element method can solve problems such as the consolidation theory of Biot. All the assumptions mentioned above are used in the finite element approach. As a matter of fact the finite element approach allows one to go beyond the above mentioned assumptions. Specifically, consolidation is treated with small time increments. Each increment is considered as a new condition where the results from the previous increment are used as an input. This allows one to use inhomogeneous material properties that can change in each increment, boundaries that change with time during the analysis, and large strains that result from smaller strains of each increment.

3.3 Elastic Consolidation around a deep circular tunnel (Carter & Booker, 1982)

When an opening is created in a saturated medium the displacements and the stresses generated are time dependent. This is a result of the two phase nature of the saturated ground.

Carter and Booker developed a closed form analysis for the consolidation due to the excavation of a long and deep circular tunnel. The following equations

are extracted from the a paper published by Booker and Carter (Elastic consolidation around a deep circular tunnel, 1982).

Before the excavation of the tunnel, the initial stress field may be described by the following equations. The total normal stress σ_v acts in the vertical direction and the total normal stress σ_H acts in the horizontal direction:

$$\sigma_H = N\sigma_v \quad (1)$$

The effective stresses are given by the equations:

$$\sigma_v = \sigma'_v + p_o \quad (2)$$

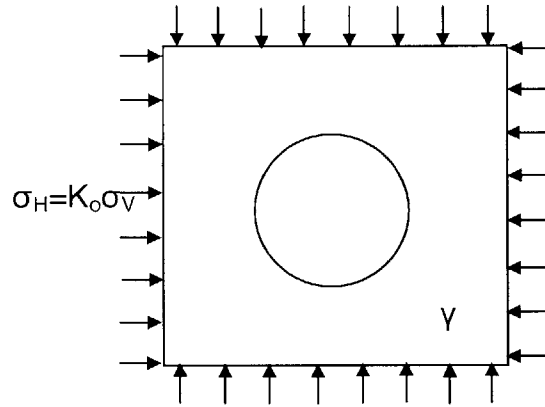
$$\sigma_H = \sigma'_H + p_o \quad (3)$$

where,

σ_v =vertical effective stress

σ_H =horizontal effective stress

p_o =in situ pore water pressure



As was mentioned in Chapter 2, the in situ stresses in polar coordinates, before the excavation of an opening, are given by the following equations:

$$\sigma_{rr} = \frac{1}{2}(\sigma_v + \sigma_H) - \frac{1}{2}(\sigma_v - \sigma_H)\cos 2\theta \quad (4)$$

$$\sigma_{\theta\theta} = \frac{1}{2}(\sigma_v + \sigma_H) + \frac{1}{2}(\sigma_v - \sigma_H)\cos 2\theta \quad (5)$$

$$\tau_{r\theta} = \frac{1}{2}(\sigma_v - \sigma_H)\sin 2\theta \quad (6)$$

General Solution

Under conditions of plane strain, the equations that describe the consolidation of an isotropic, elastic ground are:

$$\frac{\partial \sigma_{rr}}{\partial r} + \frac{1}{r} \frac{\partial \sigma_{r\theta}}{\partial \theta} + \frac{\sigma_{rr} - \sigma_{\theta\theta}}{r} = 0 \quad (7)$$

$$\frac{\partial \sigma_{r\theta}}{\partial r} + \frac{1}{r} \frac{\partial \sigma_{\theta\theta}}{\partial \theta} + 2 \frac{\sigma_{r\theta}}{r} = 0 \quad (8)$$

$$\sigma_{rr} - p = -\lambda e_v - 2G e_{rr} \quad (9)$$

$$\sigma_{\theta\theta} - p = -\lambda e_v - 2G e_{\theta\theta} \quad (10)$$

$$\sigma_{r\theta} = -G \gamma_{r\theta} \quad (11)$$

where,

λ = Lamé constant for the ground skeleton

G = elastic shear modulus

$$e_{rr} = \frac{\partial u_r}{\partial r} \quad (12)$$

$$e_{\theta\theta} = \frac{u_r}{r} + \frac{1}{r} \frac{\partial u_\theta}{\partial \theta} \quad (13)$$

$$\gamma_{r\theta} = \frac{1}{r} \frac{\partial u_r}{\partial \theta} + \frac{\partial u_\theta}{\partial r} - \frac{u_\theta}{r} \quad (14)$$

$$e_u = e_{rr} + e_{\theta\theta} \quad (15)$$

$$\nabla^2 \bar{e}_u = \frac{s}{c} \bar{e}_u \quad (16)$$

For elastic ground:

$$c = \frac{k}{\gamma_w} \cdot (\lambda + 2G) = \frac{k}{\gamma_w} \cdot 2G \cdot \frac{(1-2\nu)}{(1-2\nu)} \quad (17)$$

where,

c =coefficient of consolidation

k =coefficient of isotropic permeability

γ_w =unit weight of pore fluid

ν =Poisson's ratio for ground skeleton

u_r = radial displacement

u_θ =circumferential displacement

\bar{e}_v = Laplace transform of volume strain

If t is the time elapsed after the tunnel excavation, the Laplace tranform of the volume strain is:

$$\bar{e} = \int_0^{\infty} \exp(-st) e_v(t) dt \quad (18)$$

The governing equations of consolidation may be written in the following form:

$$(\lambda + 2G) \frac{\partial e_v}{\partial r} - \frac{G}{r} \frac{\partial \omega}{\partial \theta} = \frac{\partial p}{\partial r} \quad (19)$$

$$(\lambda + 2G) \frac{1}{r} \frac{\partial e}{\partial \theta} + G \frac{\partial \omega}{\partial r} = \frac{1}{r} \frac{\partial p}{\partial \theta} \quad (20)$$

$$\nabla^2 \bar{e}_v = \frac{s}{c} \bar{e}_v \quad (21)$$

If the deformation function φ is used, then the latter equations may be written as:

$$p = G\varphi + (\lambda + 2G)e_u \quad (22)$$

$$-\frac{1}{r} \frac{\partial \omega}{\partial \theta} = \frac{\partial \varphi}{\partial r} \quad (23)$$

$$\frac{\partial \omega}{\partial r} = \frac{1}{r} \frac{\partial \varphi}{\partial \theta} \quad (24)$$

$$\nabla^2 \bar{e}_u = \frac{s}{c} \bar{e}_u \quad (25)$$

The solutions will have the form:

$$\left. \begin{aligned} u_r &= U_r \cos(n\theta + \varepsilon) \\ u_\theta &= U_\theta \cos(n\theta + \varepsilon) \\ p &= P \cos(n\theta + \varepsilon) \\ \sigma_{rr} &= S_{rr} \cos(n\theta + \varepsilon) \\ \sigma_{\theta\theta} &= S_{\theta\theta} \cos(n\theta + \varepsilon) \\ \sigma_{r\theta} &= S_{r\theta} \sin(n\theta + \varepsilon) \\ e_u &= E_u \cos(n\theta + \varepsilon) \\ \omega &= \Omega \sin(n\theta + \varepsilon) \\ \varphi &= \Phi \cos(n\theta + \varepsilon) \end{aligned} \right\} \quad (26)$$

With substitution to the equations (23), (24) and (25) the following equations are formed:

$$-\frac{n}{r}\Omega = \frac{\partial\Phi}{\partial r} \quad (27)$$

$$-\frac{n}{r}\Phi = \frac{\partial\Omega}{\partial r} \quad (28)$$

$$\frac{\partial^2 \bar{E}_u}{\partial r^2} + \frac{1}{r} \frac{\partial \bar{E}_u}{\partial r} - \frac{n^2}{r^2} \bar{E}_u = \frac{s}{c} \bar{E}_u \quad (29)$$

After solving equations (27), (28) and (29) for the transforms of displacement coefficients U_r and U_θ , the general solution can be expressed in terms of six independent solutions:

$$\begin{pmatrix} \bar{U}_r \\ \bar{U}_\theta \\ \bar{P} \\ \frac{2G}{s} \bar{S}_{rr} \\ \frac{2G}{s} \bar{S}_{\theta\theta} \\ \frac{2G}{s} \bar{S}_{r\theta} \end{pmatrix} = [M] \begin{pmatrix} A_1 \\ A_2 \\ A_3 \\ A_4 \\ A_5 \\ A_6 \end{pmatrix} \quad (30)$$

where,

$[M]$ is given in Appendix I.

A_1, \dots, A_6 coefficients that can be found from the boundary conditions of the problem

The coefficients U_r can be derived from the equations (30) with the application of complex inversion theorem. For a general function $f(t)$ the inversion is given by :

$$f(t) = \frac{1}{2\pi i} \int_c \bar{f}(s) e^{st} ds \quad (31)$$

Chapter 4

Application of Numerical Methods in Tunnel Engineering

4.1 Introduction

The goal of this chapter is to introduce numerical methods for solving engineering problems as an alternative solution to other computational methods such as the analytical methods of solution.

Numerical methods represent a complex group of computational methods. What makes them different from the other computational methods is their capability to simulate actual and complex conditions. Their use allows one to solve many practical problems, such as non-linear material behavior, variations in material properties and other factors that different geologic conditions impose.

The choice of a computational method depends on its capability to satisfy the needs of a particular problem. For uncomplicated problems a simple computational method can give satisfactory results. If more complex problems are to be solved then the precision and accuracy that a numerical solution may offer, is in many cases preferred.

Sometimes more than one computational method can be used for a particular problem. In tunnel engineering, an analytical method can be used for a preliminary design of the tunnel, where a numerical method can be used during the final design for a detailed analysis. In each case the geotechnical engineer has to identify the difficulties of the problem and choose the appropriate solution method.

4.2 Applicability of Numerical Methods

One of the main uses of the numerical solutions in simulations of tunnel excavation is the calculation of the stresses, strains and displacements. In other cases, additional analyses that are very common in tunnel design such as the determination of the plastic zone or even the generation of pore pressures are also performed.

In each analysis, the generation and interpretation of the results is done according to the level of accuracy and the purpose for which these analyses are performed.

In general these analyses can be grouped in two categories:

a) Qualitative analysis

Qualitative analyses do not give exact numbers as results but their main purpose is to enhance the conceptual understanding of the problem and the engineering principles in general. Specifically in a tunnel excavation analysis, the impact of parameters that describe the tunnel or the surrounding ground, on the stress distribution around the tunnel, can be considered to be a qualitative analysis.

Another form of qualitative analysis are parametric or sensitivity analyses. Such analyses aim to find the impact of some parameters on the tunnel and the surrounding mass. This analysis will consider different parameters and how they affect the behavior of the tunnel. A sensitivity analysis is performed when the different parameters of the tunnel and the surrounding mass are known and the goal, through this analysis, is to identify the impact of some parameters such as the tunnel geometry or the tunnel's depth on the stress distribution or the displacements around the tunnel.

Other parameters that can be checked during the sensitivity (parametric) analysis are the tunnel excavation sequence and the time dependency of the excavation stages.

b) Quantitative analysis

The main purpose of this analysis is to determine all the required values that will affect the final design of the tunnel. The design values relate not only to the structure itself, but also to the effect on the surrounding structures.

These results might as well be used for back analysis of a problem. For instance, during the construction of a tunnel where field measurements are performed, these results can be used for verification of the design procedure, or even for adjustment of further design of the tunnel.

4.3 Numerical Methods - Description and Comparison

A number of several numerical methods are used in tunnel engineering. Some of these methods are presented in the following table. Three different models are presented, with the associated numerical methods used.

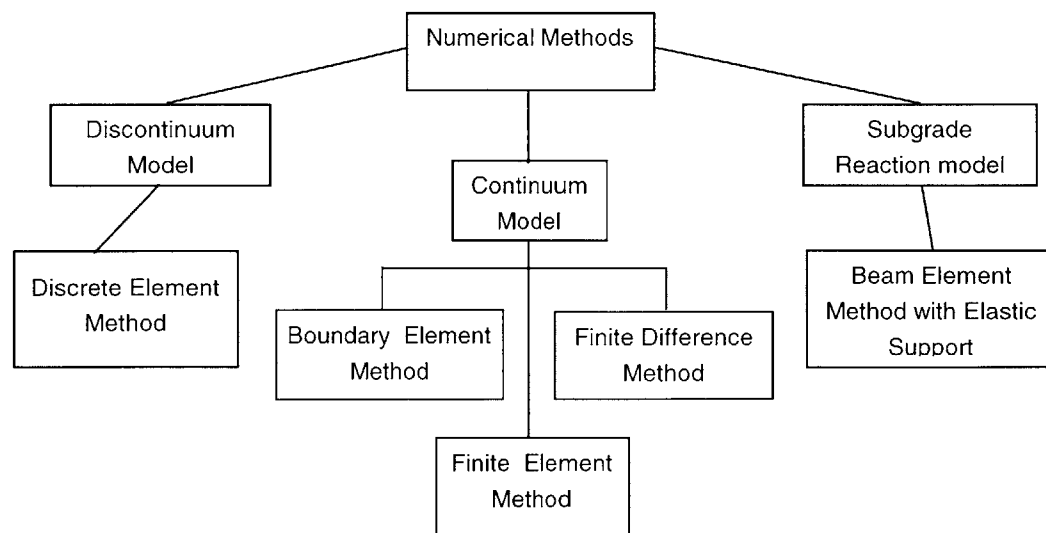


Figure 4.1 Common Numerical Methods used in Engineering

All of the numerical analysis methods mentioned above can be applied individually or they can be combined in a hybrid form. Each one of them can be applied according to the problem that has to be solved.

4.3.1 Modeling with Finite Elements

The main solution method applied in this thesis is the Finite Element Method. Regardless of the physical nature of the problem, the subsurface is modeled as a continuum. This is the first step in the application of this method.

Thus the continuum is divided into an equivalent system of smaller continua, a limited number of elements - each of simple geometry - that are called finite elements. All these elements form the finite element mesh. Some examples of generated meshes are shown at the following figures.

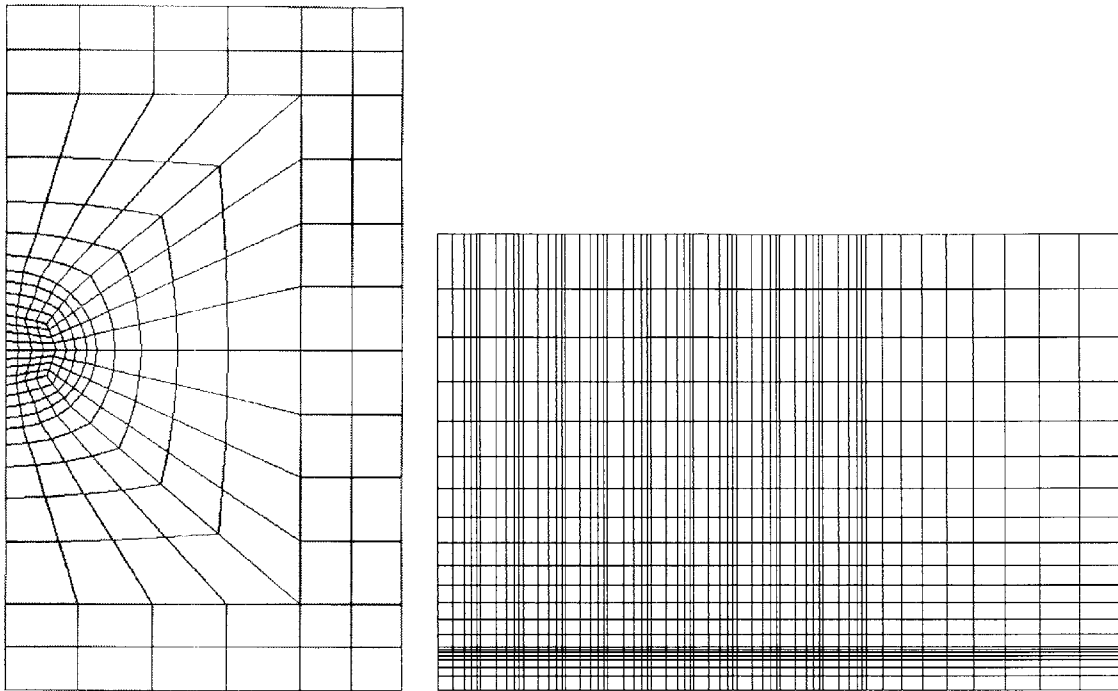


Figure 4.2 Examples of 2-D mesh

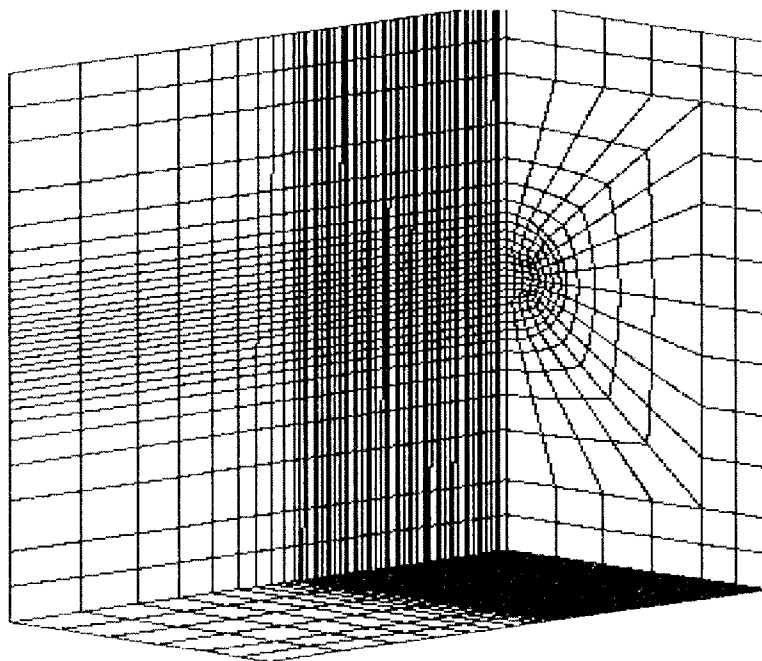


Figure 4.3. 3-D mesh formed by solid elements

The elements that form the mesh are assumed to be connected at certain points called nodal points. As shown at the following figures the nodal points can be located at the corners of the elements or at mid points, depending on the precision required in the analysis.

These nodes are the points where the displacements are calculated during the analysis. The nodal displacements are related to the displacements at every point inside each element, depending on the type of the element used. From the displacement field in the elements the strains and stresses can also be calculated.

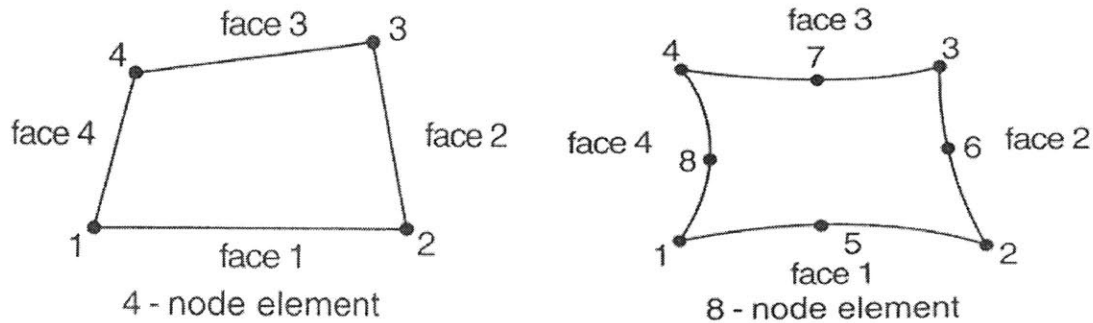


Figure 4.4 Node and face numbering for generalized plain strain elements
(Source: Abaqus Theory Manual)

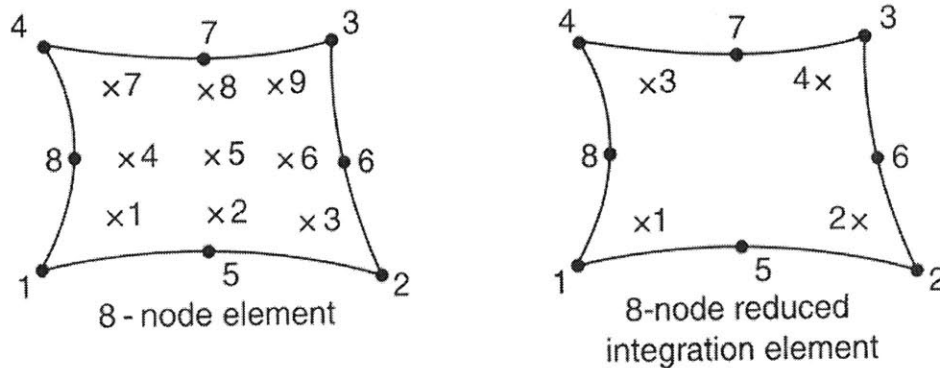


Figure 4.5 Numbering of Integration points for output results in plain strain elements
(Source: Abaqus Theory Manual)

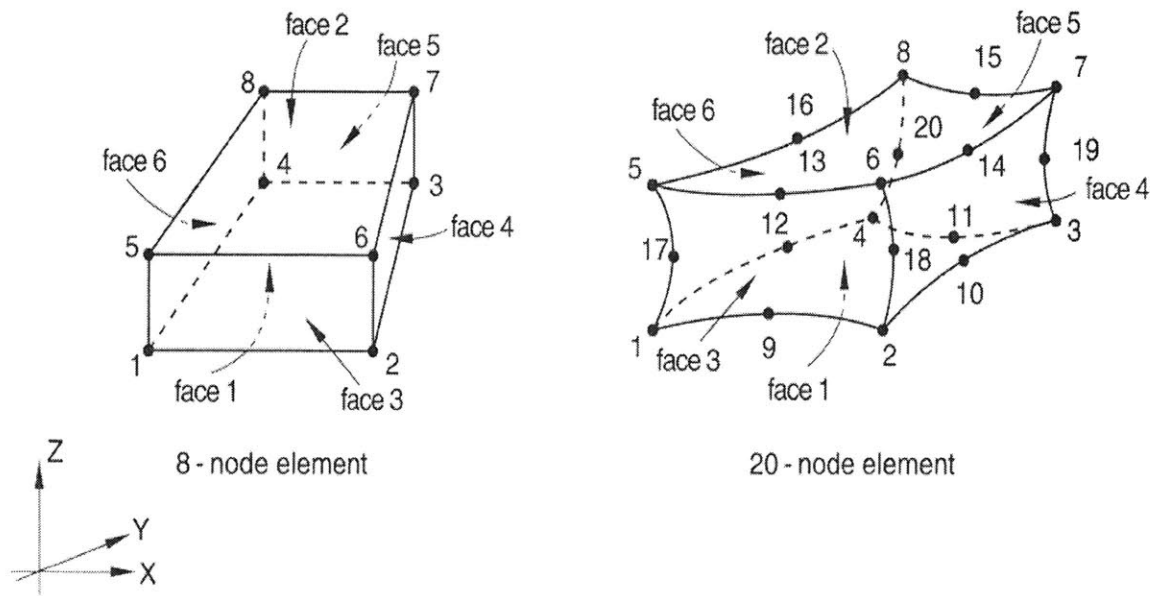


Figure 4.6 Numbering of nodes and faces in solid elements
(Source: Abaqus Theory Manual)

Basic characteristic of the finite element method is that the finite elements are analyzed separately with the physical and constitutive properties assigned individually in each one of them. The different equations for the stiffness and the properties of the elements are formulated and are assembled so as to get the equations for the total structure. This interconnection between the elements makes the analysis a highly complex mathematical model.

The continuum can represent a physical body of ground where the excavation of a tunnel is performed. In this model, we are interested in several values such as displacements, stresses or even potential flow. These are the unknown quantities in a tunnel simulation. Quantities such as stresses and water flow quantities can be calculated from the displacements and the flow potential respectively.

The mesh that is created by the different elements represents the model that simulates the excavation. The analysis of this model is performed with the solution of the equation matrix that includes all the equations from the different

elements. A global stiffness matrix is created for the whole structure to relate the known with the unknown quantities. This global stiffness matrix is formed by adding all the stiffnesses of each of the elements.

The main advantage of the finite element method is that it allows the simulation and the analysis of complex underground conditions. This numerical solution method allows the simulation of complex constitutive laws, different material properties (homogeneous and non-homogeneous), as well time dependent construction methods.

4.4 Mathematical Formulation

As mentioned before the basic concept when generating a finite element model that will be analyzed, is that the domain that is modeled, is discretized into smaller elements that are connected with each other sharing the same nodal points. Any variables calculated at the nodal points are used to calculate these variables inside these elements.

All these calculations are performed with the use of different mathematical expressions that describe the behavior of the model analyzed.

Under certain loading conditions, the load is transferred through the model mesh to the nodes. With the assumption of specified material properties for each of the discretized elements, the nodal displacements and the internal stresses are calculated after a determination of a stiffness matrix that will model the soil domain.

The nodal displacements and the internal displacements are related with an internal set of linear expressions:

$$D_{11}\Phi_1 + D_{12}\Phi_2 + D_{13}\Phi_3 + \dots + D_{1n}\Phi_n = U_1$$

$$D_{21}\Phi_1 + D_{22}\Phi_2 + D_{23}\Phi_3 + \dots + D_{2n}\Phi_n = U_2$$

$$\cdot \quad \cdot \quad \cdot \quad \cdot \quad \cdot$$

$$\cdot \quad \cdot \quad \cdot \quad \cdot \quad \cdot$$

$$\cdot \quad \cdot \quad \cdot \quad \cdot \quad \cdot$$

$$D_{n1}\Phi_1 + D_{n2}\Phi_2 + D_{n3}\Phi_3 + \dots + D_{nn}\Phi_n = U_n$$

Where, D_{ij} : internal displacement

Φ_{ij} : shape factors

U_n : nodal displacement

These relations can be presented in the form of matrices:

$$\begin{Bmatrix} D_1 \\ D_2 \\ \dots \\ \dots \\ D_n \end{Bmatrix} = \begin{bmatrix} \phi_{11} & \phi_{12} & \phi_{13} & \dots & \dots & \phi_{1n} \\ \phi_{21} & \phi_{22} & \phi_{23} & \dots & \dots & \phi_{2n} \\ \dots & \dots & \dots & \dots & \dots & \dots \\ \dots & \dots & \dots & \dots & \dots & \dots \\ \phi_{n1} & \phi_{n2} & \phi_{n3} & \dots & \dots & \phi_{nn} \end{bmatrix} \begin{Bmatrix} U_1 \\ U_2 \\ \dots \\ \dots \\ U_n \end{Bmatrix}$$

or

$$\{D_i\} = [\Phi] \{U_n\}$$

where, $\{D_i\}$ is the internal displacement of a finite element vector

$[\Phi]$ is the shape matrix

$\{U_n\}$ is the nodal displacement vector

The internal strains can be calculated in the same way with derivation of the last equations.

$$\{\epsilon_i\} = [B] \{U_n\}$$

where, $\{\epsilon_i\}$ is the strain vector

$[B]$ is the displacement matrix

$\{U_n\}$ is the nodal displacement vector

In order to calculate the strain vector, the stiffness matrix has to be defined.

This matrix

$$\begin{Bmatrix} \varepsilon_1 \\ \varepsilon_2 \\ \dots \\ \dots \\ \varepsilon_n \end{Bmatrix} = \begin{Bmatrix} U_1 \\ U_2 \\ \dots \\ \dots \\ U_n \end{Bmatrix} \begin{bmatrix} B_{11} & B_{12} & B_{13} & \dots & \dots & B_{1n} \\ B_{21} & B_{22} & B_{23} & \dots & \dots & B_{2n} \\ \dots & \dots & \dots & \dots & \dots & \dots \\ \dots & \dots & \dots & \dots & \dots & \dots \\ B_{n1} & B_{n2} & B_{n3} & \dots & \dots & B_{nn} \end{bmatrix}$$

The internal stresses can be calculated from the strain vector, by using the following equation:

$$\{\sigma_i\} = [D] \{\varepsilon_i\}$$

where, $\{\varepsilon_i\}$ is the strain vector

$[D]$ is the stiffness matrix

$\{\sigma_i\}$ is the stress vector

The stiffness matrix can be calculated using the energy equation, by defining the work that is generated from nodal forces that create nodal displacements.

Many scientists have developed several stiffness matrices for different elements such as plain strain, axisymmetric stress, and 3D elements, for the development of the mathematical formulations of the finite element analysis.

Chapter 5

Modeling a Tunnel Excavation

5.1 Introduction

What can be achieved with the generation of a numerical model is the accurate reproduction of the real conditions in a tunnel excavation problem. This offers the opportunity to predict and interpret the behavior of the surrounding ground as well as the response of the tunnel itself.

In many cases this procedure can be very complicated as there are many unknown parameters when a real condition is simulated. The uncertainty about the ground parameters, the tunnel behavior, as well as the inability to represent the ground response by formulating the appropriate constitutive laws, are some of the reasons for certain simplifying assumptions. Even with these assumptions the results can be accurate enough, so that they can be beneficial to the geotechnical engineer.

5.2 Modeling the Ground Subsurface

The selection of the model is one of the most important steps in the simulation of a problem. The size of the mesh as well as the size and the type of the elements that generate it, must be appropriate so as to ensure accuracy in the model and subsequently in the results.

Using a simple model with simplified assumptions can be one of the reasons for the omission of important parameters that directly affect the behavior of the tunnel and the surrounding area. In a similar way a complex model, although providing accurate results, can increase the cost of the analysis, as the definition of several parameters can be a complicated procedure. The results in the simulation are calculated in a way that a possible

mistake in the definition of the parameters can be multiplied by the end of the simulation. For example the stresses calculated in an analysis result from the integration of the displacements.

The first step in a simulation is to set the constitutive laws that will describe in the most appropriate way the stress-strain relationship in the ground. For geotechnical engineering problems some of the main constitutive laws used are linear elastic, elastic-plastic, linear visco-elastic and elasto-visco-plastic.

During the simulation of the ground certain assumptions are considered, such as the homogeneity of the medium and its isotropy. In many cases though, the ground parameters may vary with time. These changes are often related to creep effects or consolidation.

5.3 Simulation of Tunnel Advance

With the excavation of a tunnel and the subsequent placement of the support, there is a change in the stress field at the tunnel perimeter and in the surrounding medium. Depending on the prevailing conditions around the tunnel, this change may be continuous or in stages during its lifetime. The knowledge and understanding of the deformations associated with these changes, is necessary so as to interpret and explain the behavior of the tunnel support.

The excavation sequence and the installation of the liner during the excavation of a tunnel are the most important parameters to consider in the design phase. When a computer analysis is performed for the simulation of a tunnel excavation, the construction phases and their sequence must be simulated in order to obtain realistic results. However, taking into consideration the effect of staged excavation, more complex simulations can be created that in many cases might eventually decrease the accuracy and the integrity of the results. In any case, the main goal is the accurate and realistic modeling of the problem under investigation.

5.3.1 Change of Equilibrium during Construction

Before the excavation of the tunnel there is a static equilibrium in the medium. The process of tunneling creates a new equilibrium. This equilibrium is continuously changing, depending on the various stages of tunnel construction and placement of supports, until a final equilibrium is reached.

A region of changing stresses, characterized by increased vertical pressure, travels ahead of the advancing of the tunnel. Changes of equilibrium conditions are also felt at a considerable distance behind the face. The distribution of stresses has a three-dimensional character near the face, but approaches a two-dimensional state as the face advances. The rate at which the two-dimensional state is approached is influenced by the rate of advance of the face in relation to the time dependent behavior of the medium.

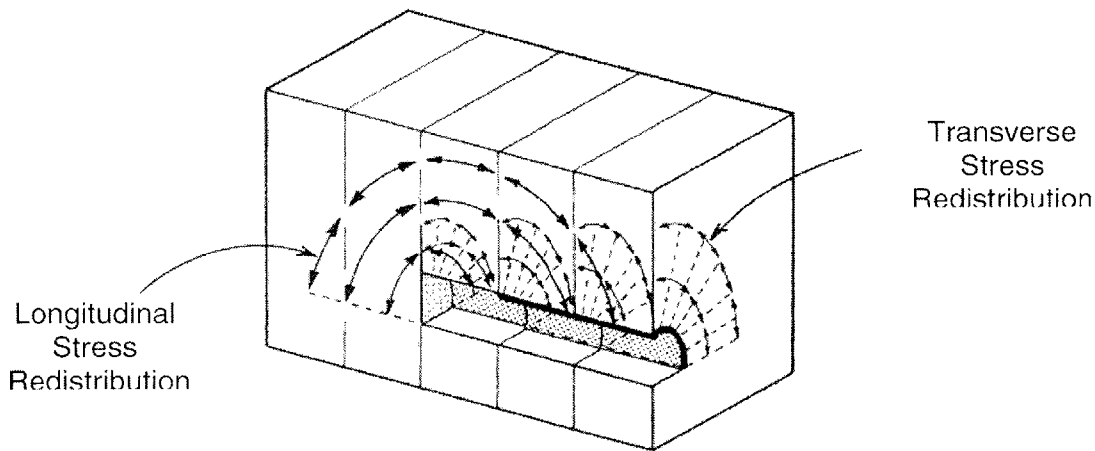


Figure 5.1. Load transfer in three-dimensional model
(Source: Underground Structures, 1989)

Changes in the stress equilibrium cannot take place without deformations in the medium. If supports are employed these will deform as well. There is always an immediate deformation response to a change in equilibrium conditions, and commonly there is an additional, time dependent response.

In a water-bearing medium, the excavation of a tunnel changes the pore water pressures around the opening and flow of water is induced. In fine grained materials with low permeability, the establishment of hydrostatic or hydrodynamic equilibrium is not immediate. The associated time-dependent changes in effective intergranular pressures in the medium lead to time-dependent deformations. Time lags may also be associated with visco-elastic or visco-plastic phenomena such as creep in the medium itself or along joint planes in the medium.

Whatever the cause of the time lags, their most important effect is that the final equilibrium for a set of boundary conditions is not often reached before new changes in boundary conditions occur.

5.4 Effect of Water and Consolidation

With the excavation of a tunnel in a fully saturated mass, two types of time dependent behavior occur in the surrounding ground. The first time dependent behavior is related to creep deformation or stress relaxation. The second behavior is caused due to the dissipation of the excessive pore water pressures in the surrounding ground, where there is an apparent loss of strength of materials.

In tunnel construction a common phenomenon is that drainage occurs in the surrounding ground due to the excavation process. With progressing tunnel advance the area is subjected to additional groundwater drainage into the tunnel opening. When the surrounding ground is partially or fully saturated, the stress field is influenced by negative pore pressures that build up behind the tunnel liner. The dissipation of these pore pressures affect the vertical stresses in the surrounding mass and eventually the stress applied on the liner.

5.5 2d and 3d Analysis of a Tunnel Excavation

Tunnel excavation is a complex procedure that usually has a three-dimensional character. This three dimensionality is often related to the geometry of the problem and particularly to the zone near the excavation face. Figure 5.2 depicts the way in which this three dimensionality is encountered. With the excavation advance there is a redistribution of stresses in both the longitudinal and the transverse direction. This effect and the generation of displacements in this zone can create a stability problem.

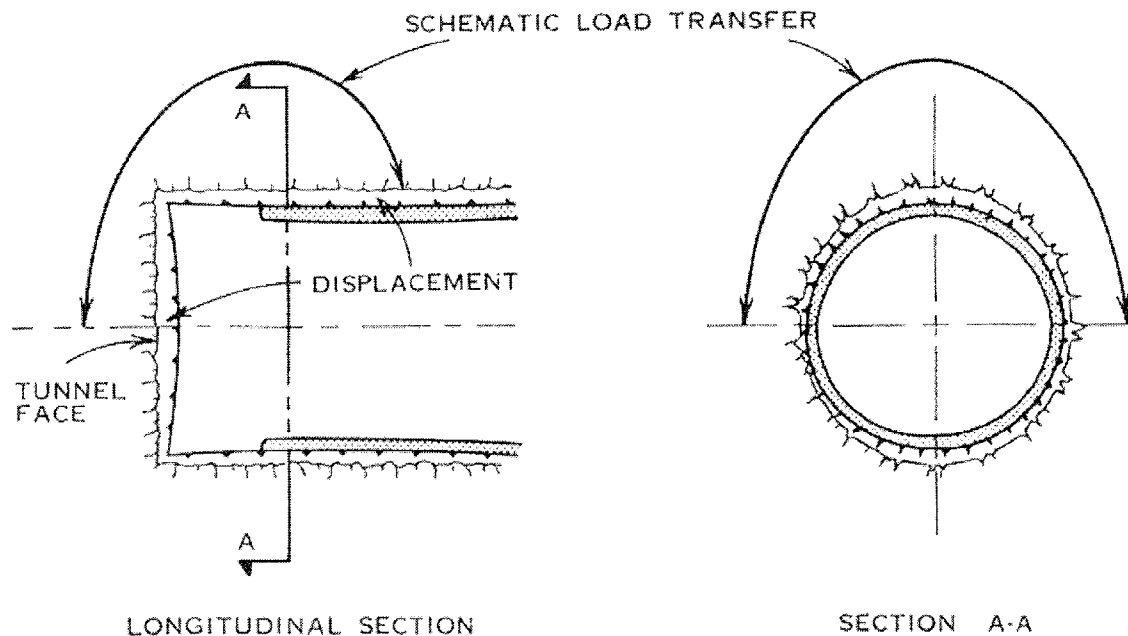


Figure 5.2 Three-dimensional character of a tunnel excavation
(Source: Underground Structures, 1989)

Apart from the problem of the geometry of the analyzed zone, a three-dimensional model is necessary when the subsurface behaves differently in the three dimensions.

The most significant advantage of the 3d model is its ability to simulate various stress fields. In contrast to the simpler 2d models, it allows the consideration of the horizontal stresses perpendicularly to the tunnel as well as

along its axis. This effect of variability of the horizontal stresses will be examined in a later chapter. Figure 5.3 compares the stress conditions of a complete 3d model to those of an axisymmetric 2d model.

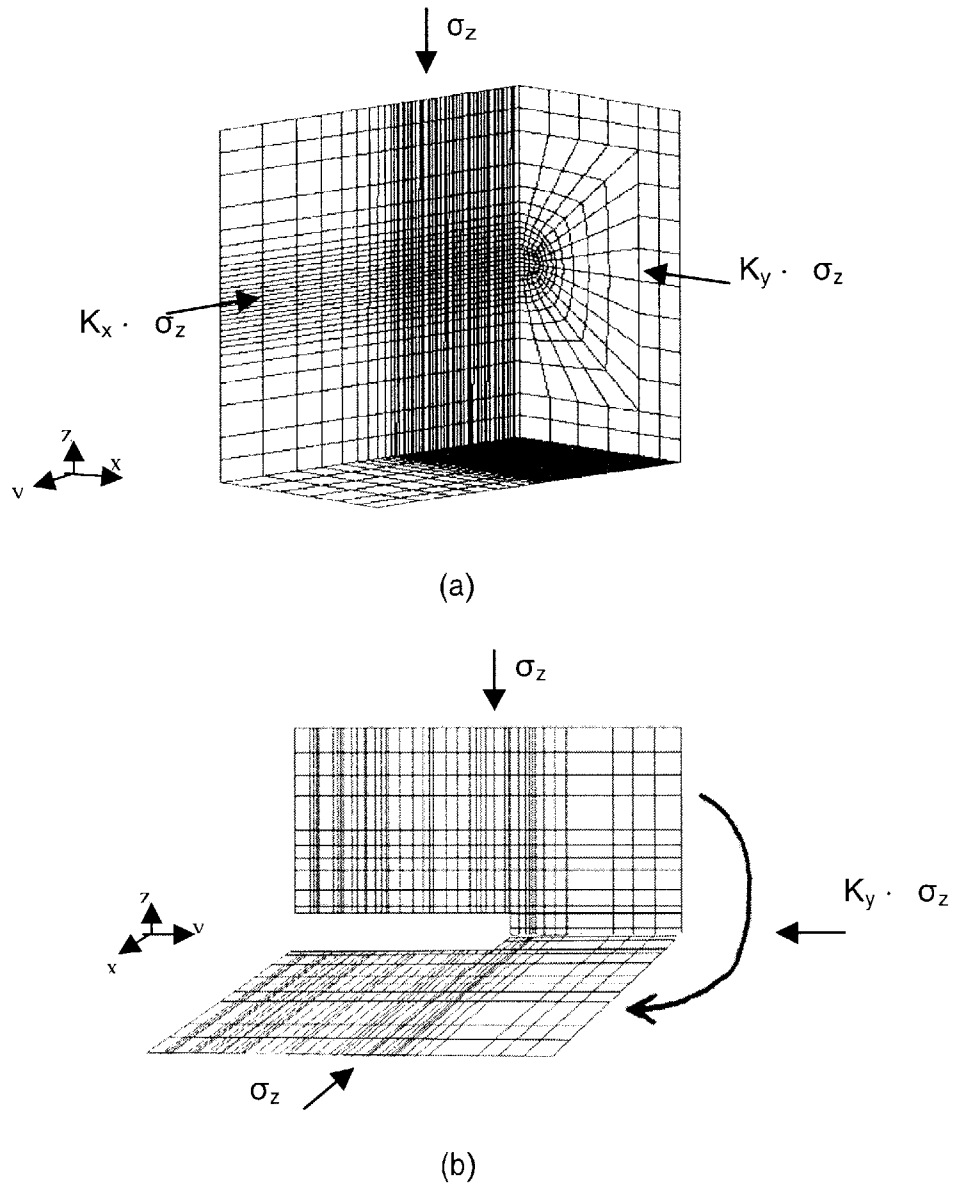


Figure 5.3 a) 3d model with different principal stresses in all three directions
b) axisymmetric 2d model with two principal stresses being equal

The influence of the coefficient of horizontal stresses has been analyzed in the past by Chen & Lin (1997). Initially they investigated the effect of in-situ stresses on the deformation behavior of the tunnels, excavated in multiple stages by three-dimensional numerical analysis. The purpose of their survey was to study the effect of tunnel driving direction with respect with the maximum horizontal stress direction.

From the results of their analysis presented in figure 5.4, we can see the variation of the tangential stress and the tunnel deformation with different values of coefficients K_x and K_y (figure 5.5). The tangential stresses and the deformations were calculated at the crown and at the level of the springline along the tunnel axis.

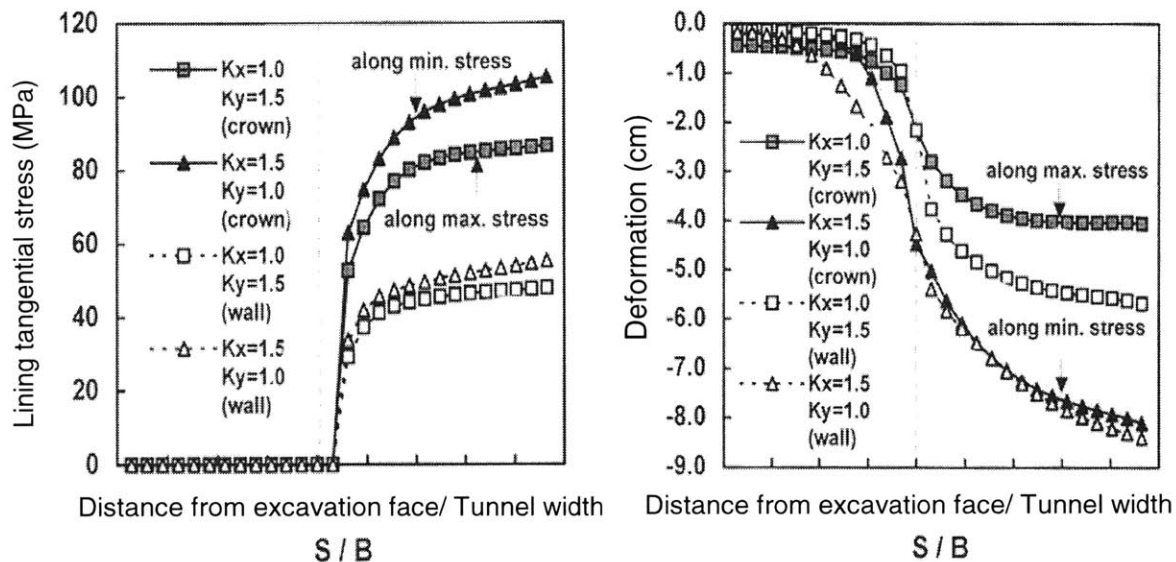


Figure 5.4 Effect of in-situ stresses on tunnel deformation and tangential stresses on a tunnel lining (Chen & Lin 1997)

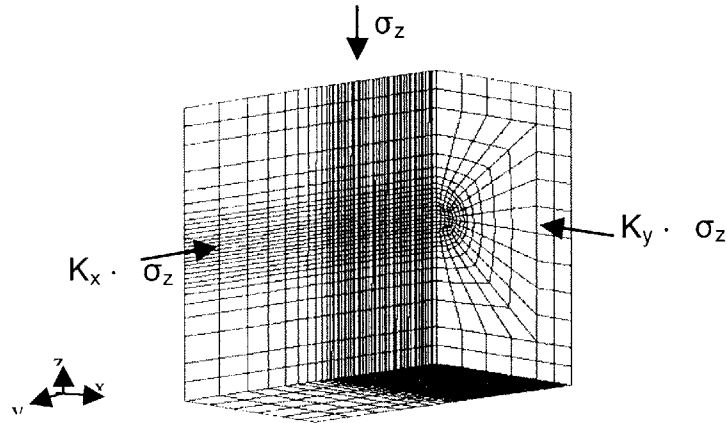


Figure 5.5 Coefficients of horizontal stresses used in the analysis

There are certain assumptions that can be made during the simulation of a tunnel excavation, such as the homogeneity of the surrounding mass and the isotropy of the stress field. These assumptions allow one to use simpler (non 3-d) simulations with acceptable accuracy of the results. Typical two-dimensional models are the axis-symmetric and the plane strain model. Although a 2d model cannot consider the effect of the tunnel advance on the real stress redistribution around the face, it can capture satisfactorily the deformations ahead of the tunnel face.

An axisymmetric model is restricted to an isotropic, radially homogeneous and continuous ground, and cylindrical tunnels. The ground properties as well as the geometry of the tunnel cannot vary with the angle of rotation of the tunnel axis but can vary along the tunnel axis.

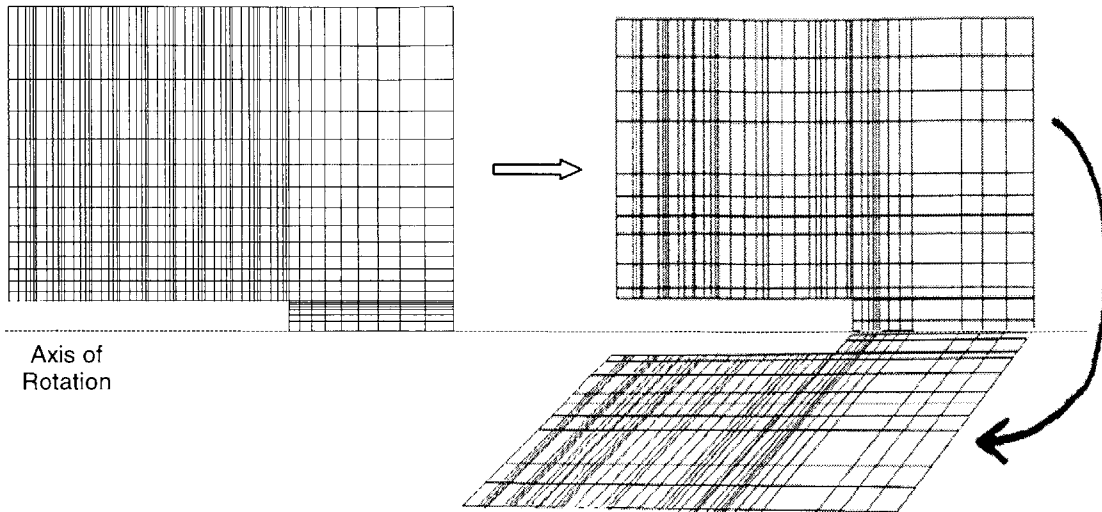


Figure 5.6 Axis Symmetric model with rotation to simulate a 3d problem

In the plane strain model a cross section of the tunnel with an infinite length is examined. The behavior of the tunnel and of the surrounding area are considered constant along the tunnel axis. The main advantage of this model is the simplicity and low cost compared to three-dimensional finite element analyses. It can be used in cases where the ground conditions do not change along the tunnel. The plane strain model is widely used for the analysis of stresses during the simulation of a tunnel excavation. This model cannot take into account the effect of the excavation process but can give enough input for the tunnel design.

Some of the limitations of the two 2d models can be overcome by combining them. This will be done, to some extent in the following chapters where results from the axisymmetric model will be used in the plane strain model. As will be shown, during the advance of the face of the tunnel, the axisymmetric model can show the deformation of the ground in front of the face before any means of support is installed. This input can be used in the plane strain model, for the analysis of different sections of the tunnel.

In conclusion, the 3d model can:

- Represent the actual initial stresses around the opening with different coefficients K_x and K_y (figure 5.3)
- Model the three-dimensional character of the stress redistribution due to the excavation advance
- Produce results in three dimensions
- Model the real ground conditions such as anisotropy in the material behavior and permeability
- Exactly reproduce an excavation process

By definition the two-dimensional models do not have the same capabilities as the three-dimensional models. However, with the combination of two-dimensional models, one can obtain results that approach reasonably moderate cases.

Chapter 6

Two Dimensional Modeling of a Tunnel Excavation

6.1 Introduction

Normally the excavation of a tunnel and the subsequent placing of the support are performed in stages. In most cases though, the design of the support after the excavation, ignores the effect of excavation.

The performance of a tunnel is greatly influenced by the excavation and support procedure, as well as by the initial and long term ground behavior. The proper consideration and the better understanding of these effects on support design and installation, should lead to more economic and efficient tunnel construction.

In this analysis a two-dimensional finite element model has been used in order to study the influence of the rate of advance of the face of excavation and time of support application on the behavior of the tunnel. This analysis continues by examining the effect of consolidation during excavation and placement of the liner.

As discussed earlier, tunnel excavation is actually a three-dimensional problem but it can be usually analyzed by a two-dimensional model. The basic idea behind all 2-d models for simulating tunnel excavation is to capture the deformation which occurs ahead of the tunnel face by some means without performing a 3-d analysis. This is especially important when the design of the temporary lining is of concern. A number of approaches have been proposed from design charts developed from 3-d analyses (Kielbassa & Duddeck 1991).

Although the numerical technique employed in this study is not new, the results presented show the importance of the effect of consolidation on the stresses on the lining, during a staged excavation of a tunnel.

6.2 Problem Description

In this first part of the analyses, an axisymmetric model is used for the elastic analysis of a staged tunnel excavation. The excavation is modeled in 10 steps of 1m each with application of a concrete liner simultaneously with the excavation at different distances from the face.

Three different scenarios of excavation are examined, each in both dry and wet conditions. In each scenario the lining is placed 1m, 2m and 3m behind the excavation face, leaving an unsupported length $l_u=1\text{m}$, $l_u=2\text{m}$ and $l_u=3\text{m}$ respectively. An example of the three scenarios of excavation is shown in the figure below (Figure 6.1). At the beginning of the excavation when the liner has not been placed yet, the first section of the ground is excavated. In subsequent steps, 1m of liner per step is placed, leaving an unsupported tunnel length of $l_u=1$, $l_u=2\text{m}$ and $l_u=3\text{m}$ depending on the scenario.

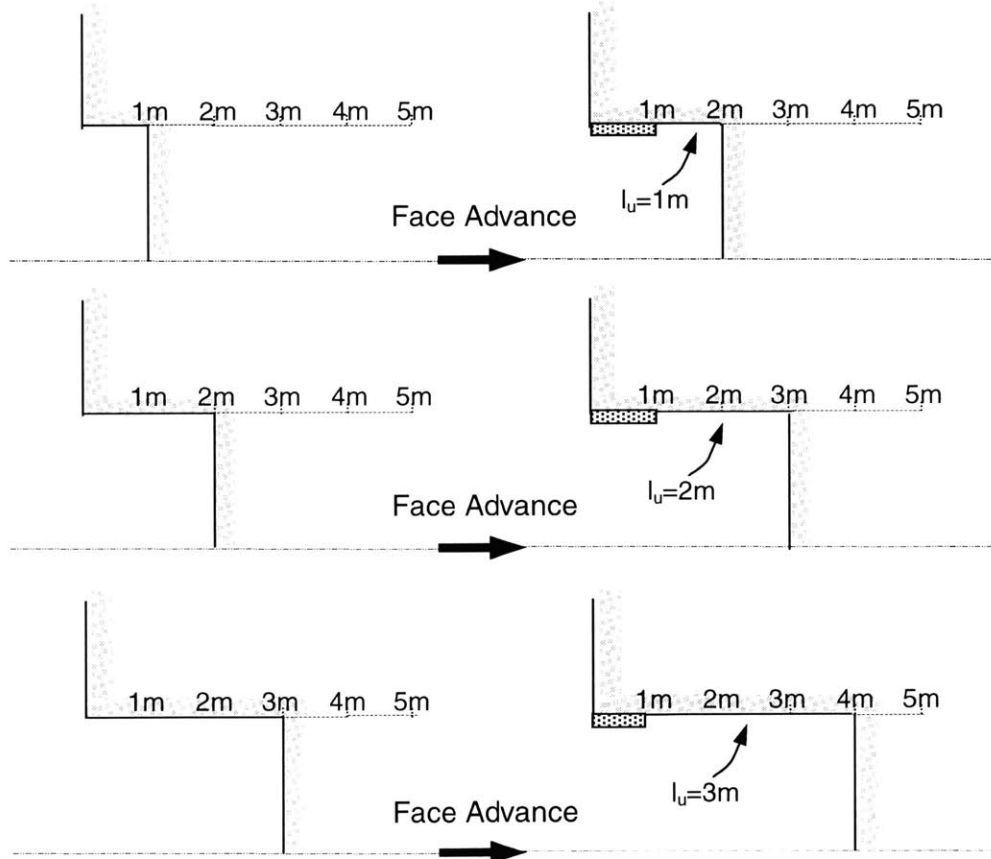


Figure 6.1 Axisymmetric model of a full advance excavation with three different unsupported lengths examined

6.2.1 Ground Behavior

In this investigation the ground was assumed to be homogeneous and linear elastic. The stiffness or deformation modulus was considered constant in the entire model, with no change close to the face of the excavation. Obviously, these assumptions simplify the behavior of the groundmass.

Ground Properties

$E=150000 \text{ KPa}$

$\nu=0.3$

Permeability: 10^{-9} m/sec

$\gamma=20 \text{ KN/m}^3$

6.2.2 Tunnel Geometry

The tunnel is circular and it is supported with the placement of a concrete liner, which is installed in stages as the excavation advances. It has a radius $\alpha=4.5$, which remains constant along the tunnel axis. The liner placed at the tunnel periphery is simulated by concrete elements with a thickness of $t=0.5\text{m}$ (In the next chapter in which the three-dimensional model is used, the simulation of the liner is performed with finite shell elements).

Tunnel Properties

Tunnel Depth: 100m

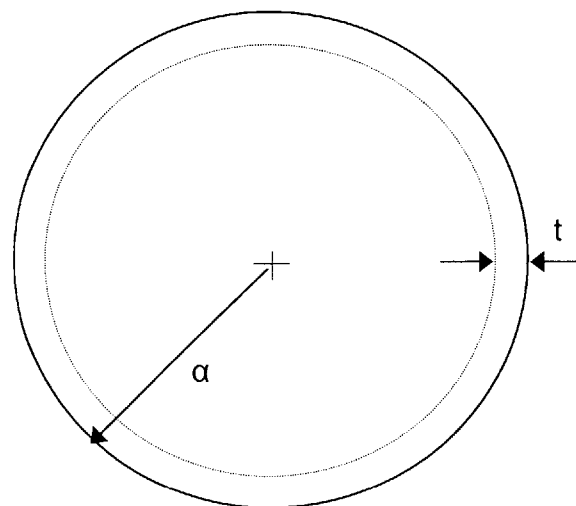
Tunnel radius: $\alpha=4.5\text{m}$

$E_c=25000000 \text{ KPa}$

$\nu_c=0.25$

$\gamma=25 \text{ KN/m}^3$

Thickness $t=0.5\text{m}$



6.2.3 Staged Excavation

During the excavation of a tunnel, the original stress field in the ground changes considerably before the first support system installed, affecting the stabilization of the opening.

Depending on the stress release around the tunnel and at the face of excavation, a small portion of the primary stresses is acting on the lining. This effect can also be examined when using a two-dimensional model, but without the ability to control the horizontal stresses perpendicularly to the tunnel axis. This limitation can be overcome with a three dimensional model (examined in chapter 7).

During the excavation of the tunnel the ground responds to each step of excavation. Stresses normal to the surface of the tunnel are released followed by inward displacements (assuming homogeneous surrounding ground for each step of excavation). These stresses and displacements increase, to reach finally a maximum value at some distance from the face.

The excavation of the tunnel is performed in several steps in order to approach reality. In each step, the face of the excavation advances 1m. In the following step the excavation proceeds further 1m while at the same time the liner is placed behind (figure 6.2).

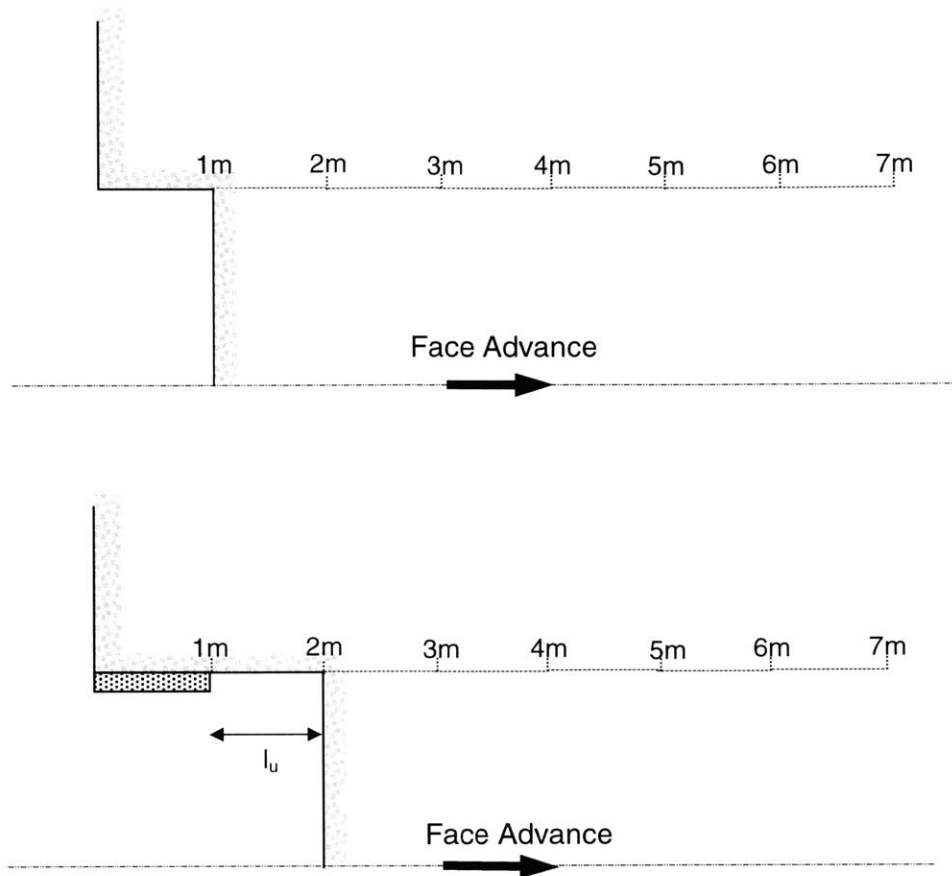


Figure 6.2 Simulation of the excavation

6.2.4 Consolidation during Excavation

Part of the analysis refers to the excavation of the tunnel in a fully saturated medium. The effect of consolidation is taken into account during the staged excavation.

As mentioned above, the excavation of the tunnel is performed in 10 steps. Each step represents 1m of full-face advance. During the excavation of the tunnel, the surrounding ground is allowed to consolidate. The permeability of the ground is $k=10^{-9}$ m/sec, while the liner that is placed after excavation is considered impermeable.

In the first step of the simulation the first 1m is excavated. At this point this section of the tunnel remains unsupported, and the mass is allowed to consolidate for 1 day. In the next step the excavation advances one more meter, while at the same time the liner is placed in the section of the tunnel that was excavated in the first step. This time between two consecutive steps is constant for the whole excavation and equal to 1 day. Hence, after the end of the excavation that is simulated (10m of excavation), the total time of consolidation will be 10days.

6.5 Numerical Simulation of the Excavation

6.5.1 Numerical Code

Abaqus is a powerful general-purpose finite element package which has been designed for the analysis of complex nonlinear problems. At first sight, it may therefore seem inappropriate for beginners in finite element analysis. However Abaqus is relatively easy to use and while complex problems require complex input files, simple problems require only simple input data.

Essentially, the finite element analysis is a method of solving partial differential equations and so Abaqus can be used to solve many types of field problem. However the program was really written for modeling mechanical systems and so it is most suitable for problems in which the field variable is displacement, temperature, etc. It can also be applied for various geotechnical applications giving solutions to many complex problems.

6.5.2 Building the Model

In order to investigate the effect of consolidation during a tunnel excavation, an axisymmetric FEM model was initially constructed. The following figure 6.3 depicts the element pattern around a flat face of a tunnel, circular in cross section. The FEM model used in the present analyses is a body of revolution whose axis is identical with the axis of tunnel denoted by the x-axis.

The examined region is represented by the meshed rectangle (figure 6.3). Along the limits of the model the normal components of displacement are zero. In the case of a fully saturated medium, drainage is allowed in all the directions.

The type of elements that was used in the model was CAX8P, pore pressure-axisymmetric elements with 8 nodes.

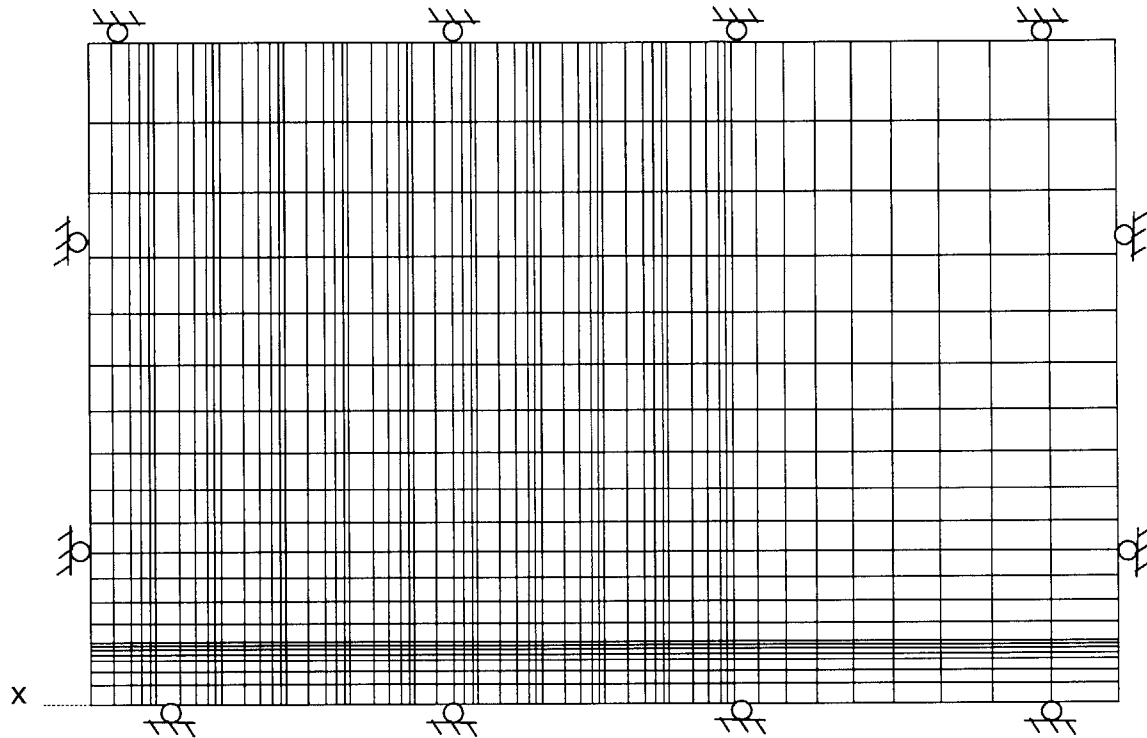


Figure 6.3 Axisymmetric model used in the analysis

6.5.2.1 Simulation Steps

The steps described earlier in the chapter, represent the real conditions during the excavation and support of a tunnel. The main goal when applying the numerical methods for the analysis is to simulate the problem in a realistic way.

Real conditions are simulated by using several steps in the input file. These steps include the definition of the initial stress conditions, of the boundary constraints during the excavation, and finally of the excavation sequence.

The steps mentioned below refer to the simulation of a tunnel in dry conditions where no consolidation takes place. In a saturated ground where

consolidation is considered, the steps include the consolidation procedure. A schematic diagram of the excavation sequence and a short description of the steps followed are shown in Appendix II.

Initial Stress Field

The initialization of stresses is performed before any of the steps that simulate the excavation. In Abaqus the initialization of stresses is considered a model command, so it is not included in any step functions.

The sources of the initial stresses are the weight of submerged soil, according to γ of the ground. One of the main limitations of the two-dimensional axisymmetric model is that with the rotation of the model around the tunnel axis, it is not possible to define a coefficient of lateral stresses perpendicular to the tunnel axis. In any case the horizontal stress will be equal to the vertical stress.

In the model, the vertical stress is kept constant at 2000 MPa (the tunnel is located at 100m depth). For reasons mentioned above, the horizontal stress perpendicular to the tunnel axis has the same value as the vertical stress. A different coefficient of horizontal stresses $K_0=0.5$ can be assigned along the tunnel axis (Figure 6.4).

(The effect of the limitation in the definition of different coefficients K_0 in the model, will be examined in the next chapter where the same tunnel excavation will be simulated in three-dimensions).

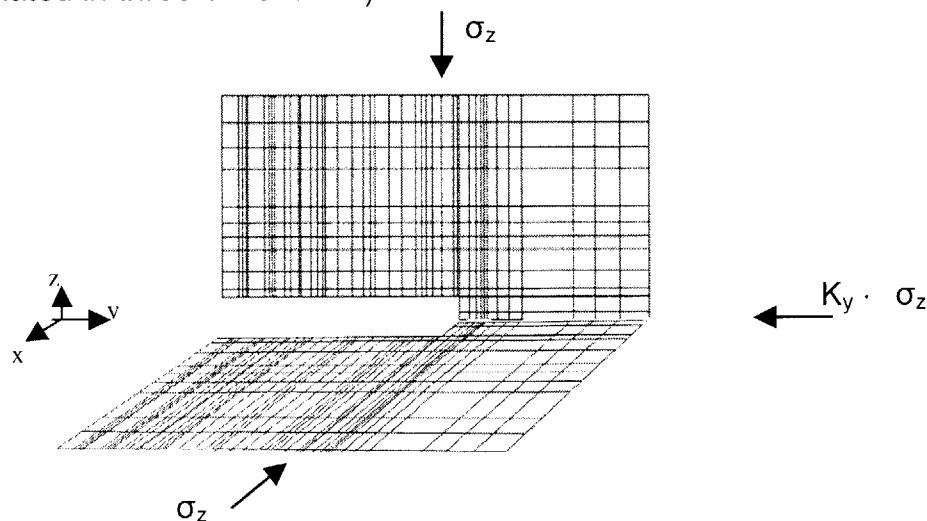


Figure 6.4 Definition of initial stress field

Generation of the concrete elements - Step 1 (dry case) – Step 0 (sat. case)

Due to a limitation of Abaqus in assigning two different material properties for the same elements and in the same model, a new element set with the properties of concrete had to be created in this step.

Immediately after its generation, the new set is deactivated in order to avoid potential conflict with the existing elements that simulate the ground.

Start of Excavation Sequence – Step 2 (dry case) – Step 1+Step2 (satur. case)

In this step the first section of the tunnel is excavated. The liner still remains inactive. Depending on the excavation scenario, the section of the tunnel excavated is 1m, 2m or 3m, creating an initial unsupported section of equivalent length.

In the case of the excavation in saturated ground, the excavation of the first section of ground, is performed in two steps, since this the initialization of pore pressures is performed at the same time.

(The simulation of consolidation is explained later in paragraph 6.5.3)

Excavation and placement of the liner (dry case)

Steps 3 - 12 ($l_u=1m$), 3 -11($l_u=2m$), 3 -10 ($l_u=3m$).

These steps simulate the excavation advance. For the three scenarios the excavation advances by 1m while in the same step the liner is placed in the section that was excavated in the previous step. An example of the initial excavation phase was shown in figure 6.1. In the model the placement of the liner is simulated by activating the concrete elements that were created in step 1. This procedure, i.e. step 3, is repeated until the face has reached the desired end point (excavation of 10m).

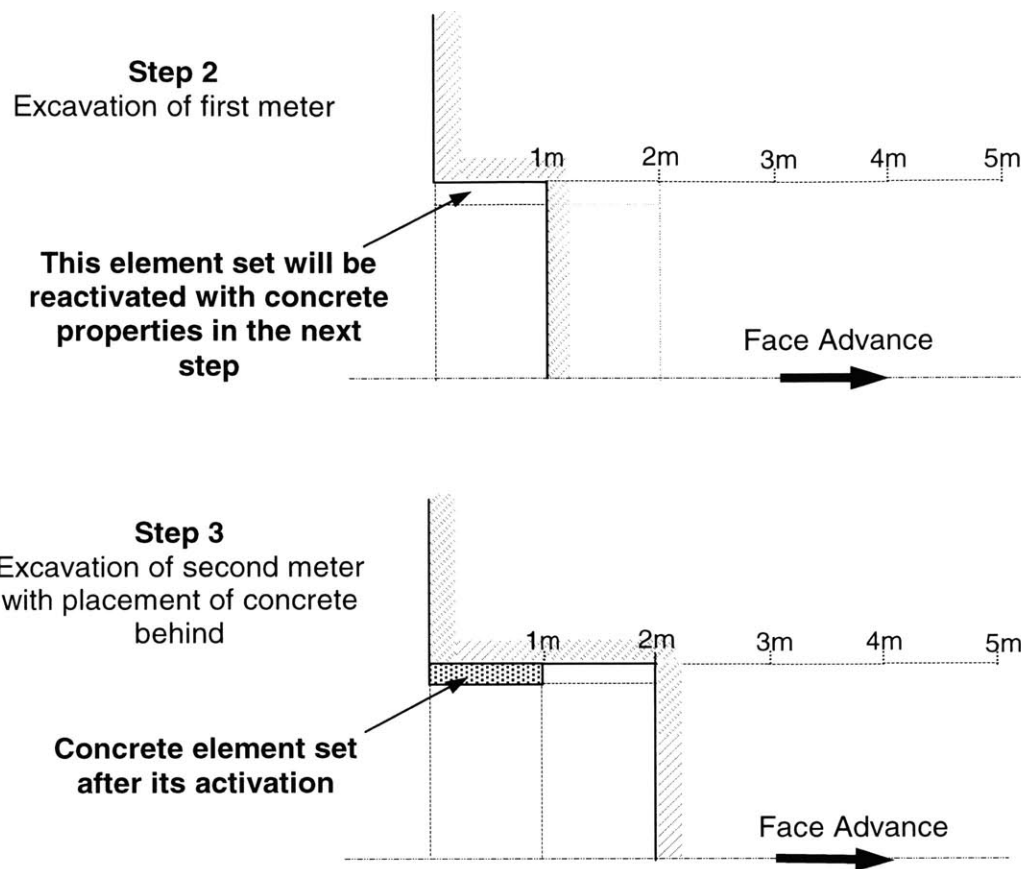


Figure 6.5 Excavation sequence during the analysis

6.5.3 Time Stepping during Consolidation

Consolidation is run in two steps. The first step is a single increment analysis with an initial time step, with no drainage allowed across the excavated surfaces of the roof and the face. This establishes the initial solution: uniform pore pressure equal to the load throughout the body, with no stress carried by the skeleton (zero effective stress). This initialization is performed once and for the whole simulation.

In the second step of this procedure the actual consolidation is then performed using automatic time stepping. For this reason the Step 1 and Step 2 in the case of consolidation is equivalent to the Step 2 in the case of dry

ground. This procedure of consolidation is performed for all the following steps of the simulation.

The accuracy of the time integration for the second procedure, during which drainage is occurring, is controlled by the parameter UTOL. This parameter specifies the allowable pore pressure change per time step. Even in a linear problem UTOL controls the accuracy of the solution, because the time integration operator is not exact (the backward difference rule is used). In this case UTOL is chosen according the load applied or the initial stress field. Since this value is relatively large it should only give moderate accuracy; this is considered to be adequate for the purposes of the example.

An important issue in such consolidation problems is the choice of initial time step. As the governing equations are parabolic, the initial solution, (immediately after the sudden change in load) is a local, “skin effect” solution. With a finite element mesh of reasonable size for modeling the solution at later time (when the change in pore pressure have diffused into the bulk of the body ground), the initial solution will be modeled poorly. With smaller initial time steps the difficulty becomes more pronounced. As in any transient problem, the spatial element size and the time step are related to the extent that time steps smaller than a certain size give no useful information. This coupling of the spatial and temporal approximations is always most obvious at the start of diffusion problems, immediately after prescribed changes in the boundary values. For this particular case the issue has been discussed in detail by Vermeer and Verruijt (1981), who suggest the simple criterion.

$$\Delta t \geq \frac{\gamma_w}{6Ek} (\Delta h)^2$$

where,

Δh is the characteristic element size near the disturbance (that is near the draining tunnel perimeter in our case), E is the elastic modulus of the soil skeleton, k is the soil permeability, and γ_w is the specific weight of the permeating fluid. Based on the solution of the equation an initial time step Δt is used.

6.6 Analysis of Results

6.6.1 Displacement at the Liner

Part of the analysis is to examine the effect of the excavation process on the displacement of the lining. After 10m of excavation, the displacement at the interface of the lining and the ground is examined. Recall that different scenarios were selected with unsupported tunnel length ranging from $l_u=1\text{m}$ to 3m. The reference points for all the graphs that are going to be presented are shown in figure 6.6.

The steps performed in both the dry and fully saturated cases, are shown and explained in Appendix II. In these two cases the whole analysis is performed in 10 steps (when $l_u=3\text{m}$) to 12 steps (when $l_u=1\text{m}$). In the analysis and interpretation of the results, every step is going to be referred by the day in which it is performed.

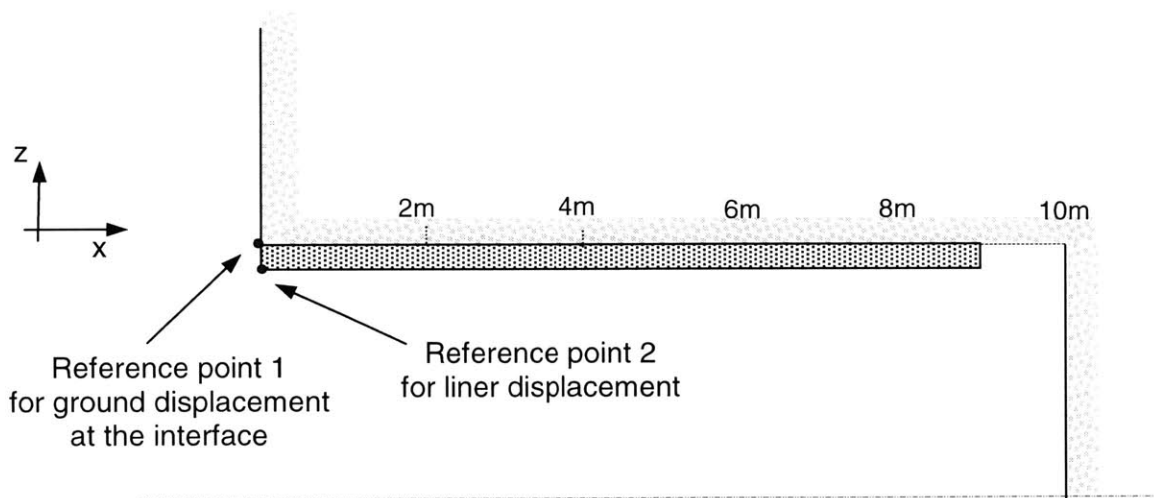


Figure 6.6 Location of the reference point for the calculation of the displacement of the lining

In the following graphs of figures 6.7 and 6.8, the displacements of the liner at the reference point 2, are shown. In the case of the dry ground, the liner is activated during the second day. The first displacement of the liner is recorded at the end of the second day, at the beginning of which it was activated in the model.

In the case of the saturated ground, the displacement of the liner starts after its activation during the second day. During the first day, the ground was excavated and was allowed to consolidate for a day, until the excavation advanced one step and the liner was activated.

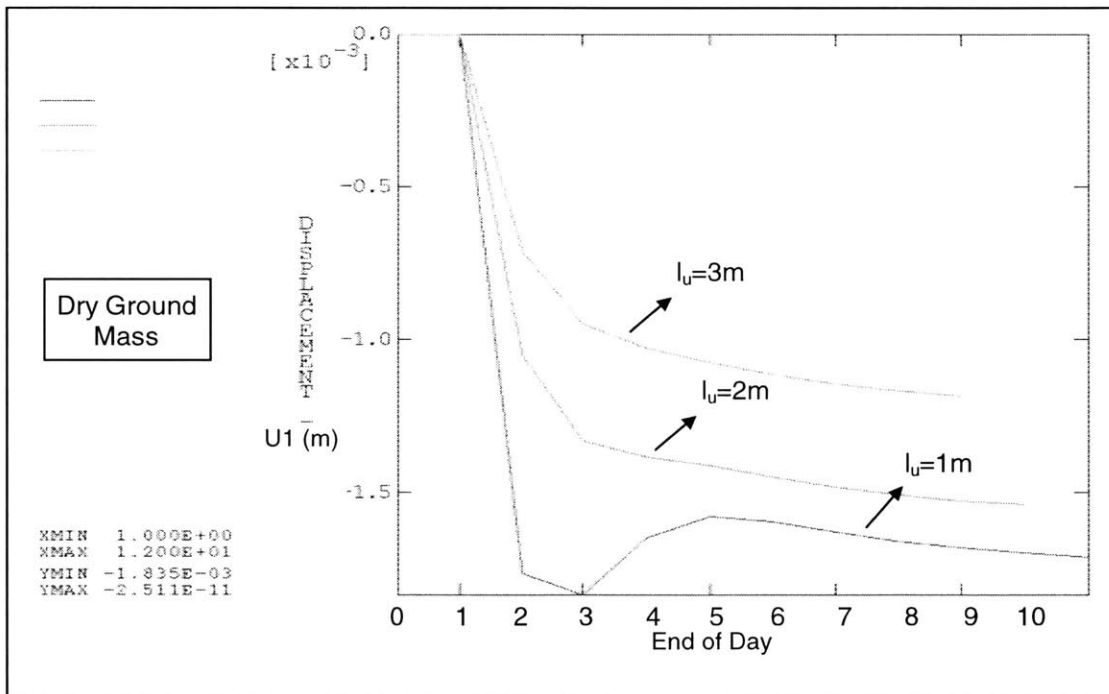


Figure 6.7 Displacement in z direction for reference point 2 in dry ground

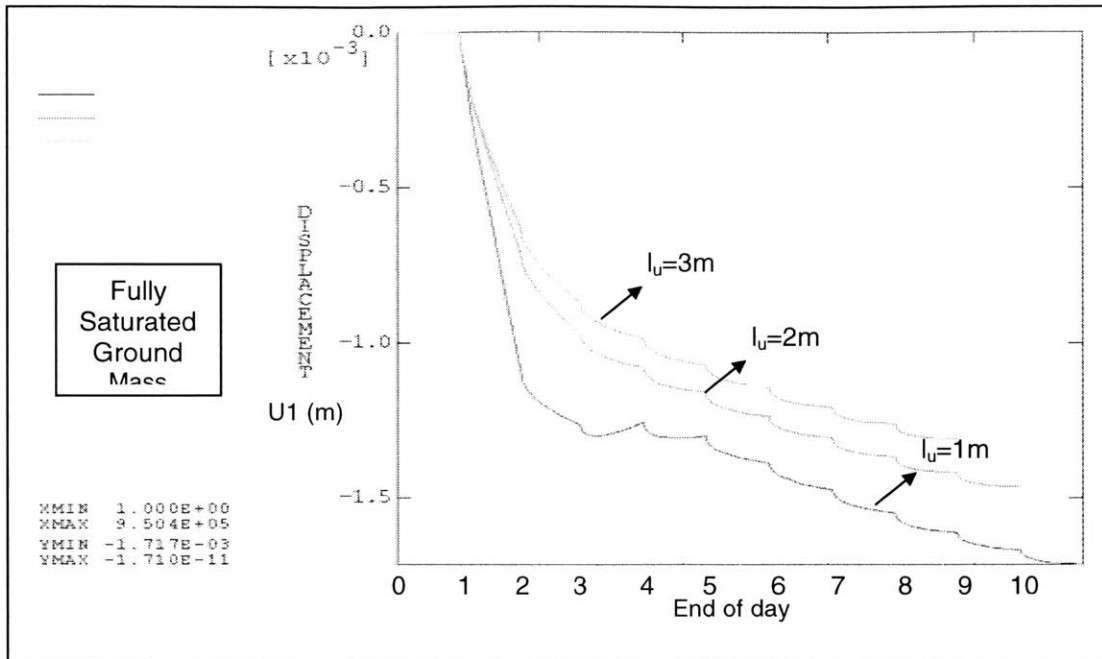


Figure 6.8 Displacement in z direction, for reference point 2 in fully saturated ground

Comparing the two cases, in dry and saturated ground (graph of figure 6.9), we can see that in the case of dry ground, most of the displacements are released early in the excavation process, (by the end of the day 5 or 6 when the excavation face has advanced 5m). With consolidation taken into account, the displacement is released more slowly.

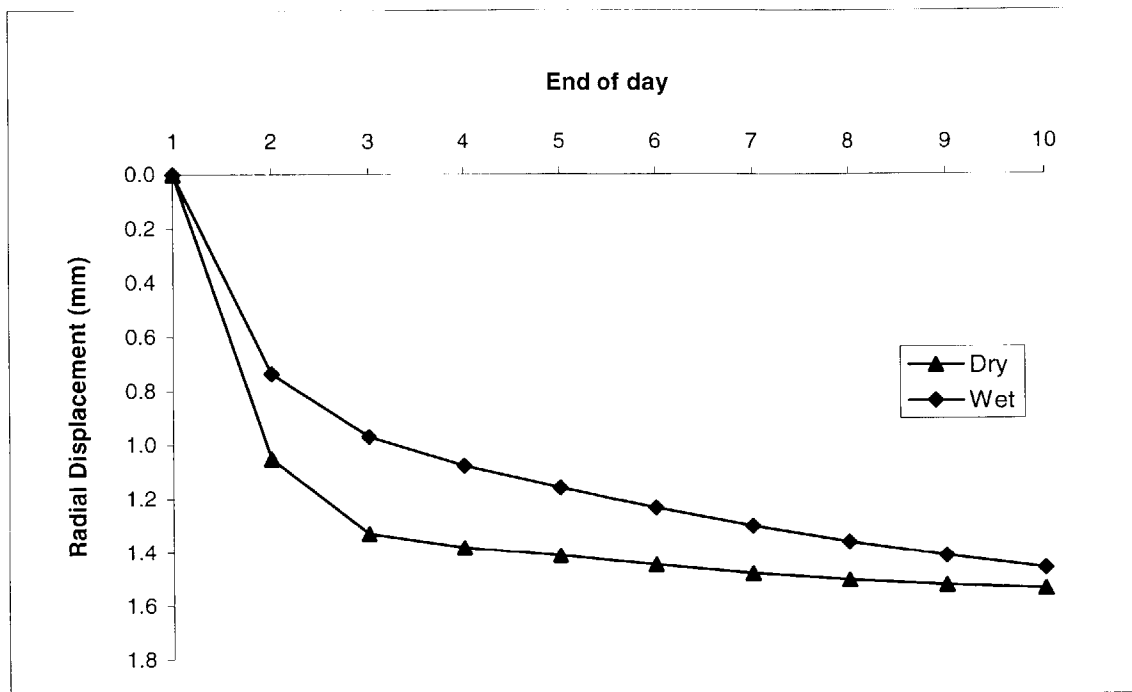


Figure 6.9 Displacement in z direction, for reference point 2 in dry and fully saturated ground ($l_u=2m$)

Some comments can also be mentioned for the effect of the unsupported length l_u in both dry and saturated ground. In figures 6.7 and 6.8 it was shown that the variation of l_u has an effect on the displacement of the liner. Greater unsupported length leads to smaller displacements of the liner, since in that case most of the displacement has been after excavation and before the placement of the liner.

This release of displacements can be shown in figures 6.10 and 6.11 where the displacement of the ground above the liner is shown. In both dry and saturated ground (figures 6.10 and 6.11 respectively), the displacement in the z direction increases with an increase of the unsupported length. Figure 6.12 shows this displacement in dry and saturated ground for two different values of the unsupported lengths.

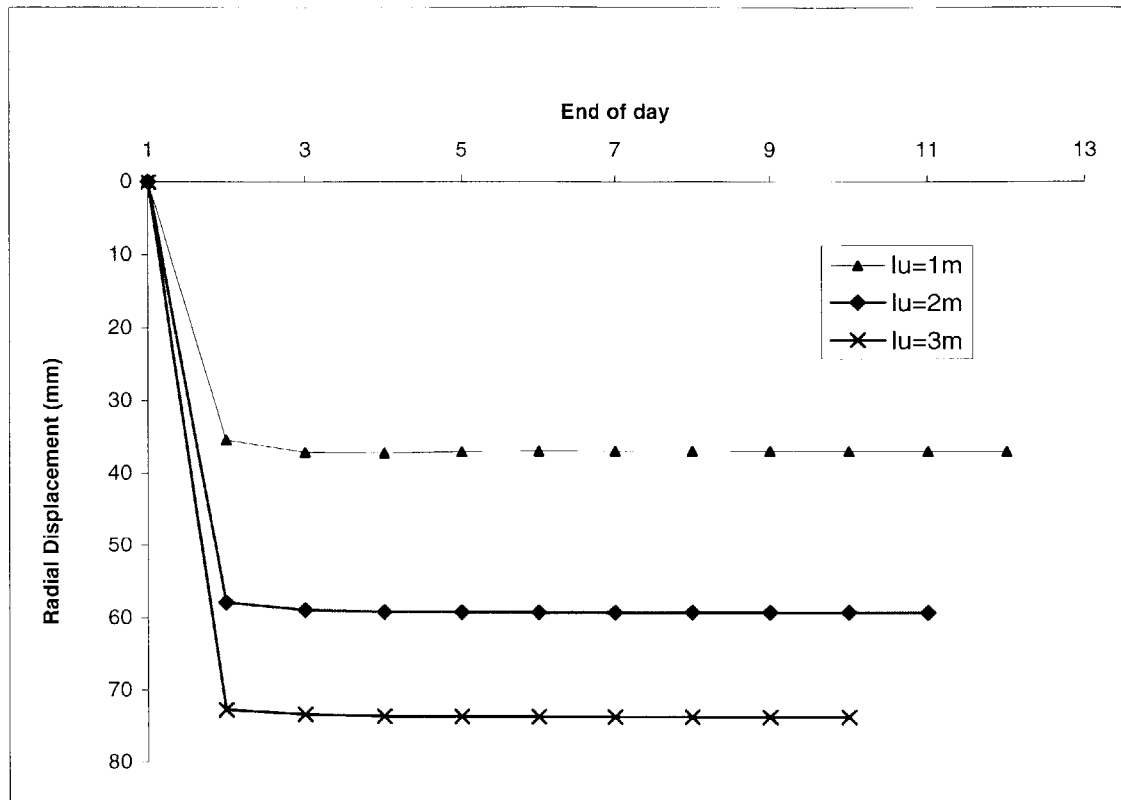


Figure 6.10 Displacement in z direction, for reference point 1 in dry ground

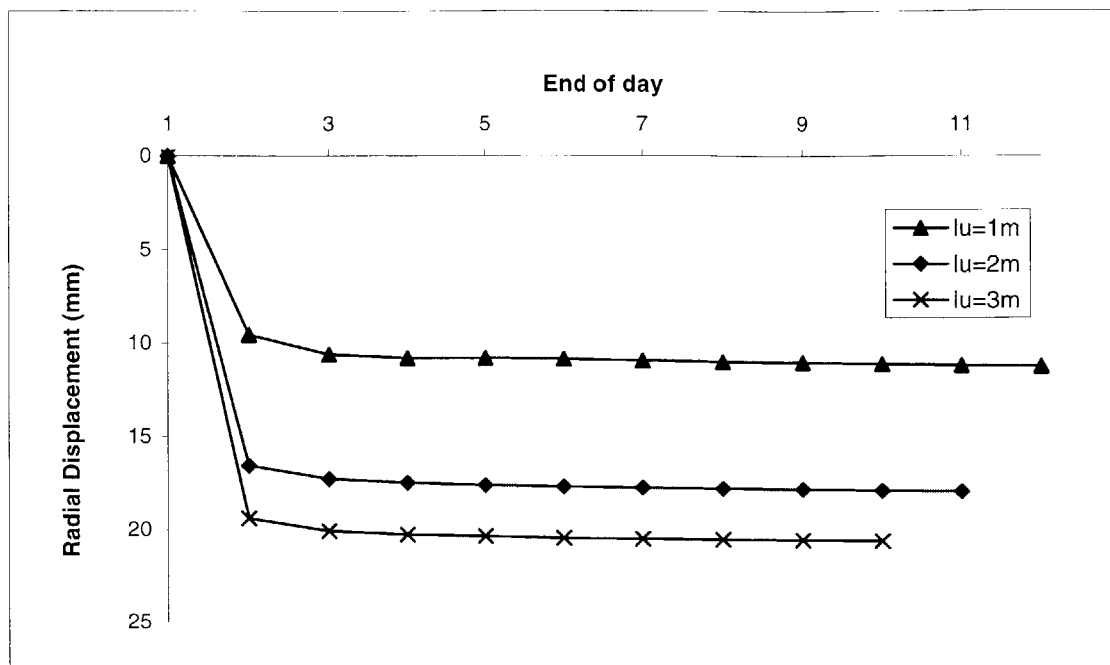


Figure 6.11 Displacement in z direction, for reference point 1 in fully saturated ground

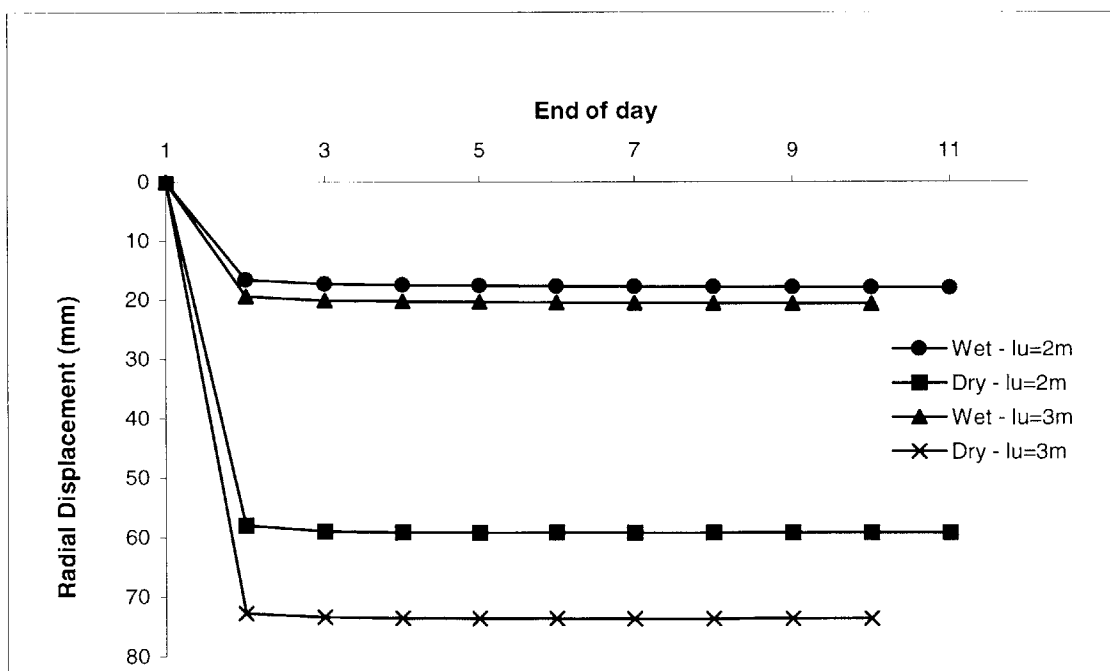


Figure 6.12 Displacement in z direction, for reference point 1 in dry and fully saturated ground

Comparison of Radial Stress on the liner for dry and fully saturated ground

One of the most important issues in this simulation was to examine the effect of consolidation on the stresses in the liner, with the advance of the tunnel excavation. The following figure 6.13 shows, the reference point for the calculation of the radial stress acting on the liner.

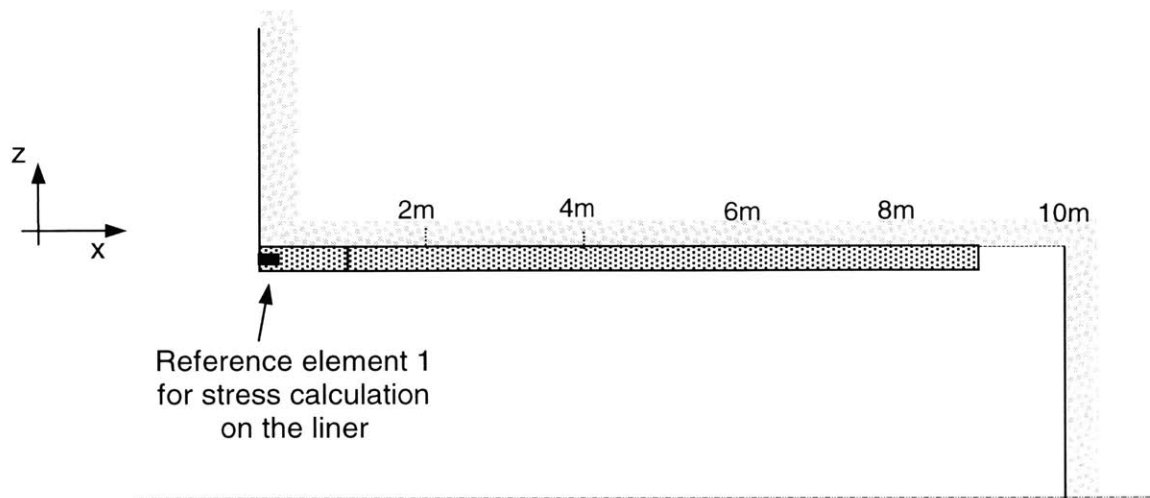


Figure 6.13 Location of the reference point for the calculation of the radial stress acting on the lining

The variation of the radial stress in the z direction for both dry and saturated ground is shown in figures 6.14 and 6.15.

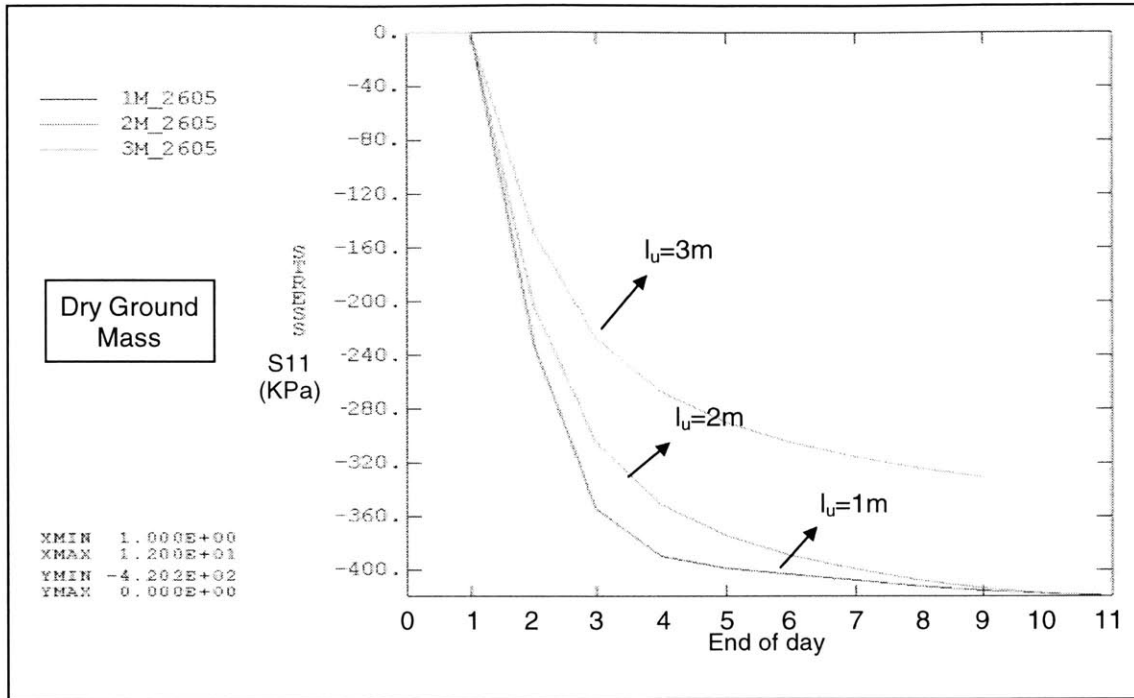


Figure 6.14 Radial Stress S_{11} in z direction in dry ground (reference element 1)

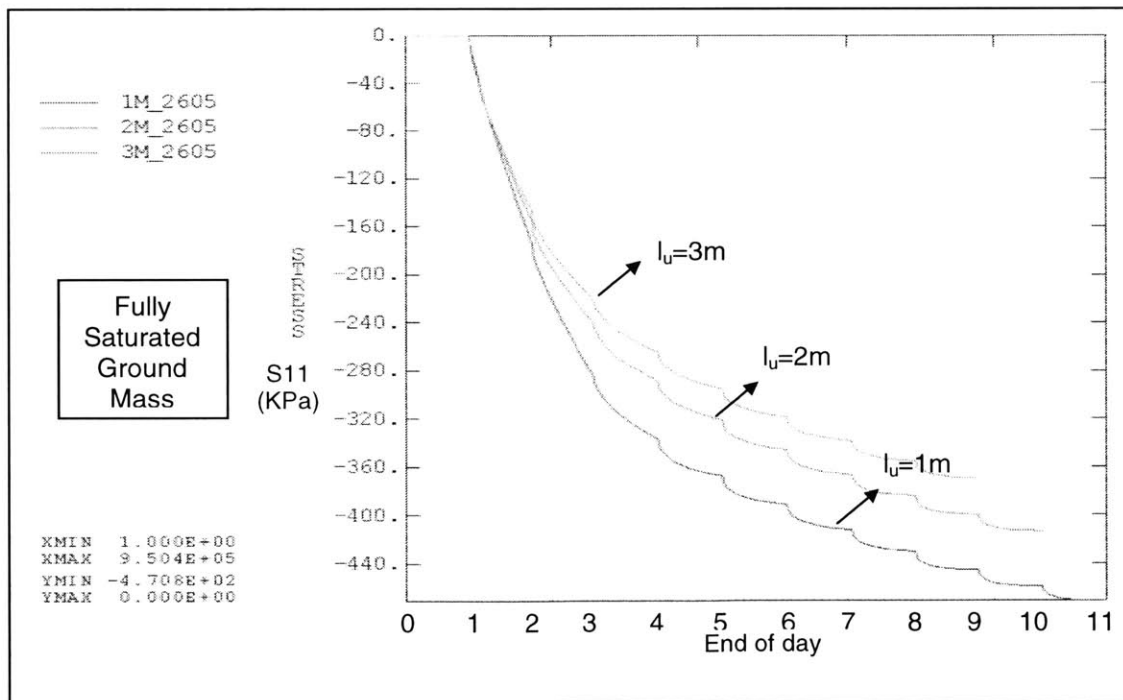


Figure 6.15 Radial Stress S_{11} in z direction, in fully saturated ground (reference element 1)

The variation of the unsupported length of the tunnel during excavation has an effect on the development of stresses in the lining. In both dry and saturated conditions, a greater unsupported length leads to smaller stresses acting on the lining. As shown earlier in the chapter, a high value of l_u , leads to a release of greater displacements before the excavation of the area.

Comparing the results of the dry and the saturated ground, an increase of the stresses is observed when the consolidation effect is taken into account (Figure 6.16). In each case the stress applied on the lining increases with the advance of the excavation face. In the case of dry ground and when the excavation face is at a distance of 5m from the reference element 1, the stress acting on the liner has reached almost 90% of its final value. With the consolidation effect, the stress on the lining increases throughout the considered excavation sequence and reaches a maximum which is 10-15% higher than the stresses that develop when the ground is dry.

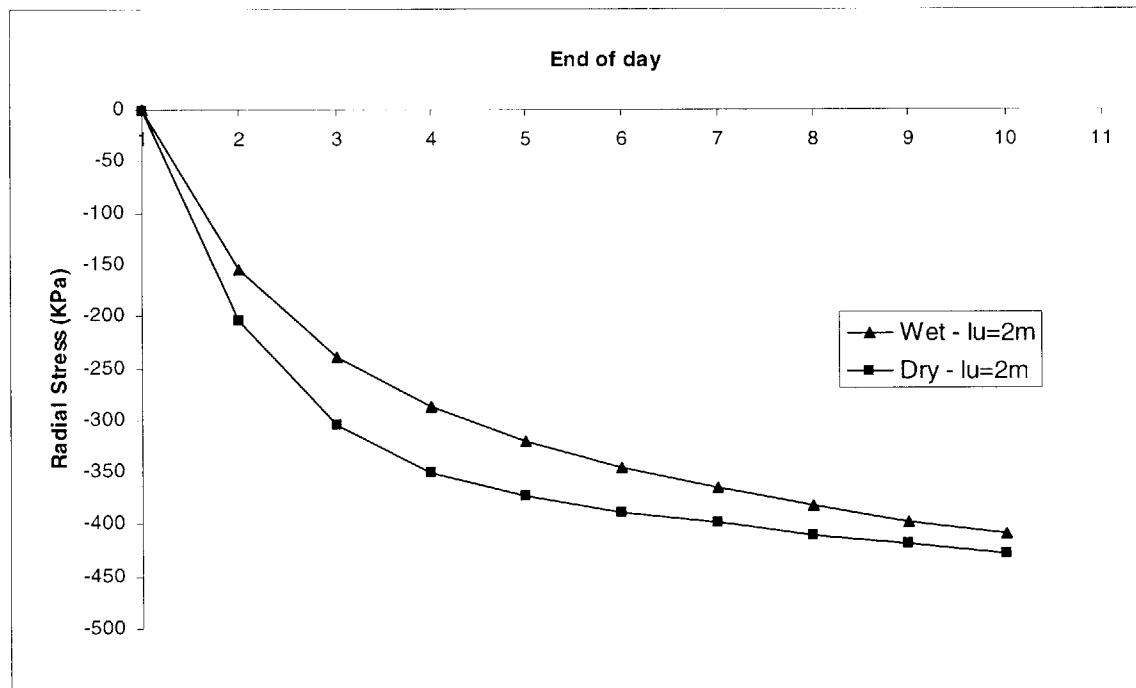


Figure 6.16 Comparison of radial stresses in z direction in dry and fully saturated ground, for $l_u=2m$ – (reference element 1)

Variation of pore pressures with time, above the liner

During the excavation of the tunnel in the saturated mass, the surrounding mass consolidates, affecting the stress release and the generation of displacements. The following figures present the dissipation of pore pressures with time, at different distances from the liner. Figure 6.17 depicts the reference points for the pore pressure calculation.

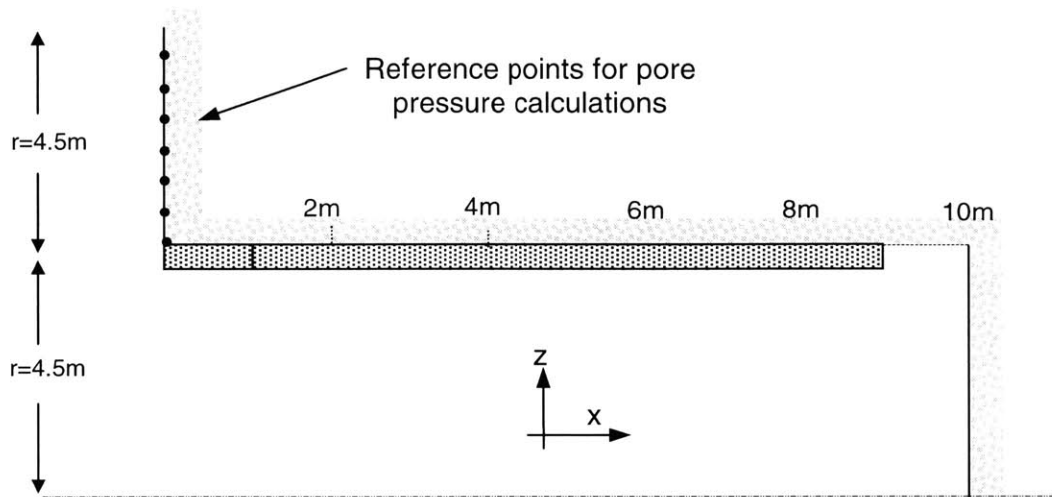


Figure 6.17 Location of the reference points for the calculation of the pore pressures above the lining

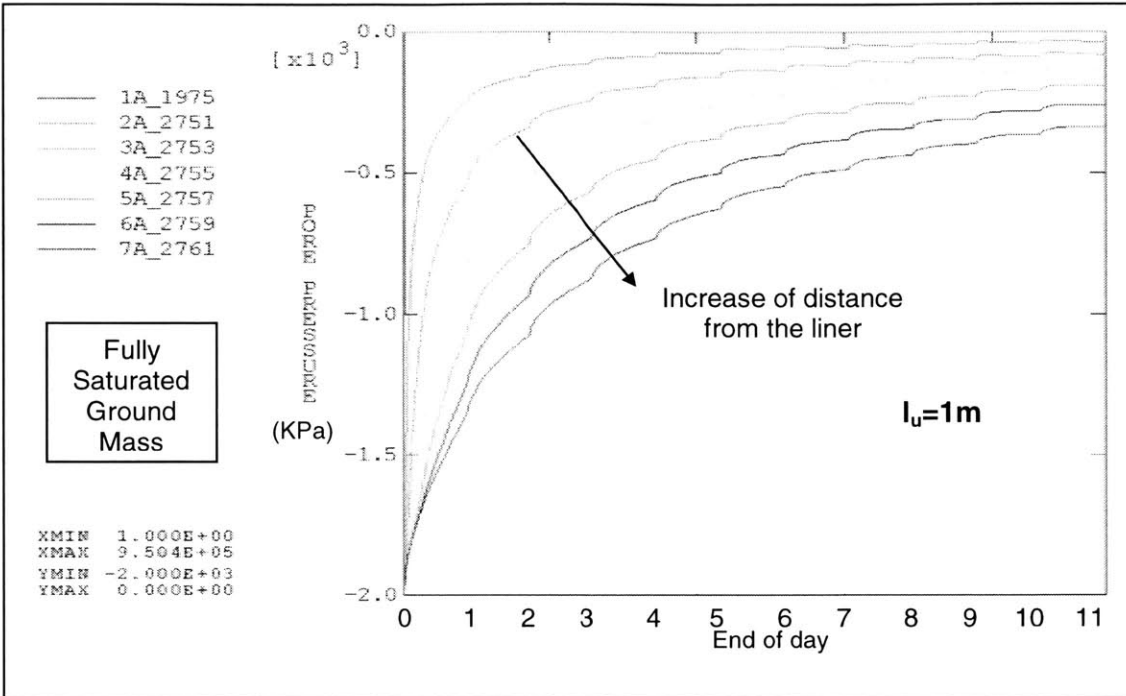


Figure 6.18 Dissipation of pore pressures with time, above the lining with unsupported tunnel length $l_u = 1\text{m}$

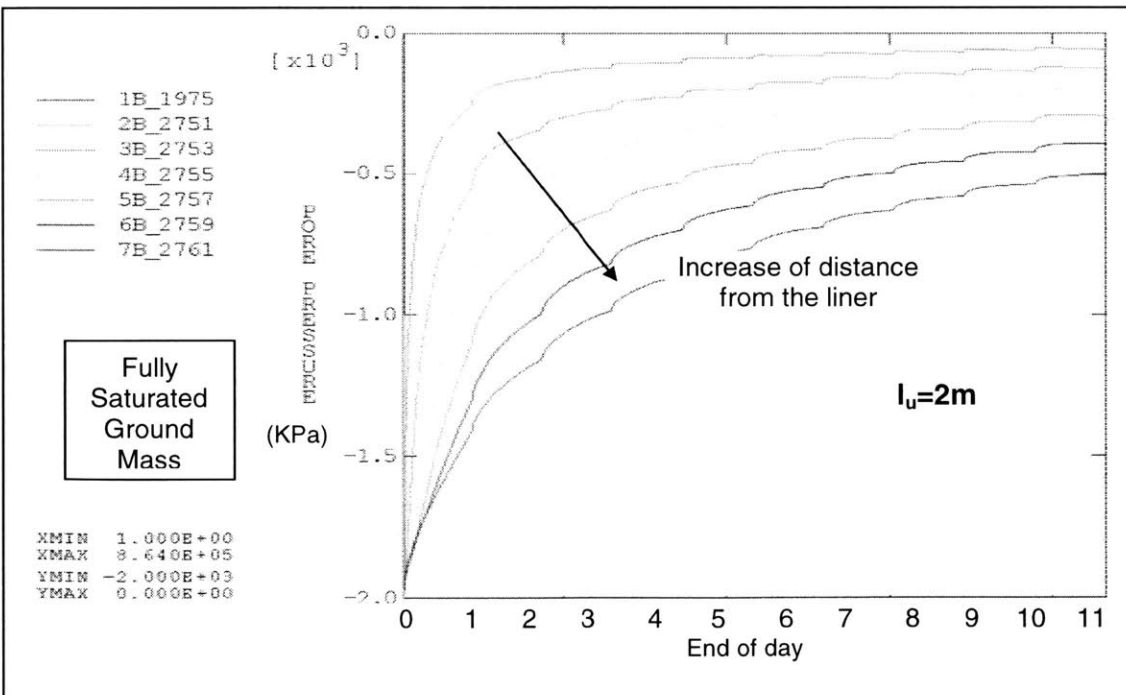


Figure 6.19 Dissipation of pore pressures with time, above the lining with unsupported tunnel length $l_u = 2\text{m}$

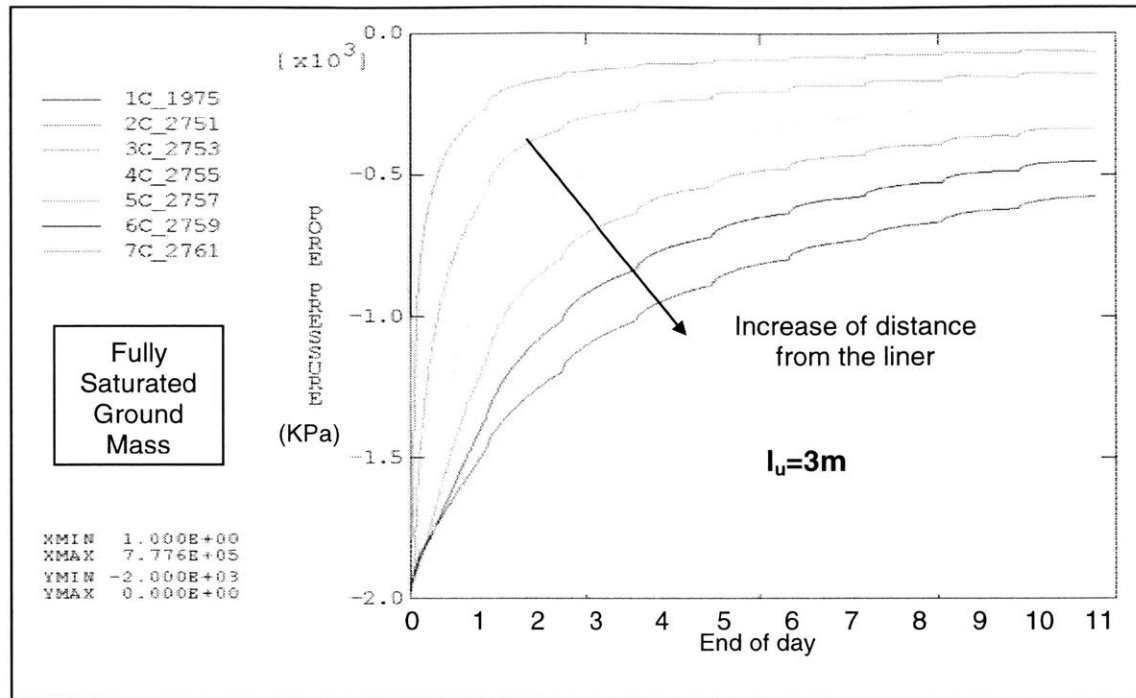


Figure 6.20 Dissipation of pore pressures with time, above the lining with unsupported tunnel length $l_u=3\text{m}$

After the initialization of stresses, and before the beginning of excavation, the pore pressure is 2000 KPa. When the excavation begins the pore pressures start dissipating. Figure 6.21 is a comparative graph for the dissipation of pore pressures at a point that is located 3.5 m above the lining. As shown earlier a greater unsupported length leads to smaller stresses in the liner. Pore pressure dissipation can be related to this stress development. With an increase of l_u the stresses are smaller leading to a slower pore pressure dissipation above the liner. Hence, when the unsupported length of the tunnel is smaller, water is forced out of the surrounding ground faster causing quicker pore pressure dissipation.

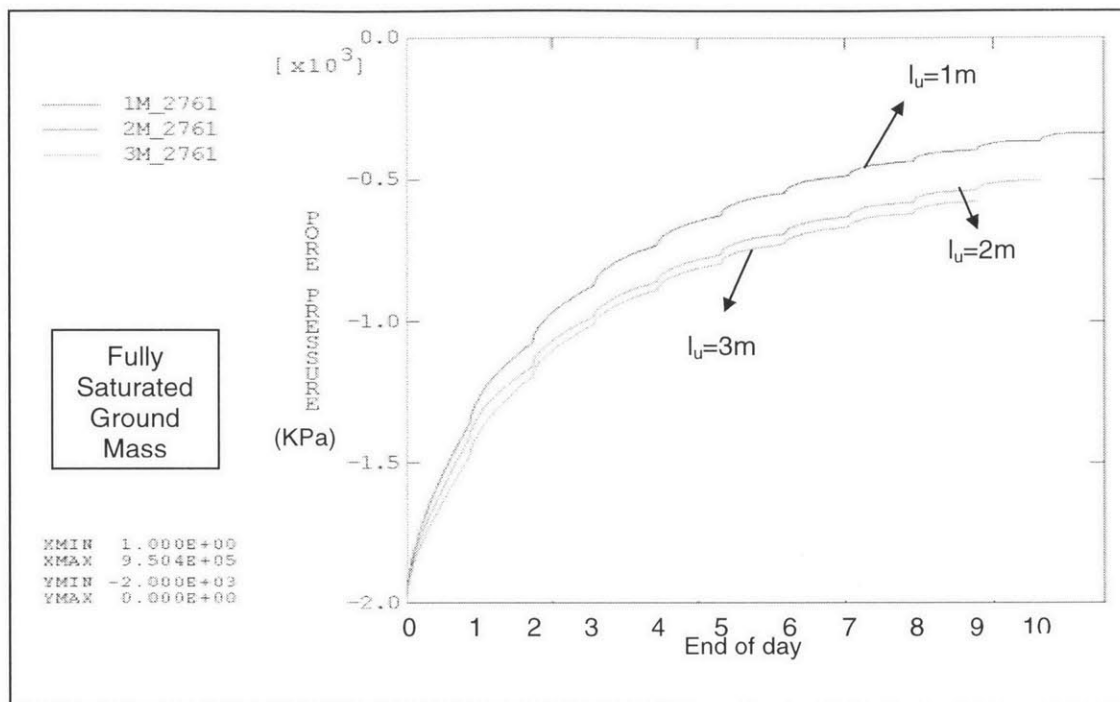


Figure 6.21 Dissipation of pore pressures with time, above the lining with variation of the unsupported tunnel length l_u

Chapter 7

Three Dimensional Modeling of a Tunnel Excavation

7.1 Introduction

The analysis performed in this chapter consists of two parts. The first part examines the effect of the variation of the initial stress field. The purpose is to show the importance of the relation between the vertical and the horizontal stresses, and how it affects the stress distribution during a staged tunnel excavation. A three dimensional model is used.

This variation of vertical and horizontal stresses was mentioned as one of the limitations of the axisymmetric model compared to the three-dimensional model. In the axisymmetric model, only the coefficient of lateral to vertical stresses along the tunnel axis can be controlled, which in most cases has less effect on the stress and displacement variation.

In the second part, the results of the 3d model are compared to the axisymmetric model, using the same tunnel and ground properties. This comparison will show the differences in the accuracy of the results obtained from a 2d and a 3d model.

7.2 Analysis Description

A three-dimensional model is used for the elastic analysis of a staged tunnel excavation in dry ground. The ground properties as well as the tunnel geometry are the same as those used in chapter 6.

Ground Properties

$E=150000$ KPa

$\nu=0.3$

Permeability: 10^{-9} m/sec

$\gamma=20$ KN/m³

Tunnel Properties

Tunnel Depth: 100m - Tunnel radius: $r=4.5$ m

$E_c=25000000$ KPa

$\nu_c=0.25$, $\gamma=25$ KN/m³

Thickness $t=0.5$ m

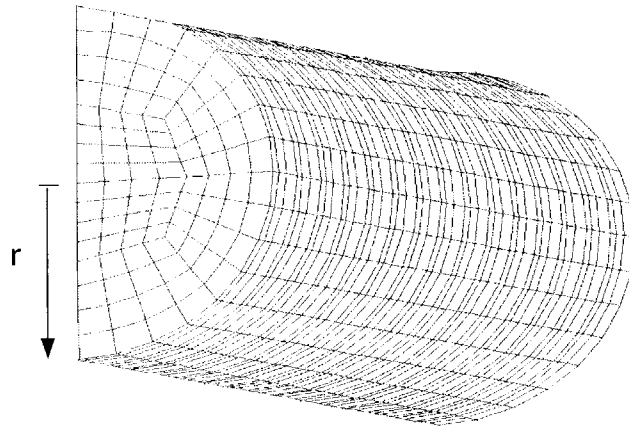


Figure 7.1 Tunnel Cross Section

7.2.1 Staged Excavation

The staged excavation of the tunnel is simulated in steps. Each step simulates the excavation advance and the placement of the liner. The excavation rate is 1m per day.

In each step a section of 1m of the tunnel is excavated. At the same time the liner is placed in the previously excavated section and at a distance of 1m from the face. Thus an unsupported length $l_u=1\text{m}$ (previously defined in section 6.3) is created.

7.2.2 Stress Variation

As mentioned, one of the purposes of the analysis is to show the effect of different coefficients of horizontal stresses. Two different cases of stress variation are examined as shown in Figure 7.2.

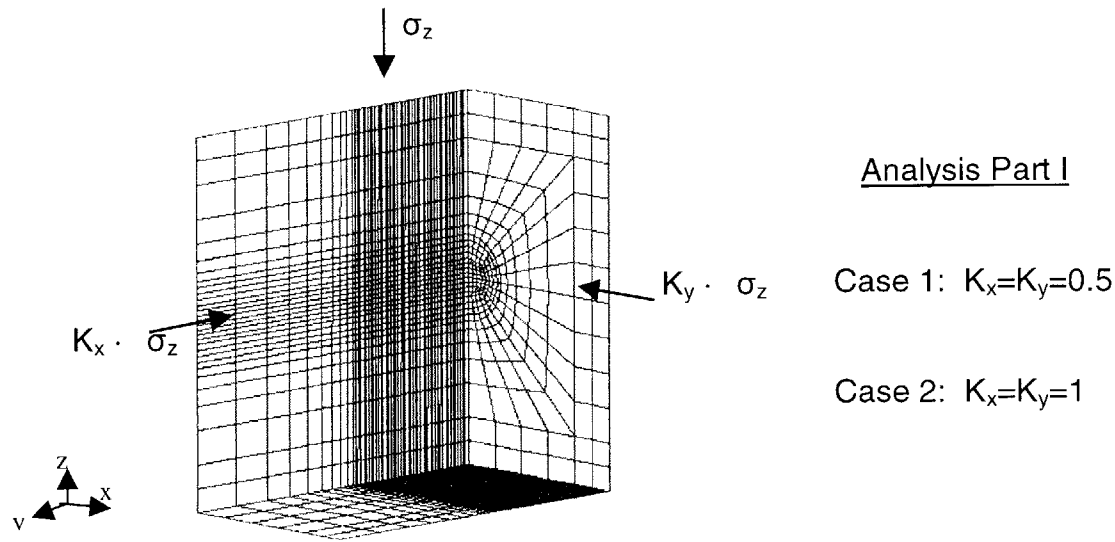


Figure 7.2 Horizontal stresses applied in the analysis

The stress field of case 2 is also used in the axisymmetric model, which will be compared to the 3d model later in this chapter (Section 7.4)

7.3 Numerical Simulation of the Excavation

7.3.1 Building the Model

A three dimensional finite element model will be used for analysis in this study. Figure 7.3 shows this finite element mesh, after the ground excavation is completed. Only half of the ground is shown in the figure because of the symmetry along the vertical centerline of the opening. The tunnel is located at a depth of 100m. However in the model used, only 19m are shown (distance from the center of the tunnel to the top surface of the model). The remaining (100-19) m are treated as the overburden above the opening.

The horizontal dimension of this model is 19m from the vertical opening centerline to its domain boundary. The radius r , of this opening is 4.5m. The domain of this model measured from the edge of opening to model

boundaries, either horizontal or vertical, is chosen to be three times of the opening diameter.

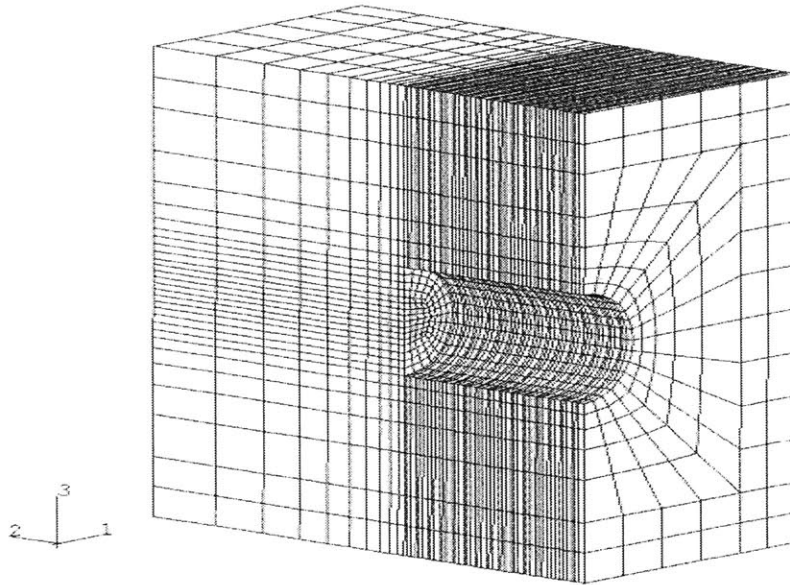


Figure 7.3 Mesh of the three-dimensional model simulating the excavation of a tunnel

For the three-dimensional finite element, 8-node linear tetrahedrons were chosen (C3D8). For the simulation of the lining that was placed at the tunnel periphery, 4-node doubly curved general purpose shells (S4) were used.

This is one difference between the 3d model and the axisymmetric model. In the axisymmetric model, the placement of the concrete liner as a support for the tunnel was simulated with two-dimensional solid elements. In the 3d model the liner is simulated with shell elements, which offer a more realistic simulation of the liner behavior.

7.3.2 Simulation Steps

The simulation of the staged excavation follows the same sequence as that of the two-dimensional analysis. These steps are defined in the input file of the simulation.

Step Description

<u>During</u>	<u>Action</u>
Step 1	Initialization of geostatic stresses
Step 2	Activation and deactivation of concrete elements
Step 3	Excavation of first 1m
Step 4	Excavation of second meter and activation of concrete at 1 st meter
Step 5	Excavation of third meter and activation of concrete at 2 nd meter
Step 6	Excavation of fourth meter and activation of concrete at 3 rd meter
Step 7	Excavation of fifth meter and activation of concrete at 4 th meter
Step 8	Excavation of sixth meter and activation of concrete at 5 th meter
Step 9	Excavation of seventh meter and activation of concrete at 6 th meter
Step 10	Excavation of eighth meter and activation of concrete at 7 th meter
Step 11	Excavation of ninth meter and activation of concrete at 8 th meter
Step 12	Excavation of tenth meter and activation of concrete at 9 th meter
Step 13	Excavation of third meter and activation of concrete at 10 th meter

Step 1 - Initialization of geostatic stresses

During the initialization of the stress field, the vertical stress in the whole model is kept constant (no variation with depth). Since the tunnel examined is located at a depth of 100m, a vertical stress 2000 KPa due to the overburden is used.

Step 2 - Activation and deactivation of concrete shells

In a same way as in the case of the axisymmetric model, the shell elements which in later steps will represent the liner of the tunnel, are activated. Immediately and in the same step these elements are deactivated to avoid conflict with the existing ground elements. Their activation will start in the next steps where the liner will be placed.

Step 3 - Excavation of 1st meter

The first meter of ground is excavated. The liner is not placed yet at the periphery of the tunnel. Its placement will begin in the next step when the excavation face has advanced one meter.

Steps 4-13 - Excavation and placement of the liner

These steps simulate the excavation of the tunnel and the placement of the lining at the tunnel periphery. The placement of the concrete is simulated with the activation of the shell elements that were created in step 2.

7.4 Analysis of the Results

The analysis consists of two parts. In the first part (section 7.4.1) the effect of the variation of the coefficient of horizontal stresses is examined. Continuing in the second part (section 7.4.2) the results obtained will be compared with those of the axisymmetric model.

7.4.1 Effect of K_0 variation in a 3d Model

Figure 7.4 shows the reference points for the interpretation of the results.

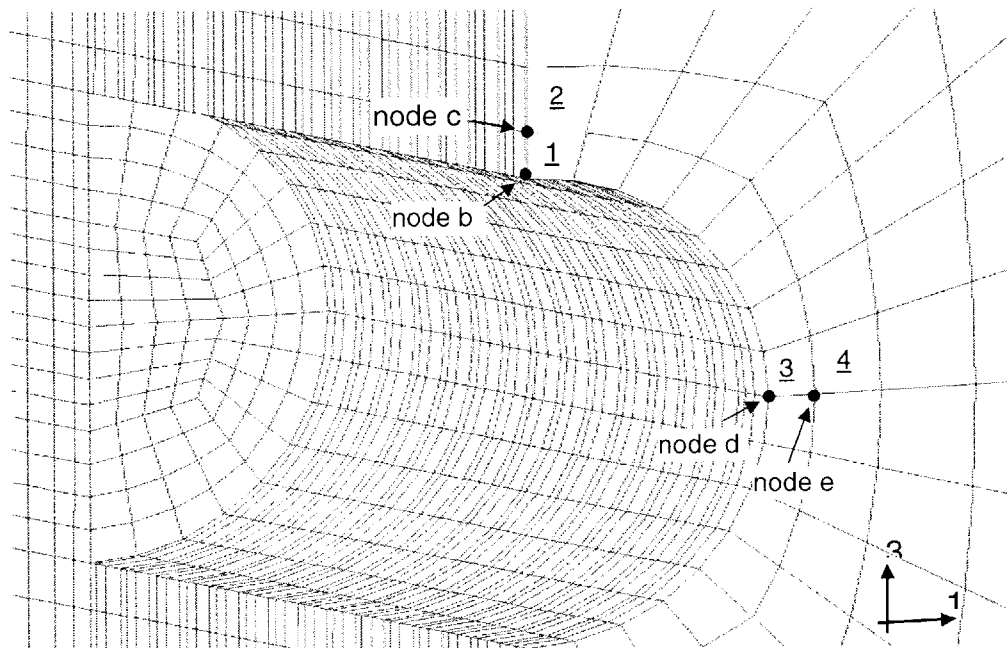


Figure 7.4 Reference points and elements used for the interpretation of results

The tunnel deformation is different for each of the two different coefficients of lateral stresses. Figure 7.5 shows the deformation of the tunnel after excavation with two different initial stress fields. In the case of $K_0=0.5$ the tunnel is deformed into an elliptical shape since the resistance of the ground is less in the horizontal direction. When $K_0=1$, the tunnel is deformed inwards, uniformly in both directions.

This effect is shown in figures 7.6 and 7.7 where the displacements of the tunnel in the crown and at the springline are shown. As shown in figure 7.6, the displacement in the crown is greater when $K_0=0.5$ than when $K_0=1$.

Similarly in figure 7.7, the horizontal displacement at the level of the springline is positive (outward displacement) for $K_0=0.5$, while for $K_0=1$ the side is displaced towards the center of the tunnel.

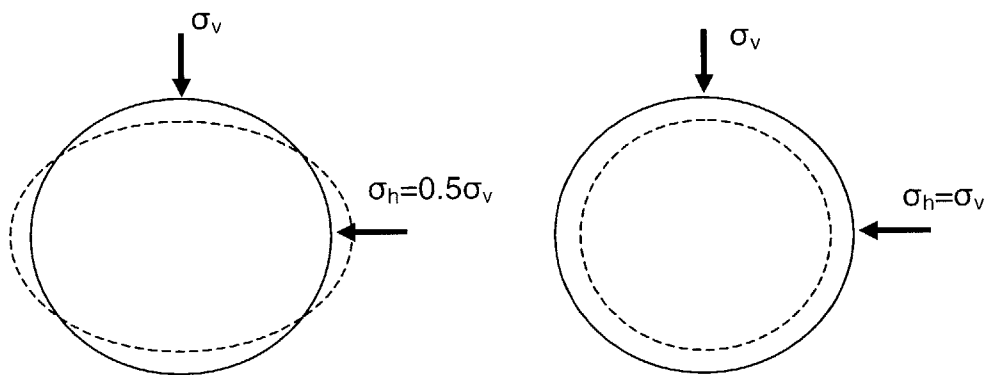


Figure 7.5 Tunnel deformation for $K_0=0.1$ and $K_0=0.5$

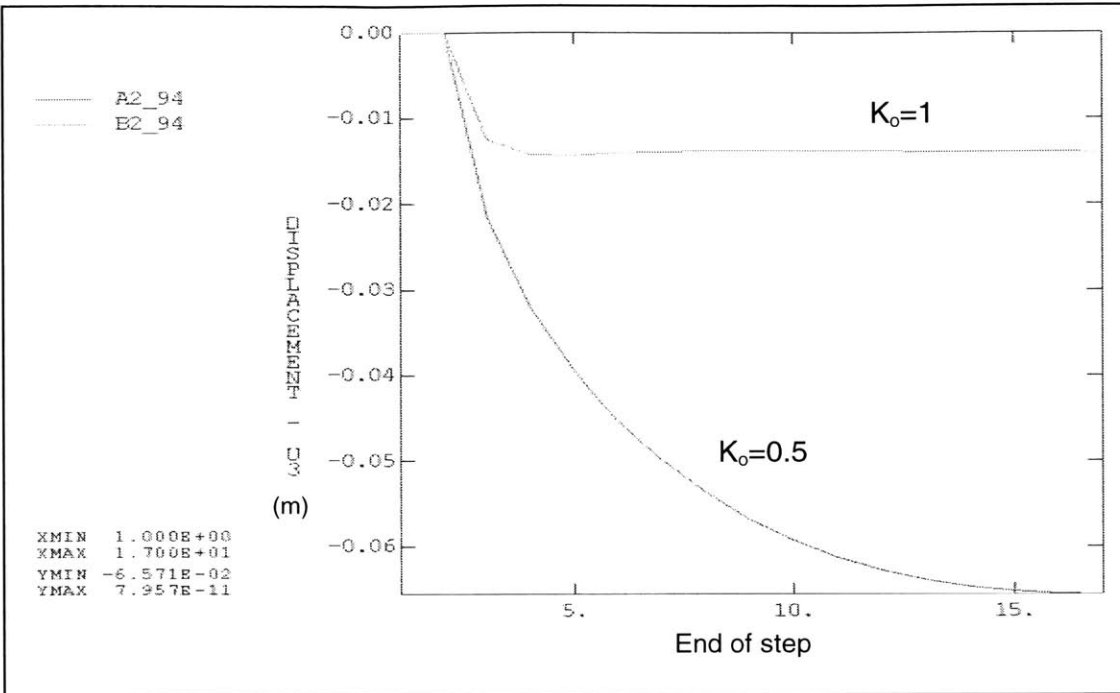


Figure 7.6 Radial convergence in crown (reference point c - figure 7.4)

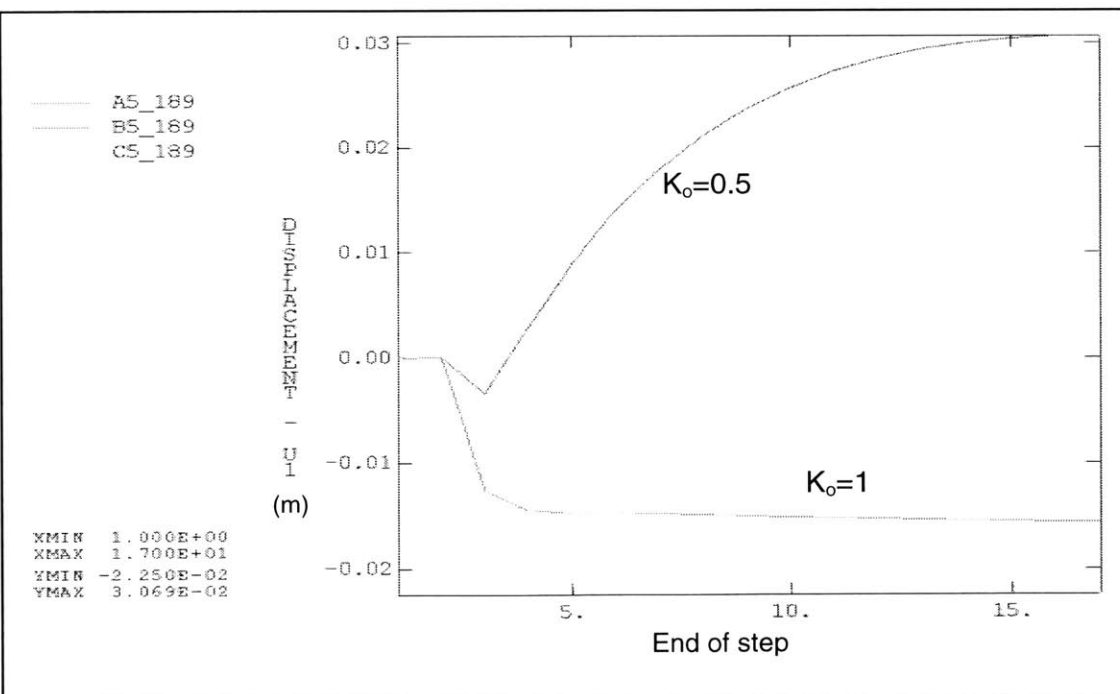


Figure 7.7 Radial convergence at springline (reference point e - figure 7.4)

The radial stresses (in direction 3 – figure 7.4) in the ground, during the tunnel excavation are shown in figures 7.8 and 7.9. Figure 7.8 shows the variation of the radial stress in the crown (in direction 3) of the tunnel, at the boundary of the excavation (element 1 – Figure 7.4), while figure 7.9 shows the stress variation in the element 2 in the ground and above the liner.

At the end of step 1, when the initialization of stresses is completed, the vertical stress in both cases is $\sigma_v=2000$ KPa. At the end of step 3, when the first meter is excavated, the radial stresses decrease. Since the element examined is located at the boundary of the excavation, the stress should normally decrease to zero immediately after excavation. The reason this does not appear in the graph, is that the values shown are the average for the element and not for the point at the interface.

In the case when $K_o=0.5$, the radial stress in the crown is less than for $K_o=1$. Most initial stresses are released after the excavation at the end of step 1, generating greater displacements in the crown and the face. With the excavation advance the radial stress decreases down to a minimum stress 500 KPa.

When $K_o=1$, the radial stress decreases from the initial 2000 KPa to a stress value close to that obtained in the case of $K_o=0.5$. After the third step the radial stress increases again up to a 1200 KPa.

Comparing the two models with $K_o=0.5$ and $K_o=1$, we observe that in the case of $K_o=1$, the radial stresses in the crown of the tunnel are greater.

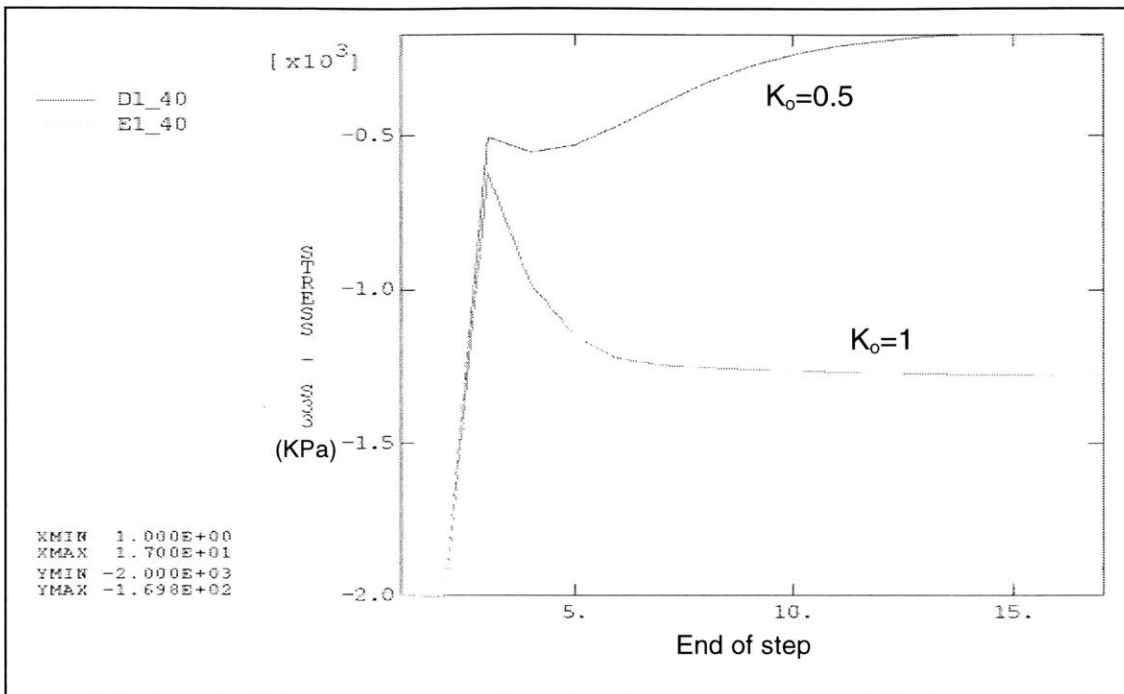


Figure 7.8 Radial stress (direction 3 – Figure 7.4) in the crown of the tunnel (reference element 1 - figure 7.4)

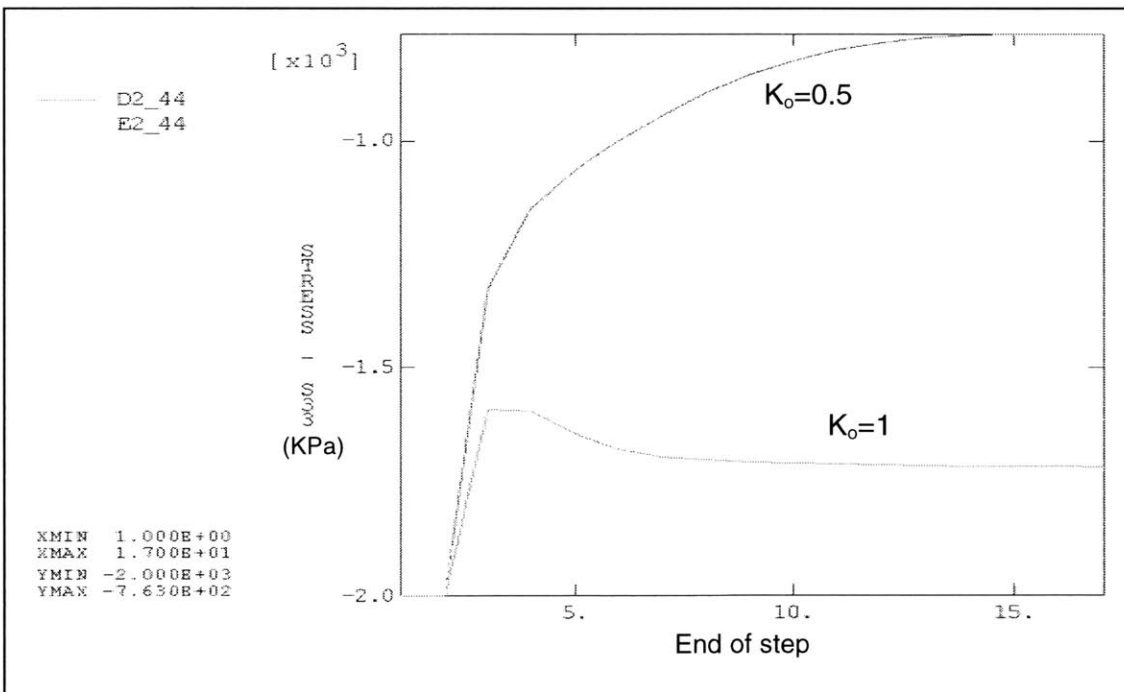


Figure 7.9 Radial stress (direction 3 – Figure 7.4) in the crown (reference element 2 - figure 7.4)

7.4.2 Comparison of 3d and Axisymmetric Model

It was mentioned in chapter 5, that one of the limitations of the axisymmetric model is that it does not allow to specify the horizontal stresses perpendicularly to the tunnel axis. A coefficient $K_o=0.5$ in the axisymmetric model specifies the horizontal stresses only along the tunnel axis. The horizontal stresses perpendicularly to the tunnel axis, which are of greater importance, are always equal to the vertical stresses.

The effect of the coefficient of horizontal stresses will be examined here. The purpose of this analysis is to show how this limitation of the axisymmetric model can affect the results obtained during the simulation of a tunnel excavation.

In the following figure 7.10, the displacement in the crown is compared for the axisymmetric and the three-dimensional model.

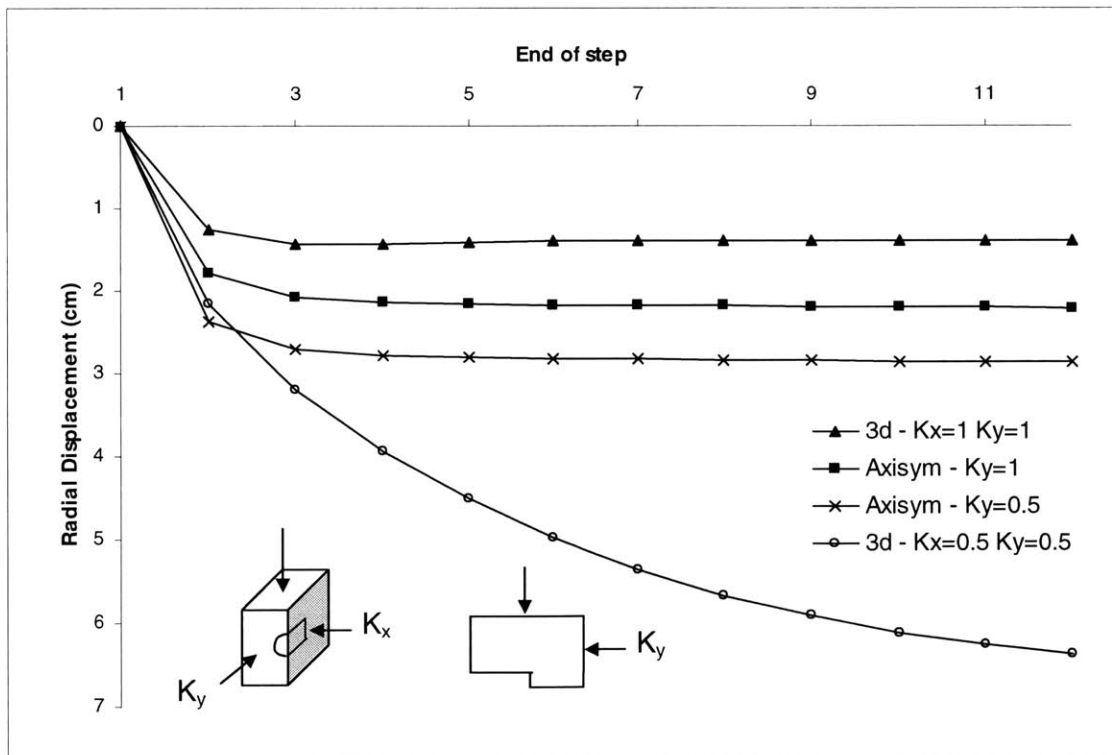


Figure 7.10 Comparative graph of radial displacements in the crown for the axisymmetric model and the 3d model (reference point c - figure 7.4)

The following coefficients of lateral stresses are examined in the two models:

- 1) Three-dimensional model
 - a. Equal principal stresses in all three directions ($K_x=K_y=1$)
 - c. Two equal horizontal principal stresses ($K_x=K_y=0.5$)
- 2) Axisymmetric model
 - a. Two equal principal stresses ($K_y=1$)
 - b. Two different principal stresses ($K_y=0.5$)

When the principal stresses are equal in all directions, the displacement produced with the axisymmetric model is greater than that with the 3d model. The difference in the maximum displacement is about 35%.

The comparison of the 3d model with $K_x=K_y=0.5$ to the axisymmetric model with $K_y=0.5$, shows the limitations of the latter. In this case the axisymmetric model produces only about half the displacements of the 3d model.

Similarly, the radial stresses in the crown, at the interface ground-liner and at the ground above the liner, are presented in figures 7.11 and 7.12, where the two models are compared.

In figure 7.11, where the reference element is at the interface ground-liner, the comparison of the axisymmetric model with the 3d model ($K_x=K_y=1$) shows that the stresses in both models initially decrease until the end of step 2, up to which the tunnel remains unsupported. The stresses approach the zero value during the second step when the excavation of the first meter is performed.

This is expected since the nodes that are located at the excavation surface have zero stress immediately after excavation. In the case of the 3d model the stresses do not decrease to zero, because the stress calculated at the element is an average of the stress of its corner nodes. This difference between the axisymmetric and the 3d model is due to the different type of elements used in each case. During the next steps the radial stresses increase as the excavation advances. This is caused by the installation of the liner, which prevents any additional displacement of the tunnel (the additional displacement is very small

compared that produced when no liner is in place), thus increasing the radial stress at the tunnel periphery.

When the 3d model ($K_x=K_y=0.5$) and the axisymmetric model ($K_y=0.5$) are compared, the final stress right at the interface ground liner is eventually smaller than that produced with the 3d model.

In figure 7.12 the variation of the radial stress in the ground (element located above the liner) is shown. When the stress field around the tunnel is such, that $K_x=K_y=0.5$, the radial stress calculated with the 3d model is less than with the axisymmetric one. The minimum value to which the initial stresses decrease, is almost 40% lower with the 3d model than with the axisymmetric model. The opposite occurs when the two models are examined for $K_x=K_y=1$. In this case the stresses above the liner, in the crown, are much greater when a 3d model is used.

The results mentioned above show the effects of the limitation of the axisymmetric model to specify the coefficient of lateral stresses perpendicular to the tunnel axis. Due to this limitation, when the axisymmetric model is used, the stresses around the tunnel are underestimated when the principal stresses are equal in all directions and overestimated when both coefficients of the horizontal to the vertical stresses are equal to 0.5.

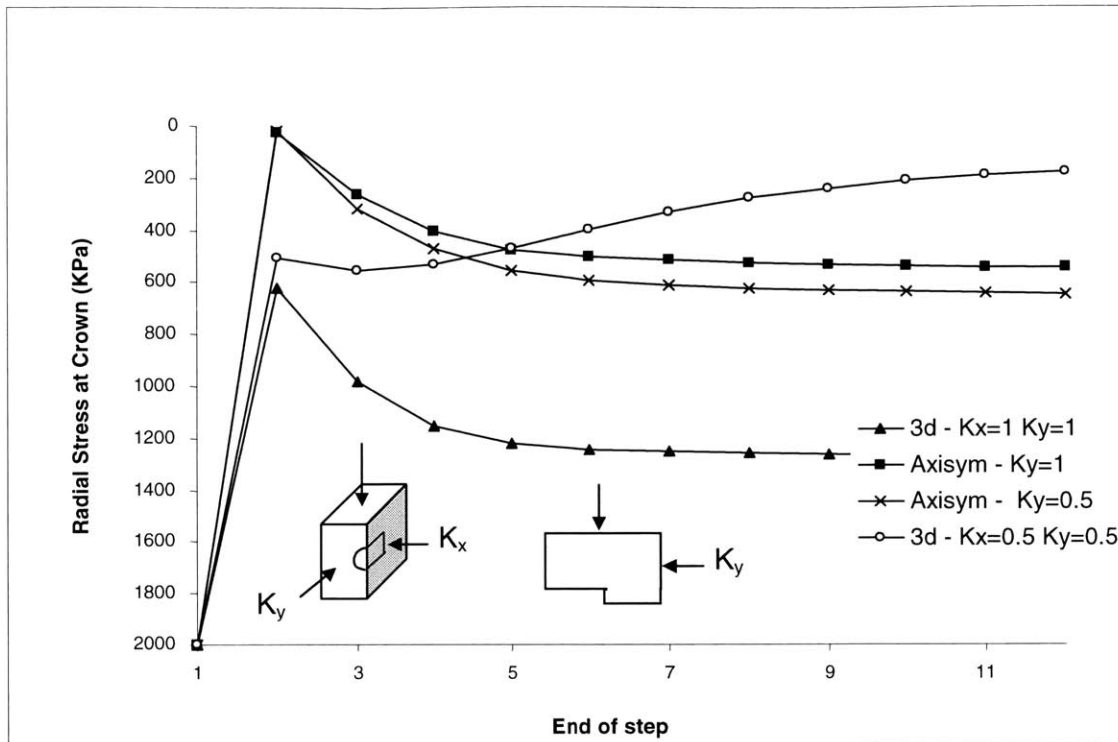


Figure 7.11 Comparative graph of radial stresses at crown, for the axisymmetric and the 3d models (reference element 1 - figure 7.4)

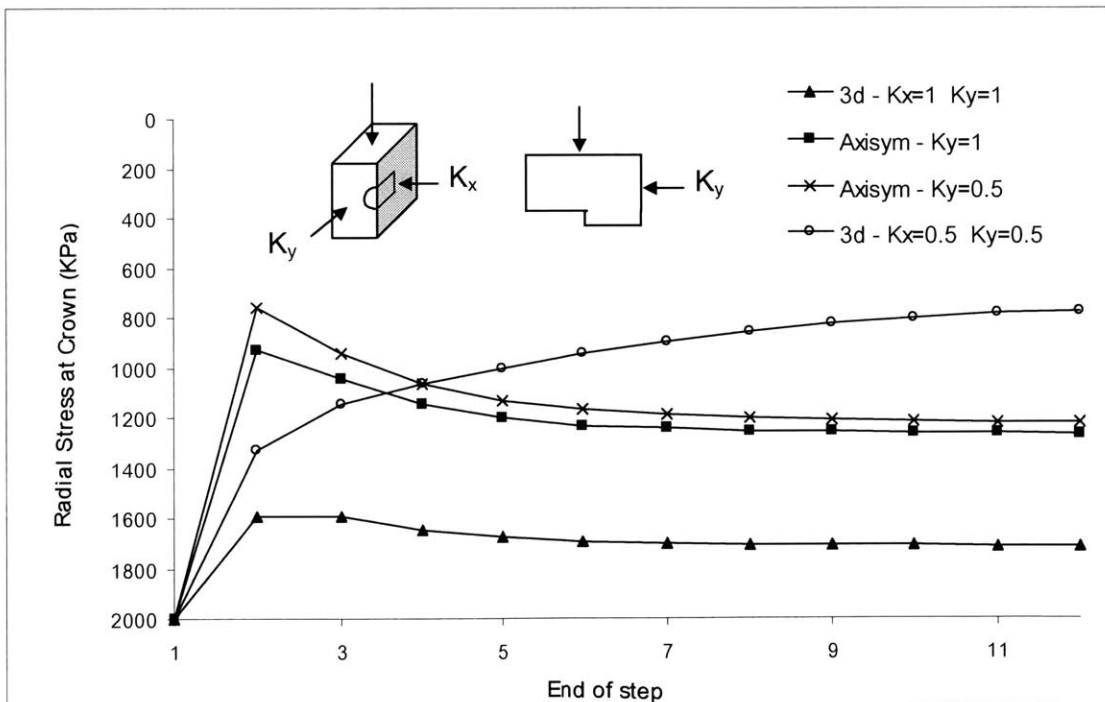


Figure 7.12 Comparative graph of radial stresses at crown, for the axisymmetric and the 3d models (reference element 2 - figure 7.4)

Chapter 8

Combination of axisymmetric and plane strain model

8.1 Introduction

The third simulation performed is a combination of an axisymmetric and a plane strain model. The purpose of the analysis is to take into account both the effect of the distance from the face at which the liner is placed and the effect of consolidation on the liner.

The response of the ground mass and how it affects the design load applied on the tunnel lining will be examined in both dry and wet conditions. A comparison of the results from this analysis to the results of the three-dimensional model can show if the two-dimensional analysis can give similar results to the more complicated 3d models.

8.2 Description of the Analysis

The analysis is divided in two parts using two different models, an axisymmetric and a plane strain model.

8.2.1 Axisymmetric Model

In the first part where an axisymmetric model is used, a full advance excavation of an unlined tunnel is examined in both dry and wet conditions. The difference to the previous analyses (chapters 6 and 7) is that the tunnel is excavated over the entire length of 90m and no liner is installed, as shown at Figure 8.1a. The initial stress field is simulated with the application of a stress, equivalent to the initial stress field, at the excavation surface (figure 8.1).

Due to these initial stresses, immediately after the excavation of the tunnel, initial displacements are released at the tunnel periphery. The magnitude of the displacement varies with the distance from the face of the excavation, to reach a maximum value far from the face. This variation of the

radial convergence of the tunnel is examined for different ground properties, in dry conditions and also in wet conditions, taking into account the consolidation effect.

8.2.2 Plane Strain Model

In the second part, a plane strain model of the same tunnel is used. The ground parameters and the tunnel geometry are the same as in the first part. This model can be considered a cross section of the axisymmetric model with the liner already in place (Figure 8.1b).

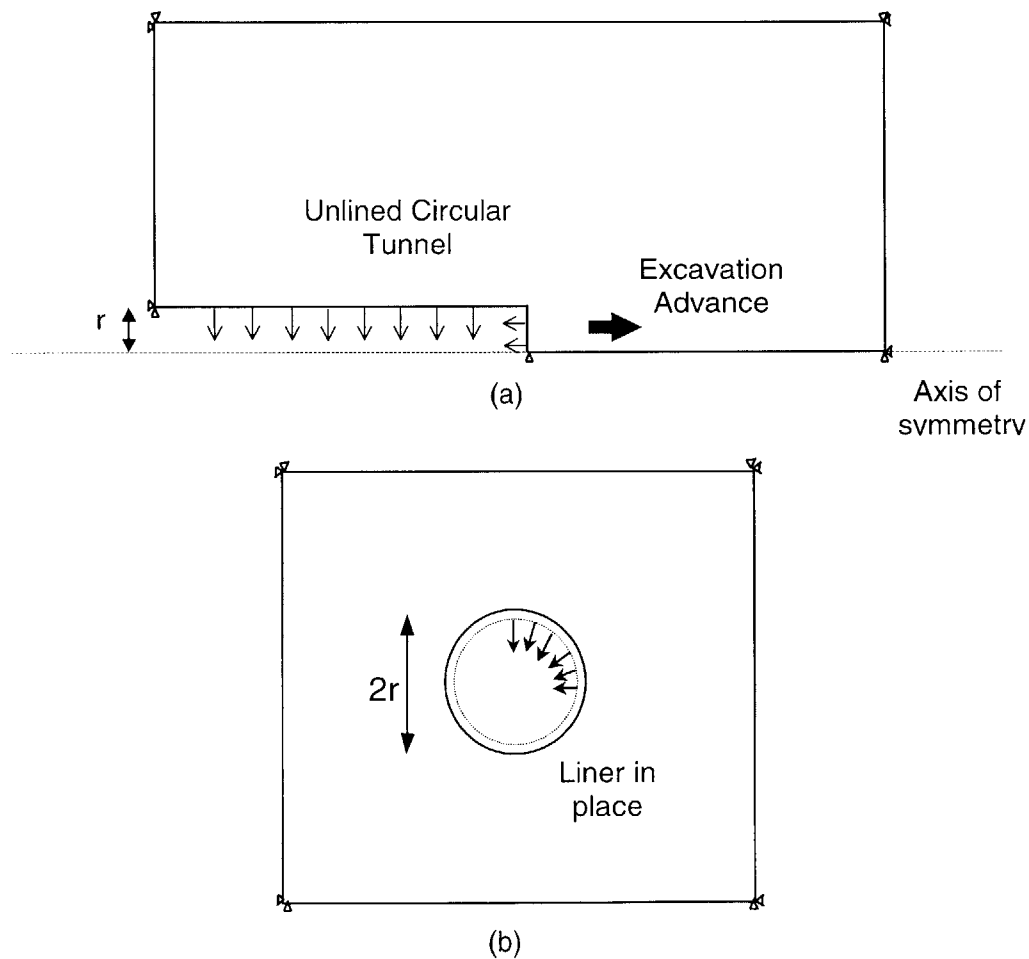


Figure 8.1 2d models used in this analysis: axisymmetric model (a) and plane Strain (b)

8.2.3 Combination of Axisymmetric – Plane Strain Models

The whole analysis is based on the combination of the results from the two analyses mentioned above, by using the tunnel periphery displacements from the axisymmetric analysis as a decreasing factor of the initial stress field of the plane strain model.

During the excavation of a tunnel the crown is displaced. This displacement starts from a zero value, ahead of the face of the excavation (usually at a distance $1-1.5D$, where D is the tunnel diameter), and increases to a maximum value at a distance where the ground mass has reached an equilibrium.

The displacement U_1 at the crown, and at a distance of 1m behind the face of the tunnel, will be calculated in this part, for both dry and wet conditions (figure 8.2). If we refer to the axisymmetric model of chapter 6, this displacement is equal to the displacement of the tunnel at 1m from the face, that is released after the excavation and before the liner is installed.

When the excavation is performed in dry conditions, this displacement depends on the properties of the ground material and usually reaches a maximum value U_{max} at a distance $2-3D$ behind the tunnel face. For dry conditions and at a distance of 1 m from the face, the displacement $U_{1,dry}$ is measured.

In wet conditions the displacement also depends on the effect of consolidation. The displacement at the same point will be less than that measured for the dry case, unless the model is allowed to consolidate until the pore pressures completely dissipate. Theoretically only after complete dissipation of the pore pressures will the displacements in dry and wet conditions will be the same. As will be mentioned in detail later in this chapter, this displacement $U_{1,wet}$ will be measured after 1 day of consolidation. For the permeabilities used in the analysis, displacement $U_{1,wet}$ will be less than $U_{1,dry}$, since consolidation of 1 day is a quite short period.

In any case the displacement of the crown, at a distance of 1m from the face, will be compared to the maximum displacement U_{max} . This is equal either to the displacement far away from the face of excavation (dry case) or after the

complete dissipation of pore pressures (wet case). Since U_{\max} is the limiting displacement for both cases, it will be used as reference value ever, if the consolidation time is not enough for complete dissipation of the pore pressures.

Two ratios will be calculated: $\frac{u_{1,\text{dry}}}{u_{\max}}$ and $\frac{u_{1,\text{wet}}}{u_{\max}}$

These ratios give the percentage of the radial displacement that is released behind the excavation face, and before the placement of the concrete lining.

The remaining $(1 - \frac{u_{1,\text{dry}}}{u_{\max}})$ and $(1 - \frac{u_{1,\text{wet}}}{u_{\max}})$, will be released after the lining is placed, in both cases of dry and wet conditions respectively.

These ratios are used in the second part of the analysis with the plane strain model. In this case the tunnel is examined with the liner in place. With the release of initial displacements, a percentage of the initial stresses was also released. This will be considered in the plane strain model to reduce the initial stresses that are going to be applied on the lining.

Specifically the stress that is applied on the surface of the liner will be multiplied by $(1 - \frac{u_{1,\text{dry}}}{u_{\max}})$ for the dry case, and by $(1 - \frac{u_{1,\text{wet}}}{u_{\max}})$ for the wet case.

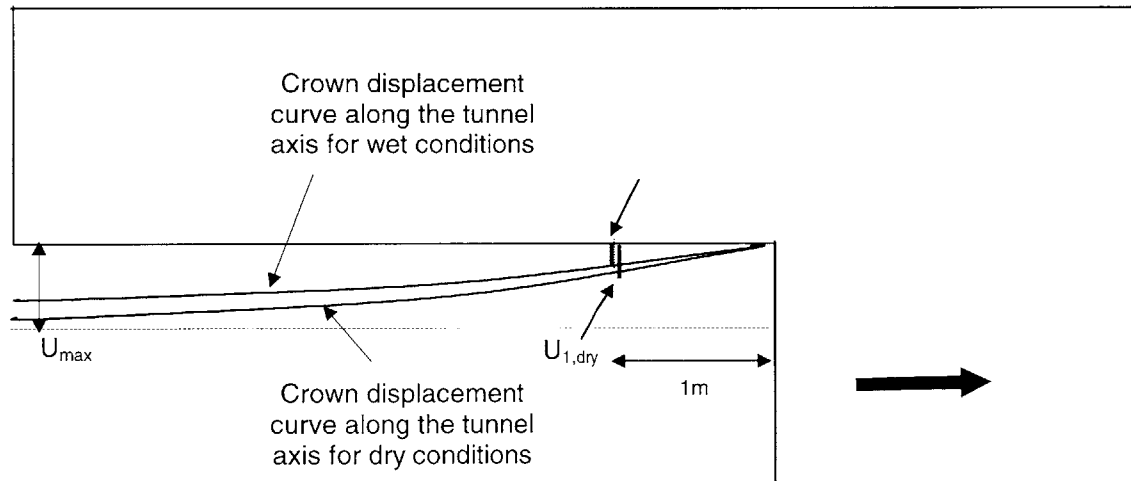


Figure 8.2 Variation of the displacements at the crown of the tunnel close the face of excavation, for dry and wet conditions.

(Note: as mentioned in section 8.2.3, the maximum displacement in wet conditions is equal to U_{\max} only after complete dissipation of pore pressures)

The plane strain model shown in figure 8.3 will be analyzed in both dry and wet conditions. In the case of saturated ground, the consolidation time is 1000 days. Thus, after the initial stresses are applied at the tunnel liner, the ground will be allowed to consolidate for the chosen period of time. This will allow the calculations of stress and displacement variation with time.

In both cases (dry and wet) the tangential stresses that act on the lining will be calculated, giving the opportunity to examine the effect of the consolidation on the behavior of the lining.

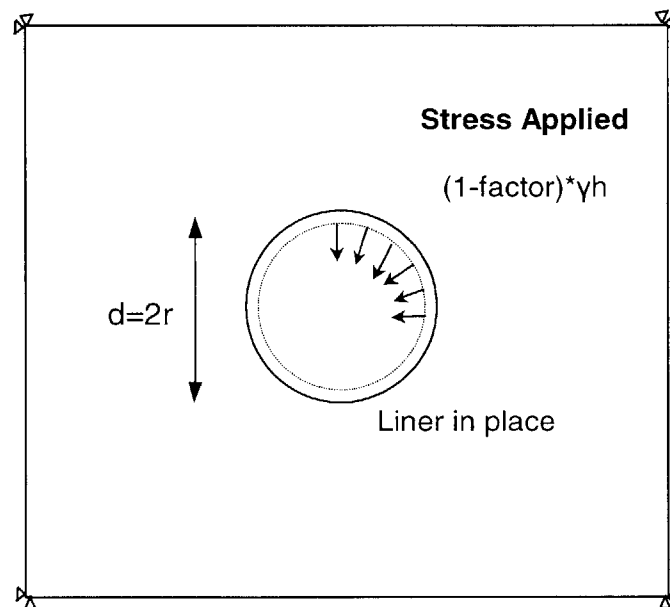


Figure 8.3 Stress field around the tunnel applied on the liner after a reduction of the initial stress field

8.3 Ground Properties and Tunnel Geometry

The ground is assumed to be homogeneous and linear elastic. The modulus of elasticity is constant throughout the groundmass. The ground properties used in the analyses are the following:

Ground Properties

$E=100000 - 150000 - 200000$ KPa

$\nu=0.3$

Permeability: $10^{-7} - 10^{-9} - 10^{-11}$ m/sec

$\gamma=20$ KN/m³

The tunnel geometry is the same in both models. The tunnel is circular with a constant radius $r=4.5$ m along the tunnel axis. In the axisymmetric model there is no liner placed. It is taken into consideration in the second part of the analysis with the plane strain model.

Tunnel Properties

Tunnel Depth: 100m

Tunnel radius: $r=4.5$ m

$E_c=25000000$ KPa

$\nu_c=0.25$

$\gamma=25$ KN/m³

Liner thickness: $t=0.5$ m

8.3.1 Effect of Consolidation

The analysis is again based on the combination of two models, axisymmetric and plane strain. The results obtained from the first model are used as an input for the second one.

The effect of consolidation is taken into account in both models. In the axisymmetric model the consolidation time is 1 day. This time represents the delay of the placement of the lining after the excavation. During that time the tunnel is displaced. The rate at which the displacements are released, will determine the reduction of the initial stress field of the plane strain model.

This rate depends on the permeability of the surrounding mass. A less permeable ground will result to smaller initial displacements because of a slower pore pressure dissipation.

In the plane strain model, the consolidation time is 1000 days. During this time, the variation of stresses and displacements with time is examined around the tunnel.

8.4 Numerical Simulation of the Excavation

8.4.1 Building the Model

Two different types of two-dimensional models were used in this simulation, an axisymmetric and a plane strain model.

The types of elements used in each case are the following:

Axisymmetric: Reduced Integration Continuum axisymmetric
with 8 nodes CAXR8

Plane Strain: Reduced Integration Continuum Plane Strain
with 8 nodes CPE8R

The boundary conditions for both models are the same. Along their limits the normal components of displacement are zero. In the case of the saturated ground, drainage is allowed in all directions.

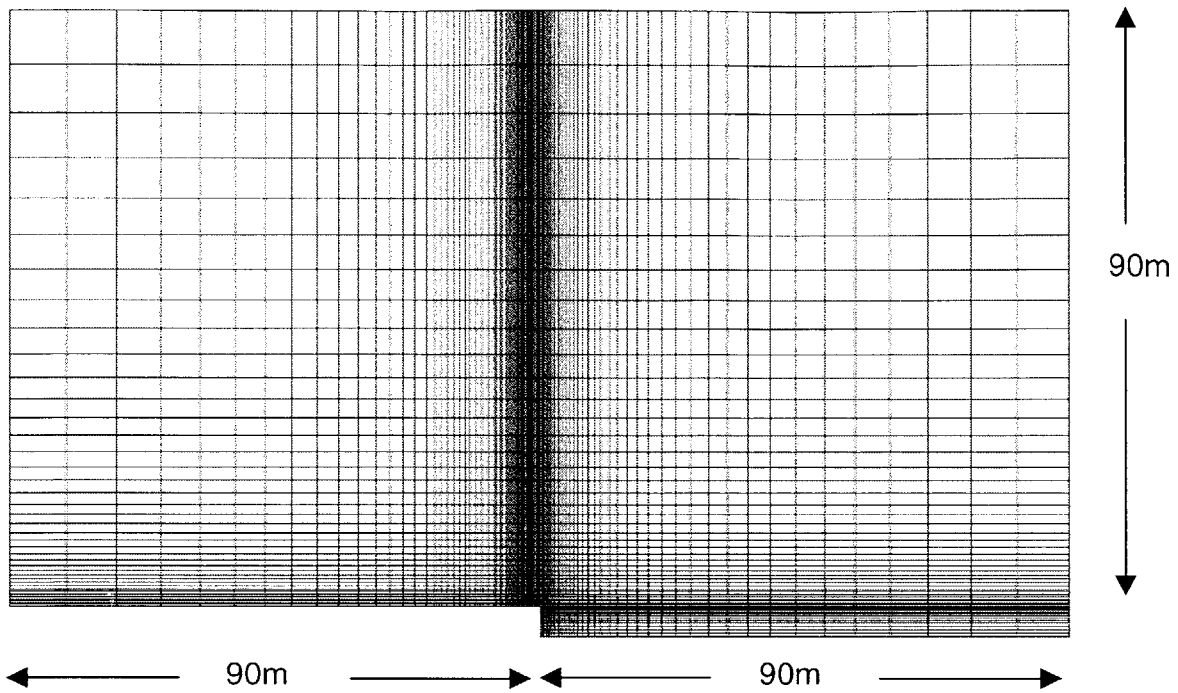


Figure 8.4 Axisymmetric model of an excavated unlined tunnel

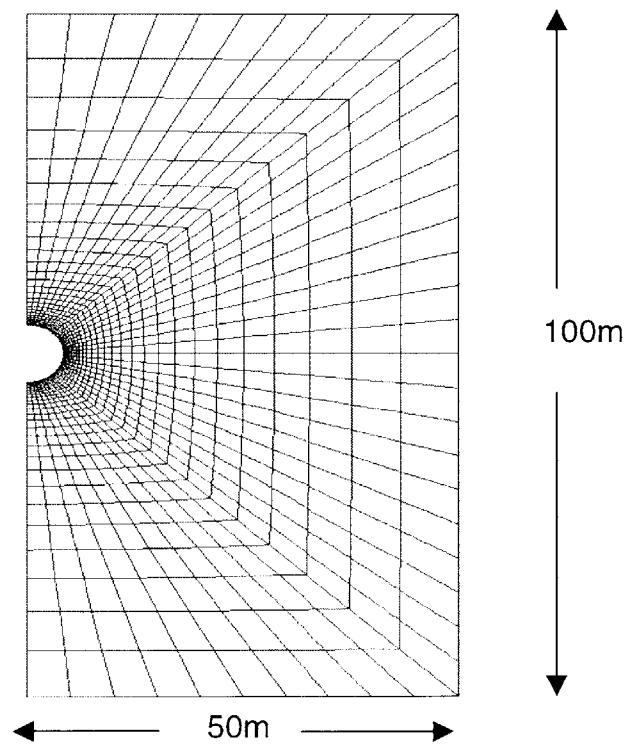


Figure 8.5 Plane strain model of an excavated tunnel with a liner in place

8.4.2 Simulation Steps

Dry Conditions

a) Axisymmetric model

The first part includes the simulation of a fully excavated unlined tunnel. This is the main difference between this model and the axisymmetric models used in previous chapters, where a staged tunnel excavation was performed.

There is only one step performed during this simulation, which again is the initialization of stresses. This is done by the application of a pressure at the surface of the excavated area equal to the stress due to the overburden (figure 8.4). Since the same pressure is applied at the crown and the face of the tunnel, the stress field initialized is uniform with $K_o=1$.

b) Plane Strain Model in dry conditions

The simulation of the plane strain model in dry conditions is also performed in one step. The tunnel examined has the same properties as before except that now a liner is already installed.

This step includes the initialization of the stress field, which is simulated by the application of a pressure at the interface liner-ground. As mentioned in section 8.2.3, this pressure is reduced by a factor, in order to take into account the release of stresses before the liner is installed. This is the only input used from the axisymmetric model. Any displacements that are generated in the mass during the analysis of the first model are not considered in the plane strain model.

Wet Conditions

a) Axisymmetric and plane strain model

In the case of wet conditions, the analysis is performed in two steps. In the first step where the initial stress field is defined, the pore pressures are initialized with no drainage allowed along the excavation surface. In the second step the actual consolidation procedure is performed. At this point the consolidation time is defined as mentioned in section 8.3.1.

8.5 Analysis of Results

8.5.1 Displacement of the Crown along the Tunnel Axis

Part of the analysis is the calculation of the displacements along the tunnel axis. The release of these displacements determines the reduction factor for the initial stress field of the plane strain model. Figure 8.6 shows the displacements at the crown of the tunnel in dry and wet conditions, along the tunnel axis.

Convergence along tunnel axis for dry and saturated ground

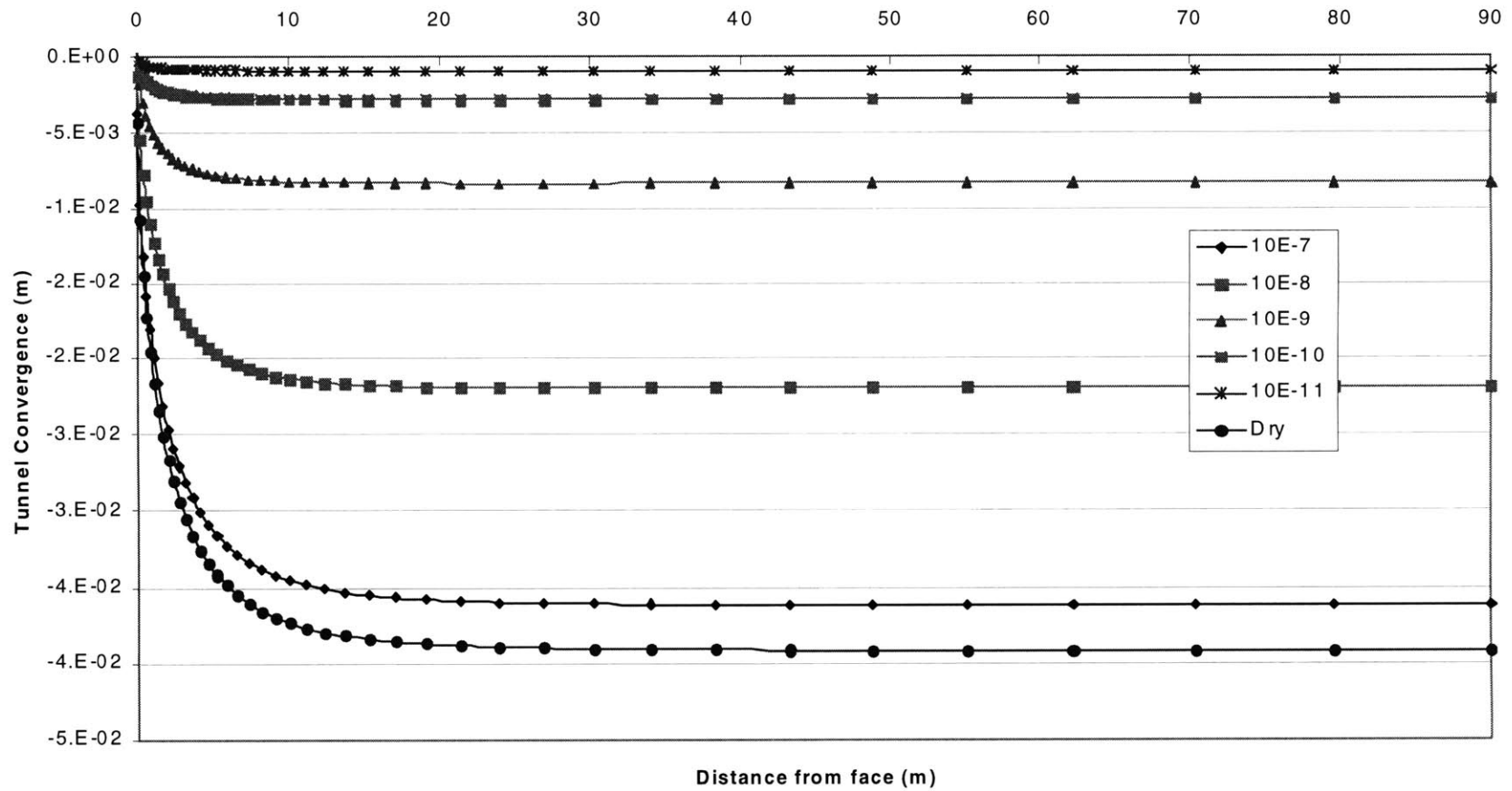


Figure 8.6 Variation of radial displacements with permeability at the crown and along the tunnel axis

The following table shows the percentage of the maximum displacements (defined in section 8.2.3) that are released at the crown of the tunnel, calculated at three different distances 1m, 2m and 3m from the face. Both dry and saturated conditions are examined. The tunnel depth is 100m and the modulus of elasticity $E=100000$ KPa. The only variable is the permeability.

	Permeability	Distance from the face		
	(m/sec)	1m	2m	3m
Dry	-	59%	71%	79%
Wet	10e-11	2%	2%	2%
	10e-9	12%	16%	18%
	10e-7	53%	65%	73%

Table 8.1 Percentage of displacements released in an unlined tunnel

When the excavation is performed in saturated ground the percentage of the displacements released is decreasing as the ground becomes less permeable, due to the slower dissipation of the pore pressures.

8.5.2 Stresses in the Liner

In the second part of the analysis, the plane strain model is used for the calculation of stresses at the tunnel liner. As discussed earlier in paragraph 8.2, the results obtained from the first part of the analysis, are used to adjust the initial stresses applied on the liner. At the time of the liner installation a percentage of the initial stresses has been released, generating displacements at the tunnel periphery.

The purpose of the analysis is to calculate the stresses in the liner intrados and extrados in dry and wet conditions.

Figure 8.7 depicts the reference points for the calculation of stresses.

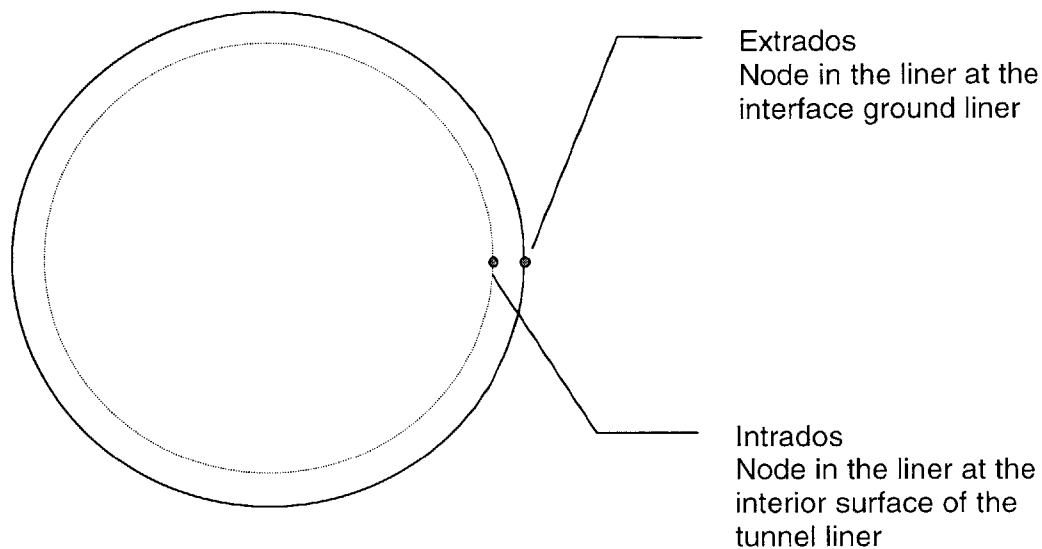


Figure 8.7 Reference points for the stress calculation

The stress variation at the two reference nodes is shown in the two graphs of figure 8.8. The effect of consolidation is obvious in both graphs. In the case of the excavation in dry ground, the tangential stress at the springline, is almost 6000 KPa, with insignificant change with the variation of modulus E . When the tunnel is in saturated ground the stresses are increased. In the case of ground with high permeability ($k=10e-7$ m/sec), the stresses are increased by almost 10%. With a decrease in permeability, the stresses in the liner increase significantly. When $k=10e-11$ m/sec the stresses are increased by almost 100%.

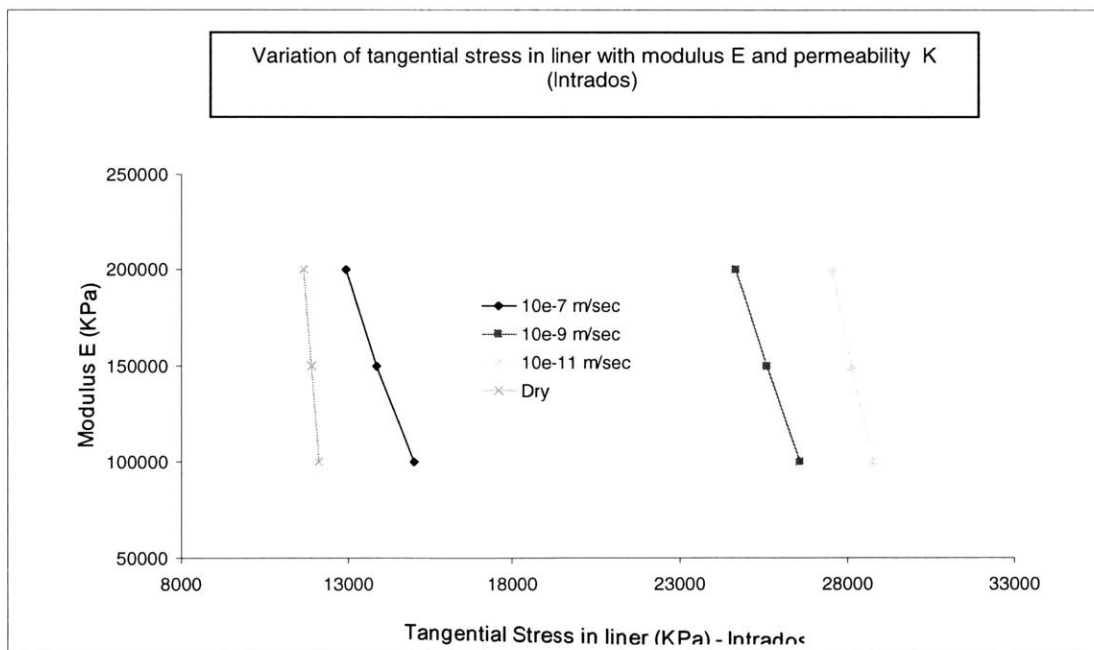
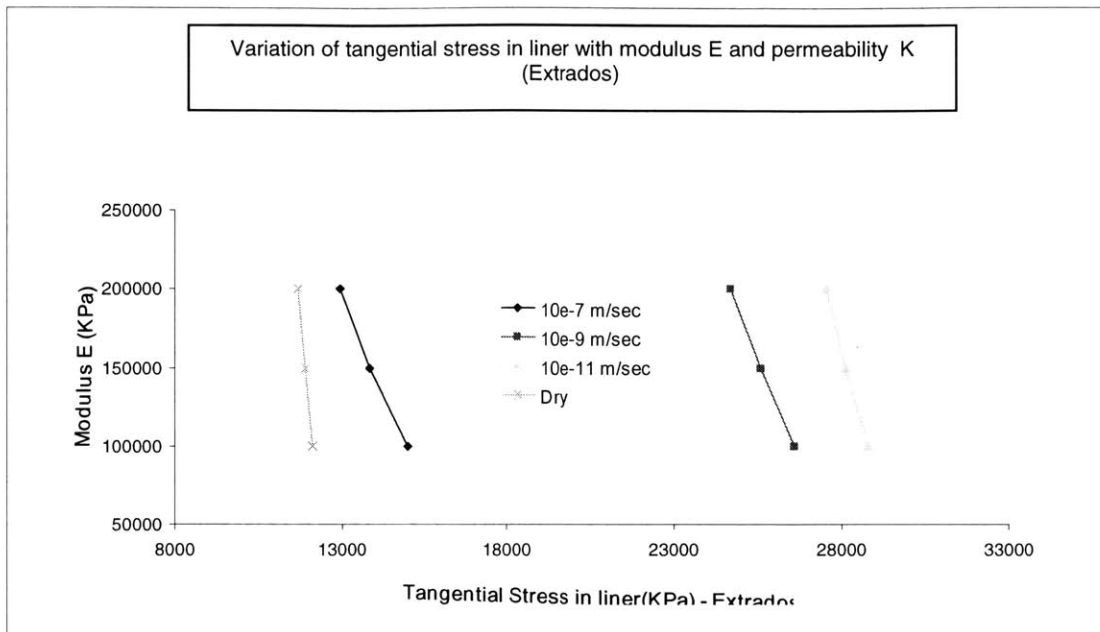


Figure 8.8 Variation of tangential stresses at intrados and extrados of liner

Chapter 9

Summary and Conclusions

9.1 Summary

In this thesis the finite element analysis method was used to simulate and investigate the staged excavation of a circular lined tunnel. The main objective was to analyze the ground-liner interaction incorporating the effect of consolidation and the three-dimensional behavior near the face of the excavation. An attempt was made also to represent this three-dimensional effect with simpler two-dimensional models.

- A two-dimensional axisymmetric model was used for the simulation of the staged excavation of a circular tunnel in dry and wet conditions; the latter to investigate the effect of consolidation. An analysis of displacements and stresses for both the liner and the ground was performed.
- A three-dimensional analysis of the same staged tunnel excavation was performed. The results obtained from this analysis were used to show the importance of the initial stress field when a tunnel excavation is simulated. At the same time, the limitations of the axisymmetric model and its inability to simulate the initial stress field around the tunnel were also examined.
- A simplified approach to simulate the three dimensional character of a tunnel excavation was also attempted. The results obtained from an axisymmetric model of an unlined tunnel were used as an input for the plane strain model of the same tunnel with the liner installed. The purpose of the analysis was to take into account both the effect of the distance from the face at which the liner is placed and the effect of consolidation on the liner.

9.2 Conclusions

9.2.1 Effect of Consolidation

- Comparing the two cases where the tunnel is excavated in both dry and wet conditions, it is observed that in the case of dry ground, most of the displacements are released early in the excavation process (when the excavation face had advanced 4-5m). With consolidation taken into account, the displacements are released more slowly.
- An increase of the stresses both in the liner and the ground is observed when the consolidation is taken into account. For both dry and wet conditions, the stress applied on the lining increases with the advance of the excavation face. In the case of dry ground and when the excavation face is at a distance of 5m from the reference location, the stress acting on the liner has reached almost 90% of its final value. With consolidation, the stress on the lining increases throughout the considered excavation sequence and reaches a maximum, which is 10-15% higher than the stresses that develop when the ground is dry.

9.2.2 Effect of Initial Stress Field

- Comparing different initial stress fields ($K_x=K_y=1$ and $K_x=K_y=0.5$) with a 3d model, it was observed that the radial stress in the crown of the tunnel is greater when the initial stress field is uniform (same principal stresses in all three directions) compared to $K_x=K_y=0.5$.
- When the 3d model is compared to the axisymmetric model, and for initial stress field of $K_x=K_y=0.5$, the radial stress in the ground calculated with the 3d model is less than that obtained with the axisymmetric one. The minimum value to which the initial stresses decrease, is almost 40% lower with the 3d model than with the axisymmetric model. The opposite occurs when the two models are examined with an initial stress field where all three principal stresses are equal. In that case the stresses in

the ground above the liner, in the crown, are much greater when a 3d model is used.

- Hence when the axisymmetric model is used for the simulation of a tunnel excavation, the stresses around the tunnel are underestimated when the principal stresses are equal in all directions and overestimated when both coefficients of the horizontal to the vertical stresses are equal to 0.5.

9.2.3 Combination of 2d Models

- When the excavation of the tunnel is performed in wet ground, the tangential stress in the liner and at the springline is increased compared to that obtained with excavation in dry conditions. In the case of ground with high permeability ($K=10e-7$ m/sec), the stresses are increased by almost 10%. With a decrease in permeability, the stresses in the liner increase significantly compared to those produced in a dry ground. When $K=10e-11$ m/sec the stresses are increased by almost 100%.

9.3 Further Recommendations

An in depth analysis was performed during the simulation of a staged tunnel excavation in dry and wet conditions. Although the finite element approach was proven to be adequate for the problem, many simplifying assumptions had to be made.

One of the major assumptions is the isotropy of the ground. A more realistic representation of the material model can be a very important topic of future research. The plastic behavior of the ground around the tunnel can also be introduced in both the 2d and the 3d models.

The displacements and the stresses that were obtained with the analyses of both models were limited to circular tunnels with full face excavation. The investigation of other tunnel cross sections and of a separate heading and bench excavation can produce interesting results.

References

1. Abaqus/Standard, User's Manual, Version 5.7, Hibbitt, Karlsson & Sorensen, Inc.
2. Abel, J.F., Fitzhugh, T. Lee, *Stress changes ahead of an advancing tunnel*, International Journal of Rock Mechanics and Mining Sciences, Volume 10, pp 673-697, 1973
3. Adachi, T., Tamura, T., Shinkawa, M., *Analytical and experimental study on tunnel support system*, Proceedings of the fourth International Conference on Numerical Methods in Geomechanics, Volume 2, pp 513-522, Edmonton, Canada, 1982
4. Allouani, M., Bahar, R., Cambou, B., Rezgui, B., *Evaluation of displacements during tunneling in soft soil*, Computer methods and advances in geomechanics, Volume 3, pp 2535-2540, Balkema, 1994
5. Al Tabaa, A., Muir Wood, D., *Horizontal drainage during consolidation: insights gained from analyses of a simple problem*, Geotechnique 41, No 4, pp 571-585, 1991
6. Aubry, D., Hujeux, J.C., *Special algorithms for elastoplastic consolidation with finite elements*, Third International Conference on Numerical methods in Geomechanics, pp 133-141, Aachen, Germany, 1979
7. Aubry, D., Kodaissi, E., *Two-phase implicit scheme for viscoplastic soil consolidation in numerical methods for transient coupled problems*, Edited by R.W. Lewis, E. Hinton and B.A. Schrefler, Pineridge Press Swansea, pp 495-508, 1984
8. Aydan, O., Kyoya, T., Ichikawa, Y., Kawamoto, T., *Three-dimensional simulation of an advancing tunnel supported with forepoles, shotcrete, steel ribs and rockbolts*, Numerical Methods in Geomechanics, pp 1481-1486, Innsbruck, 1988
9. Baumann, Th., *Numerical analysis and reality in tunneling – Verification by measurements*, Numerical Methods in Geomechanics, pp1457-1464, Balkema, Innsbruck, 1988

10. Bear, J., Verruijt A., *Modeling groundwater flow and pollution*, D. Reidel Publishing Company, Dordrecht/Boston/Lancaster/Tokyo, 1987
11. Beer, G., Booker, J.R., Carter, J.P., *Computer methods and advances in geomechanics*, Proceedings from the seventh International Conference on Computer Methods and advances in Geomechanics, Cairns, 6-10 May, 1991
12. Beer, G., Watson, J.O., *Introduction to finite and boundary element methods for engineers*, John Wiley & Sons, 1992
13. Bernat, S., Cambou, B., Santosa, P., *Modeling of soil-structure interaction during tunneling in soft soil*, Computer methods and advances in geomechanics, Volume 2, pp 1377-1382, Balkema, 1997
14. Biot, M.A., *Theory of elasticity and consolidation for a porous anisotropic solid*, J. App. Phys., Volume 26, pp 182-185, 1955
15. Biot, M.A., *Theory of elasticity and consolidation for a porous anisotropic solid*, J. Appl. Physics, 26, pp 182-185, 1955
16. Boehmer, J.W., Christian, J.T., *Plane strain consolidation by finite elements*, Prepared for the US department of transportation under Central C-85-65, Cambridge, 1969
17. Brierley, G.S. (editor), *Proceedings workshop on tunnel lining design*, Cambridge, Massachusetts, March 12 & 13, 1979
18. Brown, P.T., Booker, J.R., *Finite element analysis of excavation*, Computers and Geotechnics, Volume 1, pp 207-220, 1985
19. Carter J. P., Moore I. D. and Booker J. R., *The analysis of a lined circular opening in elastic ground*, University of Sydney, School Civil Mining Engng. Research Report, 1981
20. Carter J. P. and Booker J.R., *Elastic consolidation around a deep circular tunnel*, *Int. J. Solids Structures*, Volume 18, pp 1059-1074, 1982
21. Chaffois, S., Lareal, P., Monnet, J., Chapeau, C., *Study of tunnel face in gravel site*, Numerical Methods in Geomechanics, pp1493-1498, Balkema Innsbruck, 1988

22. Chandrasekaran, V.S. and King, G.J.W., *Simulation of an excavation using FE*, Jl. Geotech. Eng. Div., ASCE, Volume 100, pp 1086-1089, 1974
23. Chen, Yao-Chung, Lin Yao-Ming, *The influences of in-situ stresses on the deformations of tunnels*, Computer methods and advances in geomechanics, Volume 2, pp 1327-1332, Balkema, 1997
24. Chen, Wern Ping, Baldauf, S., *Prediction of ground deformations due to the excavation – Application to tunnel lining design in weak rock*, Computer methods and advances in geomechanics, Volume 3, pp 2565-2570, Balkema, 1994
25. Christian, J.T., *Undrained stress distribution by numerical methods*, Journal of the Soil Mechanics and Foundations Division, ASCE, No. SM6, Proc. pp 1333-1345, 1968
26. Christian, J.T. and Wong, I.H., *Errors in simulating excavation in elastic media by FE*, Soils and Foundations, Volume 13, pp 1-10, 1973
27. Curtis D.J., *Discussion on "The circular tunnel in elastic ground"*, Geotechnique, Volume 26(1), pp 231-237, 1976
28. Deere, D.U., Peck, R.B., Monsees, J.E., Schmidt, B., *Design of tunnel liners and support systems*, Final report, Office of High Speed Ground Transportation, US Department of Transportation, Washington, 1969
29. Desai, C.S., Christian, J.T., *Numerical methods in geotechnical engineering*, McGraw Hill, 1977
30. Dolezalova, M., *The influence of construction work sequence on the stability of underground openings*, Third International Conference on Numerical Methods in Geomechanics, Volume 2, pp 561-570, Aachen, 1979
31. Einstein, H.H., Schwartz, C.W., *Simplified analysis for tunnel supports*, Journal of Geotechnical Engineering Division, Proceedings of the American Society of Civil Engineers, Vol. 105, No GT4, April 1979
32. Einstein, H.H., Bobet, A., *Mechanized tunneling in squeezing ground- from basic thoughts to continuous tunneling*, Tunnels for people, Editors:

- J.Golser, W.J.Hinkel, W.Schubert, Proceedings World Tunnel Congress, Vienna, Volume 2, pp 619-632, Balkema, 1997
- 33.Eisenstein, Z., Ezzeldine, O., *The role face pressure for shields with positive ground control*, Tunneling and Ground Conditions, Balkema, 1994\
- 34.Eisenstein, Z., Heinz, H., Negro, A., *On three-dimensional ground response to tunneling*, Tunneling in soil and Rock, Proceedings of two sessions at GEOTECH '84, pp 128-155, American Society of Civil Engineers, 1984
- 35.Fredlund, D. G., *Consolidation of unsaturated porous media*, Proc. of the NATO Advanced Study Institute on Mechanics of Fluid in Porous Media, pp 525-578, Newark, Delaware, U.S.A., 1982
- 36.Fritz, P., *An analytical solution for axisymmetric tunnel problems in elasto-viscoplastic media*, International Journal for Numerical and Analytical Methods in Geomechanics, Vol8, pp 325-342, 1984
- 37.Galler, R., *Shotcrete-realistic modeling for the purpose of economical tunnel design*, Computer methods and advances in geomechanics, Volume 2, pp 1383-1387, Balkema, 1997
- 38.Hanafy, E.A., Emery, J.J., *Advancing face simulation of tunnel excavations and lining placement*, Ground Movements and Structures, pp 377-394, 1980
- 38.Handin, J., *Effects of pore pressure on the experimental deformation of some sedimentary rocks*, Bull. Geol. Soc. Am., Volume 69, pp 1576-1577, 1958
- 39.Handin, J., Hager, R. V. Jr., Friedman, M., & Feather, J. N., *Experimental deformation of sedimentary rocks under confining pressure: Pore pressure tests*, Bull. Geol. Soc. Am., Volume 47, pp 717-755, 1963
- 40.Hansmire, W.H., *Example analysis for circular tunnel lining Interpretation of stress-displacement measurements tunneling in soil and rock*, Proceedings of two sessions at GEOTECH '84, pp 30-45, American Society of Civil Engineers, 1984

41. Haugeneder, E., Mehl, M., *Finite element analysis of tunnel linings with emphasis on the nonlinearity of concrete*, Numerical Methods in Geomechanics, pp 1557-1565, Balkema, Innsbruck, 1988
42. Hisatake, M., *Back-analysis of tunnel lining stresses*, Computer Methods and advances in Geomechanics, pp 1479-1484, Balkema, 1991
43. Hoeg K., *Stresses against underground structural cylinders*, J. Soil Mech. Fndns. Div., ASCE Volume 94 SM4, pp 833-858, 1968
44. Kaiser, P.K., Hutchinson, D.E., *Effects of construction procedure on tunnel performance*, Proceedings of the fourth International Conference on Numerical Methods in Geomechanics, Volume 2, pp 561-569, Edmonton, Canada, 1982
45. Kielbassa, S., Duddeck, H., *Stress-strain fields at the tunneling face – Three dimensional analysis for two-dimensional technical approach*, Rock Mechanics and Rock Engineering 24, pp 115-132, 1991
46. Lingfeng, H., Jun, L., *Effect of pore water behavior on soft rock tunneling*, Computer methods and advances in geomechanics, Volume 2, pp 1367-1371, Balkema, 1997
47. Lo, K.Y., Lukajic, B., Ogawa, T., *Interpretation of stress-displacement measurements*, Tunneling in Soil and Rock, Proceedings of two sessions at GEOTECH '84, pp 107-127, American Society of Civil Engineers, 1984
48. Lo, K.Y., Ng., M.C., Rowe., R.K., *Predicting settlement due to tunneling in clays interpretation of stress-displacement measurements*, Tunneling in Soil and Rock, Proceedings of two sessions at GEOTECH '84, pp 46-75, American Society of Civil Engineers, 1984
49. Morgan H.D., *A contribution to the analysis of stress in a circular tunnel*, Geotechnique, Volume 11(1), pp 37-46, 1961
50. Moussa, A., Wagner, H., *Effect of construction speed on the behavior of NATM tunnels*, Computer methods and advances in geomechanics, Volume 2, pp 1419-1424, Balkema, 1997

51. Muir Wood, A.M., *The circular tunnel in elastic ground*, Geotechnique, Volume 25(1), pp 115-127, 1975
52. Obert, L., Duvall, W.I., *Rock Mechanics and the design of structures in rock*, John Wiley & Sons, New York
53. Ohnishi, Y., Nishigaki, Y., Kishimoto, H., Tanaka, Y., *Analysis of advancing tunnel by 2-Dimensional F.E.M.*, Proceedings of the fourth International Conference on Numerical Methods in Geomechanics, Volume 2, pp 571-578, Edmonton, Canada, 1982
54. Pande, G.N., Beer, G., Williams, J.R., *Numerical methods in rock mechanics*, John Wiley & Sons, 1990
55. Pender M.J., Elastic solutions for a deep circular tunnel, Geotechnique, Volume 30(2), pp 216-222, 1980
56. Reed, M.B., An investigation of numerical errors in the analysis of consolidation by finite elements, Int. J. Numer. Anal. Methods Geomech, Volume 8, No 2, pp 243-257, 1984
57. Sabdhu, R.S. and Wilson, E.L., *Finite-Element analysis of seepage in elastic media*, Journal of the Soil Mechanics and Foundations Division, ASCE, No. EM3, Proc. pp 641-652, 1969
58. Savioli G.B., Jacovkis P.M., Bidner M.S., *Stability analysis and numerical simulation of 1-D and 2-D radial flow towards an oil well*, Computers and Mathematics with Applications 1997, Volume 33, pp 121-135
59. Schiffman, R.L., The stress components of a porous medium, J. Geophys. Res., Volume 75, pp 4035-4038, 1970
60. Schweiger H.F., Schuller, H., Pöttler, R., Some remarks on 2-d models for numerical simulations of underground constructions with complex cross sections, Computer methods and advances in geomechanics, Volume 2, pp 1303-1308, Balkema, 1997
61. Seki, J., Noda, K., Washizawa, E., Suzuki, T., Nishimo, K., *Effect of bench length on stability of tunnel face*, Tunneling and Ground Conditions, Balkema, 1994

62. Sinha, R.S. (Editor), *Underground Structures – Design and implementation* Developments in Geotechnical Engineering, 59A, Elsevier, 1989
63. Sinha, R.S. (Editor), *Underground Structures – Design and construction*, Design in Construction, 59B, Elsevier, 1991
64. Skempton, A.W., *Effective Stress in soils*, Concrete and Rock Conf. On Pore Pressure and Suction in Soils, Butterworths, pp 4-16, 1960
65. Soliman, E., Duddeck, H., Ahrens, H., *Effects of development of shotcrete stiffness on stresses and displacements*, Tunneling and Ground Conditions, Balkema, 1994
66. Swoboda, G., *Finite element analysis of the New Austrian Tunneling Method (NATM)*, Third International Conference on Numerical Methods in Geomechanics, Volume 2, pp 581-586, Aachen, 1979
67. Swodoba, G., Moussa, A., Numerical modeling of shotcrete and concrete tunnel linings, Tunneling and Ground Conditions, Balkema, 1994
68. Swoboda, G., *Special problems during the geomechanical analysis of tunnels*, Proceedings of the fourth International Conference on Numerical Methods in Geomechanics, Volume 2, pp 605-609, Edmonton, Canada, 1982
69. Széchy, K., *The art of tunneling*, Akademiai Kiado, Budapest, 1973
70. Tazaki, K., Hirosawa, N., Furube, H., Nakazawa, A., *Design for umbrella method based on numerical analyses and field measurements*, Tunneling and Ground Conditions, Balkema, 1994
71. Vassilev, V.H., Hristov, T.N., *Influence of the heading face and a two-dimensional calculation model for tunnel linings*, Numerical methods in Geomechanics, Volume 3, pp 1551-1555, Balkema, Innsbruck, 1988
72. Vermeer P.A., Verruijt A., An accuracy condition for consolidation by Finite Elements, Int. J. Numer. Anal. Methods Geomech, Volume 5, No 1, pp 1-14, 1981
73. Verruijt, A., Computational Geomechanics – Theory and applications of transport in porous media, Kluwer Academic Publishers, 1995

74. Wagner, H., Schulter, A., *Geonumerical computations for the determination of critical deformations in shallow tunneling*, Numerical Methods in Geomechanics, pp 1531-1536, Innsbruck, 1988
75. Wanning, R., *New Austrian Tunneling method in finite elements*, Third International Conference on Numerical Methods in Geomechanics, Volume 2, pp 587-597, Aachen, 1979
76. Wittke, W., *Rock Mechanics Theory and applications with case histories*, Springer-Verlag, 1990
77. Yamatomi, J., Mogi, G., Yamaguchi, U., *Three dimensional supporting effects of tunnel face*, Computer Methods in Geomechanics, pp 1527-1532, Balkema, 1991
78. Yokoo, Y., Yamagata, K. and Nagaoka, H., *Finite element method applied to Biot's consolidation theory*, Soils and Foundation, Volume 11, No 1, pp 29-46, 1971

$$N = \begin{bmatrix} \frac{c}{s} \psi_1 & \frac{c}{s} \psi_2 & \frac{1}{4} \left(\frac{n}{n-1} \right) r^{1-n} & \frac{1}{4} \left(\frac{-n}{n+1} \right) r^{n+1} & r^{-n-1} & r^{n-1} \\ -\frac{c}{s} \frac{n}{r} \phi_1 & -\frac{c}{s} \frac{n}{r} \phi_2 & \frac{1}{4} \left(\frac{n-2}{n-1} \right) r^{1-n} & \frac{1}{4} \left(\frac{n+2}{n+1} \right) r^{n+1} & r^{-n-1} & -r^{n-1} \\ \left(\frac{\lambda+2G}{2G} \right) \phi_1 & \left(\frac{\lambda+2G}{2G} \right) \phi_2 & \frac{1}{2} r^{-n} & -\frac{1}{2} r^n & 0 & 0 \\ -\frac{c}{s} \left(\frac{n^2}{r^2} \phi_1 - \frac{1}{r} \psi_1 \right) & -\frac{c}{s} \left(\frac{n^2}{r^2} \phi_2 - \frac{1}{r} \psi_2 \right) & \left(\frac{n}{4} + \frac{1}{2} \right) r^{-n} & \left(\frac{n}{4} - \frac{1}{2} \right) r^n & (n+1) r^{-n-2} & -(n-1) r^{n-2} \\ \left(1 + \frac{n^2 c}{r^2 s} \right) \phi_1 - \frac{c}{s} \frac{1}{r} \psi_1 & \left(1 + \frac{n^2 c}{r^2 s} \right) \phi_2 - \frac{c}{s} \frac{1}{r} \psi_2 & \left(-\frac{n}{4} + \frac{1}{2} \right) r^{-n} & -\left(\frac{n}{4} + \frac{1}{2} \right) r^n & -(n+1) r^{-n-2} & (n-1) r^{n-2} \\ -\frac{c}{s} \left(\frac{n}{r^2} \phi_1 - \frac{n}{r} \psi_1 \right) & -\frac{c}{s} \left(\frac{n}{r^2} \phi_2 - \frac{n}{r} \psi_2 \right) & \left(\frac{n}{4} \right) r^{-n} & -\left(\frac{n}{4} \right) r^n & (n+1) r^{-n-2} & (n-1) r^{n-2} \end{bmatrix}$$

where $\phi_1 = K_n \left(\sqrt{\frac{s}{c}} r \right)$, $\phi_2 = I_n \left(\sqrt{\frac{s}{c}} r \right)$, $\psi_1 = \sqrt{\frac{s}{c}} K'_n \left(\sqrt{\frac{s}{c}} r \right)$, $\psi_2 = \sqrt{\frac{s}{c}} I'_n \left(\sqrt{\frac{s}{c}} r \right)$, and I_n, K_n are the modified

a) Unsupported tunnel length $l_u=1\text{m}$

Step Description for excavation in dry mass

<u>During</u>	<u>Action</u>
Step 0 (day 0)	Activation and deactivation of concrete elements
Step 1 (day 1)	Excavation of S12 and C24
Step 2 (day 2)	Excavation of S11, C23 and activation of concrete C24
Step 3 (day 3)	Excavation of S10, C22 and activation of concrete C23
Step 4 (day 4)	Excavation of S9, C21 and activation of concrete C22
Step 5 (day 5)	Excavation of S8, C20 and activation of concrete C21
Step 6 (day 6)	Excavation of S7, C19 and activation of concrete C20
Step 7 (day 7)	Excavation of S6, C18 and activation of concrete C19
Step 8 (day 8)	Excavation of S5, C17 and activation of concrete C18
Step 9 (day 9)	Excavation of S4, C16 and activation of concrete C17
Step 10 (day 10)	Excavation of S3, C15 and activation of concrete C14
Step 11 (day 11)	Excavation of S2, C14 and activation of concrete C15

Step Description for excavation in saturated mass

<u>During</u>	<u>Action</u>
Step 0 (day 0)	Activation and deactivation of concrete elements
Step 1 (day 1)	<div style="display: flex; align-items: center;"> <div style="font-size: 3em; margin-right: 10px;">{</div> <div> Excavation of S12 and C24 – initialization of pore pres. Consolidation of first excavated part </div> </div>
Step 2 (day 2)	Excavation of S11, C23 and activation of concrete C24 + Consolidation of 1 day
Step 3 (day 3)	Excavation of S10, C22 and activation of concrete C23 + Consolidation of 1 day
Step 4 (day 4)	Excavation of S9, C21 and activation of concrete C22 + Consolidation of 1 day
Step 5 (day 5)	Excavation of S8, C20 and activation of concrete C21 + Consolidation of 1 day
Step 6 (day 6)	Excavation of S7, C19 and activation of concrete C20 + Consolidation of 1 day

Step 7 (day 7)	Excavation of S6, C18 and activation of concrete C19 + Consolidation of 1 day
Step 8 (day 8)	Excavation of S5, C17 and activation of concrete C18 + Consolidation of 1 day
Step 9 (day 9)	Excavation of S4, C16 and activation of concrete C17 + Consolidation of 1 day
Step 10 (day 10)	Excavation of S3, C15 and activation of concrete C14 + Consolidation of 1 day
Step 11 (day 11)	Excavation of S2, C14 and activation of concrete C15 + Consolidation of 1 day

b) Unsupported tunnel length $l_u=2m$

Step Description for excavation in dry mass

<u>During</u>	<u>Action</u>
Step 0 (day 0)	Activation and deactivation of concrete elements
Step 1 (day 1)	Excavation of S12, S11, C24 and C23
Step 2 (day 2)	Excavation of S10, C22 and activation of concrete C24
Step 3 (day 3)	Excavation of S9, C21 and activation of concrete C23
Step 4 (day 4)	Excavation of S8, C20 and activation of concrete C22
Step 5 (day 5)	Excavation of S7, C19 and activation of concrete C21
Step 6 (day 6)	Excavation of S6, C18 and activation of concrete C20
Step 7 (day 7)	Excavation of S5, C17 and activation of concrete C19
Step 8 (day 8)	Excavation of S4, C16 and activation of concrete C18
Step 9 (day 9)	Excavation of S3, C15 and activation of concrete C17
Step 10 (day 10)	Excavation of S2, C14 and activation of concrete C16

Step Description for excavation in saturated mass

<u>During</u>	<u>Action</u>
Step 0 (day 0)	Activation and deactivation of concrete elements
Step 1 (day 1)	<div style="display: flex; align-items: center;"> <div style="font-size: 3em; margin-right: 10px;">{</div> <div> Excavation of S12,S11,C24,C23-initialization of pore pres. Consolidation of first excavated part </div> </div>

Step 2 (day 2)	Excavation of S10, C22 and activation of concrete C24 + Consolidation of 1 day
Step 3 (day 3)	Excavation of S9, C21 and activation of concrete C23 + Consolidation of 1 day
Step 4 (day 4)	Excavation of S8, C20 and activation of concrete C22 + Consolidation of 1 day
Step 5 (day 5)	Excavation of S7, C19 and activation of concrete C21 + Consolidation of 1 day
Step 6 (day 6)	Excavation of S6, C18 and activation of concrete C20 + Consolidation of 1 day
Step 7 (day 7)	Excavation of S5, C17 and activation of concrete C19 + Consolidation of 1 day
Step 8 (day 8)	Excavation of S4, C16 and activation of concrete C18 + Consolidation of 1 day
Step 9 (day 9)	Excavation of S3, C15 and activation of concrete C17 + Consolidation of 1 day
Step 10 (day 10)	Excavation of S2, C14 and activation of concrete C16 + Consolidation of 1 day

c) Unsupported tunnel length $l_u=3m$

Step Description for excavation in dry mass

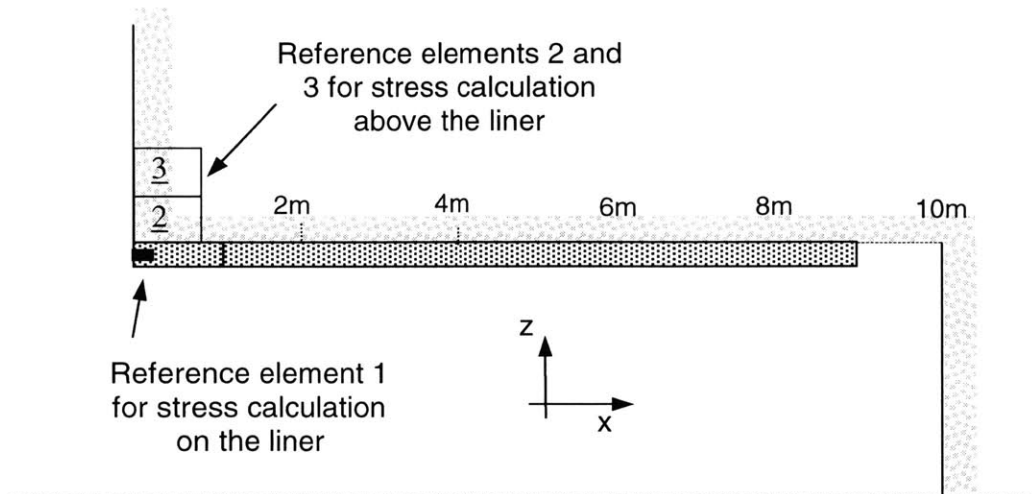
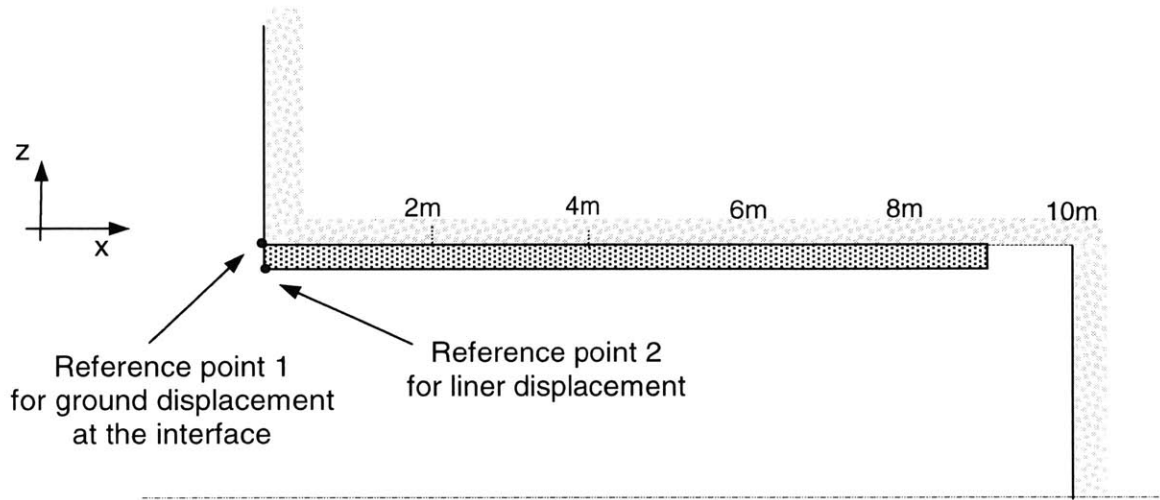
<u>During</u>	<u>Action</u>
Step 0 (day 0)	Activation and deactivation of concrete elements
Step 1 (day 1)	Excavation of S12, S11, S10, C24, C23 and C22
Step 2 (day 2)	Excavation of S9, C21 and activation of concrete C24
Step 3 (day 3)	Excavation of S8, C20 and activation of concrete C23
Step 4 (day 4)	Excavation of S7, C19 and activation of concrete C22
Step 5 (day 5)	Excavation of S6, C18 and activation of concrete C21
Step 6 (day 6)	Excavation of S5, C17 and activation of concrete C20
Step 7 (day 7)	Excavation of S4, C16 and activation of concrete C19

Step 8 (day 8)	Excavation of S3, C15 and activation of concrete C18
Step 9 (day 9)	Excavation of S2, C14 and activation of concrete C17

Step Description for excavation in saturated mass

<u>During</u>	<u>Action</u>
Step 0 (day 0)	Activation and deactivation of concrete elements
Step 1 (day 1)	<div> <div>Excav S12,S11,S10,C24,C23,C22-initialization of pore pres</div> <div>Consolidation of first excavated part</div> </div>
Step 2 (day 2)	Excavation of S9, C21 and activation of concrete C24 + Consolidation of 1 day
Step 3 (day 3)	Excavation of S8, C20 and activation of concrete C23 + Consolidation of 1 day
Step 4 (day 4)	Excavation of S7, C19 and activation of concrete C22 + Consolidation of 1 day
Step 5 (day 5)	Excavation of S6, C18 and activation of concrete C21 + Consolidation of 1 day
Step 6 (day 6)	Excavation of S5, C17 and activation of concrete C20 + Consolidation of 1 day
Step 7 (day 7)	Excavation of S4, C16 and activation of concrete C19 + Consolidation of 1 day
Step 8 (day 8)	Excavation of S3, C15 and activation of concrete C18 + Consolidation of 1 day
Step 9 (day 9)	Excavation of S2, C14 and activation of concrete C17

APPENDIX III



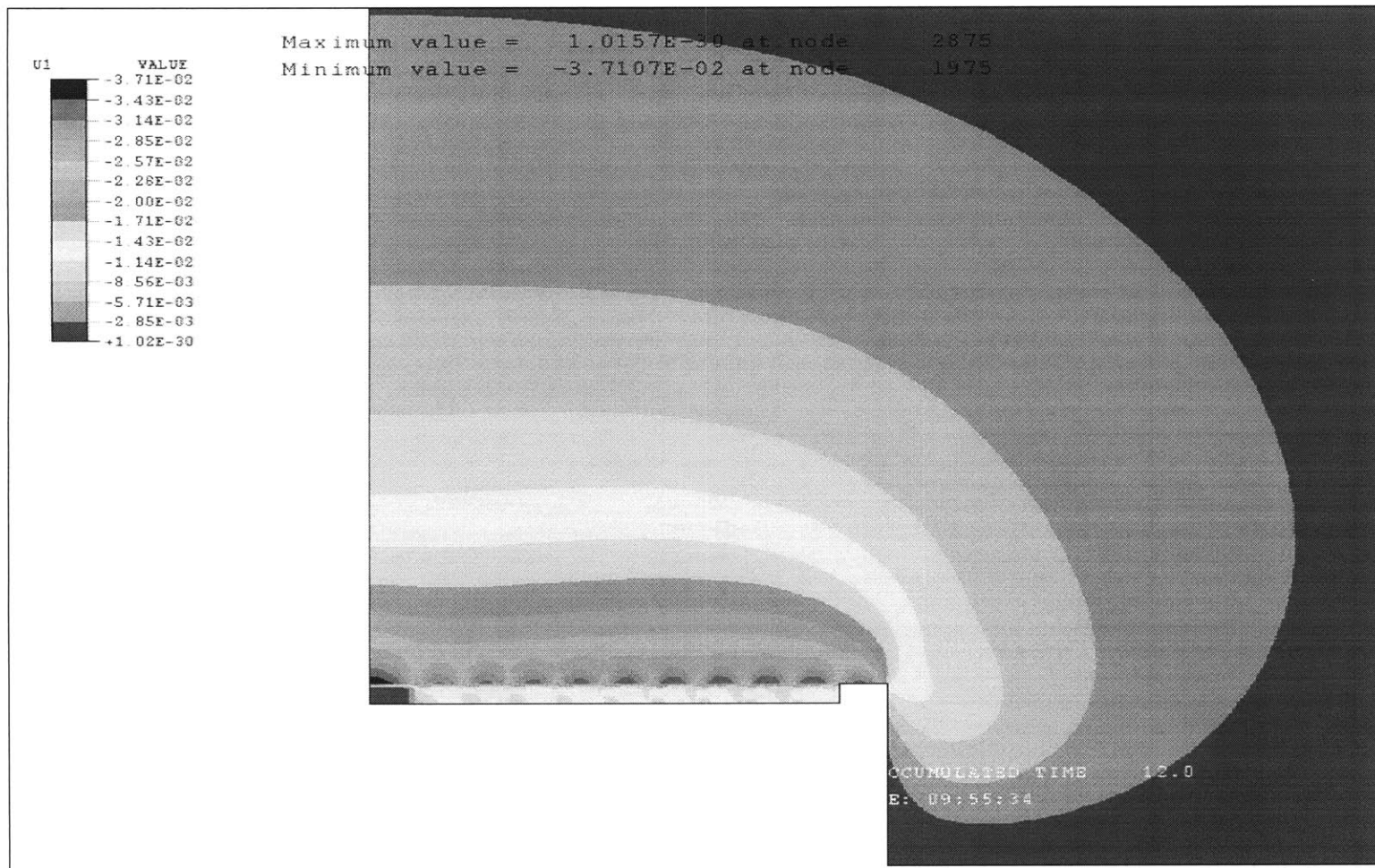


Figure 1. Displacement in the vertical direction at the end of excavation (dry conditions – $l_u=1\text{m}$)

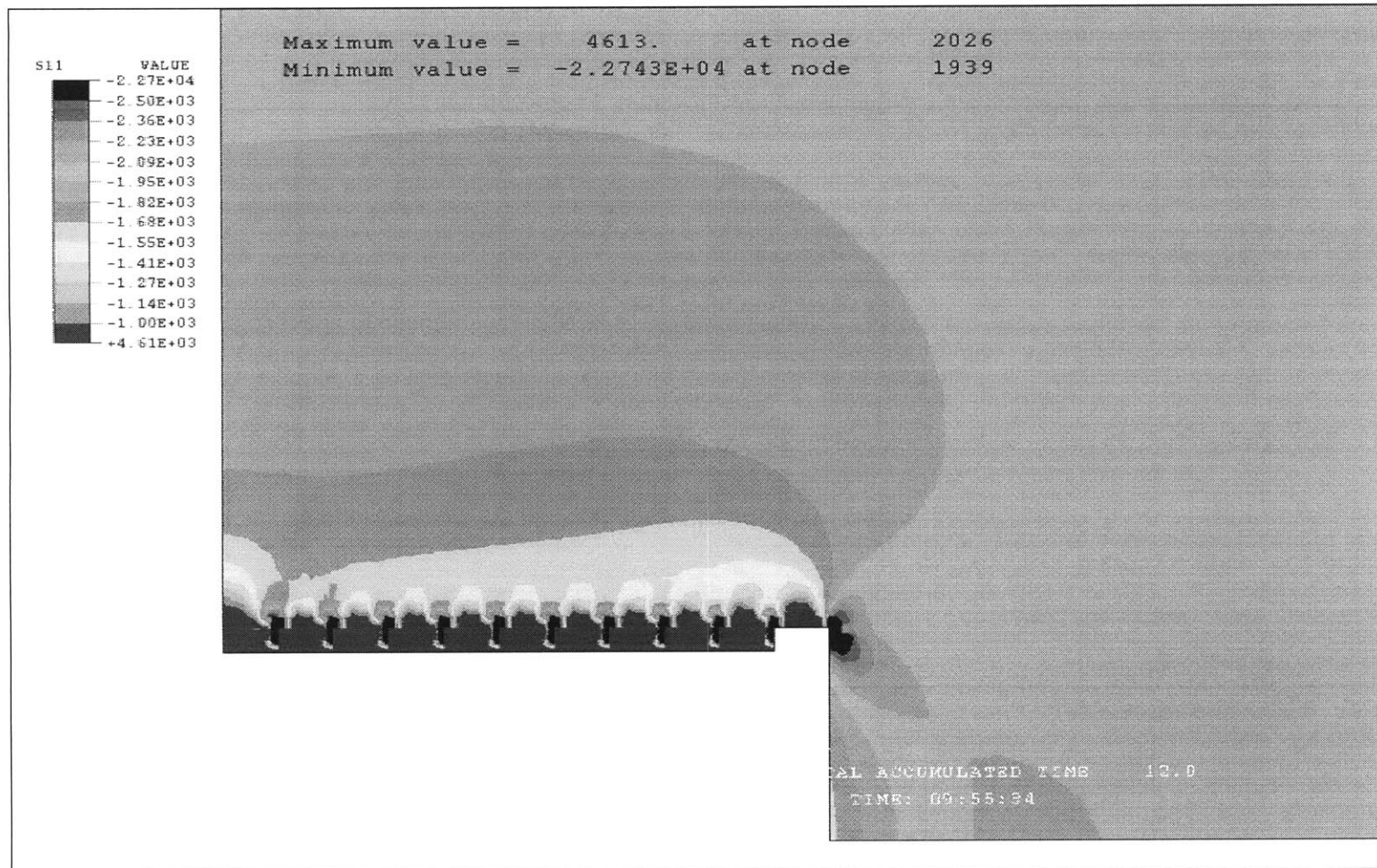


Figure 2. Stress in the vertical direction at the end of excavation (dry conditions – $l_u=1\text{m}$)

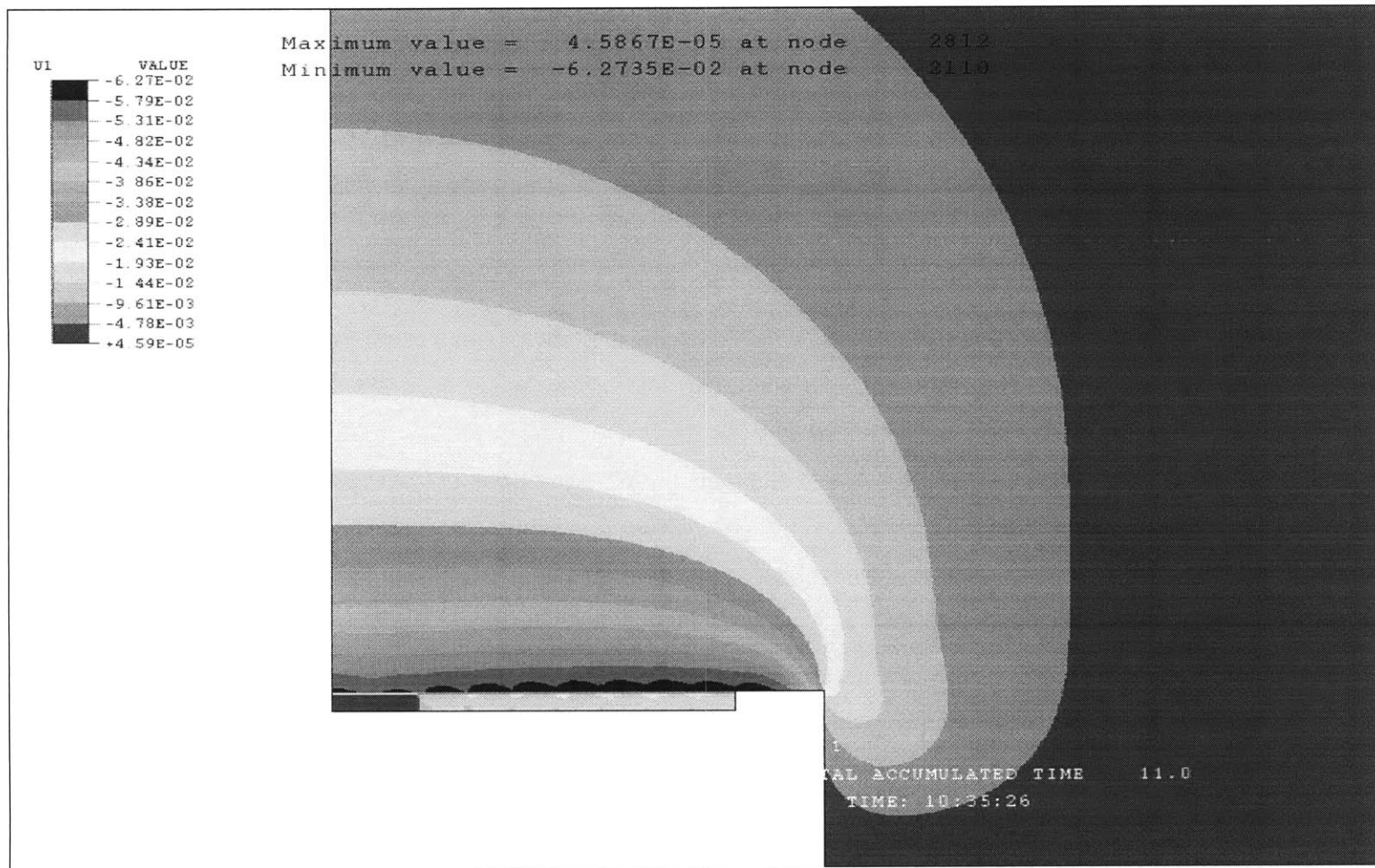


Figure 3. Displacement in the vertical direction at the end of excavation (dry conditions – $l_u=2\text{m}$)

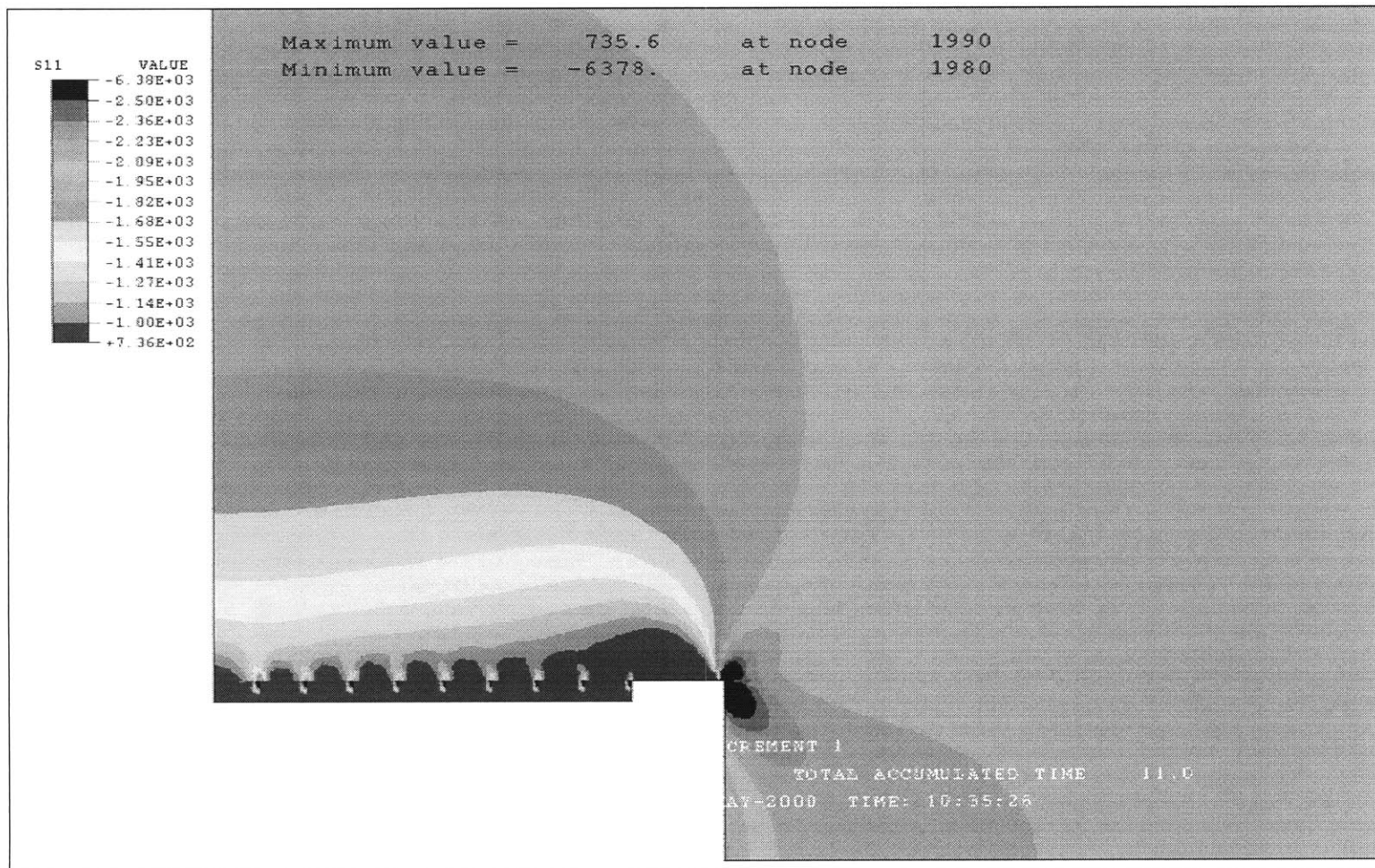


Figure 4. Stress in the vertical direction at the end of excavation (dry conditions – $l_u=2\text{m}$)

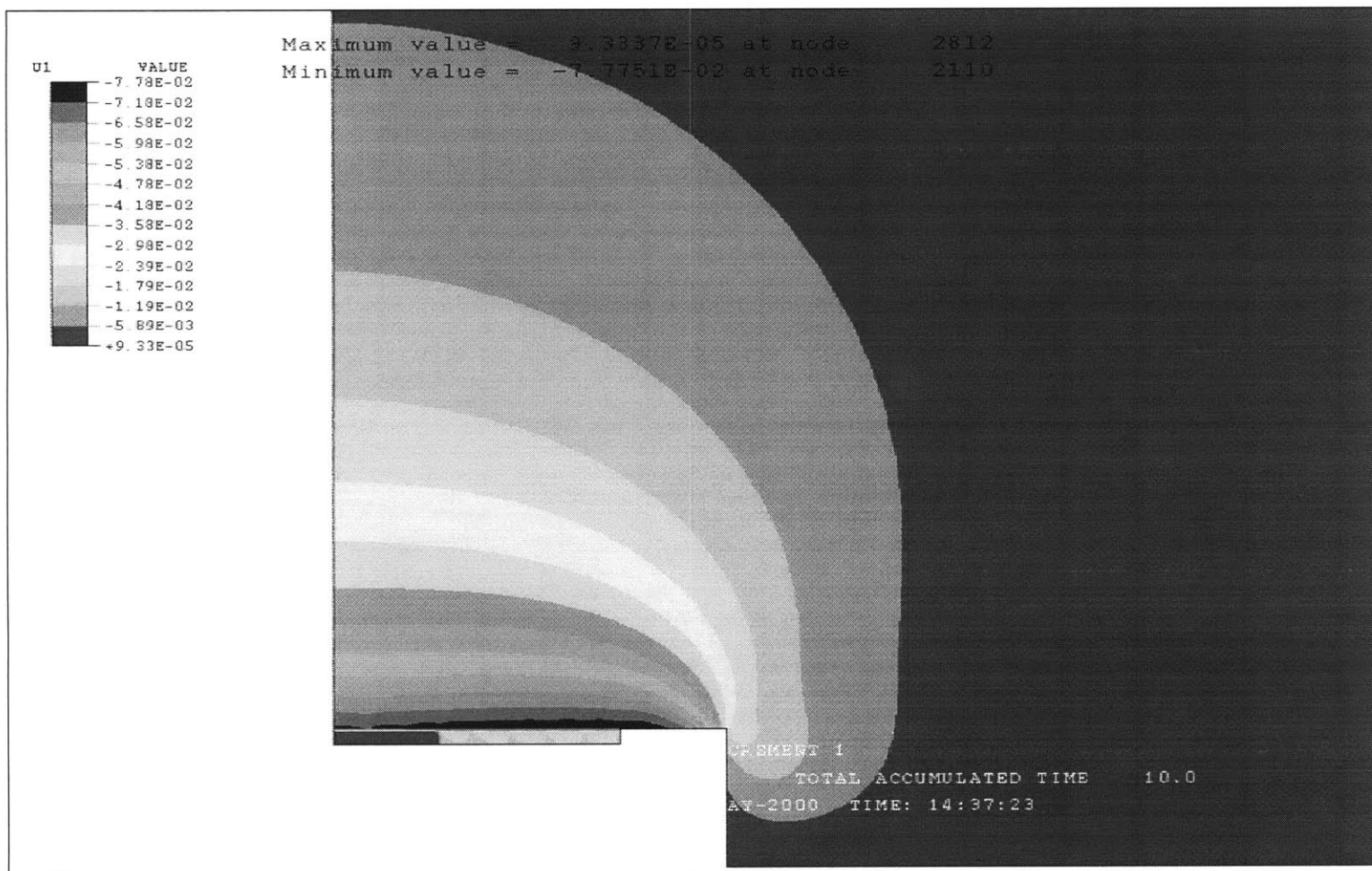


Figure 5. Displacement in the vertical direction at the end of excavation (dry conditions – $l_u=3\text{m}$)

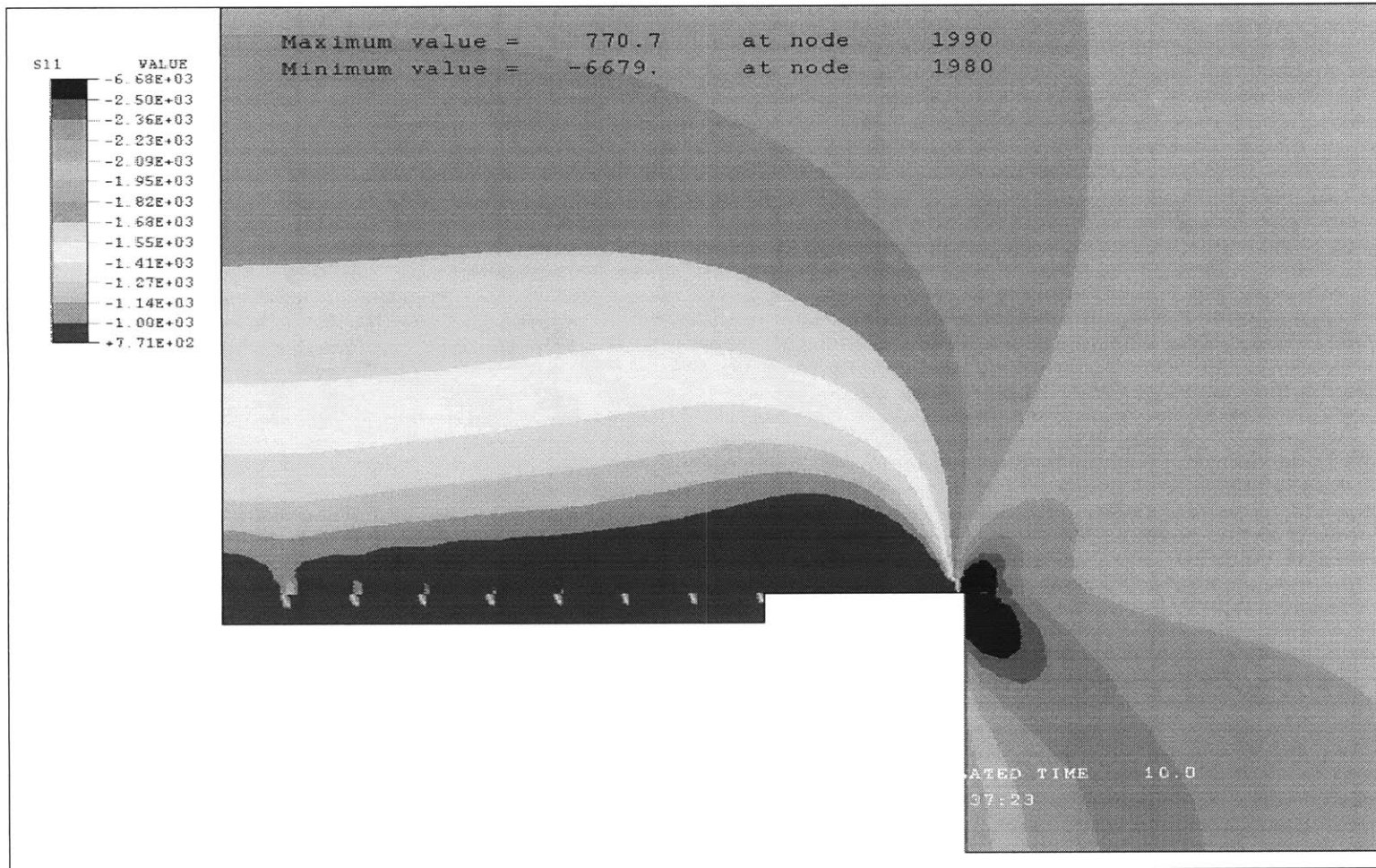


Figure 6. Stress in the vertical direction at the end of excavation (dry conditions – $l_u=3\text{m}$)

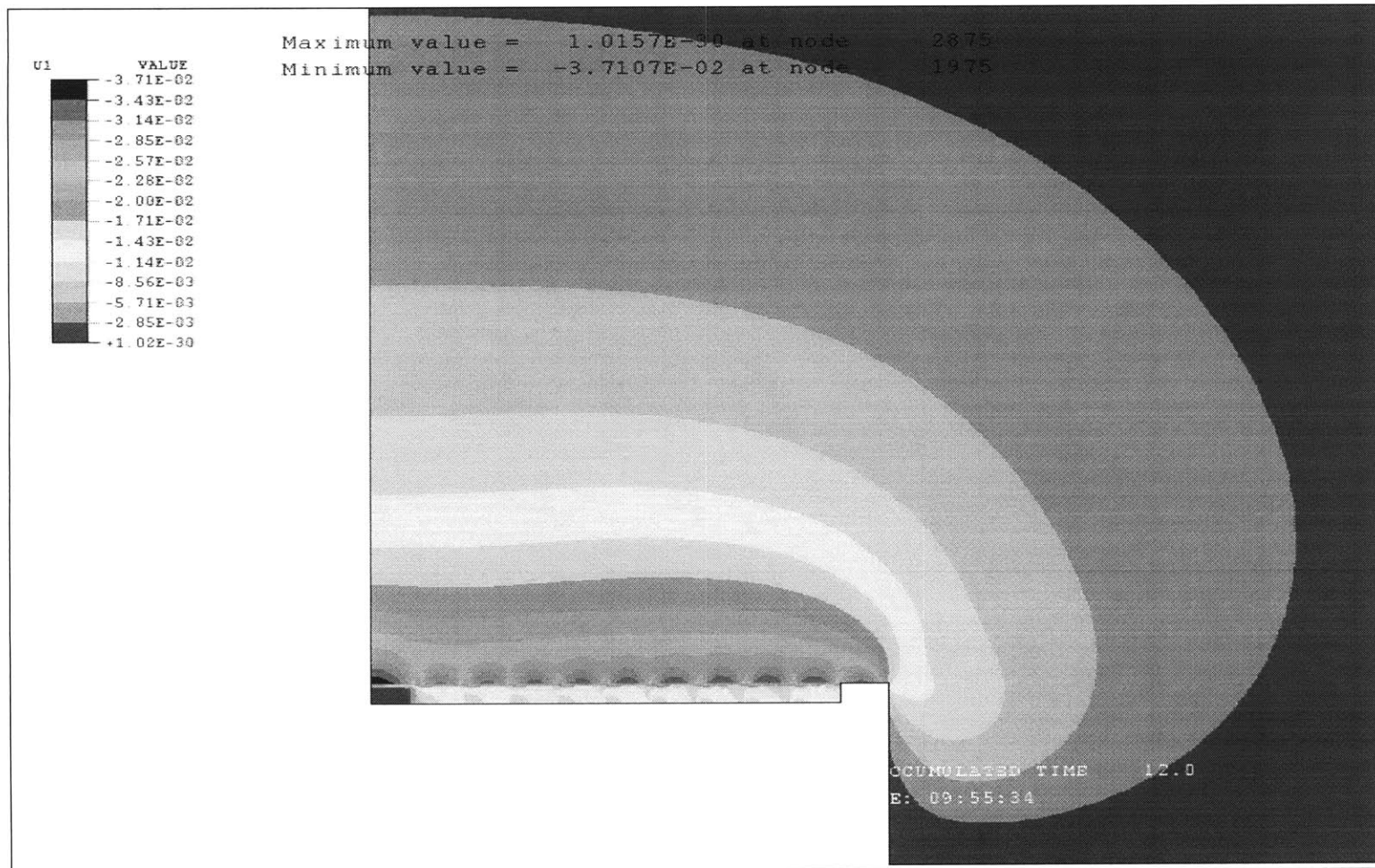


Figure 7. Displacement in the vertical direction at the end of excavation
 (wet conditions – Consolidation time=10 days - $l_0=1\text{m}$)

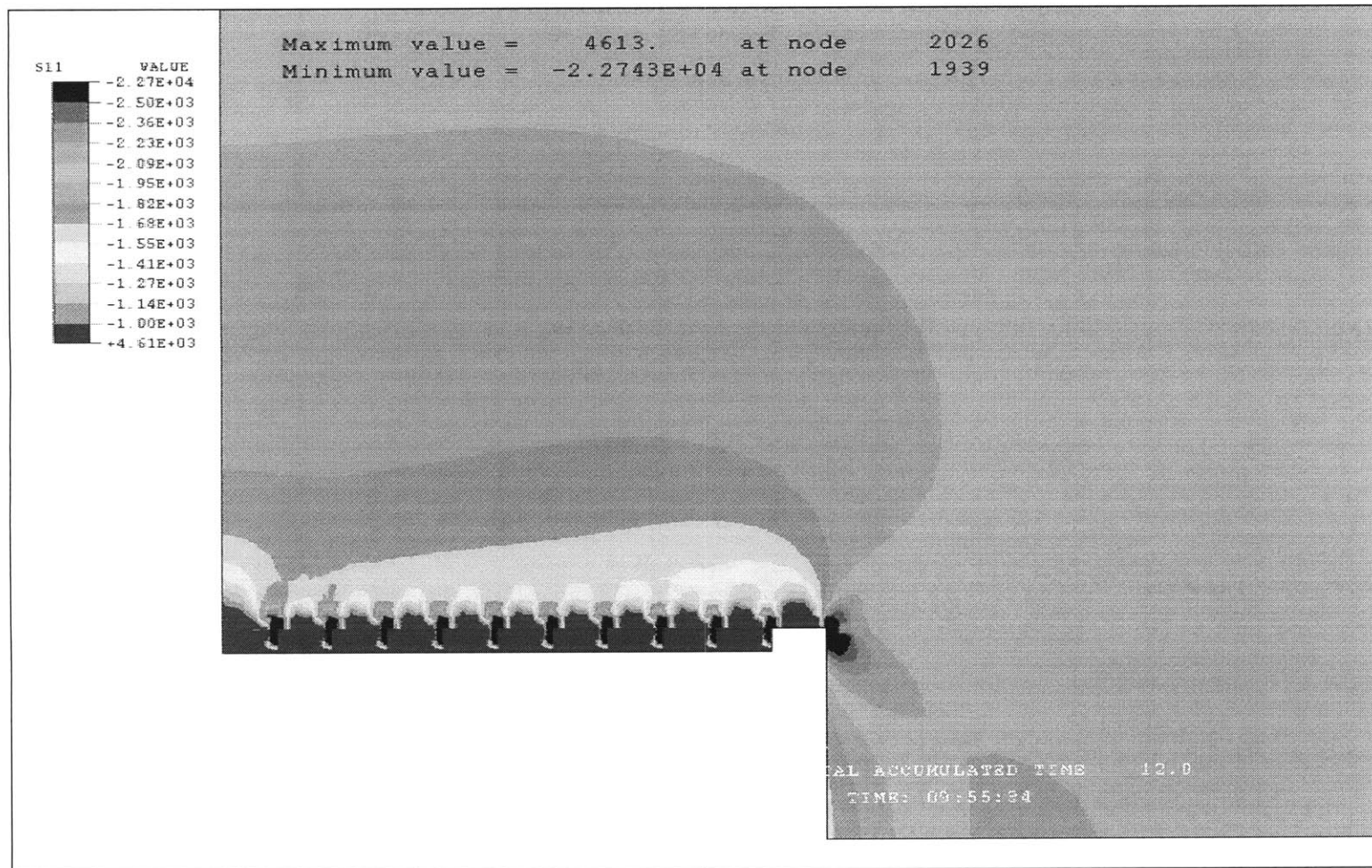


Figure 8. Stress in the vertical direction at the end of excavation
 (wet conditions – Consolidation time=10 days - $I_u=1\text{m}$)

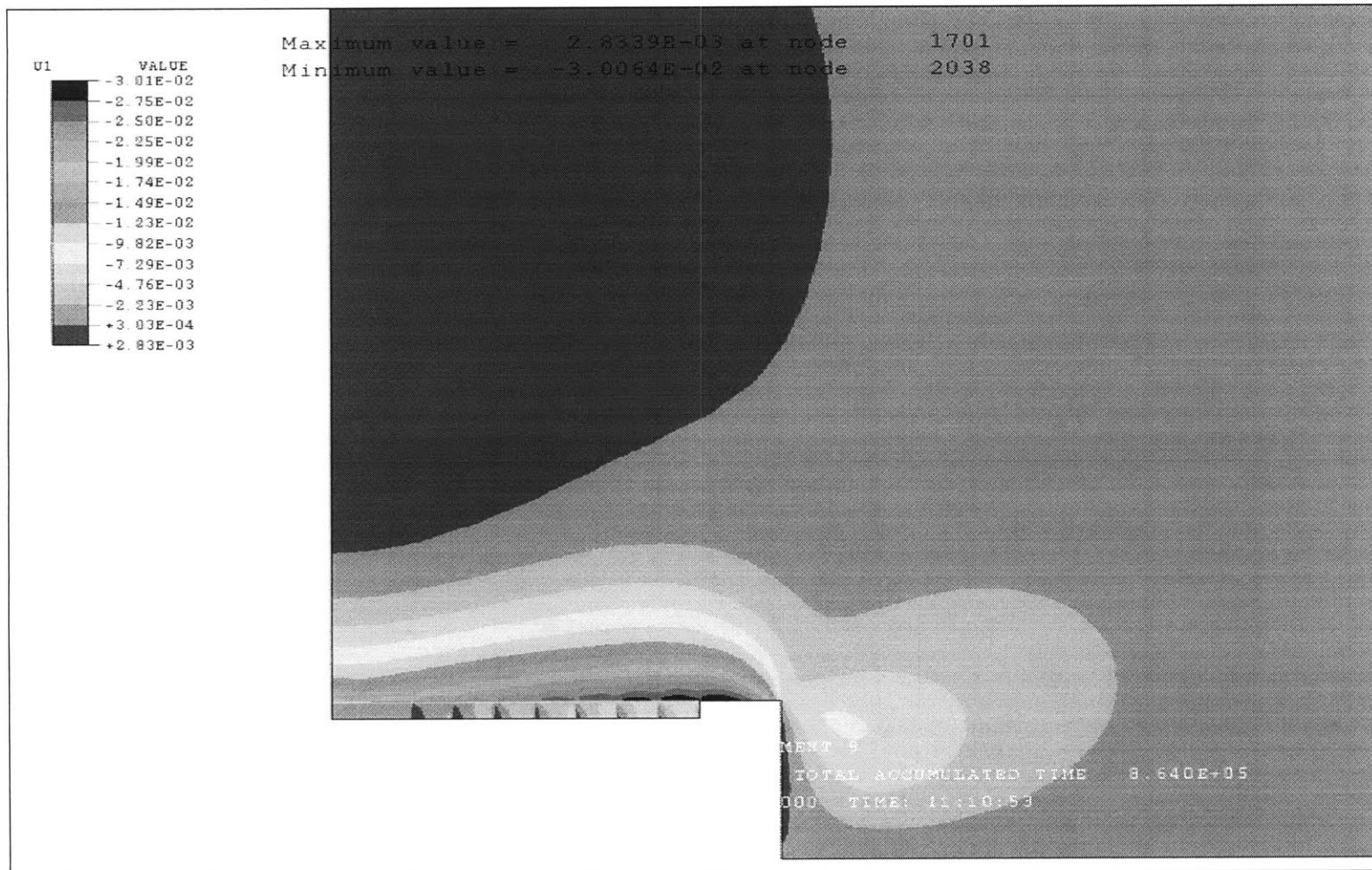


Figure 9. Displacement in the vertical direction at the end of excavation
 (wet conditions – Consolidation time=10 days - $l_u=2\text{m}$)

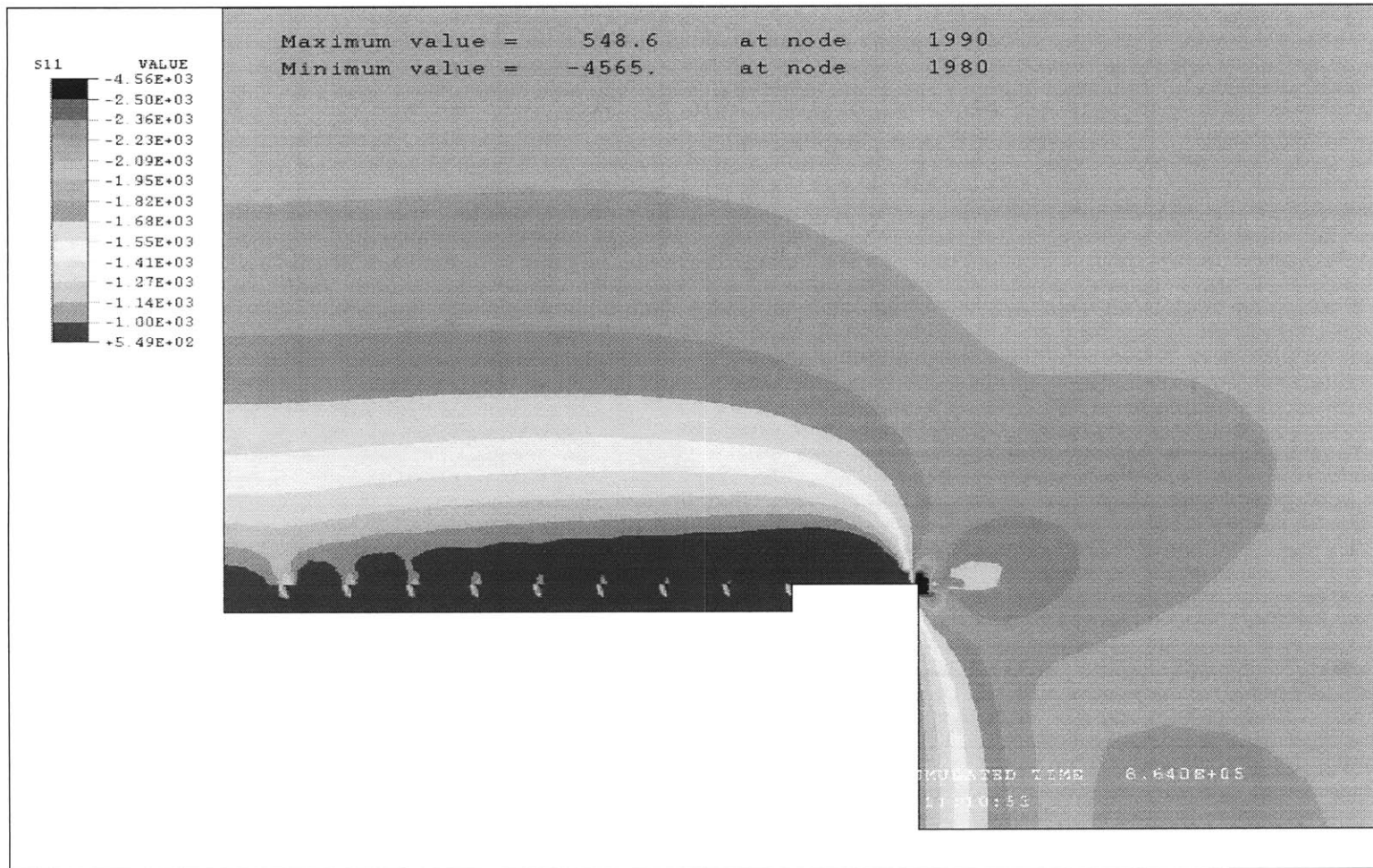


Figure 10. Stress in the vertical direction at the end of excavation
(wet conditions – Consolidation time=10 days - $l_u=2\text{m}$)

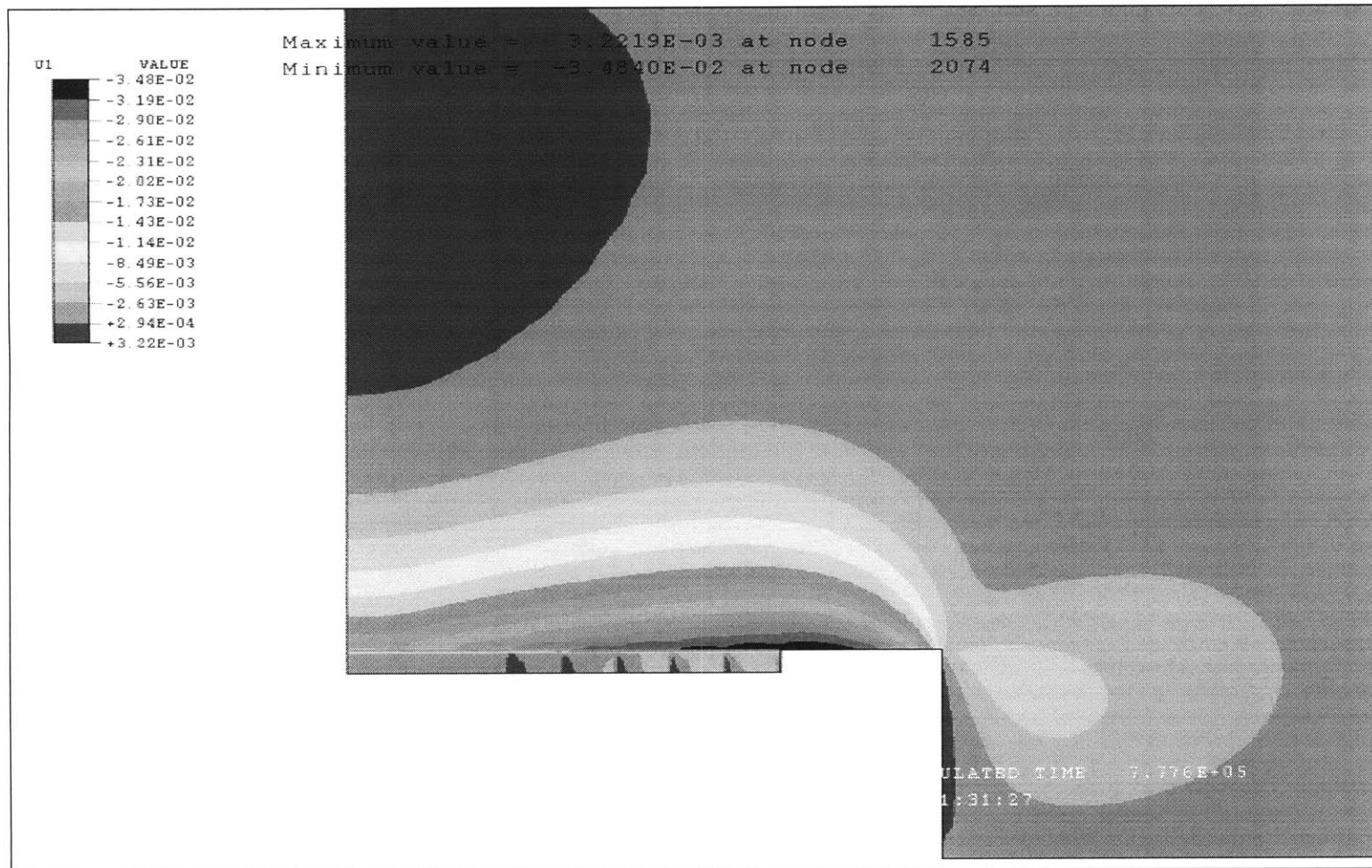


Figure 11. Displacement in the vertical direction at the end of excavation
 (wet conditions – Consolidation time=10 days - $l_u=3\text{m}$)

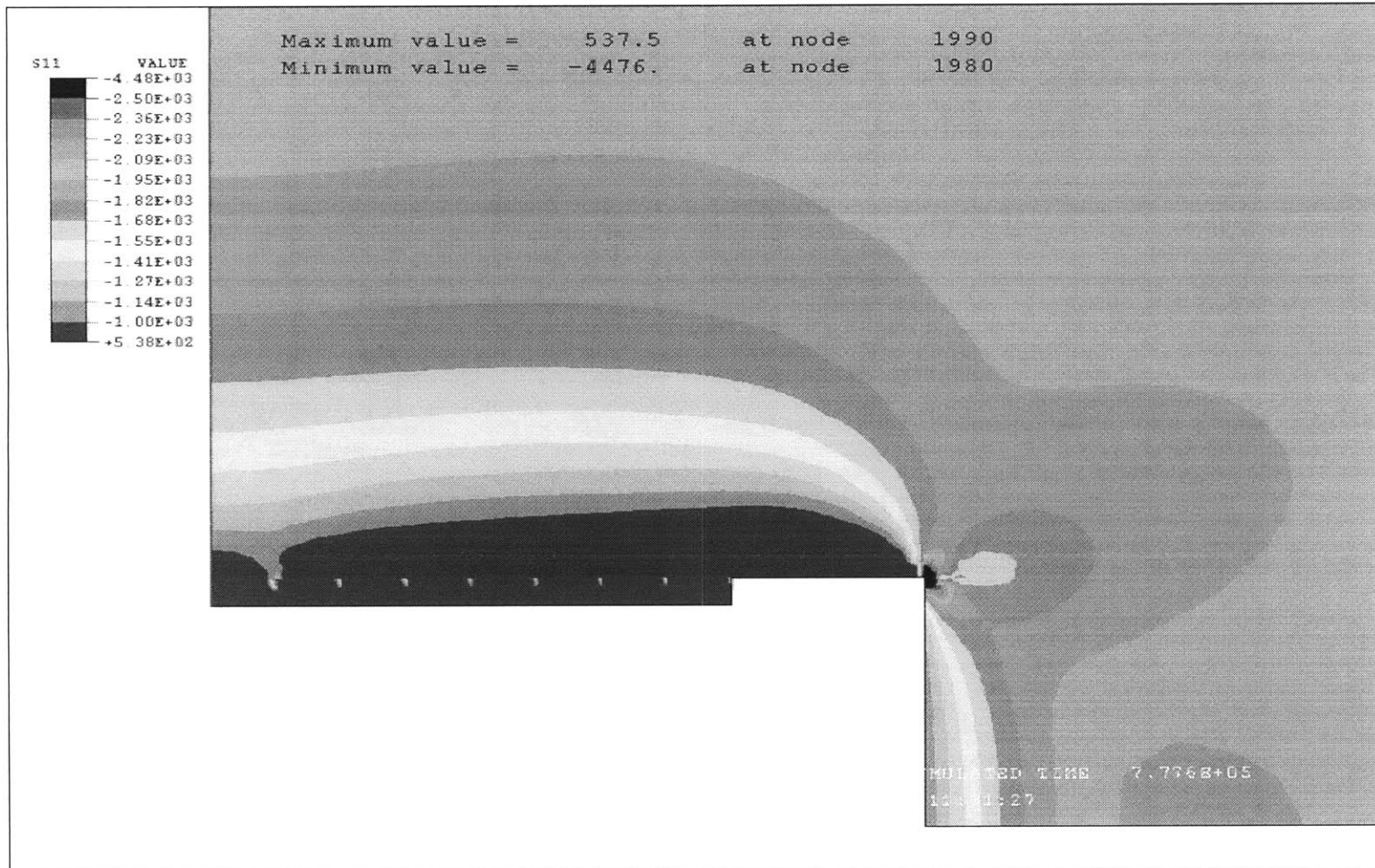


Figure 12. Stress in the vertical direction at the end of excavation
(wet conditions – Consolidation time=10 days - $l_u=1\text{m}$)

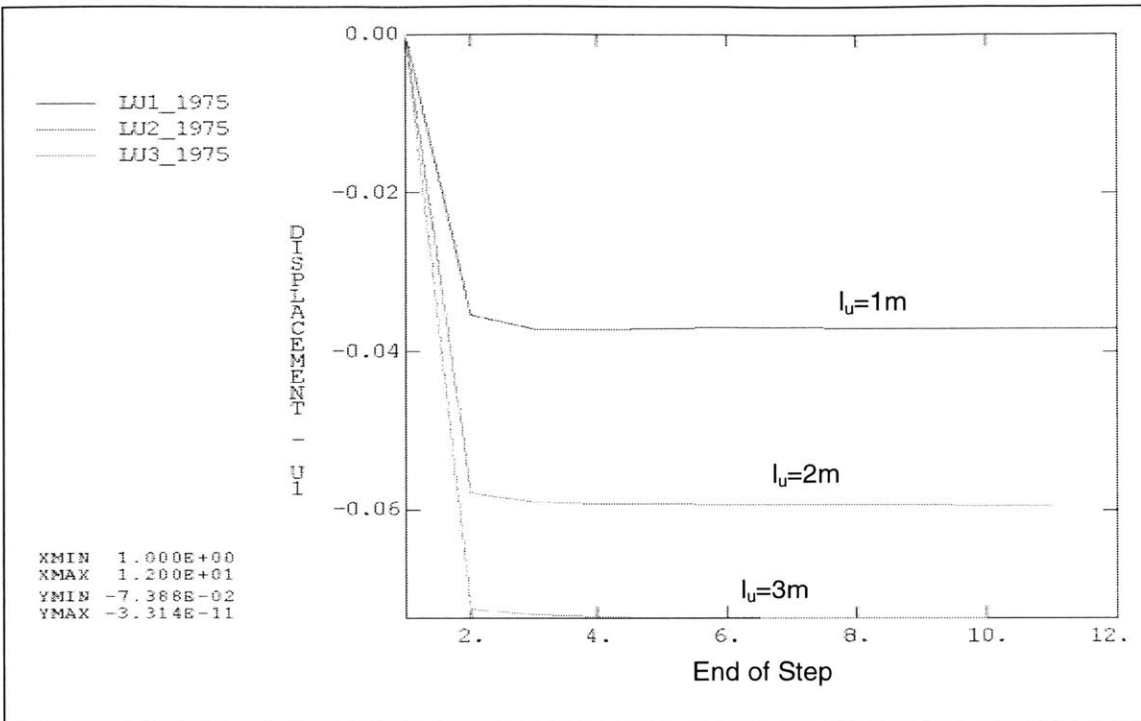


Figure 13. Variation of vertical displacement during the excavation (dry conditions – $l_u = 1m$, $l_u = 2m$, $l_u = 3m$ – reference point 1)

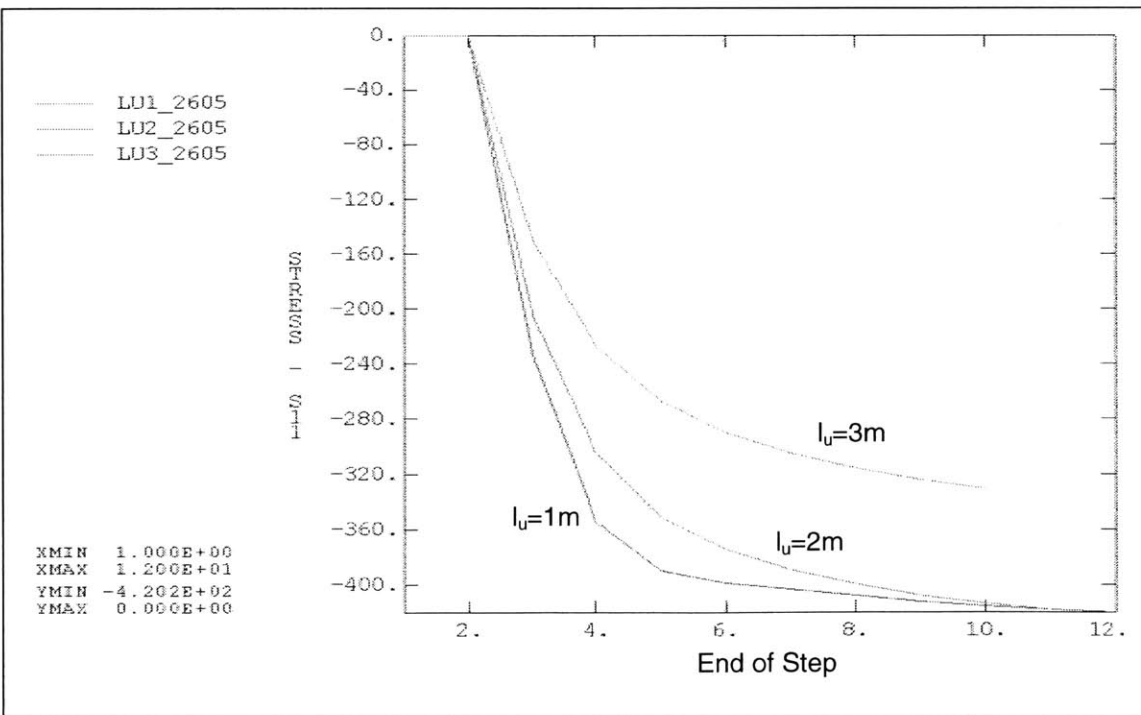


Figure 14. Variation of vertical stress during the excavation (dry conditions – $l_u = 1m$, $l_u = 2m$, $l_u = 3m$ – reference element 1)

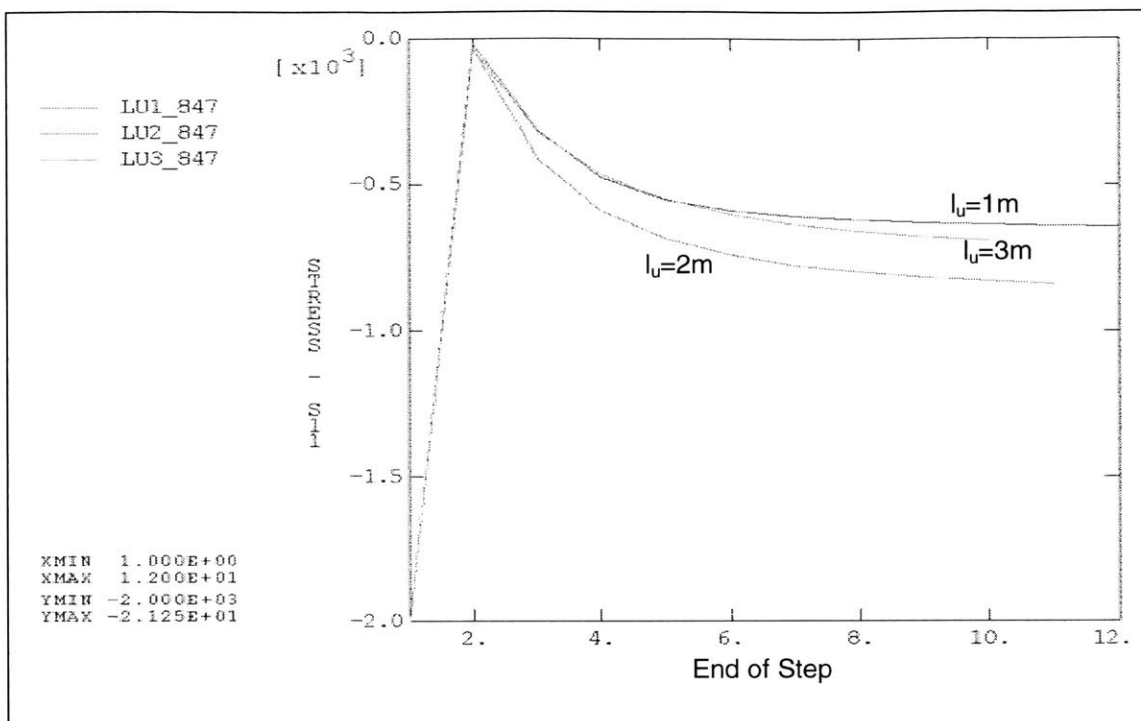


Figure 15. Variation of vertical stress during the excavation (dry conditions – $l_u=1m$, $l_u=2m$, $l_u=3m$ – reference element 2)

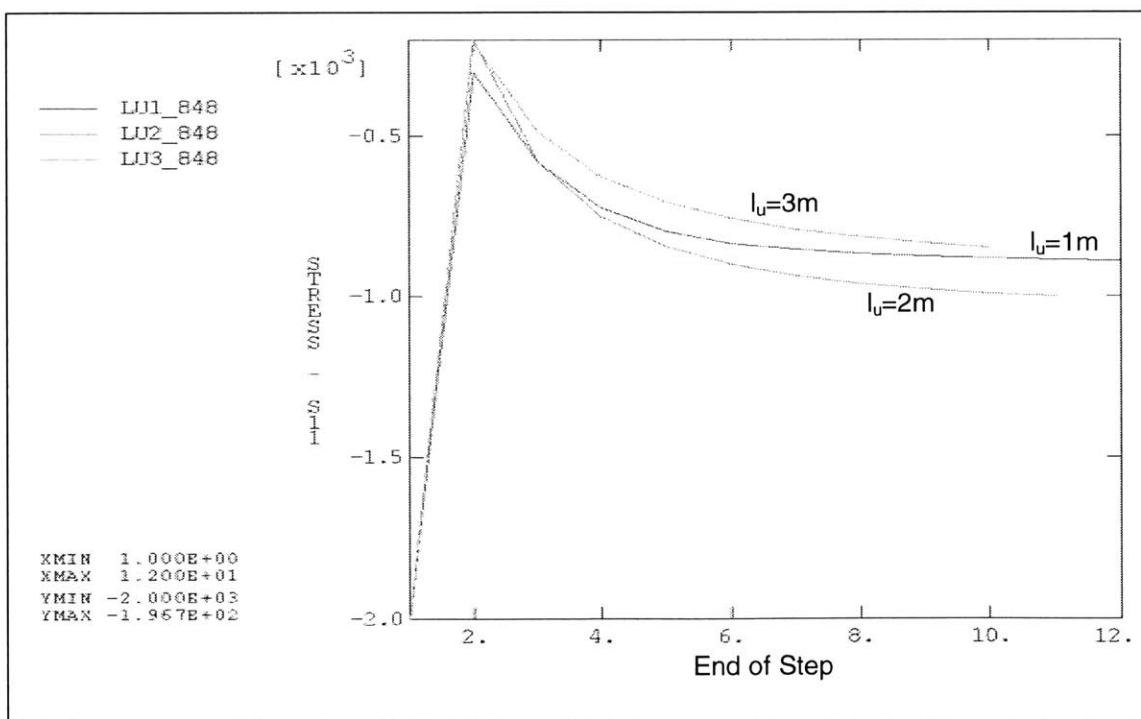


Figure 16. Variation of vertical stress during the excavation (dry conditions – $l_u=1m$, $l_u=2m$, $l_u=3m$ – reference element 3)

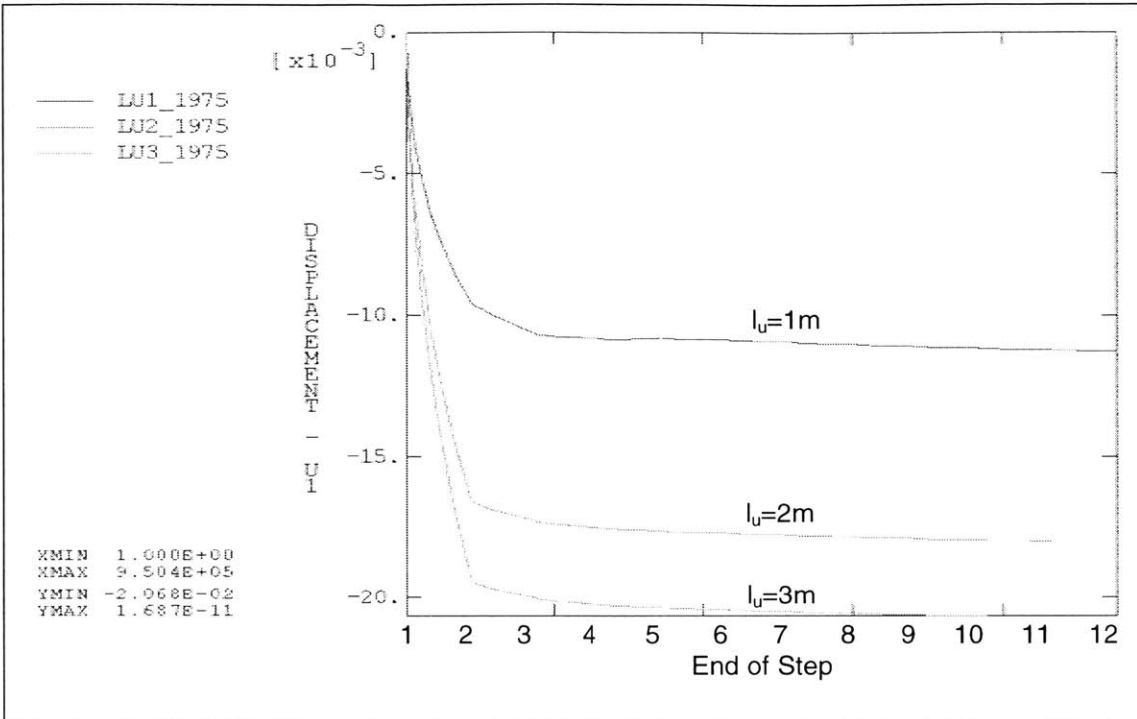


Figure 17. Variation of vertical displacement during the excavation (wet conditions – consolidation time=10days, $l_u=1m$, $l_u=2m$, $l_u=3m$ – ref. point1)

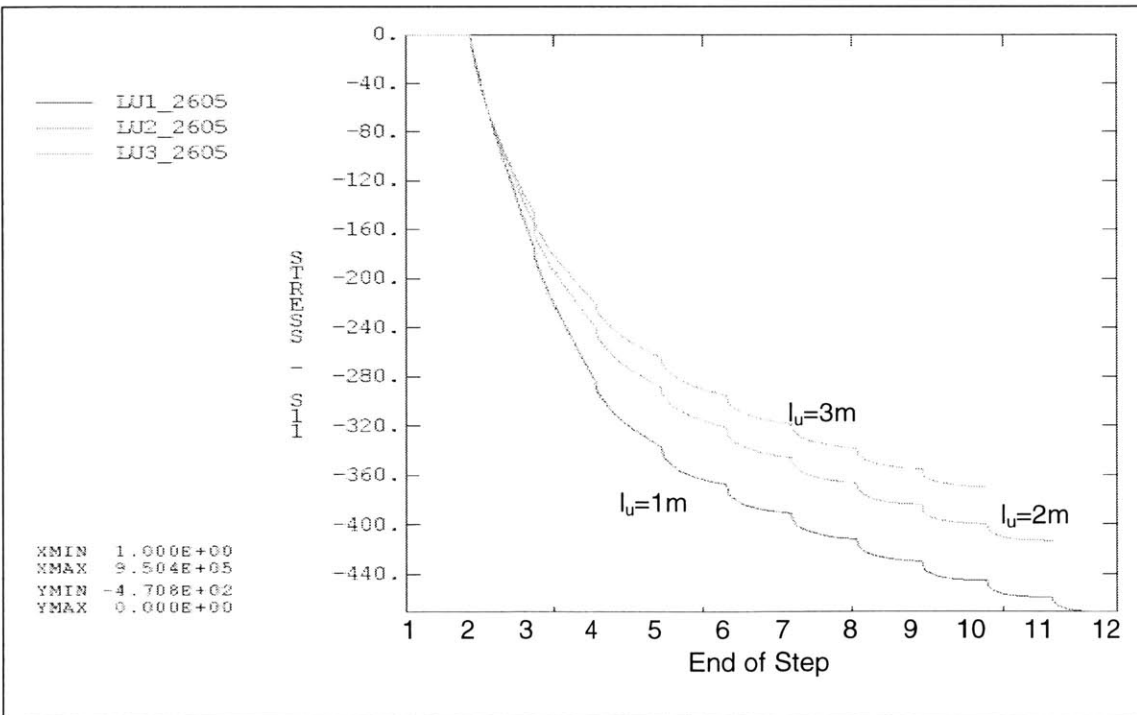


Figure 18. Variation of vertical stress during the excavation (wet conditions – consolidation time=10days, $l_u=1m$, $l_u=2m$, $l_u=3m$ – ref. elem 1)

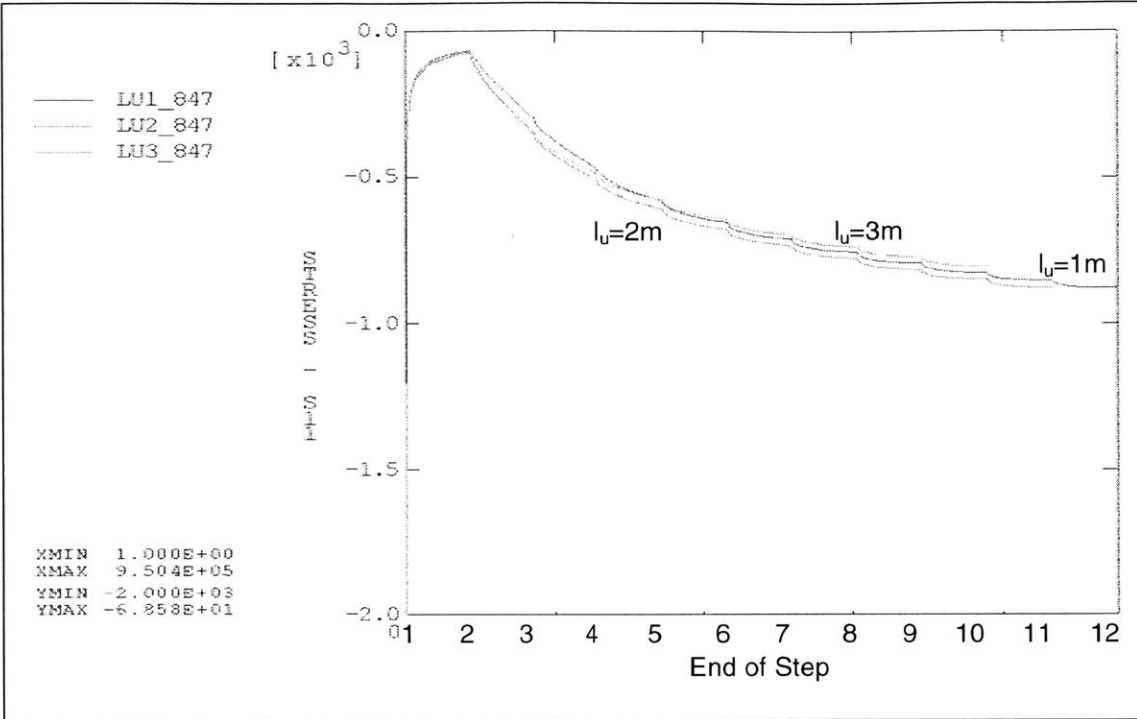


Figure 19. Variation of vertical stress during the excavation (wet conditions – consolidation time=10days, $l_u=1m$, $l_u=2m$, $l_u=3m$ – ref. elem. 2)

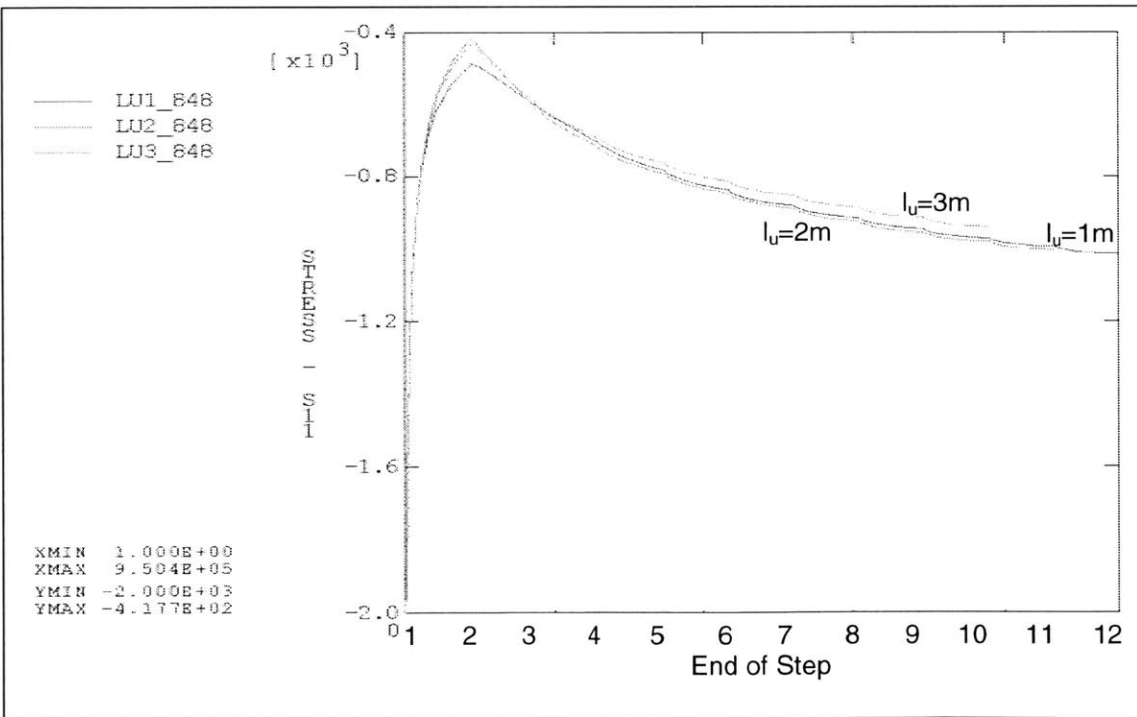


Figure 20. Variation of vertical stress during the excavation (wet conditions – consolidation time=10days, $l_u=1m$, $l_u=2m$, $l_u=3m$ – ref. elem 3)

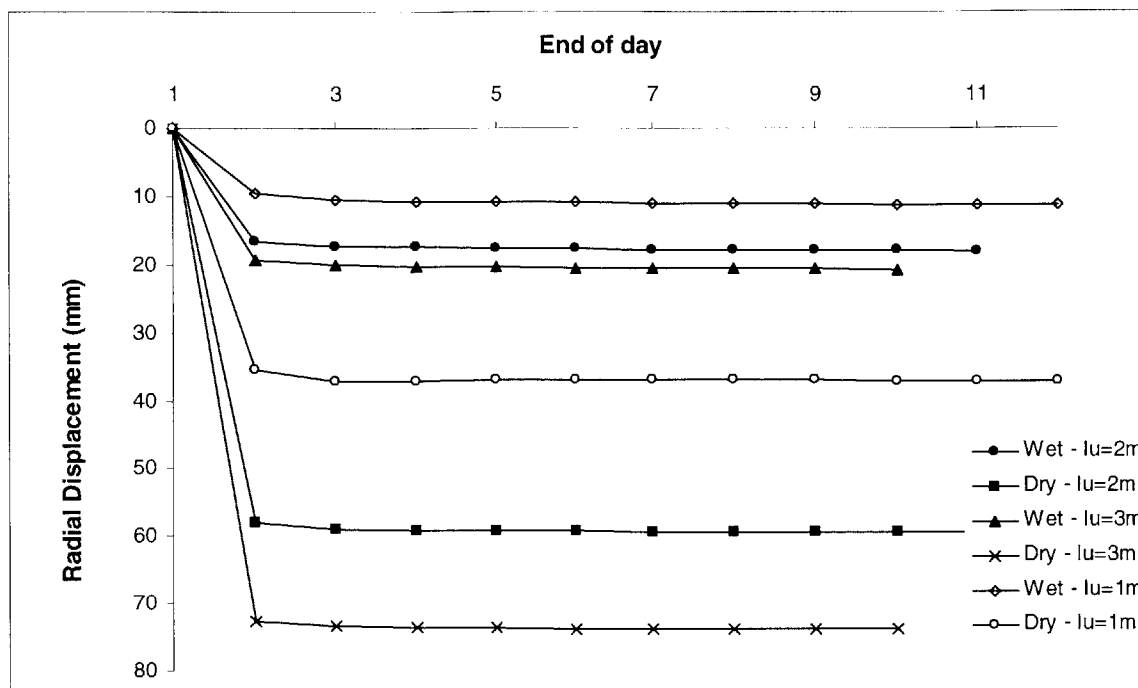


Figure 21. Variation of vertical displacement during the excavation (dry and wet – consol. time=10days, $l_u=1m$, $l_u=2m$, $l_u=3m$ – ref. point. 1)

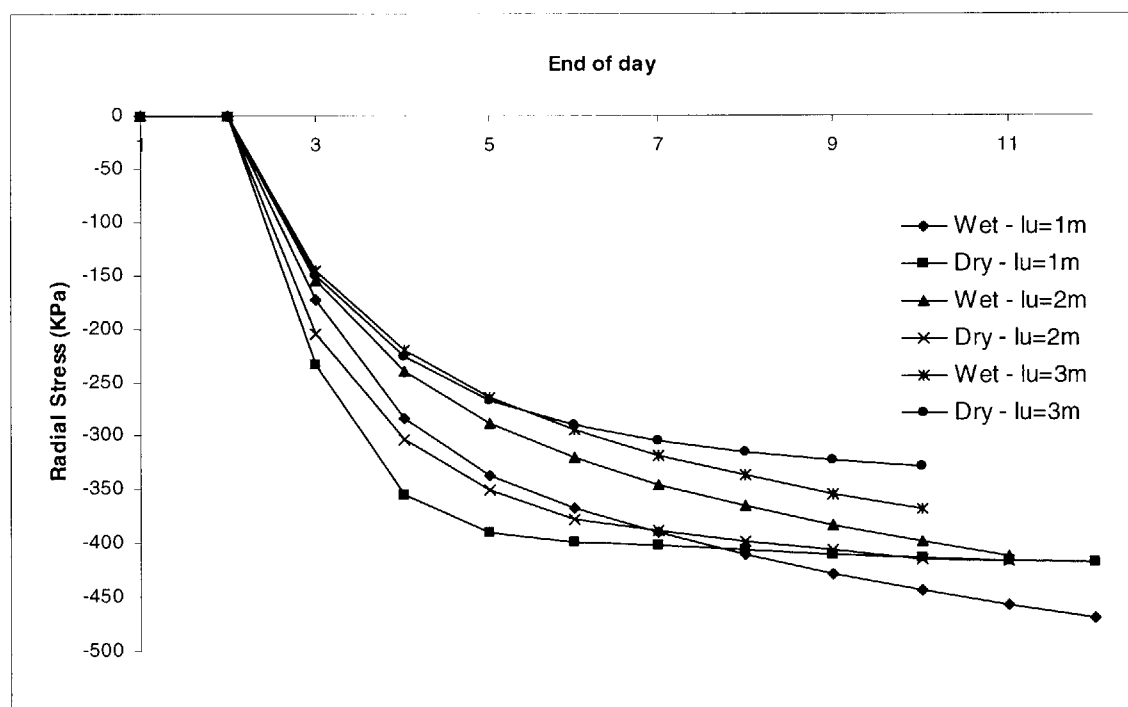


Figure 22. Variation of vertical stress during the excavation (dry and wet – consol. time=10days, $l_u=1m$, $l_u=2m$, $l_u=3m$ – ref. elem. 1)

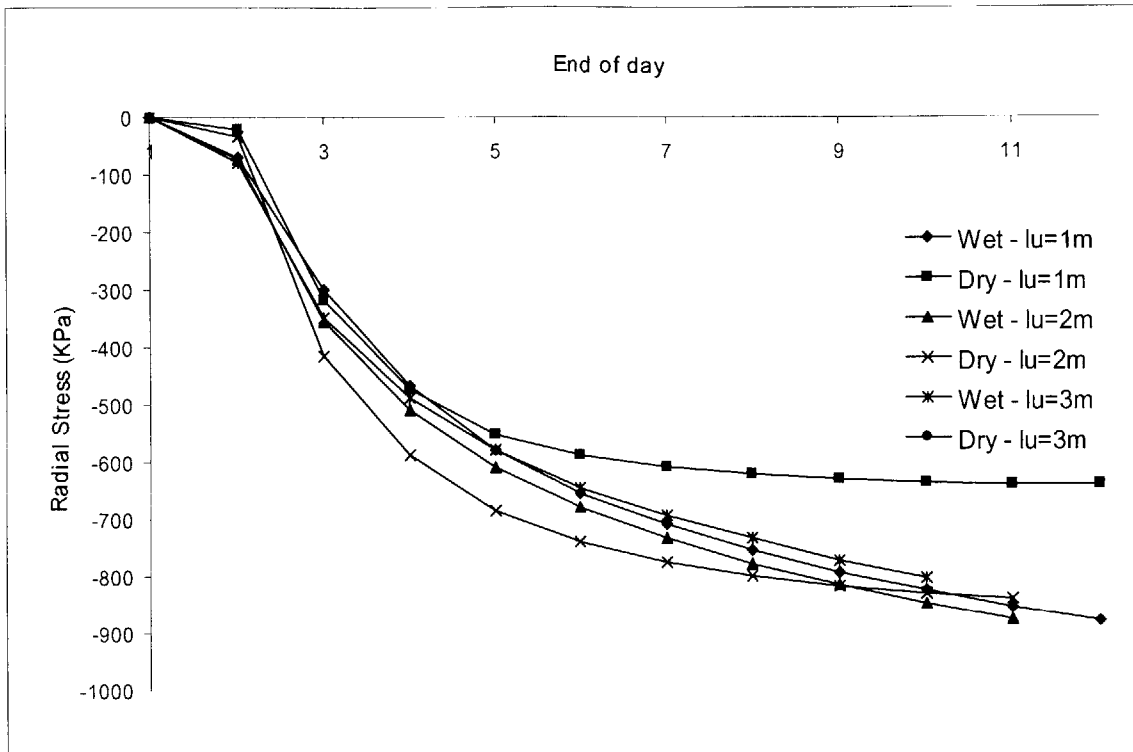


Figure 23. Variation of vertical displacement during the excavation (dry and wet – consol. time=10days, $l_u=1m$, $l_u=2m$, $l_u=3m$ – ref. point. 2)

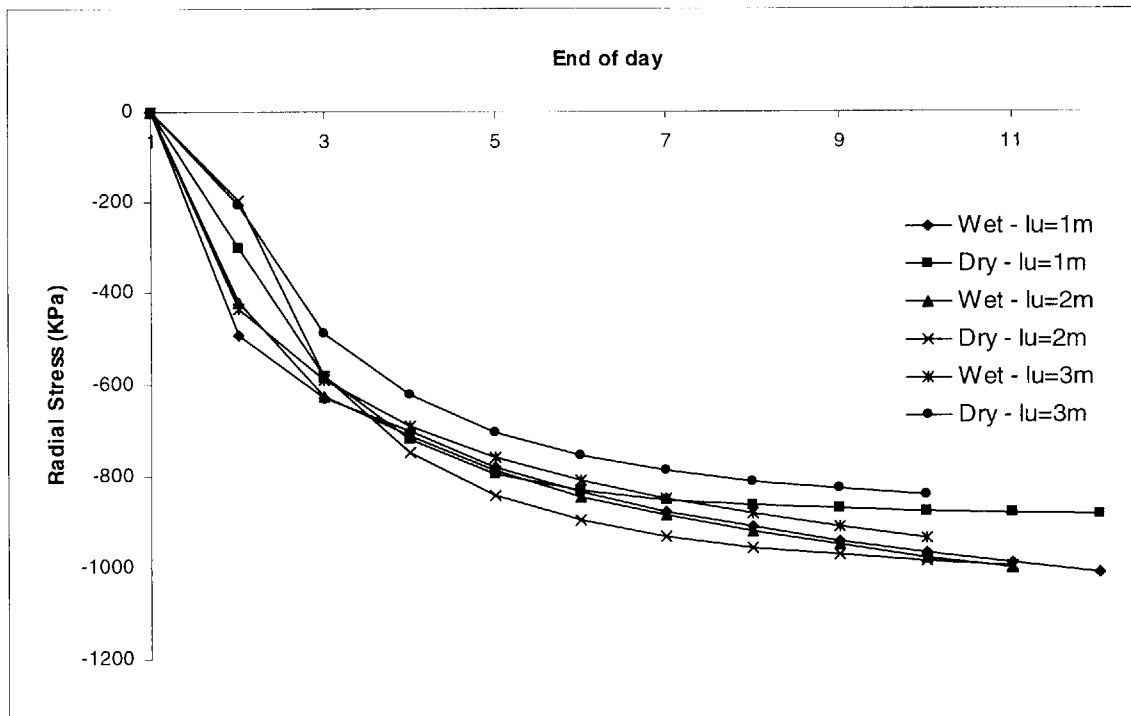


Figure 24. Variation of vertical displacement during the excavation (dry and wet – consol. time=10days, $l_u=1m$, $l_u=2m$, $l_u=3m$ – ref. point. 3)

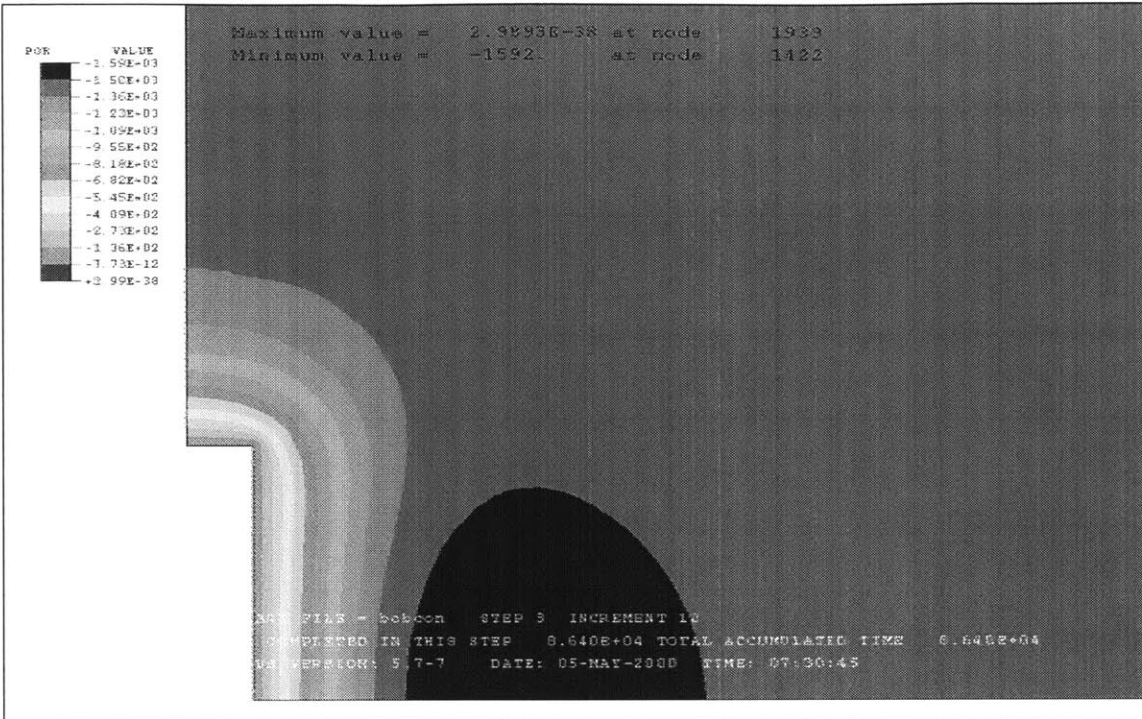


Figure 25. Variation of pore pressures after excavation of one meter (wet conditions - consolidation time=1 day - $l_u=1\text{m}$)

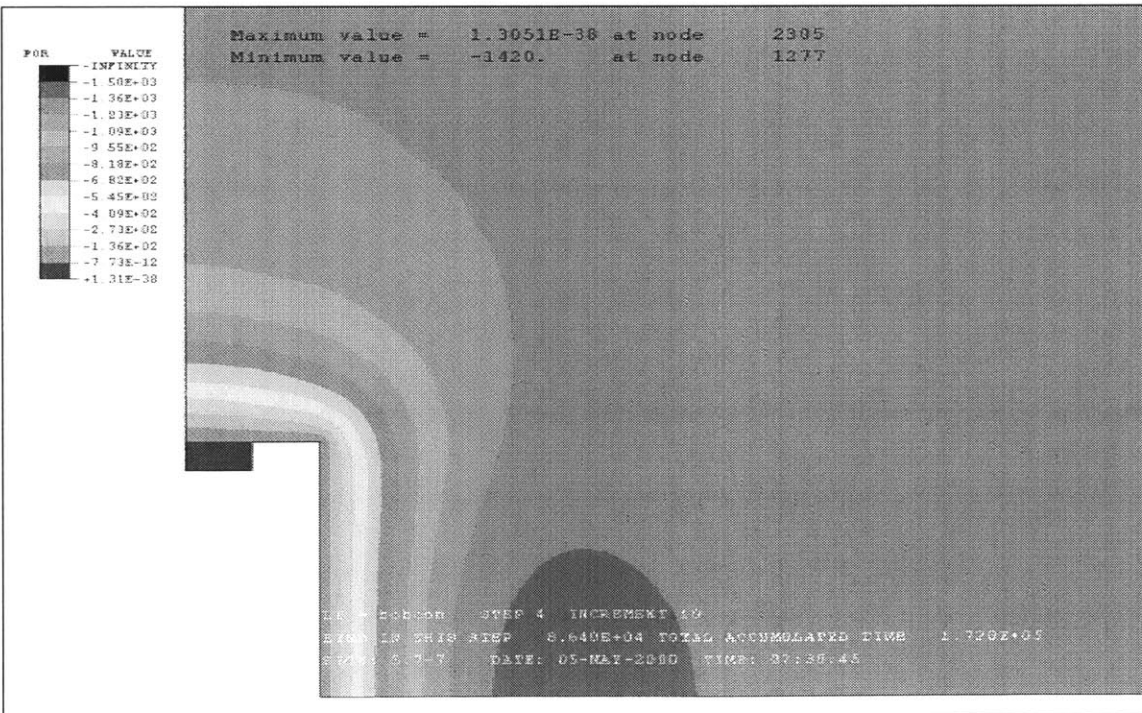


Figure 26. Variation of pore pressures after excavation of two meters (wet conditions - consolidation time=2 days - $l_u=1\text{m}$)

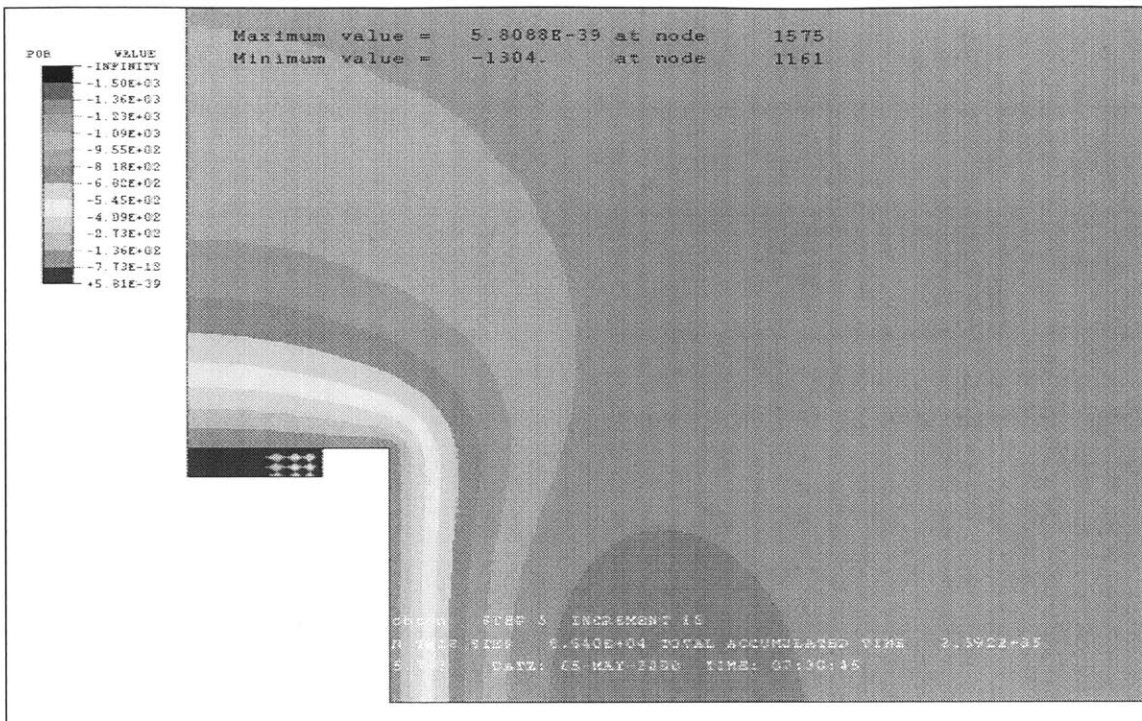


Figure 27. Variation of pore pressures after excavation of three meters (wet conditions - consolidation time=3 days - $l_u=1\text{m}$)

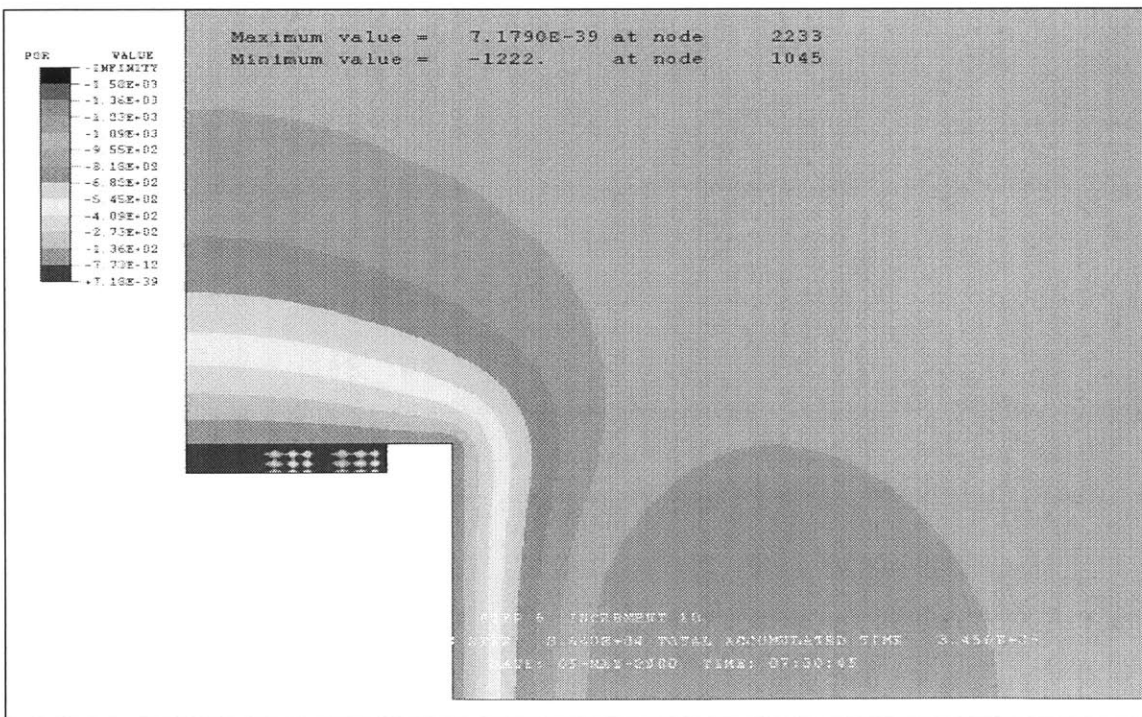


Figure 28. Variation of pore pressures after excavation of four meters (wet conditions - consolidation time=4 days - $l_u=1\text{m}$)

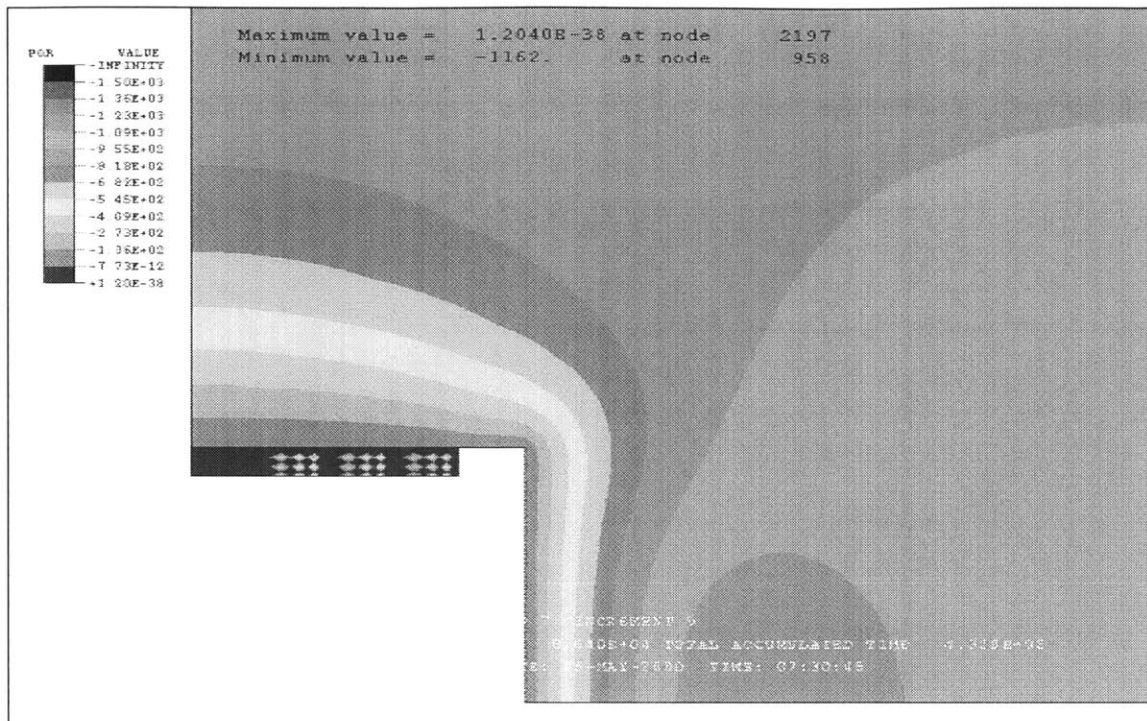


Figure 29. Variation of pore pressures after excavation of five meters (wet conditions - consolidation time=5 days - $l_u=1\text{m}$)

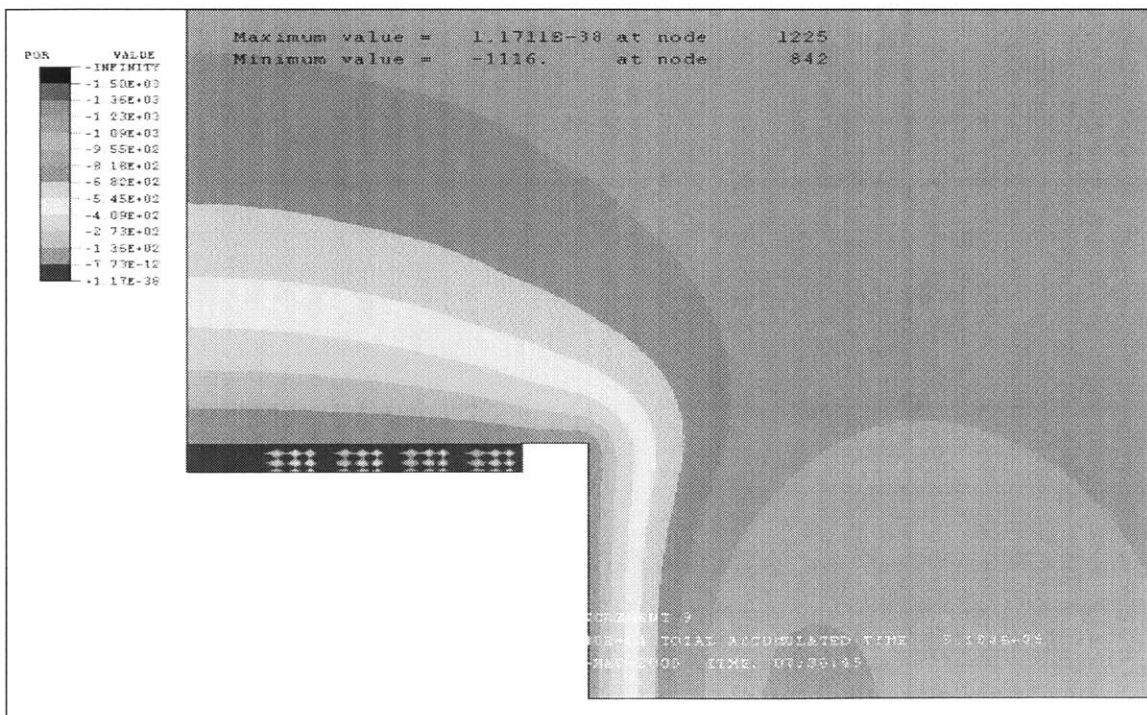


Figure 30. Variation of pore pressures after excavation of six meters (wet conditions - consolidation time=6 days - $l_u=1\text{m}$)

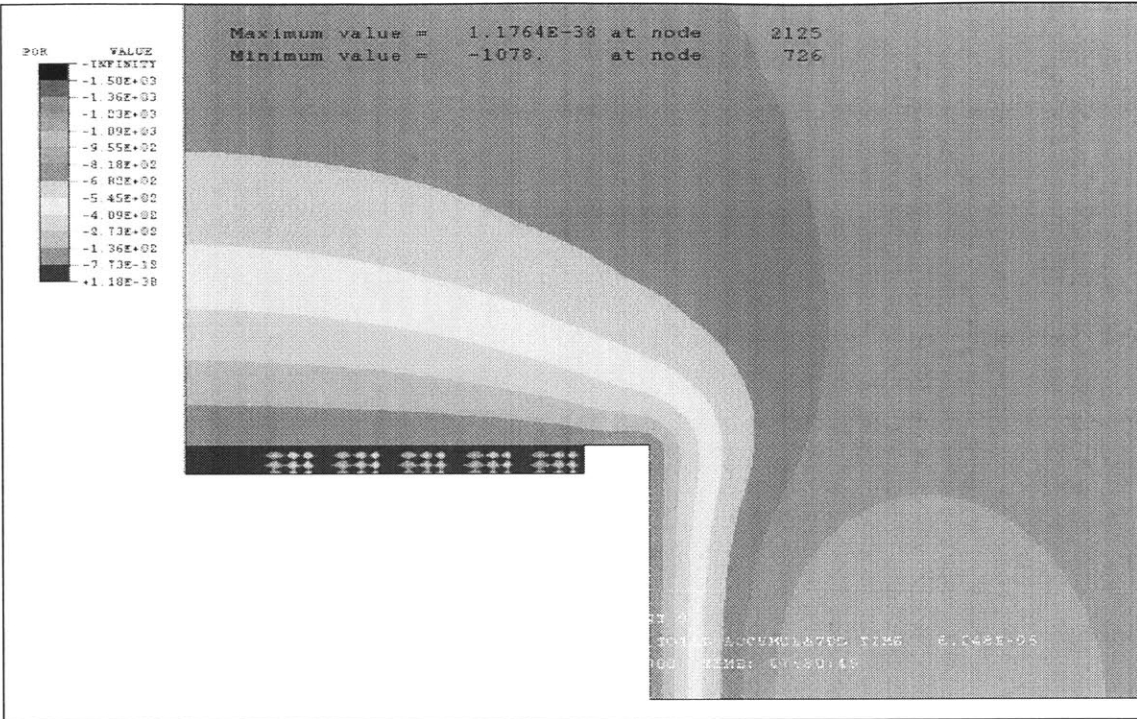


Figure 31. Variation of pore pressures after excavation of seven meters (wet conditions - consolidation time=7 days - $l_u=1\text{m}$)

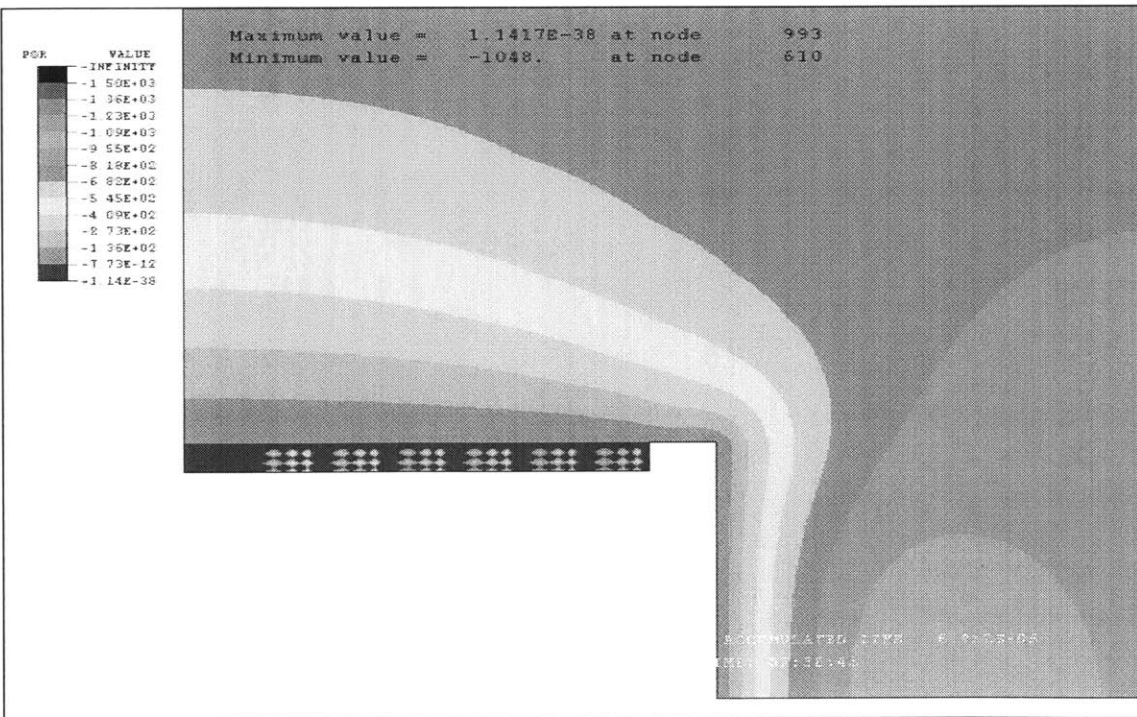


Figure 32. Variation of pore pressures after excavation of eight meters (wet conditions - consolidation time=8 days - $l_u=1\text{m}$)

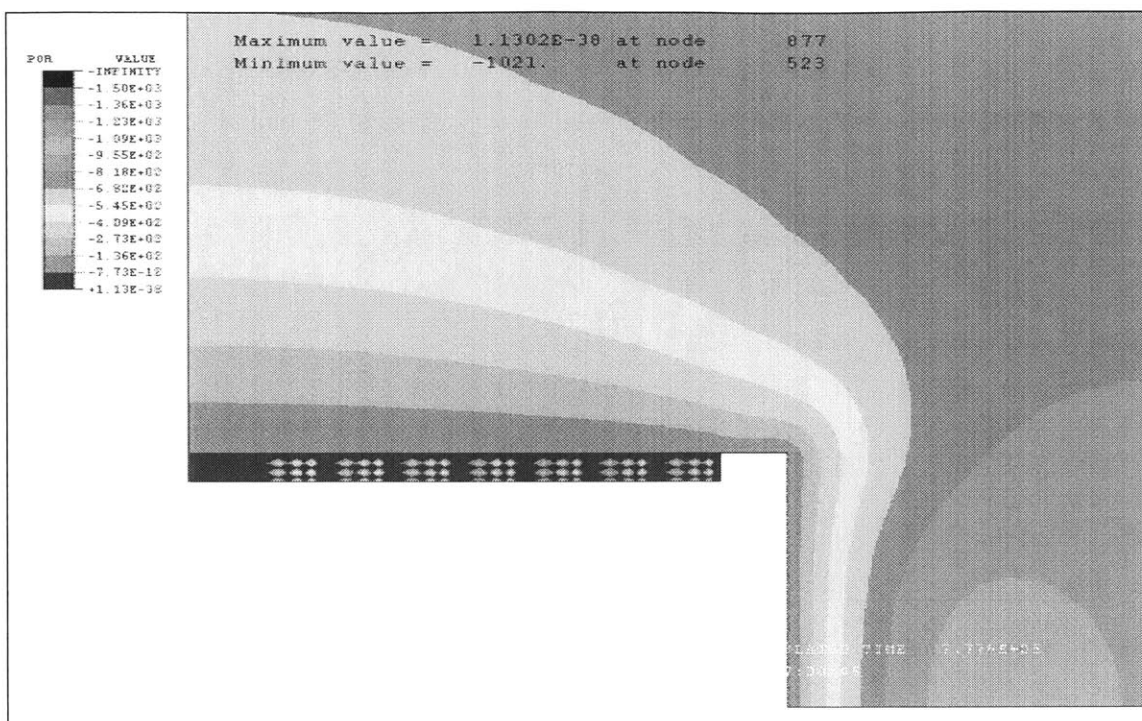


Figure 33. Variation of pore pressures after excavation of nine meters (wet conditions - consolidation time=9 days - $I_u=1\text{m}$)

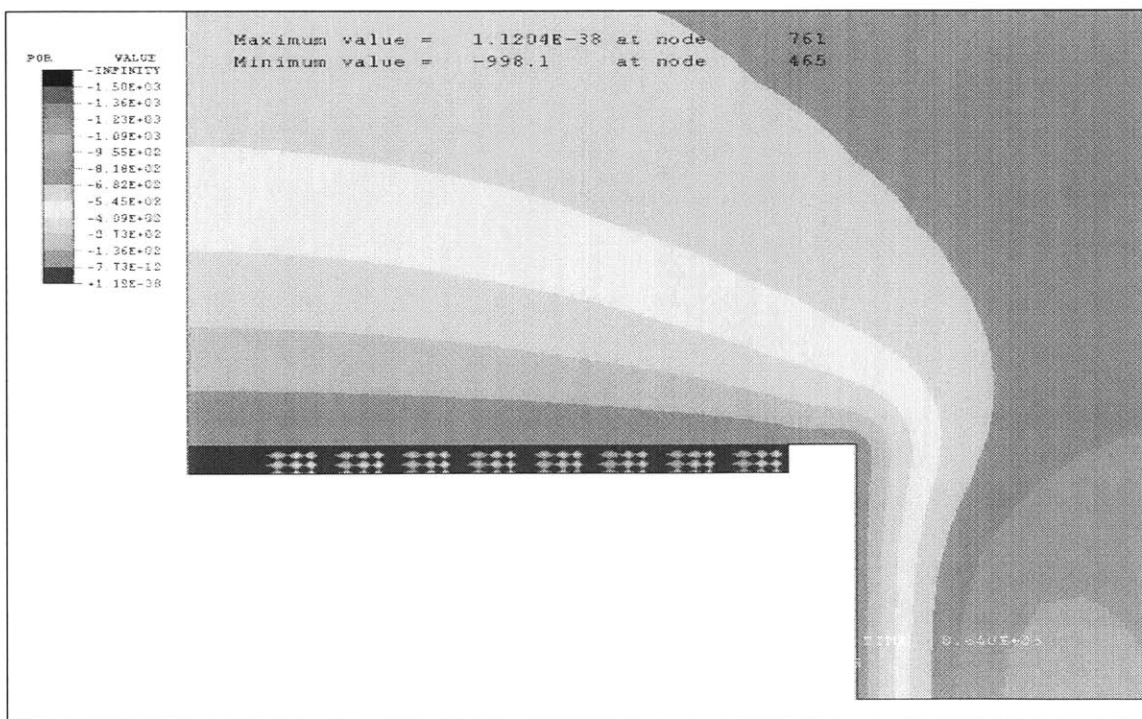


Figure 34. Variation of pore pressures after excavation of ten meters (wet conditions - consolidation time=10 days - $I_u=1\text{m}$)

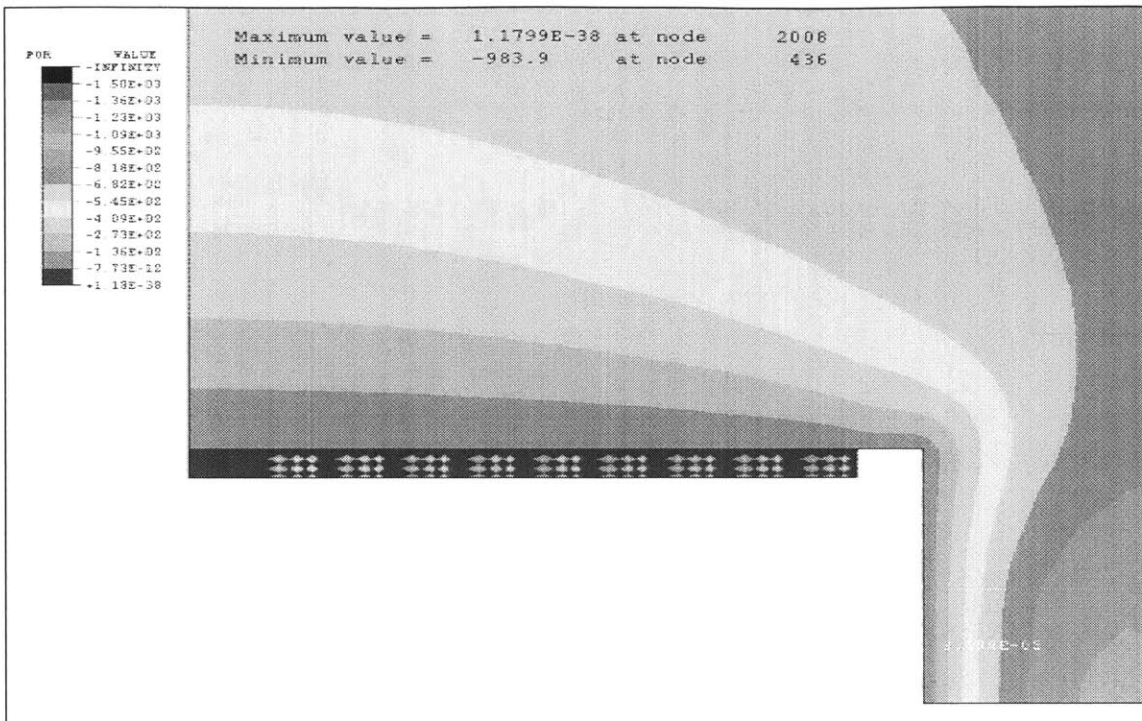


Figure 35. Variation of pore pressures after excavation of eleven meters (wet conditions - consolidation time=11 days - $l_v=1\text{m}$)

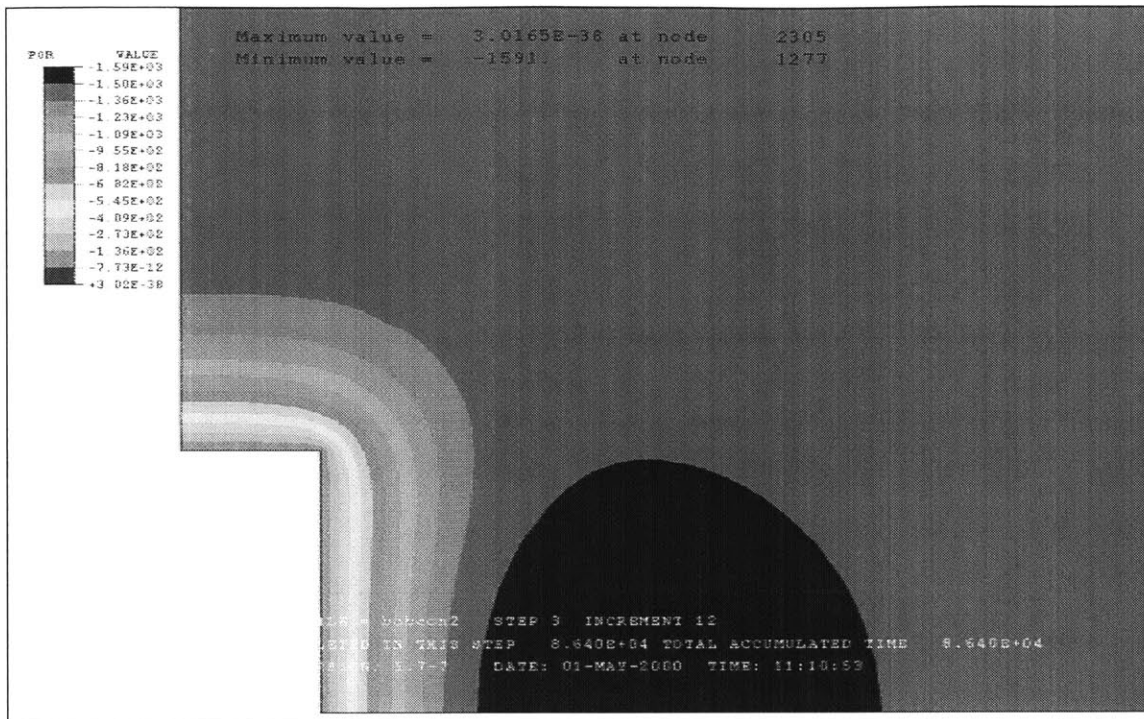


Figure 36. Variation of pore pressures after excavation of two meters (wet conditions - consolidation time=1 day - $l_u=2\text{m}$)

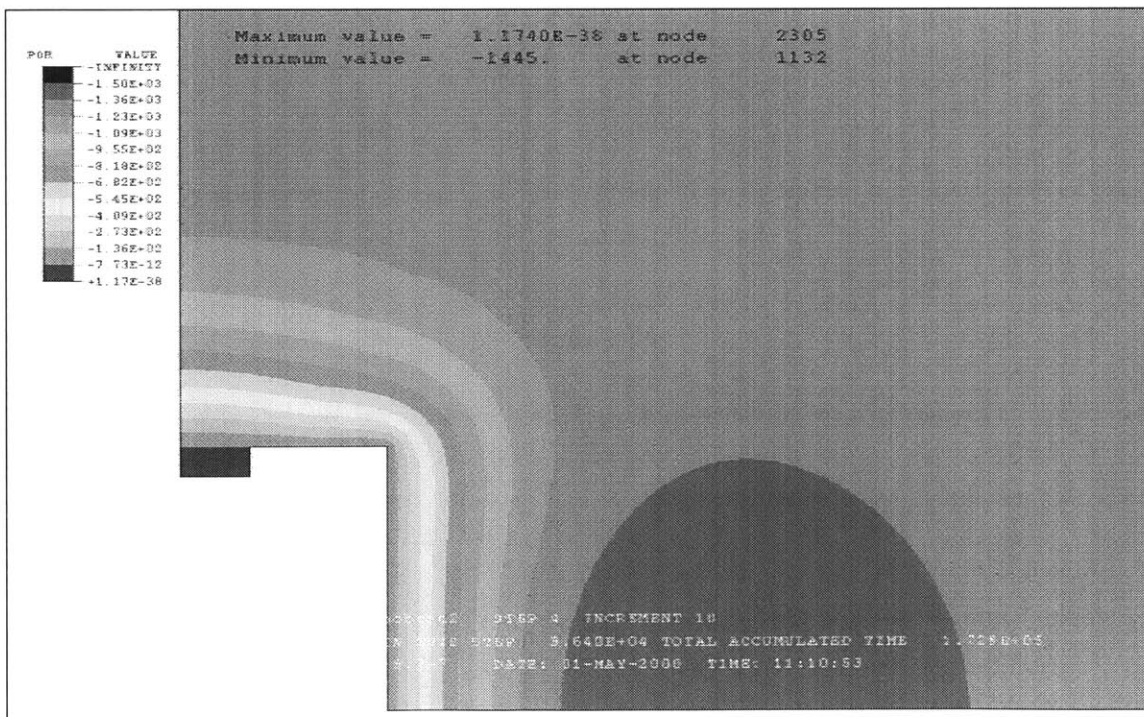


Figure 37. Variation of pore pressures after excavation of three meters (wet conditions - consolidation time=2 days - $l_u=2\text{m}$)

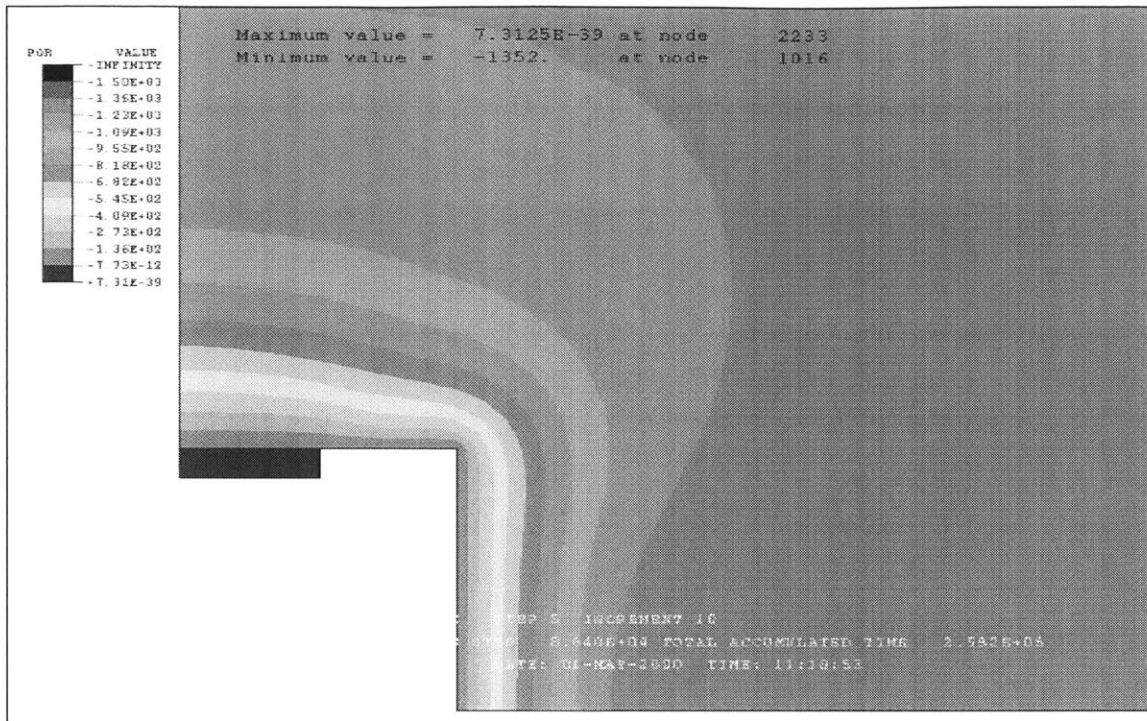


Figure 38. Variation of pore pressures after excavation of four meters (wet conditions - consolidation time=3 days - $l_u=2\text{m}$)

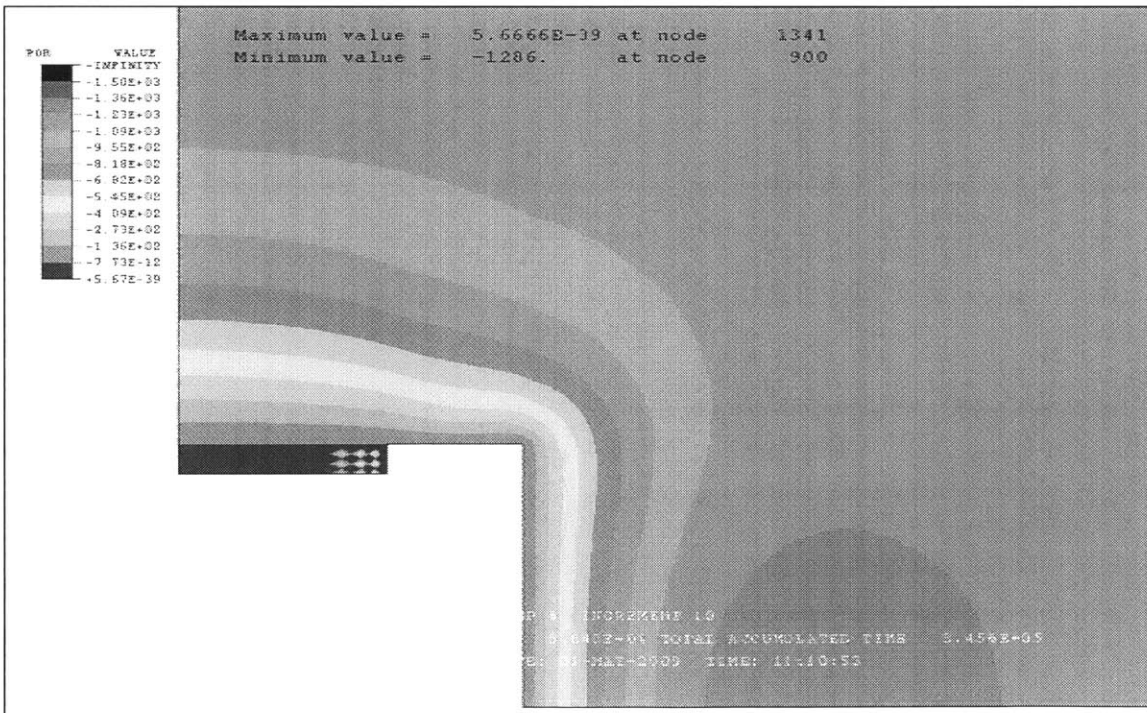


Figure 39. Variation of pore pressures after excavation of five meters (wet conditions - consolidation time=4 days - $l_u=2\text{m}$)

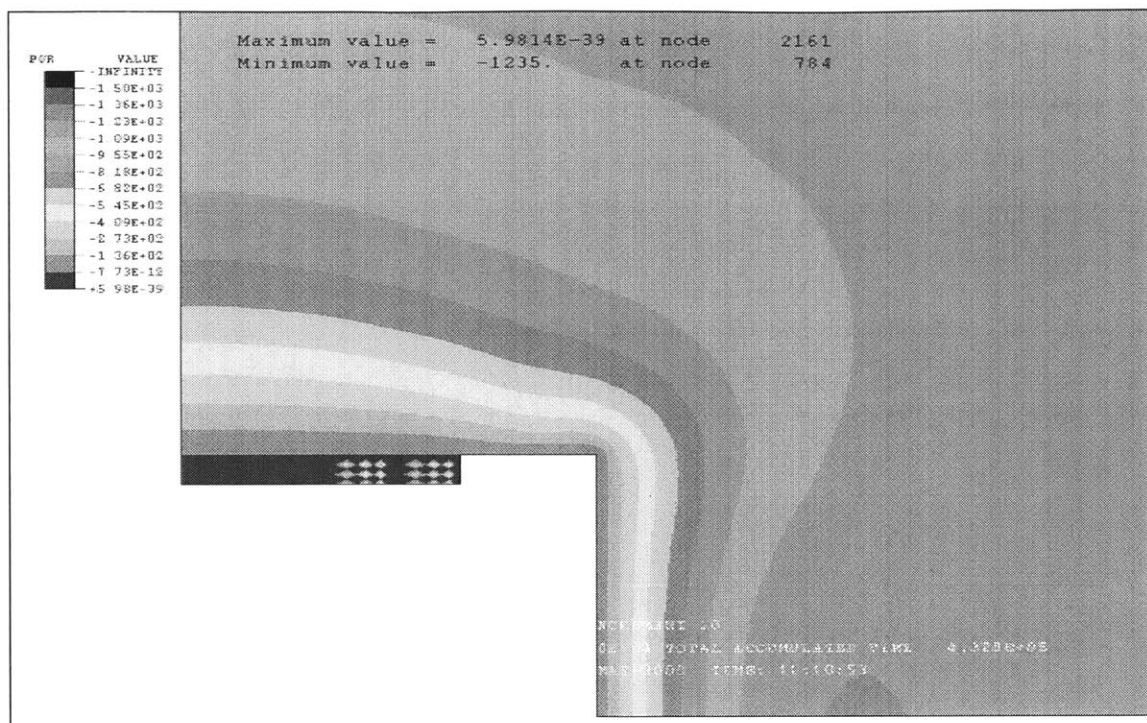


Figure 40. Variation of pore pressures after excavation of six meters (wet conditions - consolidation time=5 days - $l_u=2\text{m}$)

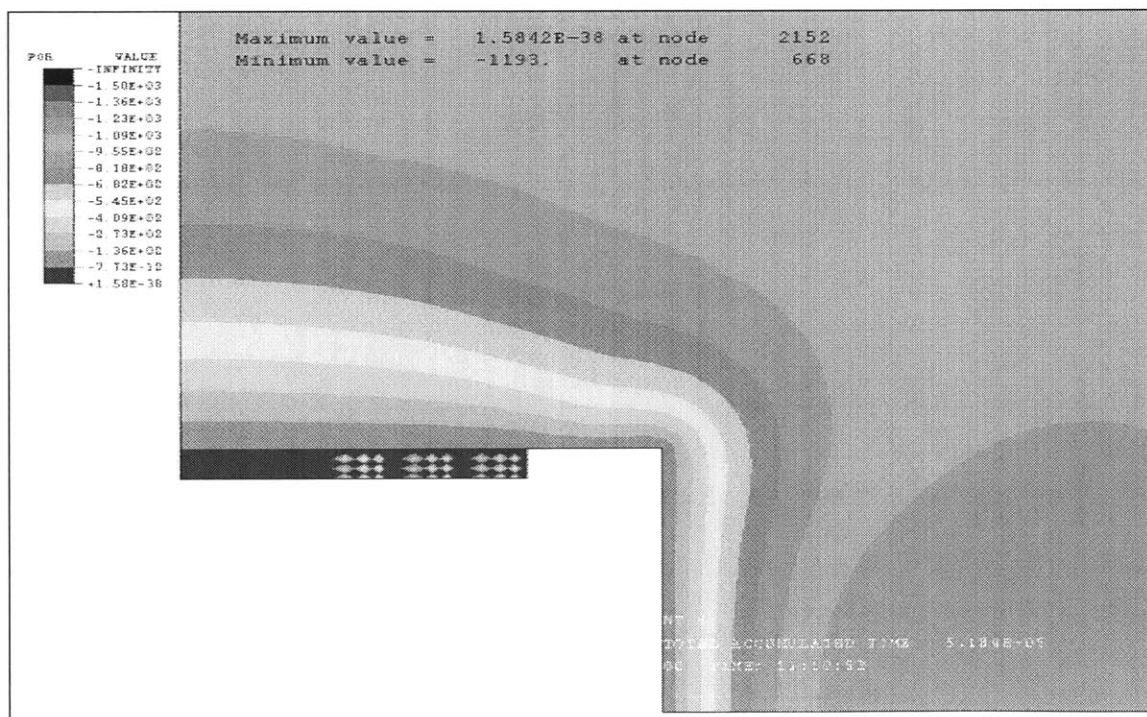


Figure 41. Variation of pore pressures after excavation of seven meters (wet conditions - consolidation time=6 days - $l_u=2\text{m}$)

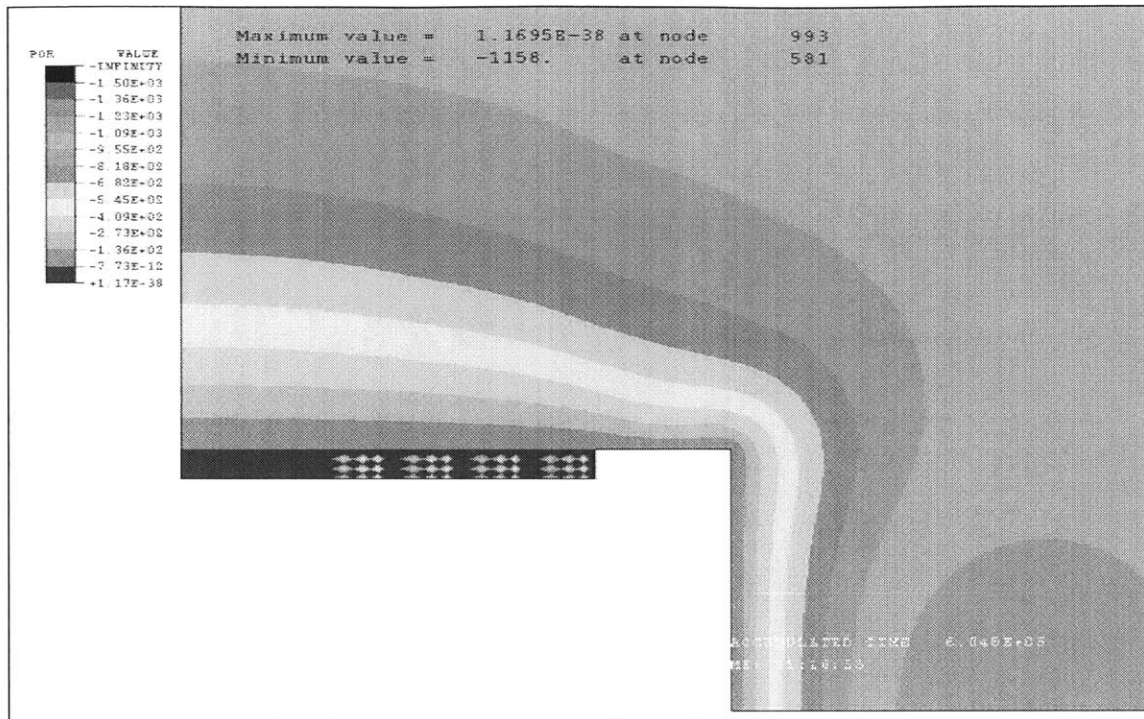


Figure 42. Variation of pore pressures after excavation of eight meters (wet conditions - consolidation time=7 days - $l_u=2m$)

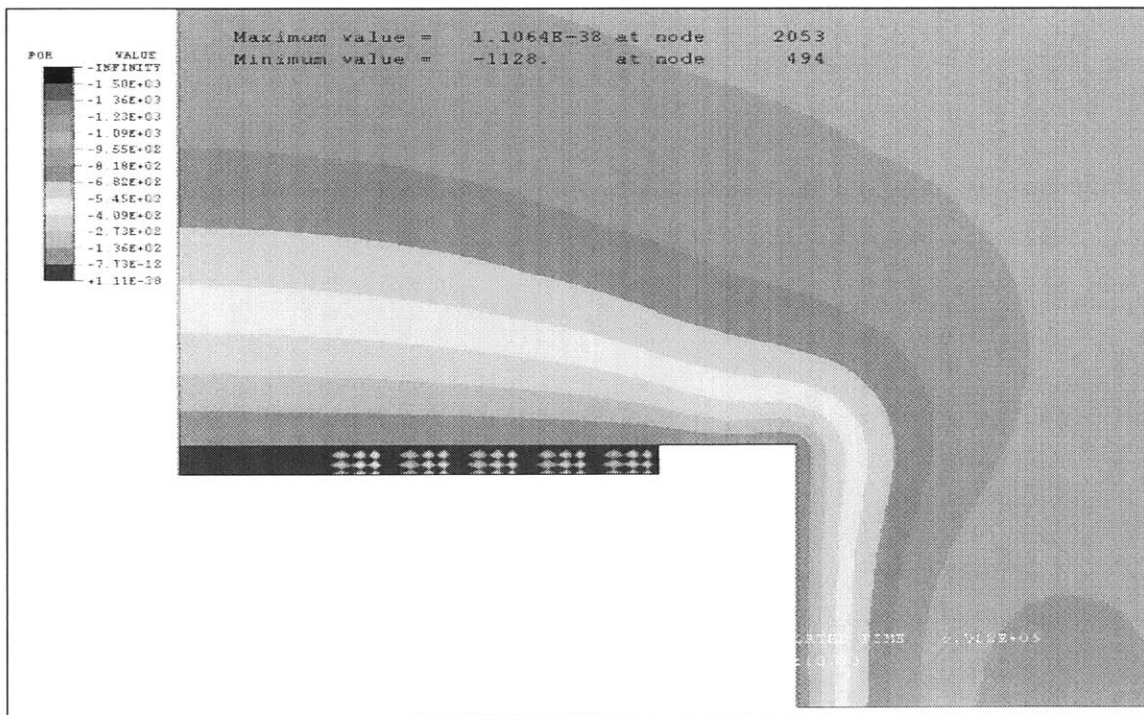


Figure 43. Variation of pore pressures after excavation of nine meters (wet conditions - consolidation time=8 days - $l_u=2m$)

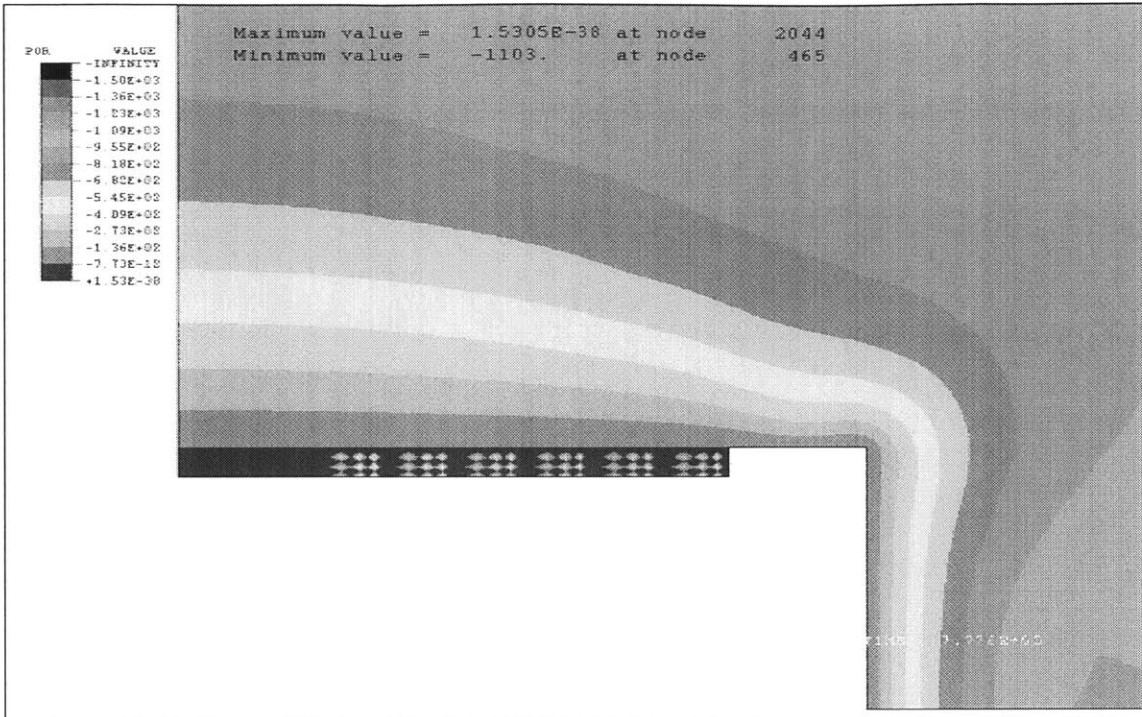


Figure 44. Variation of pore pressures after excavation of ten meters (wet conditions - consolidation time=9 days - $I_u=2m$)

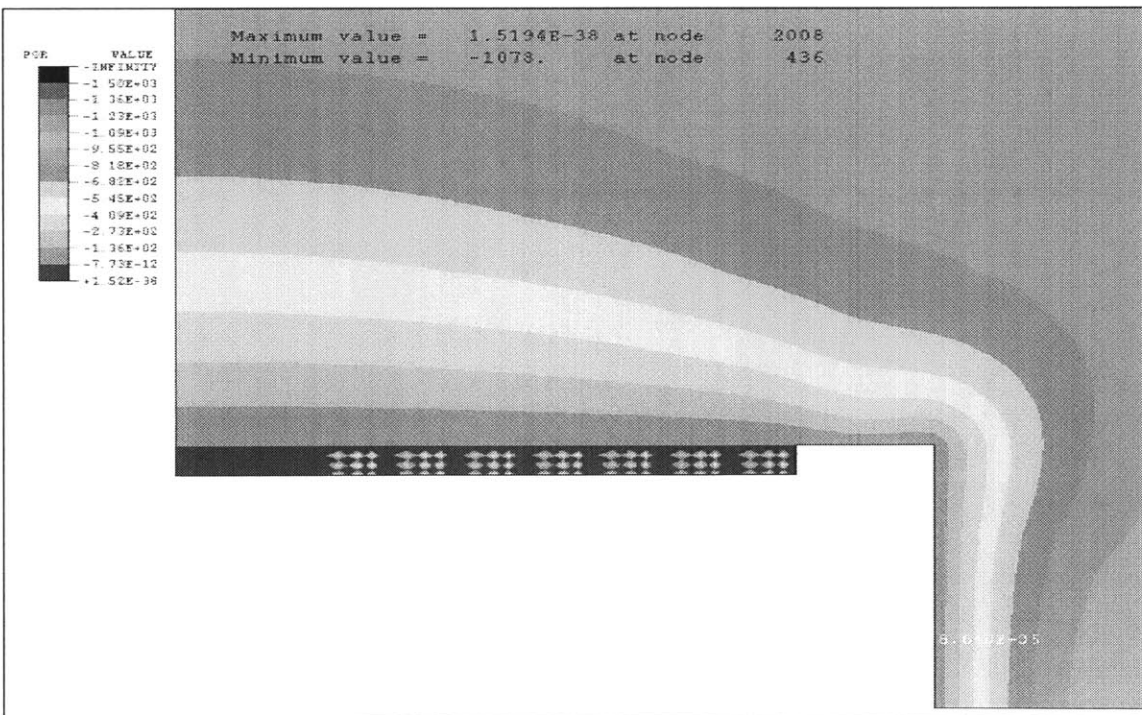


Figure 45. Variation of pore pressures after excavation of eleven meters (wet conditions - consolidation time=10 days - $I_u=2m$)

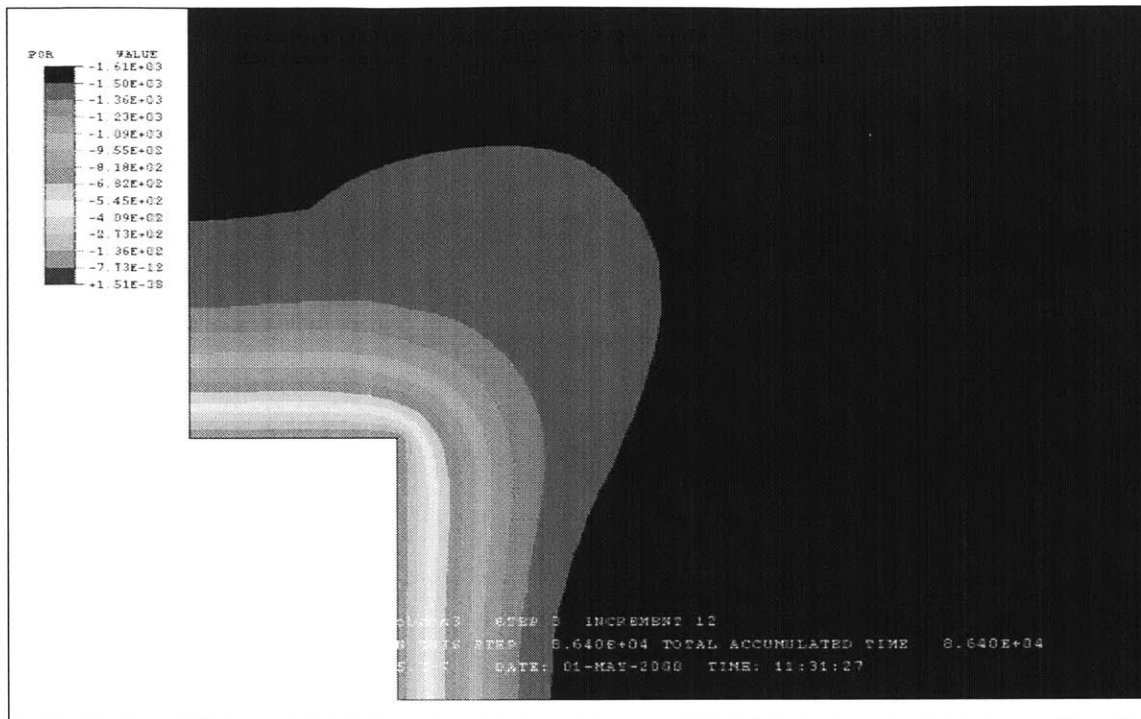


Figure 46. Variation of pore pressures after excavation of three meters (wet conditions - consolidation time=1 day - $l_u=3\text{m}$)

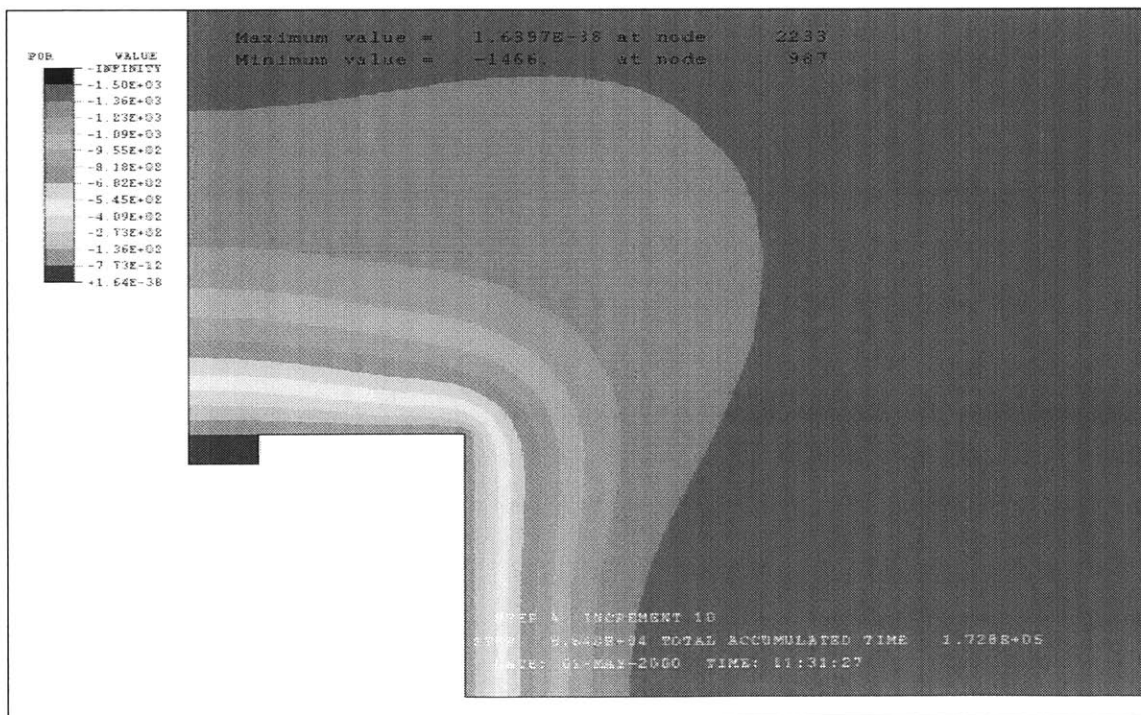


Figure 47. Variation of pore pressures after excavation of four meters (wet conditions - consolidation time=2 days - $l_u=3\text{m}$)

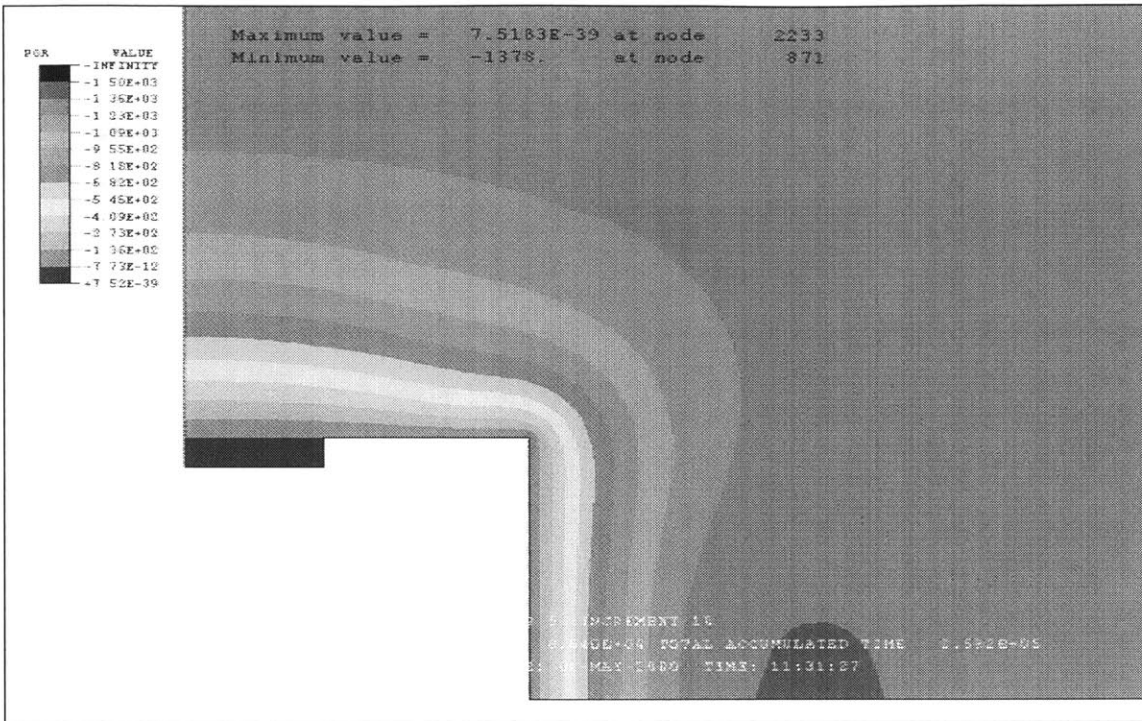


Figure 48. Variation of pore pressures after excavation of five meters (wet conditions - consolidation time=3 days - $I_u=3m$)

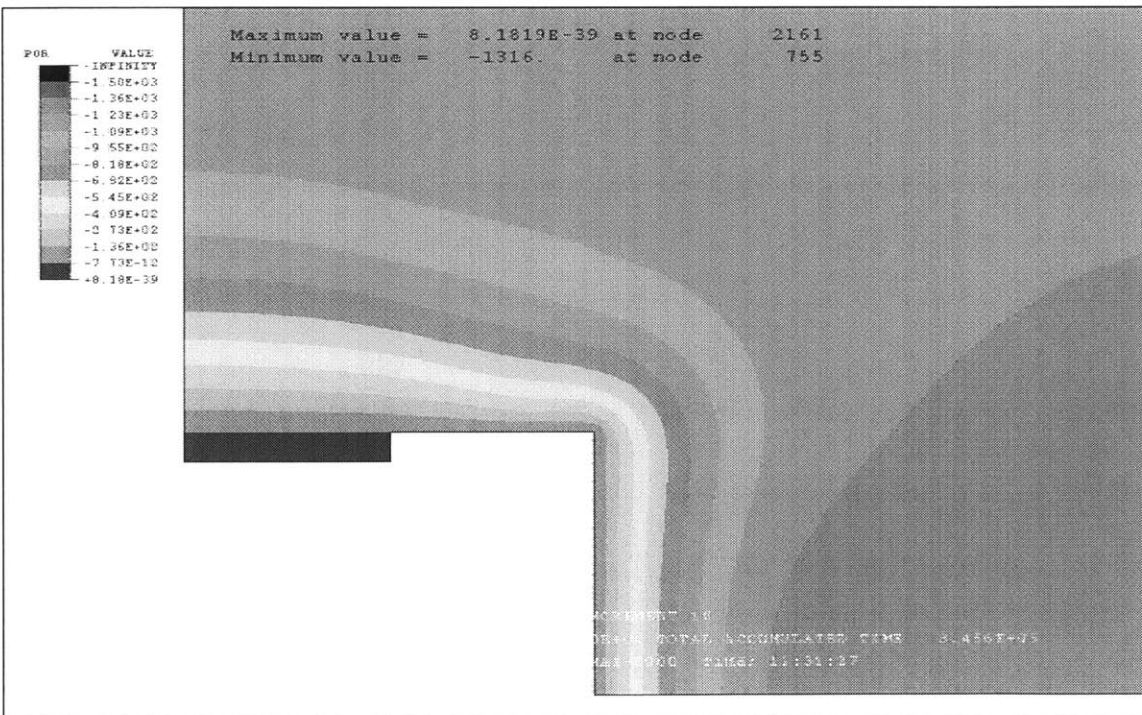


Figure 49. Variation of pore pressures after excavation of six meters (wet conditions - consolidation time=4 days - $I_u=3m$)

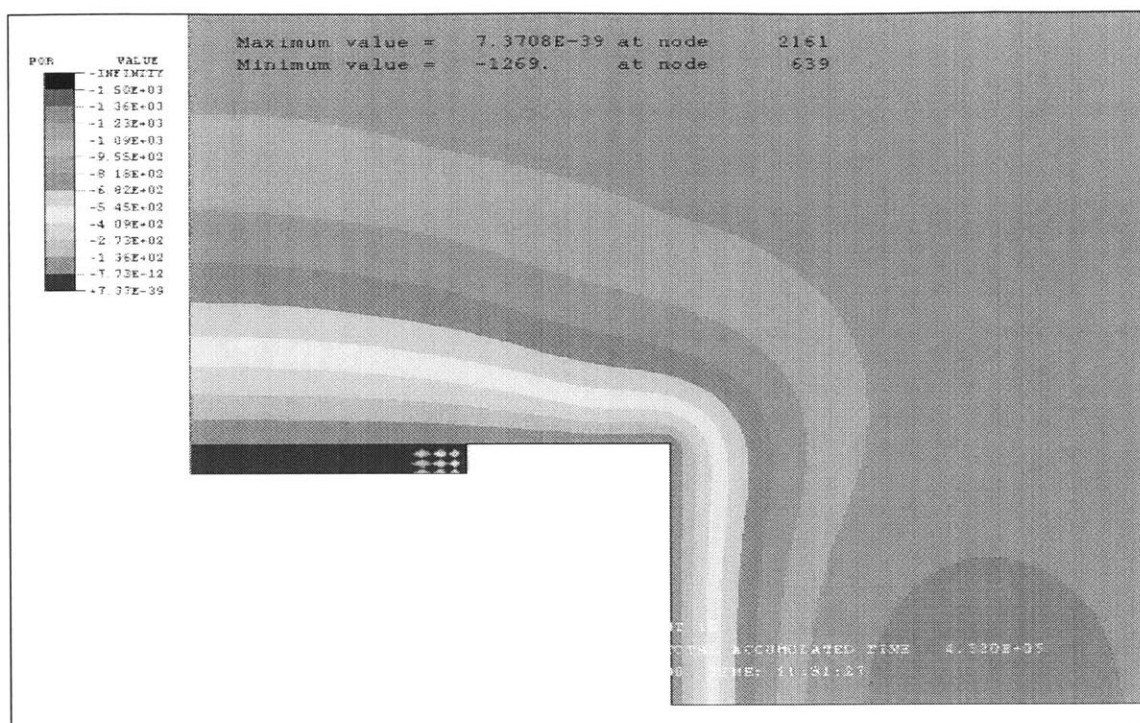


Figure 50. Variation of pore pressures after excavation of seven meters (wet conditions - consolidation time=5 days - $I_u=3\text{m}$)

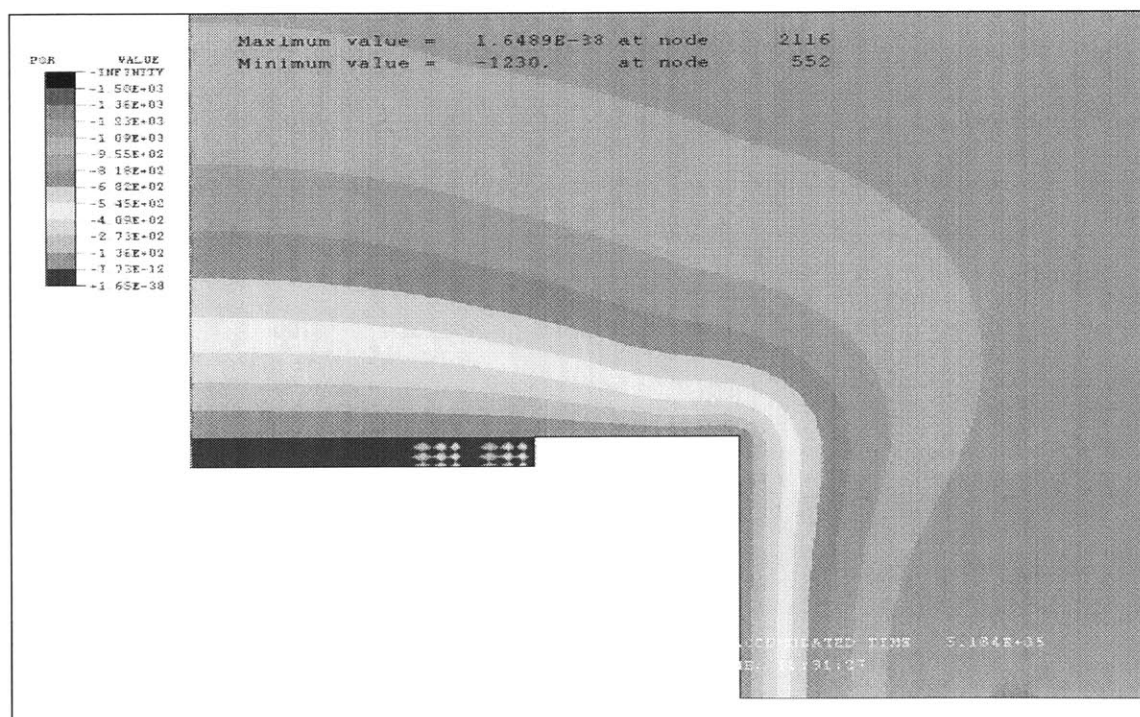


Figure 51. Variation of pore pressures after excavation of eight meters (wet conditions - consolidation time=6 days - $I_u=3\text{m}$)

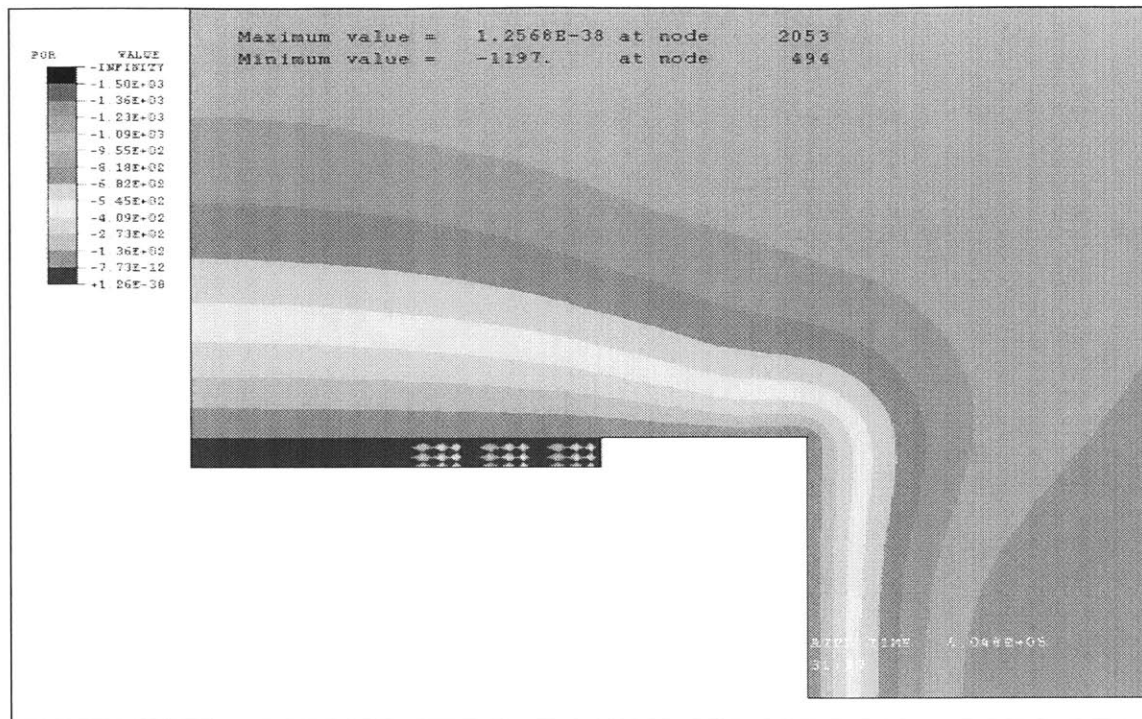


Figure 52. Variation of pore pressures after excavation of nine meters (wet conditions - consolidation time=7 days - $I_u=3\text{m}$)

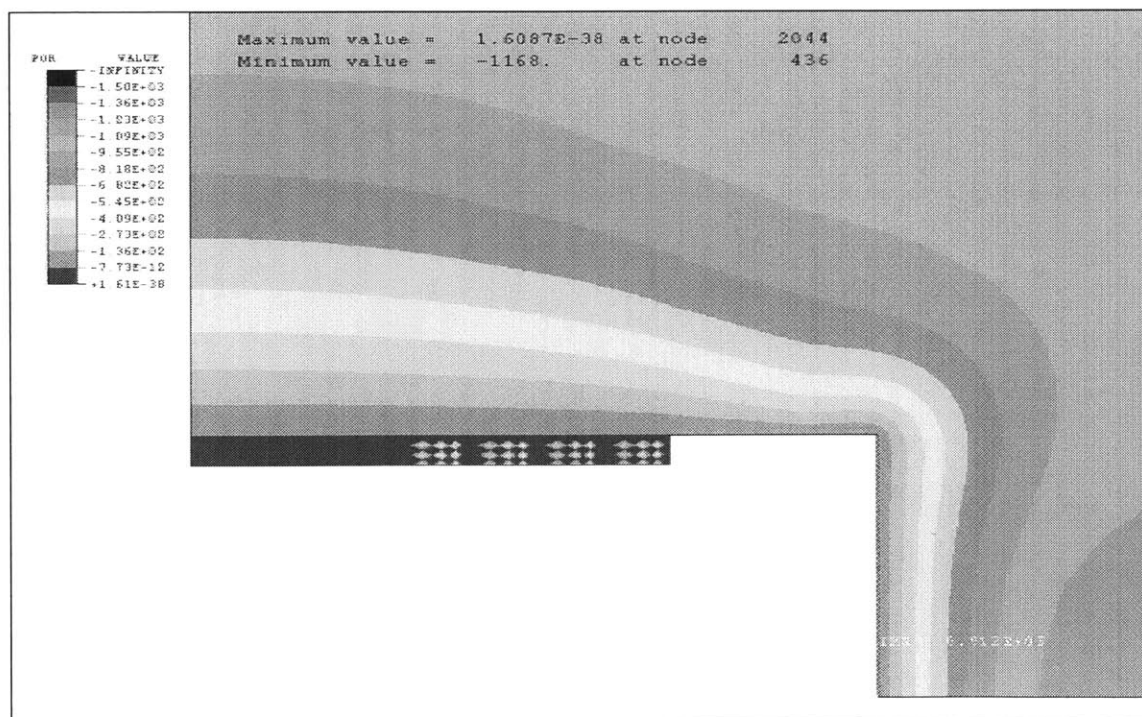


Figure 53. Variation of pore pressures after excavation of ten meters (wet conditions - consolidation time=8 days - $I_u=3\text{m}$)

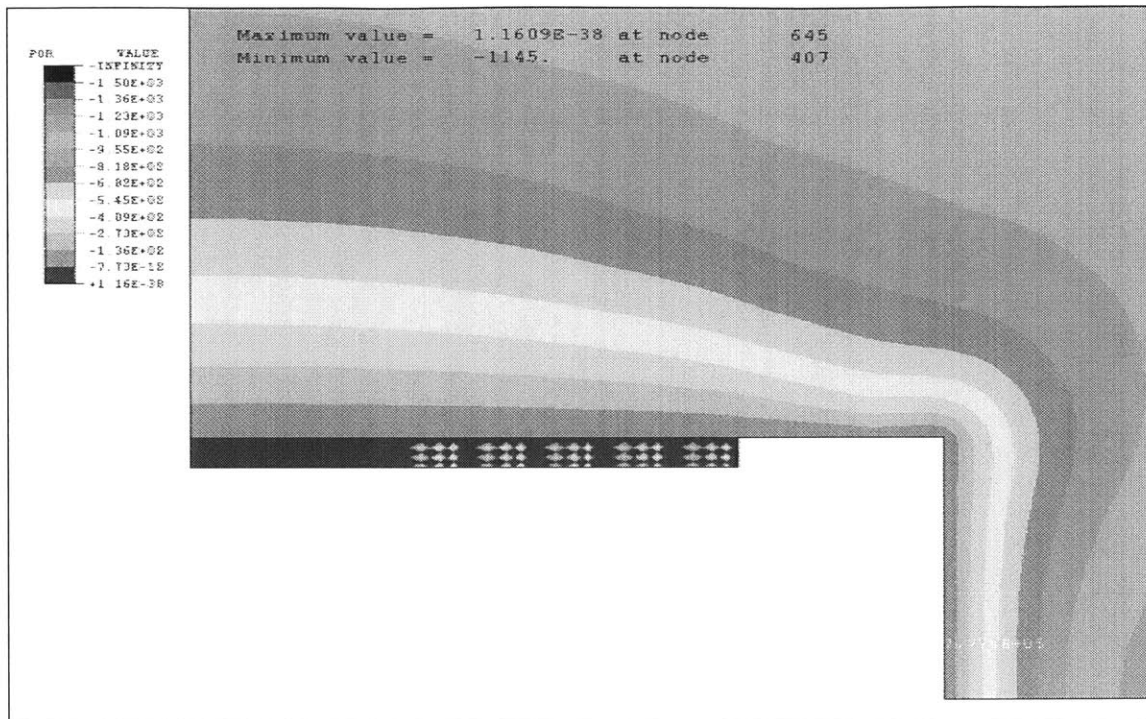
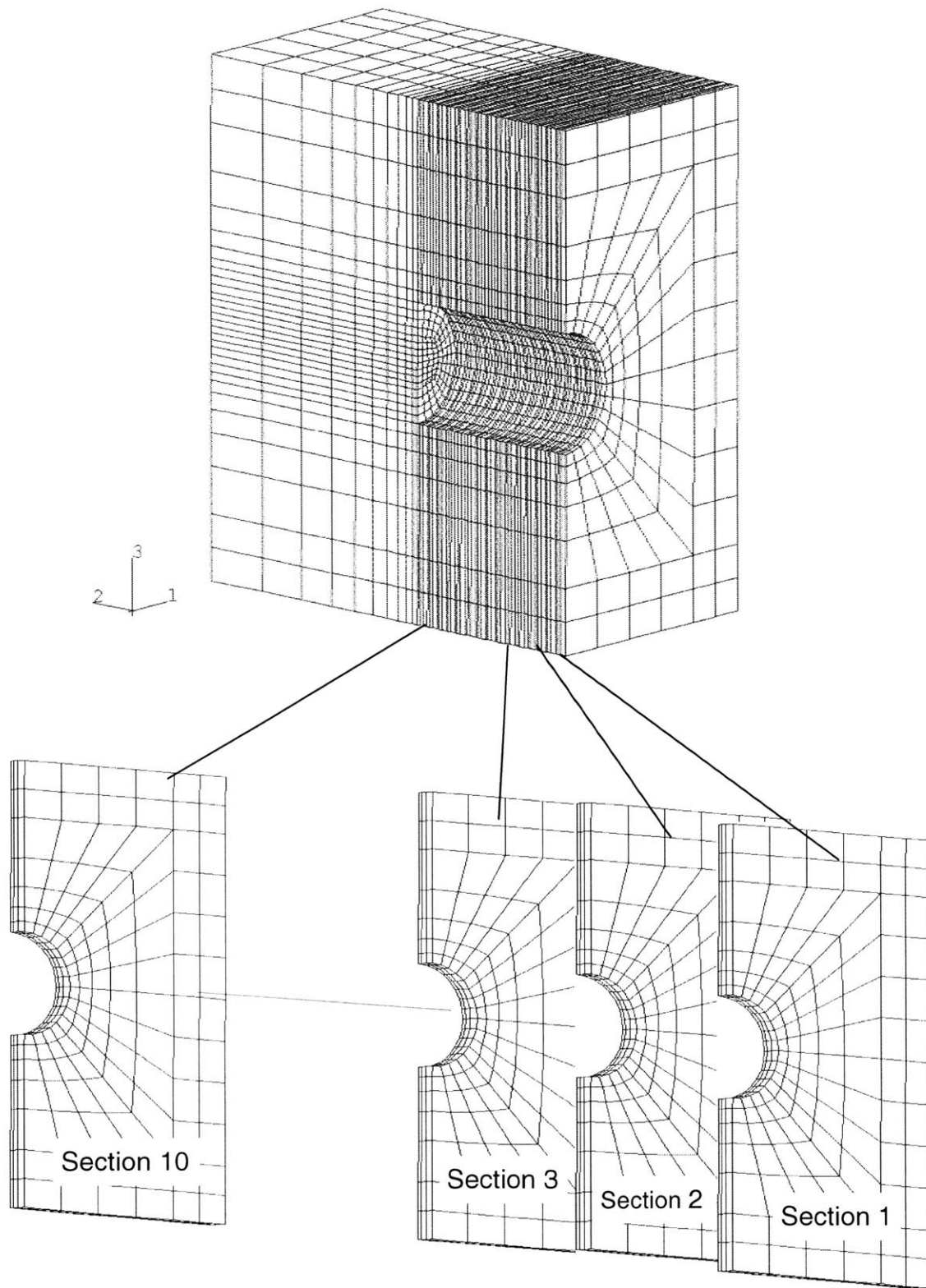


Figure 54. Variation of pore pressures after excavation of eleven meters (wet conditions - consolidation time=9 days - $I_u=3\text{m}$)

APPENDIX IV



APPENDIX IVa

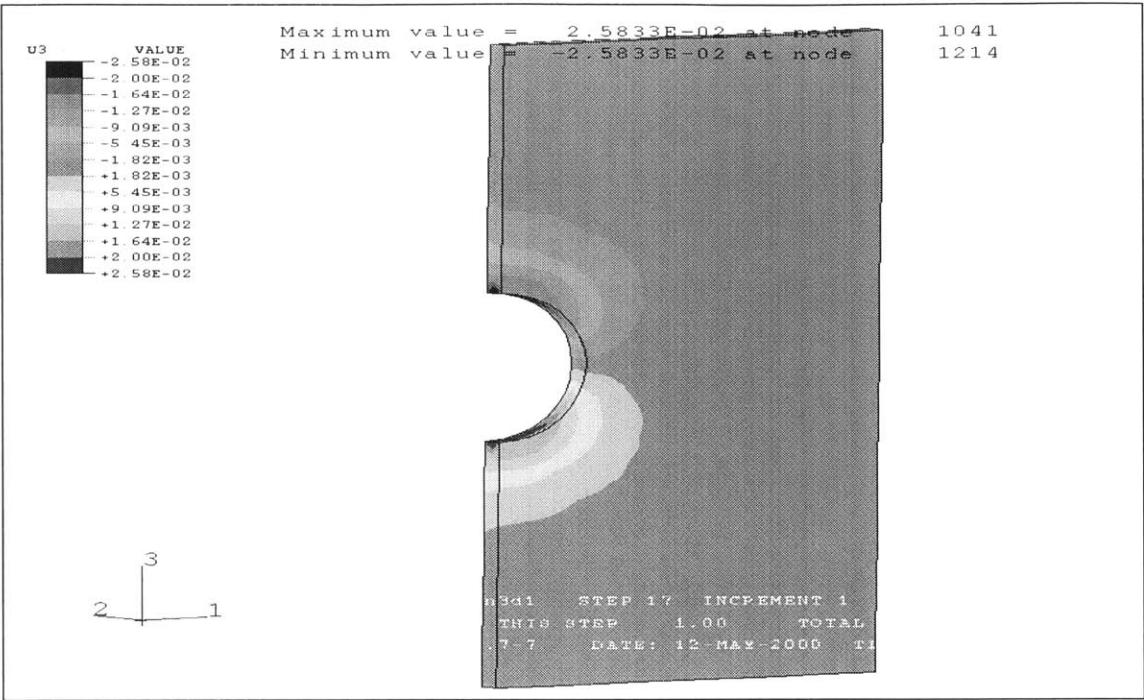


Figure 1. Displacement in the vertical direction at section 1-2
($K_x=K_y=1$ - dry conditions - $l_u=1\text{m}$ - excavation=1m)

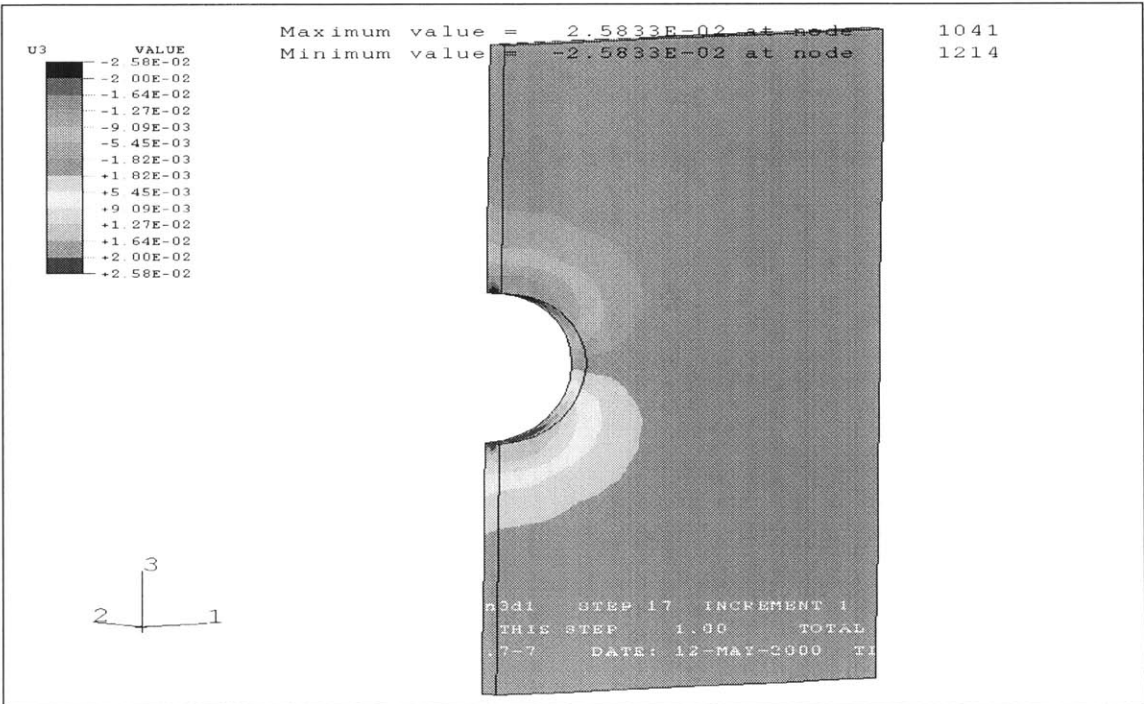


Figure 2. Displacement in the vertical direction at section 2-3
($K_x=K_y=1$ - dry conditions - $l_u=1\text{m}$ - excavation=2m)

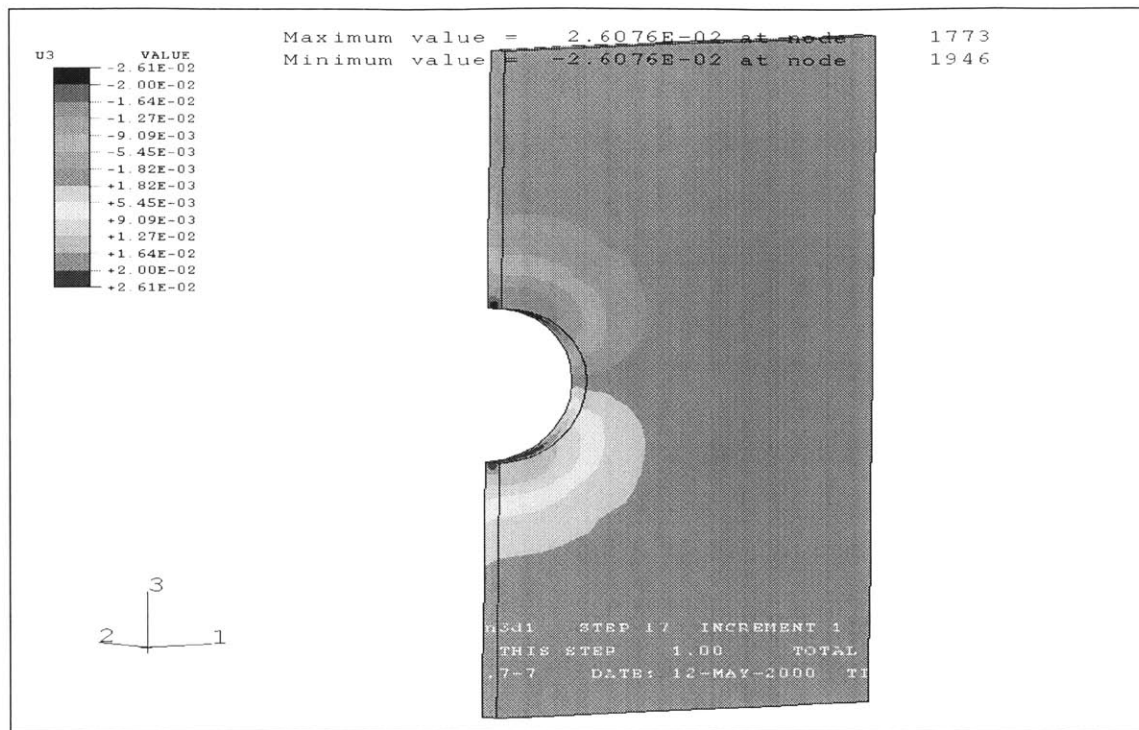


Figure 3. Displacement in the vertical direction at section 3-4
($K_x=K_y=1$ - dry conditions - $I_u=1\text{m}$ - excavation=3m)

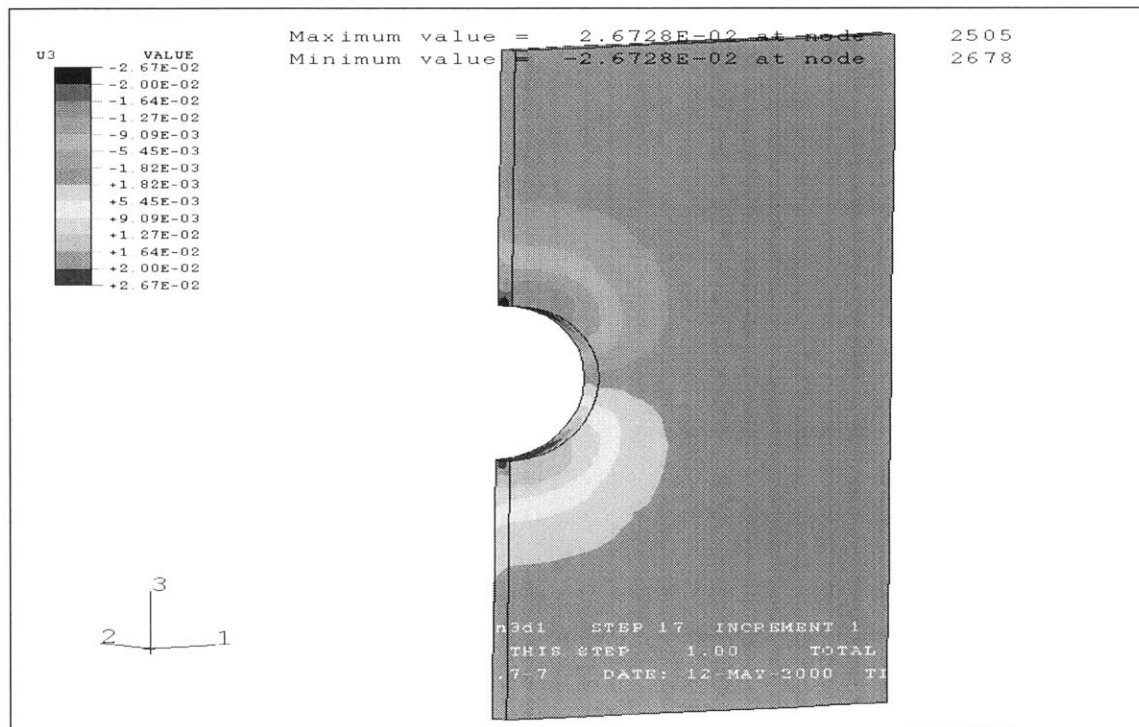


Figure 4. Displacement in the vertical direction at section 4-5
($K_x=K_y=1$ - dry conditions - $I_u=1\text{m}$ - excavation=4m)

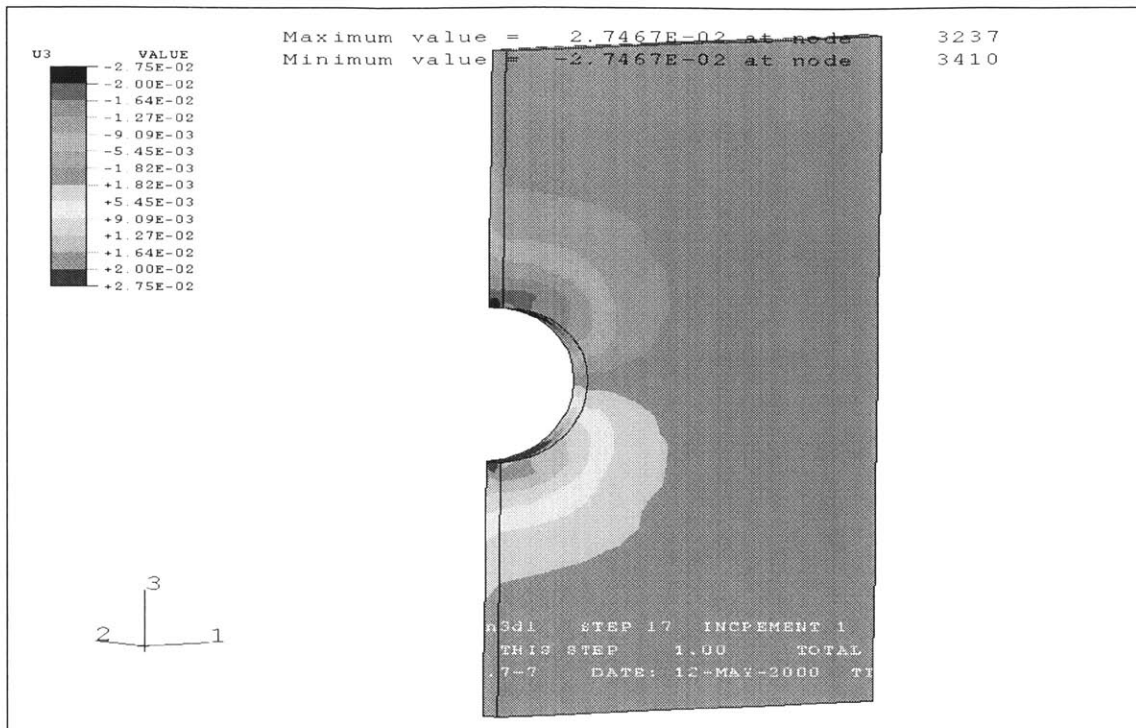


Figure 5. Displacement in the vertical direction at section 5-6
($K_x=K_y=1$ - dry conditions - $l_u=1\text{m}$ - excavation=5m)

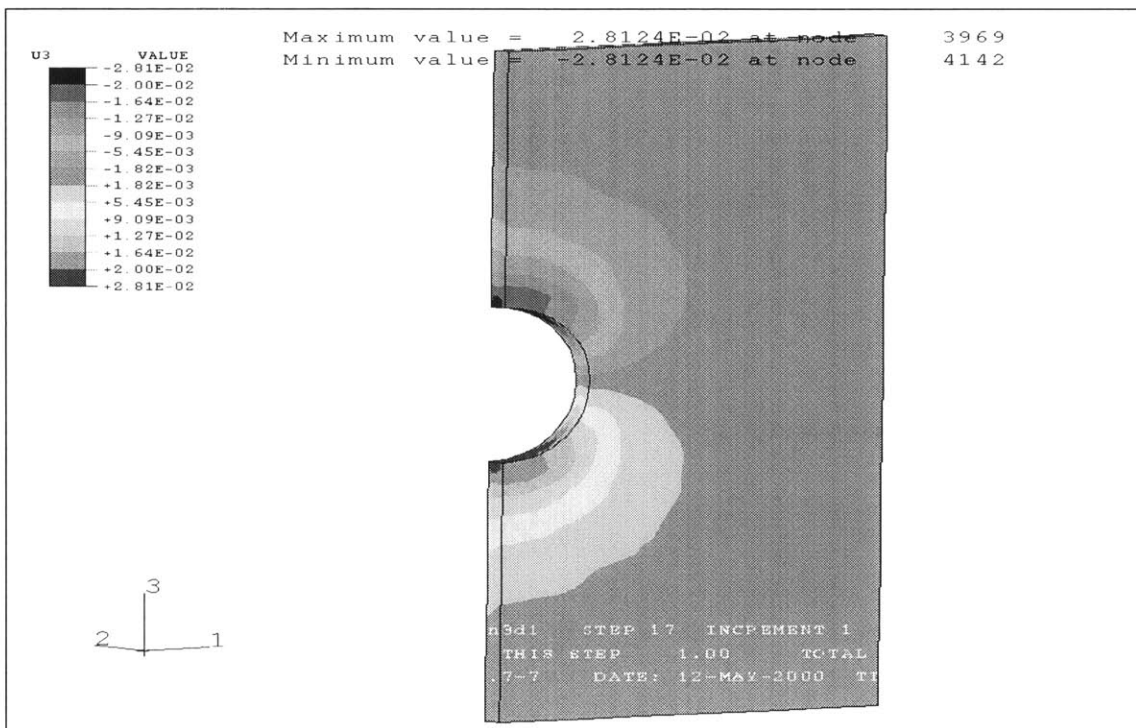


Figure 6. Displacement in the vertical direction at section 6-7
($K_x=K_y=1$ - dry conditions - $l_u=1\text{m}$ - excavation=6m)

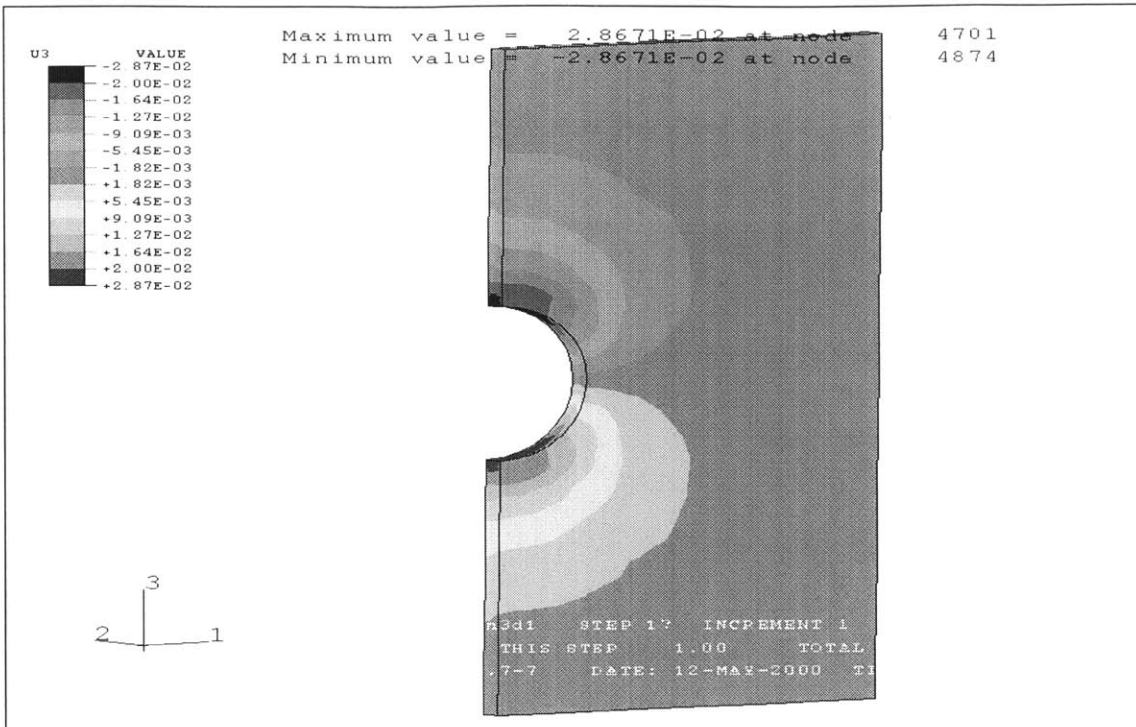


Figure 7. Displacement in the vertical direction at section 7-8
($K_x=K_y=1$ - dry conditions - $I_u=1\text{m}$ - excavation=7m)

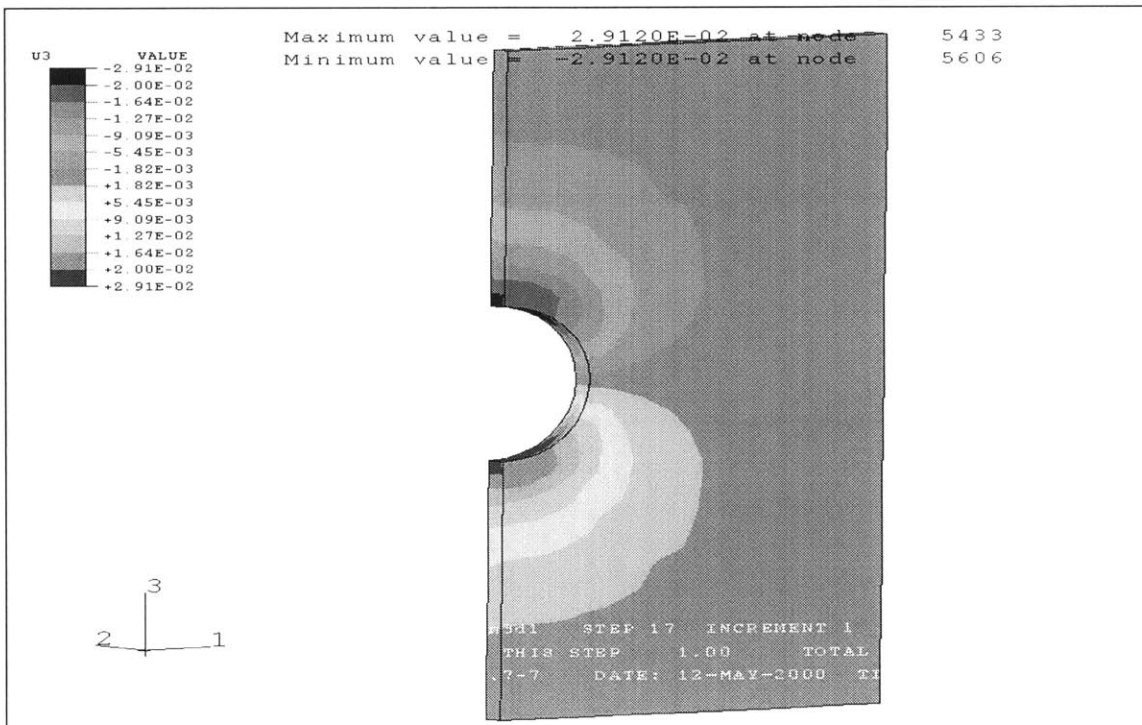


Figure 8. Displacement in the vertical direction at section 8-9
($K_x=K_y=1$ - dry conditions - $I_u=1\text{m}$ - excavation=8m)

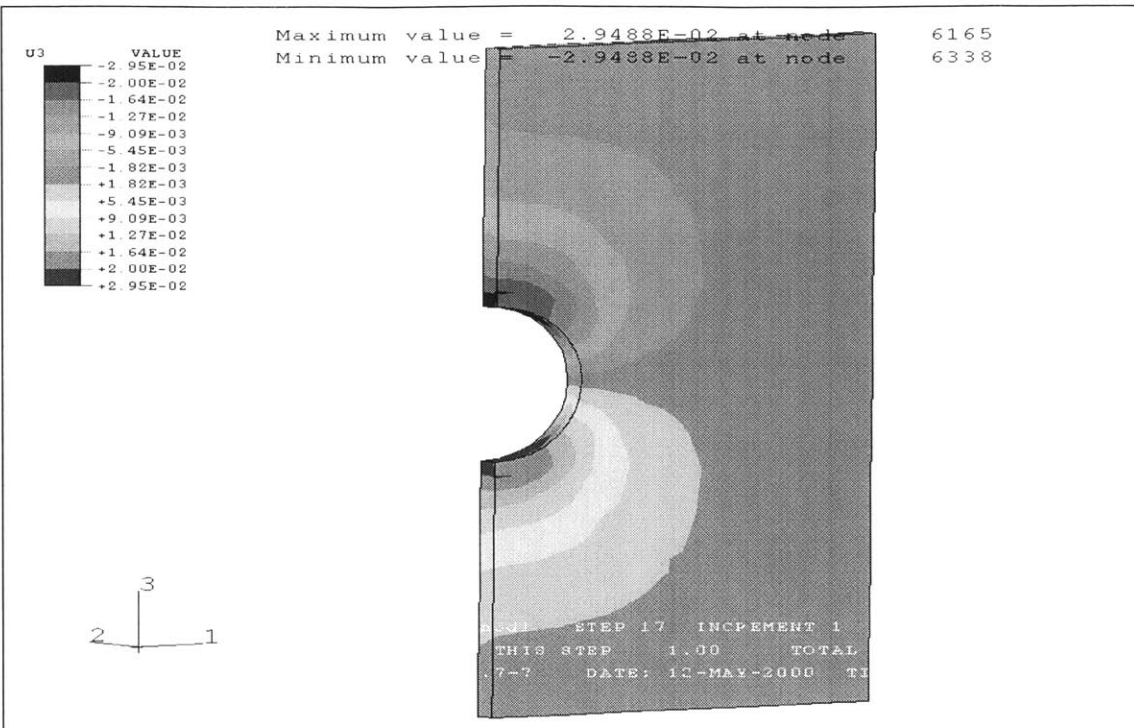


Figure 9. Displacement in the vertical direction at section 9-10
($K_x=K_y=1$ - dry conditions - $l_u=1\text{m}$ - excavation=9m)

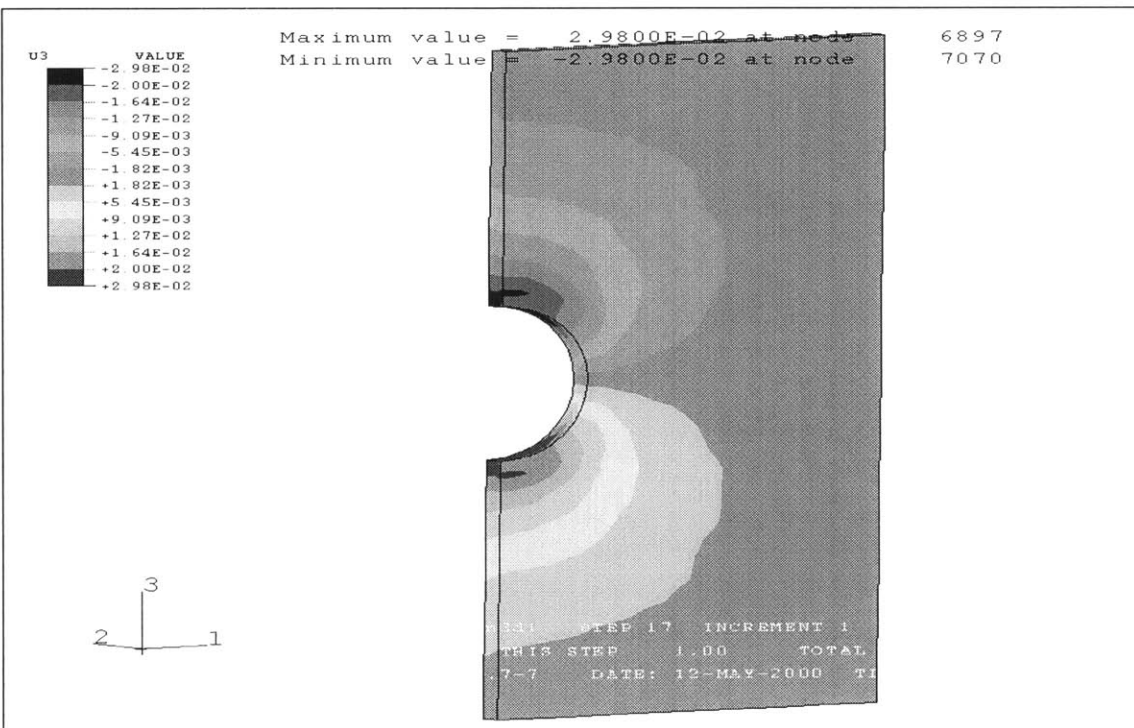


Figure 10. Displacement in the vertical direction at section 10-11
($K_x=K_y=1$ - dry conditions - $l_u=1\text{m}$ - excavation=10m)

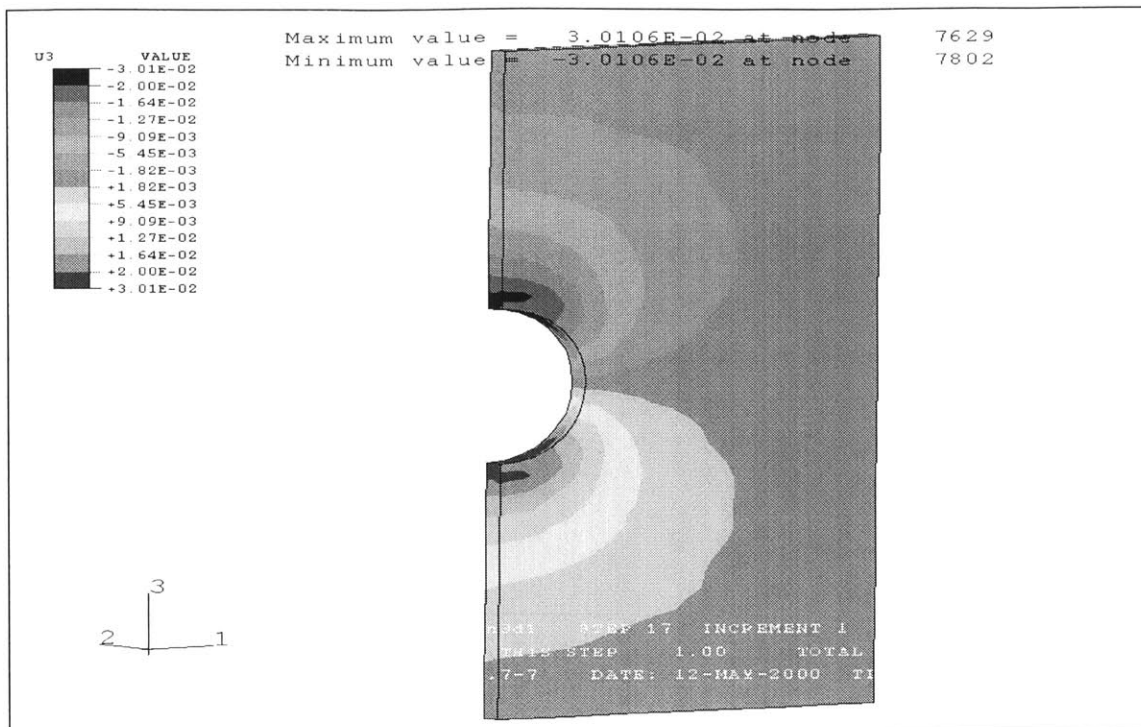


Figure 11. Displacement in the vertical direction at section 11-12
 ($K_x=K_y=1$ - dry conditions - $l_u=1\text{m}$ - excavation= 11m)

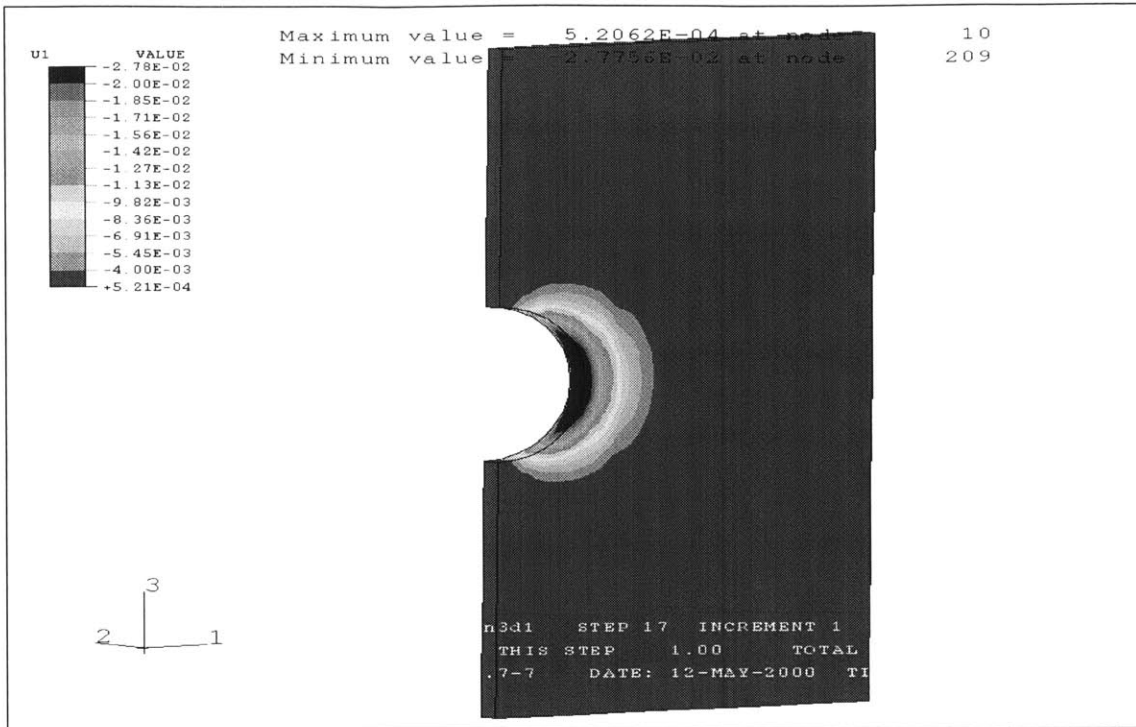


Figure 12. Displacement in the horizontal direction at section 1-2
($K_x=K_y=1$ - dry conditions - $l_u=1\text{m}$ - excavation= 1m)

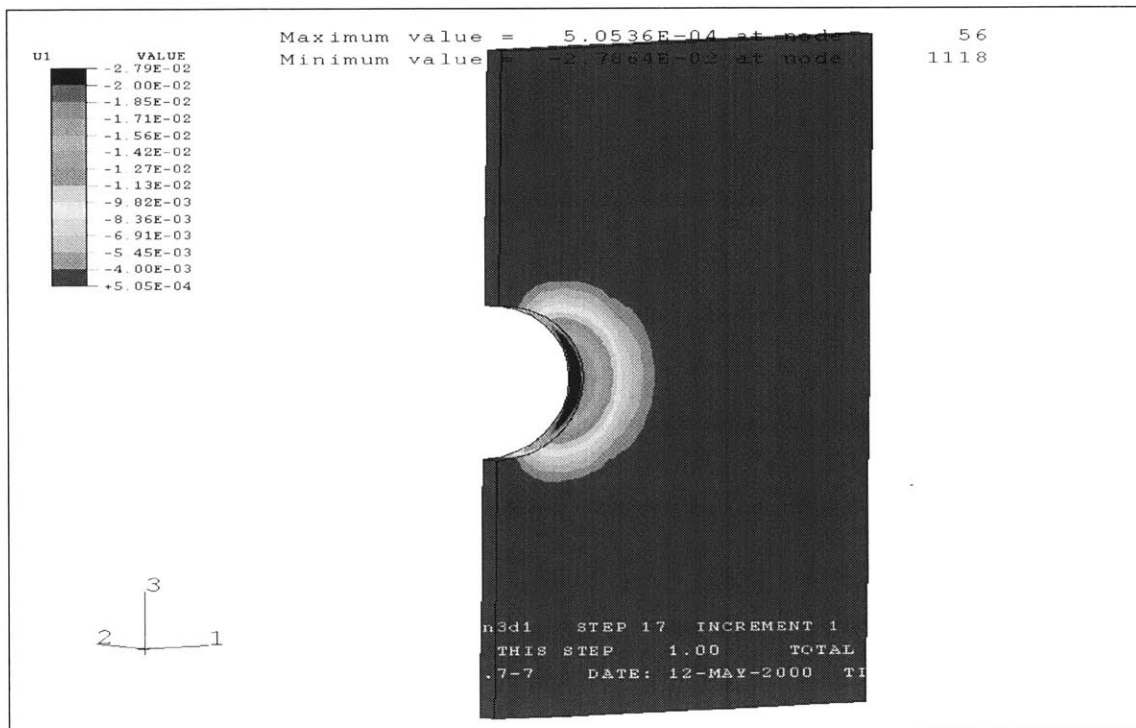


Figure 13. Displacement in the horizontal direction at section 2-3
($K_x=K_y=1$ - dry conditions - $l_u=1\text{m}$ - excavation= 2m)

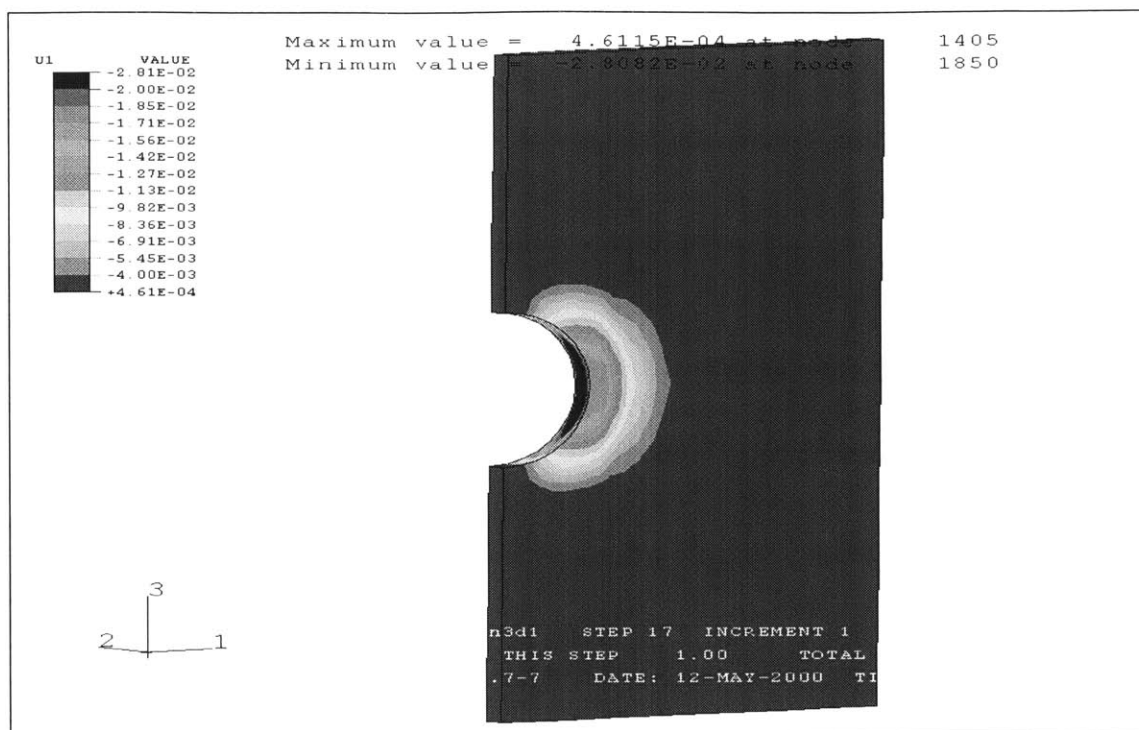


Figure 14. Displacement in the horizontal direction at section 3-4
($K_x=K_y=1$ - dry conditions - $l_u=1\text{m}$ - excavation=3m)

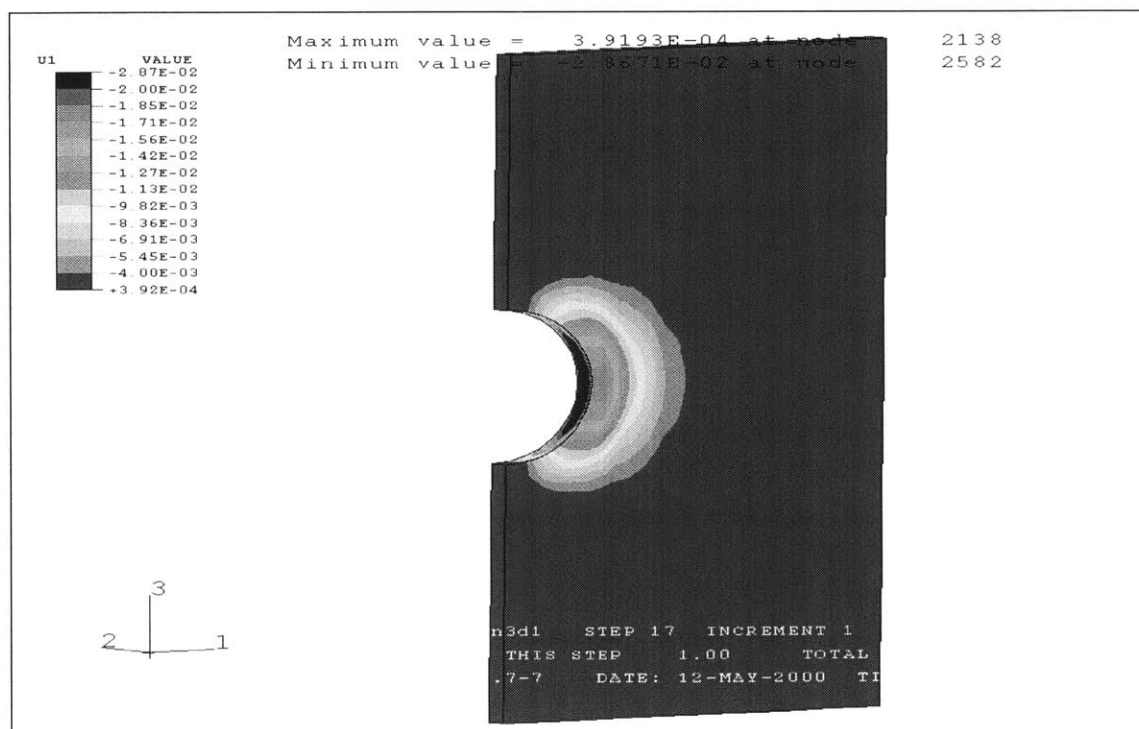


Figure 15. Displacement in the horizontal direction at section 4-5
($K_x=K_y=1$ - dry conditions - $l_u=1\text{m}$ - excavation=4m)

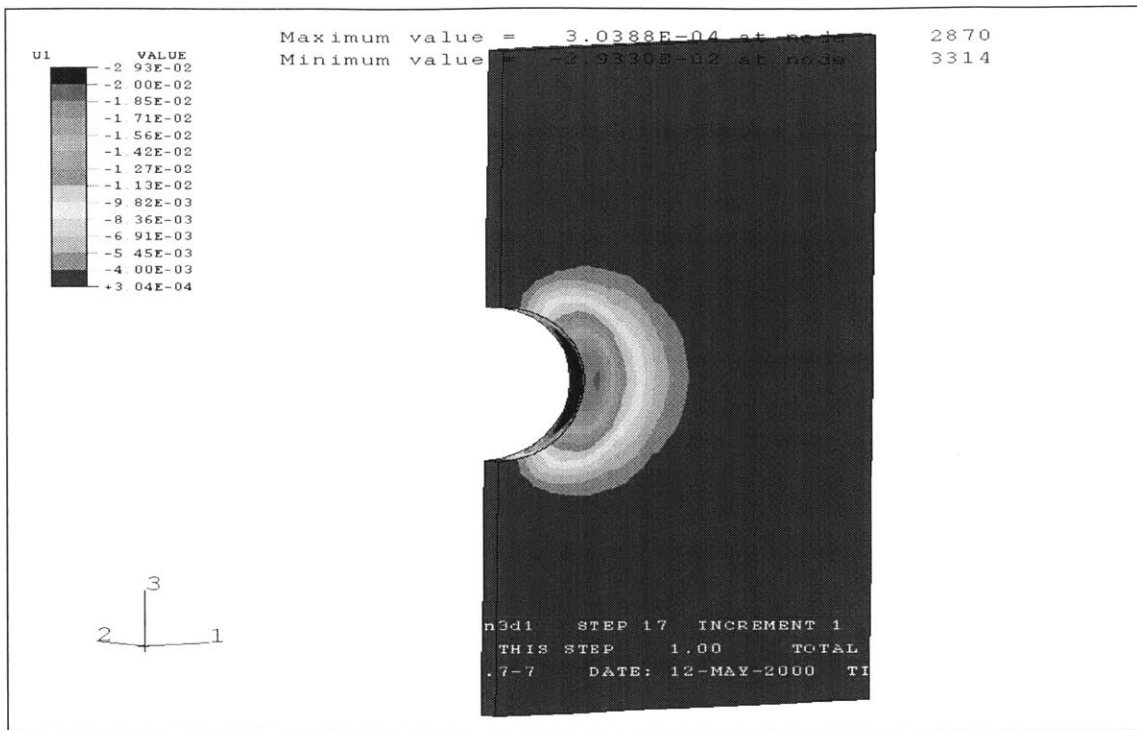


Figure 16. Displacement in the horizontal direction at section 5-6
($K_x=K_y=1$ - dry conditions - $l_u=1\text{m}$ - excavation=5m)

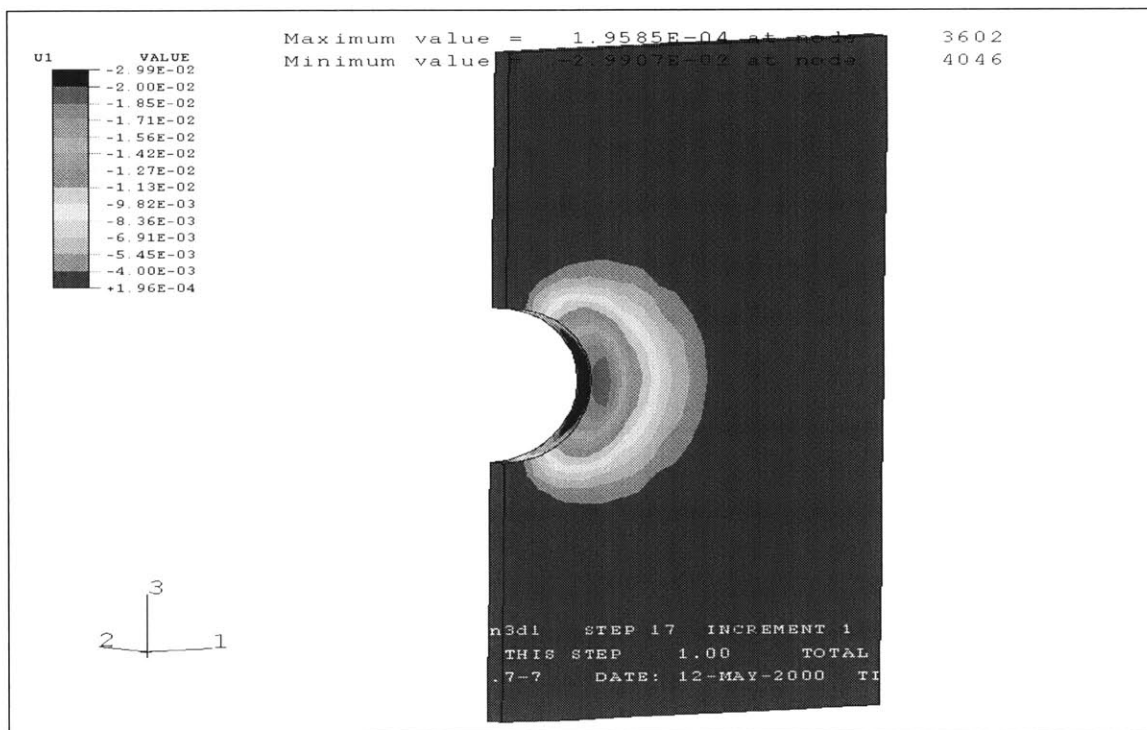


Figure 17. Displacement in the horizontal direction at section 6-7
($K_x=K_y=1$ - dry conditions - $l_u=1\text{m}$ - excavation=6m)

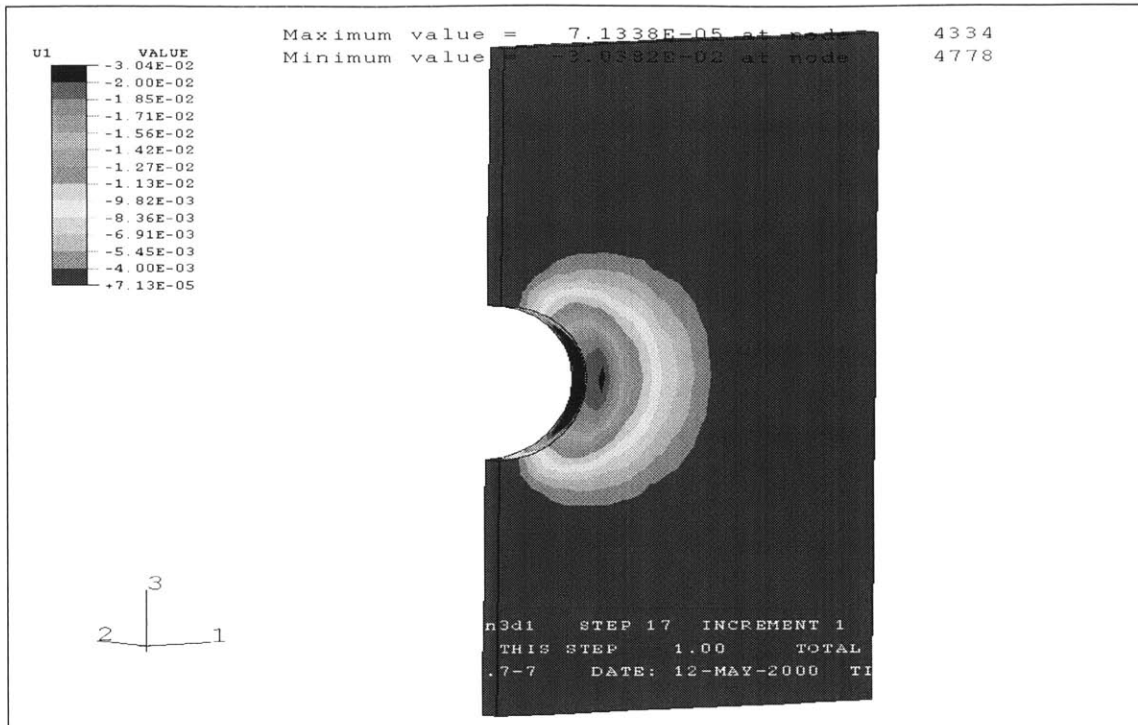


Figure 18. Displacement in the horizontal direction at section 7-8
($K_x=K_y=1$ - dry conditions - $l_u=1\text{m}$ - excavation=7m)

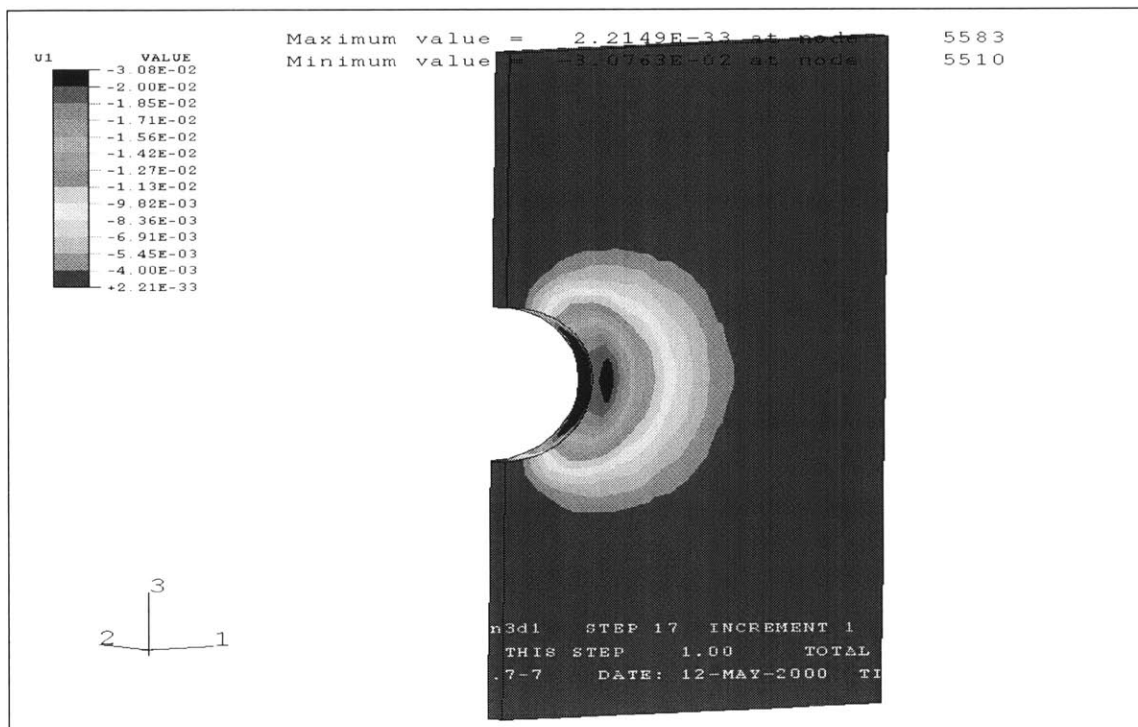


Figure 19. Displacement in the horizontal direction at section 8-9
($K_x=K_y=1$ - dry conditions - $l_u=1\text{m}$ - excavation=8m)

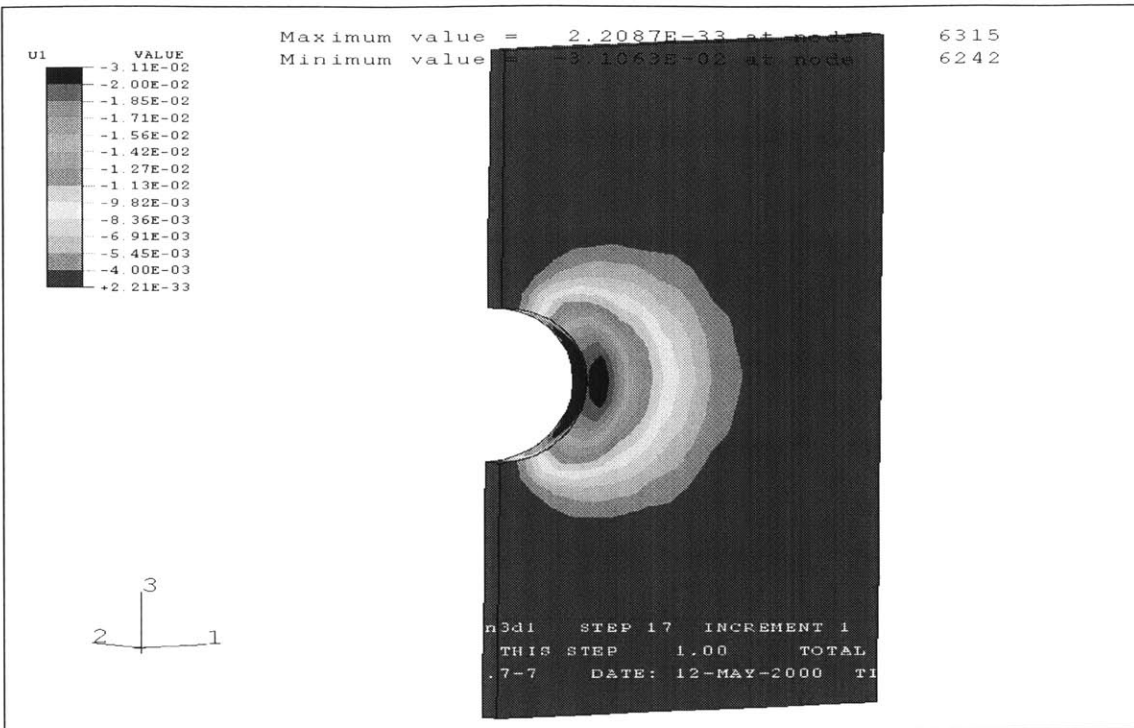


Figure 20. Displacement in the horizontal direction at section 9-10
($K_x=K_y=1$ - dry conditions - $l_u=1\text{m}$ - excavation=9m)

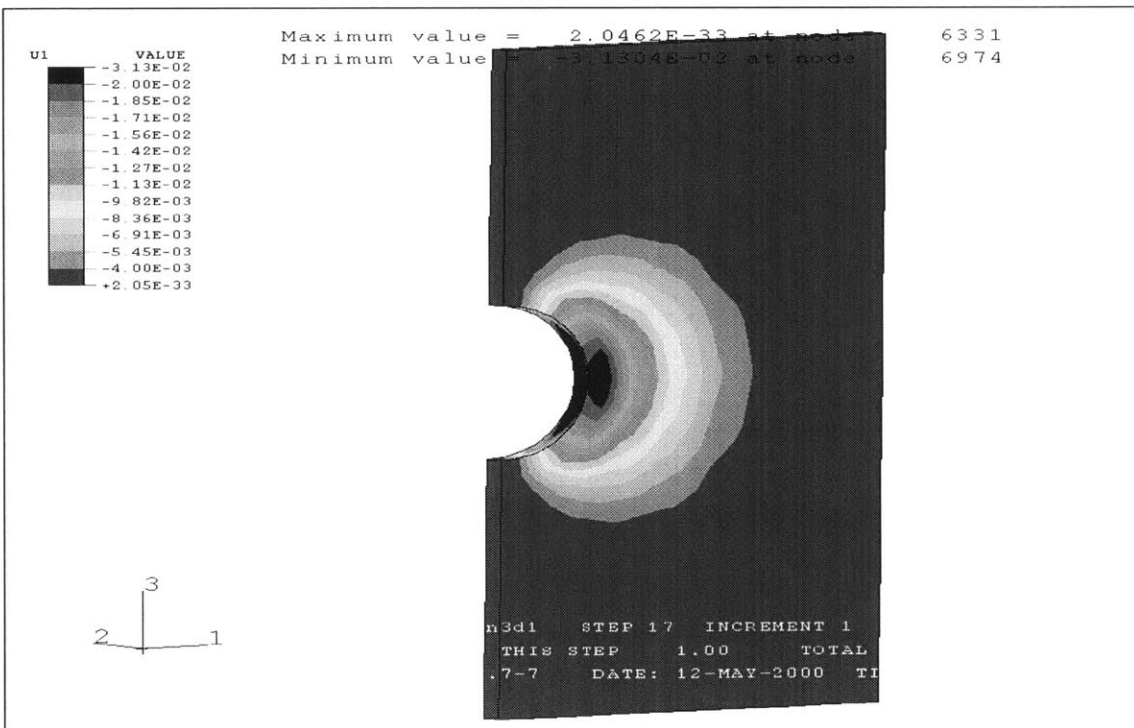


Figure 21. Displacement in the horizontal direction at section 10-11
($K_x=K_y=1$ - dry conditions - $l_u=1\text{m}$ - excavation=10m)

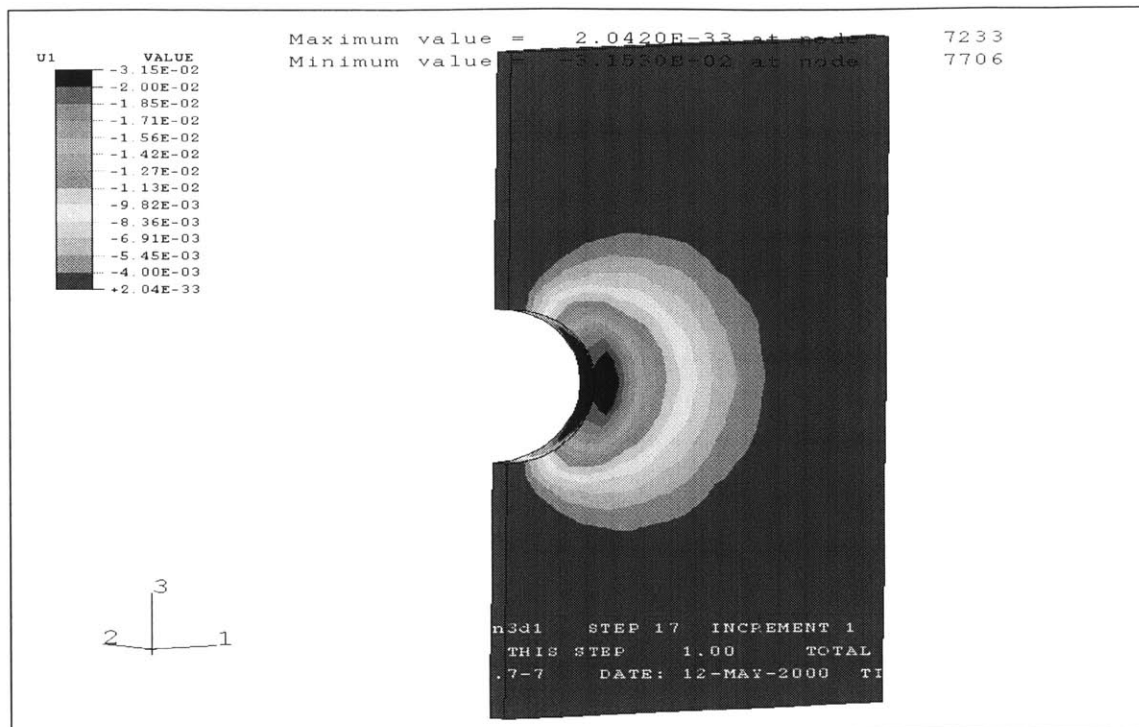


Figure 22. Displacement in the horizontal direction at section 11-12
 ($K_x=K_y=1$ - dry conditions - $l_u=1\text{m}$ - excavation= 11m)

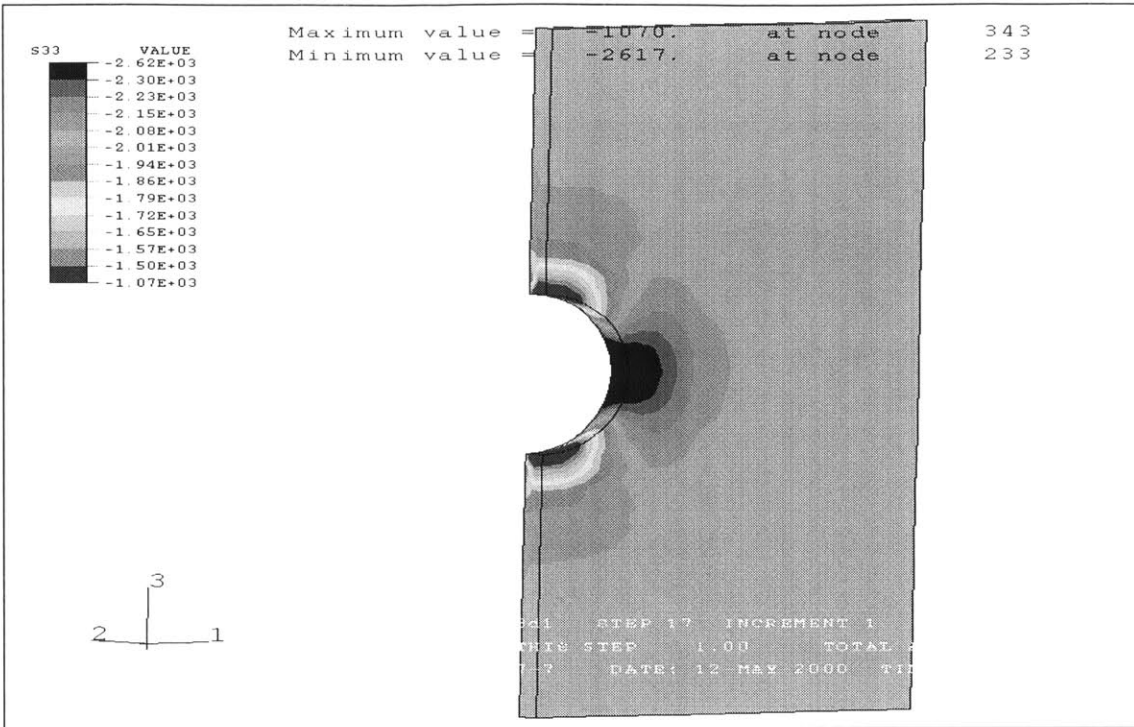


Figure 23. Stresses in the vertical direction at section 1-2
($K_x=K_y=1$ - dry conditions - $l_u=1\text{m}$ - excavation=1m)

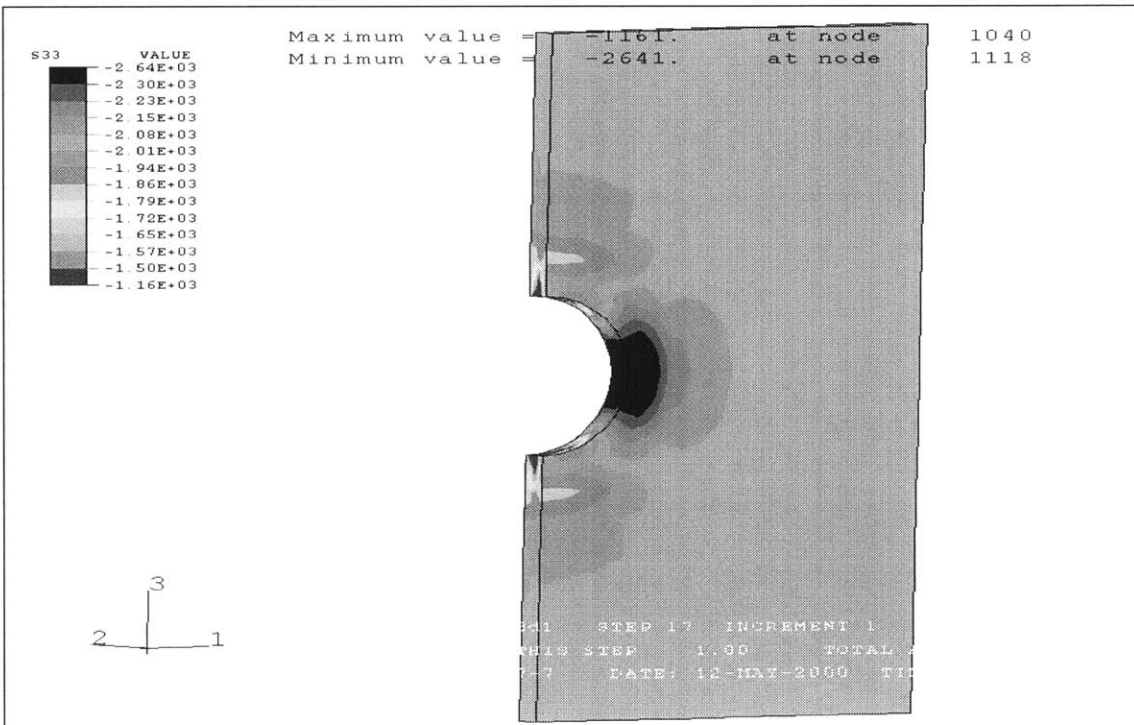


Figure 24. Stresses in the vertical direction at section 2-3
($K_x=K_y=1$ - dry conditions - $l_u=1\text{m}$ - excavation=2m)

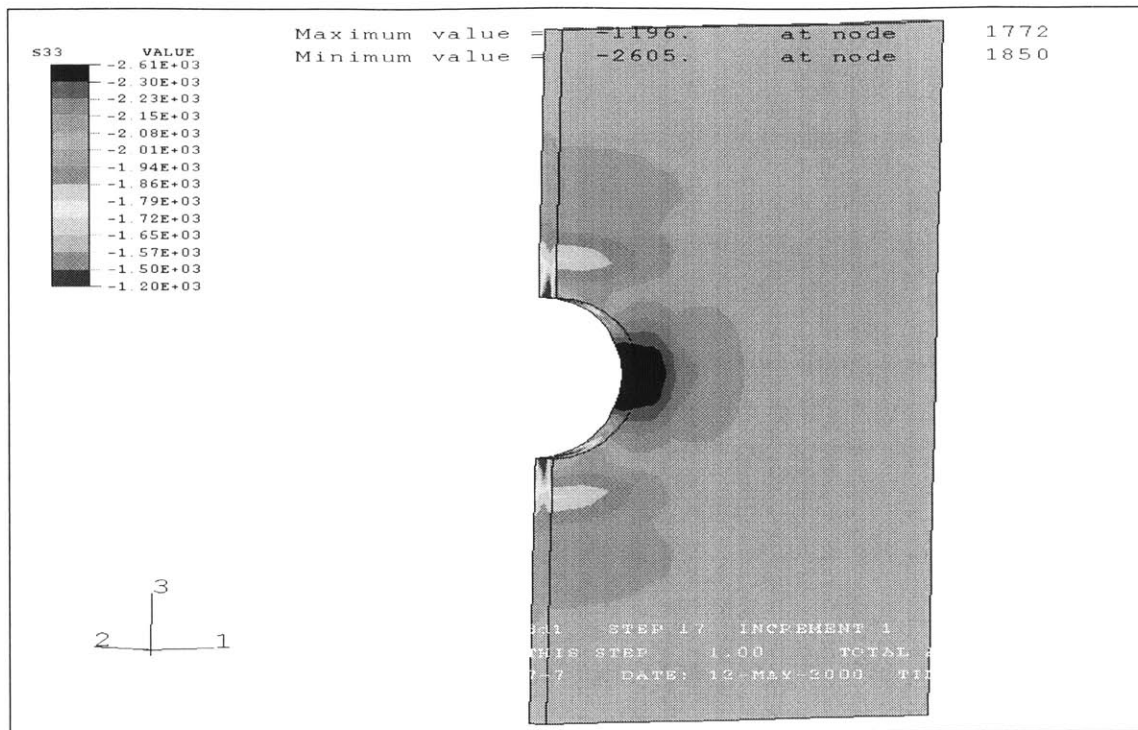


Figure 25. Stresses in the vertical direction at section 3-4
($K_x=K_y=1$ - dry conditions - $l_u=1\text{m}$ - excavation=3m)

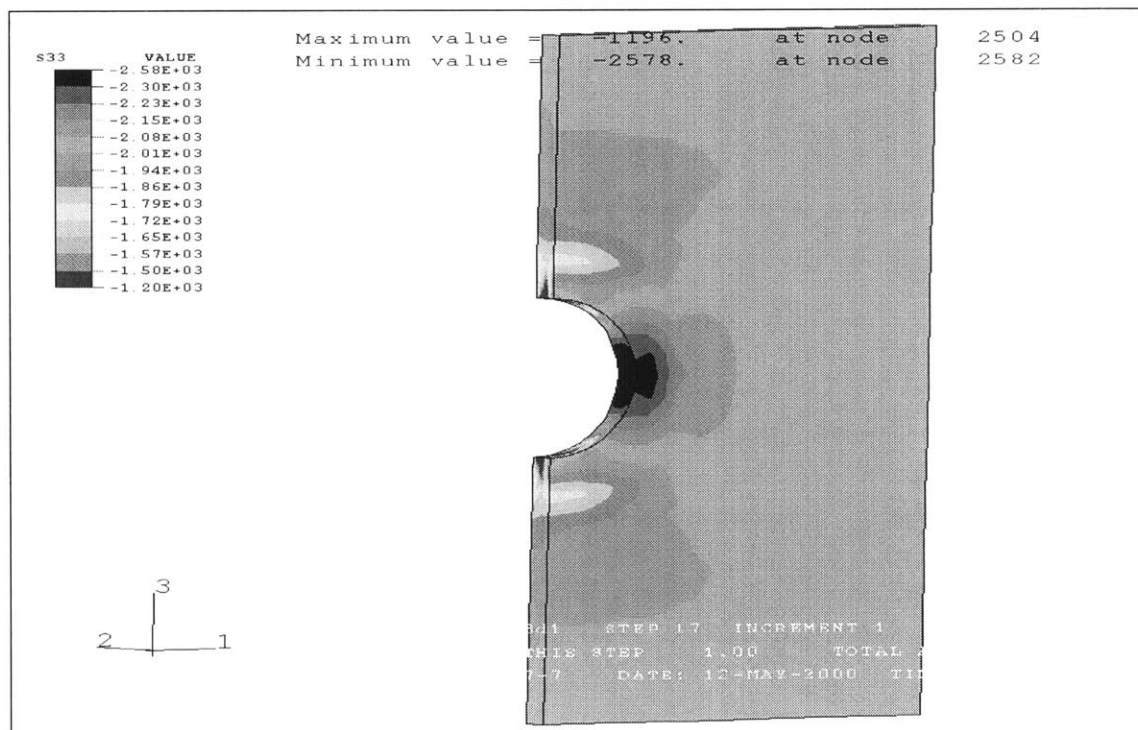


Figure 26. Stresses in the vertical direction at section 4-5
($K_x=K_y=1$ - dry conditions - $l_u=1\text{m}$ - excavation=4m)

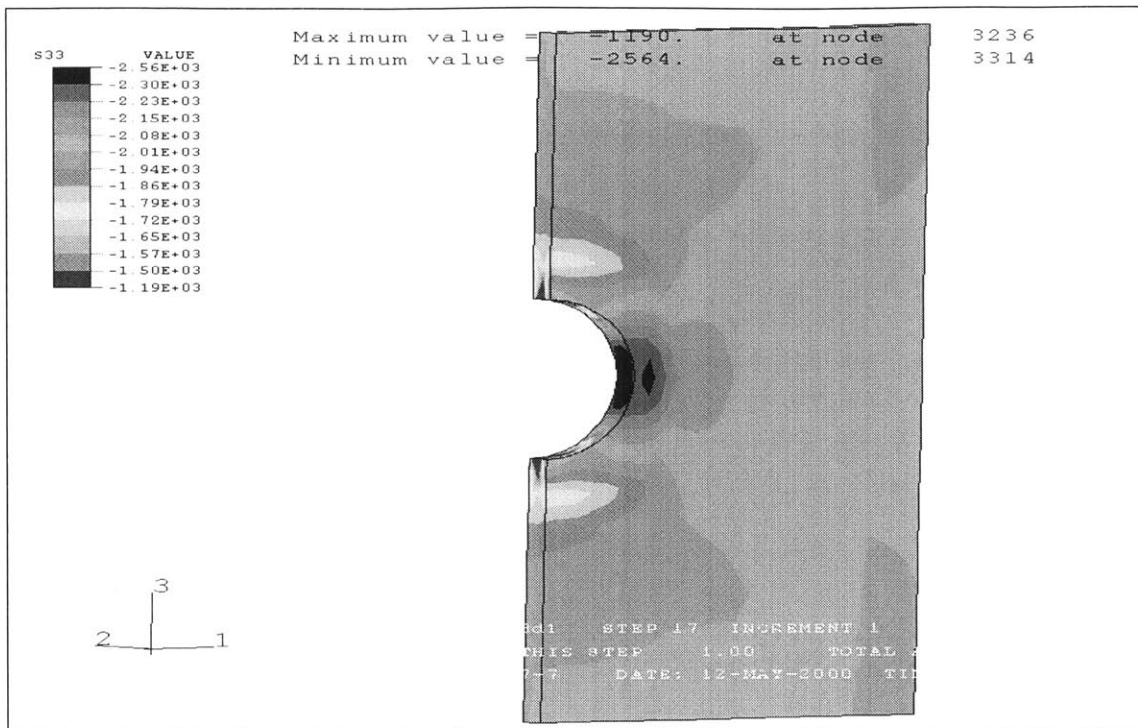


Figure 27. Stresses in the vertical direction at section 5-6
($K_x=K_y=1$ - dry conditions - $I_u=1\text{m}$ - excavation=5m)

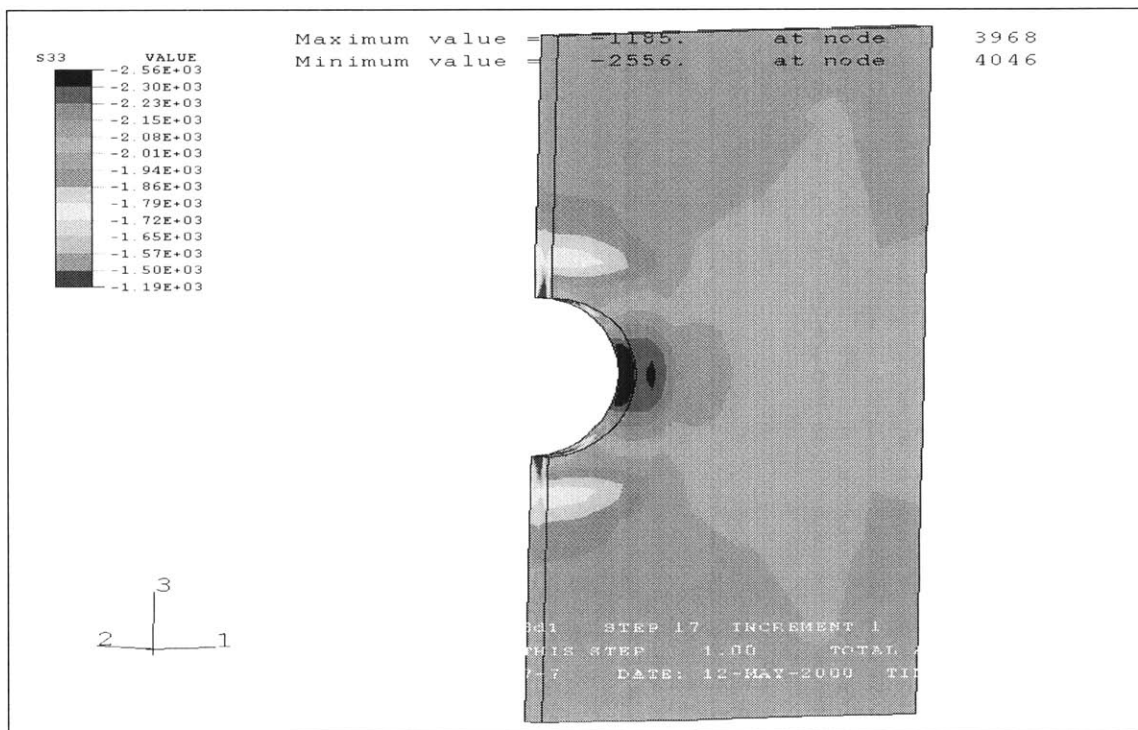


Figure 28. Stresses in the vertical direction at section 6-7
($K_x=K_y=1$ - dry conditions - $I_u=1\text{m}$ - excavation=6m)

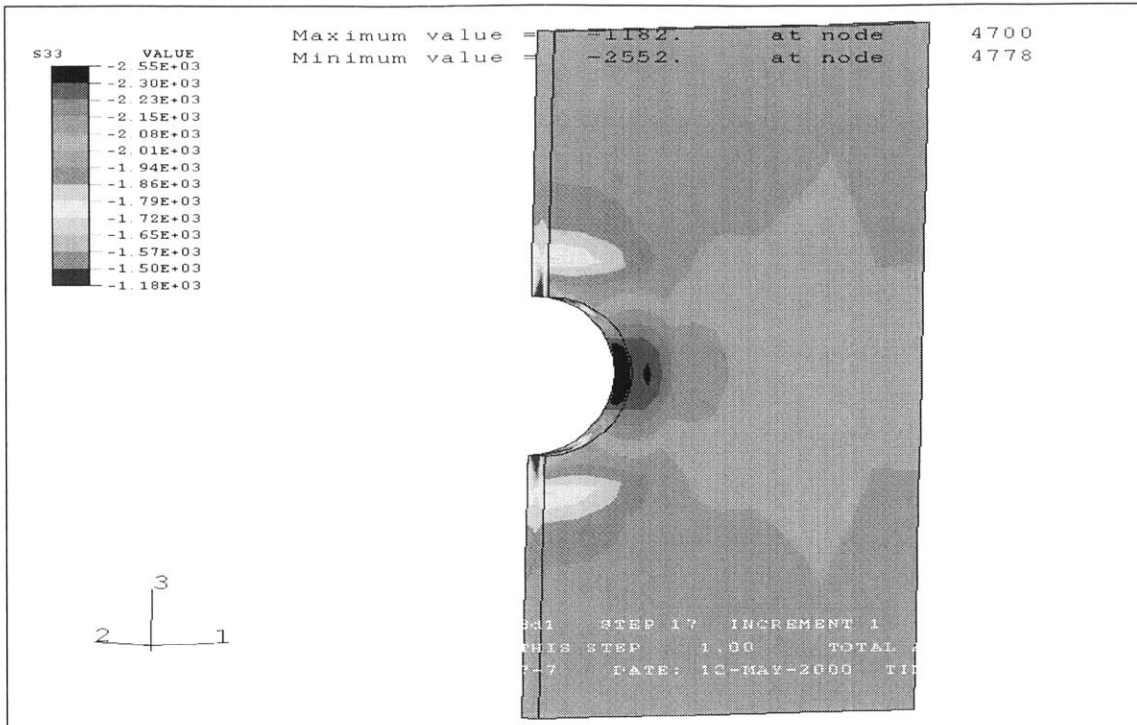


Figure 29. Stresses in the vertical direction at section 7-8
($K_x=K_y=1$ - dry conditions - $l_u=1\text{m}$ - excavation=7m)

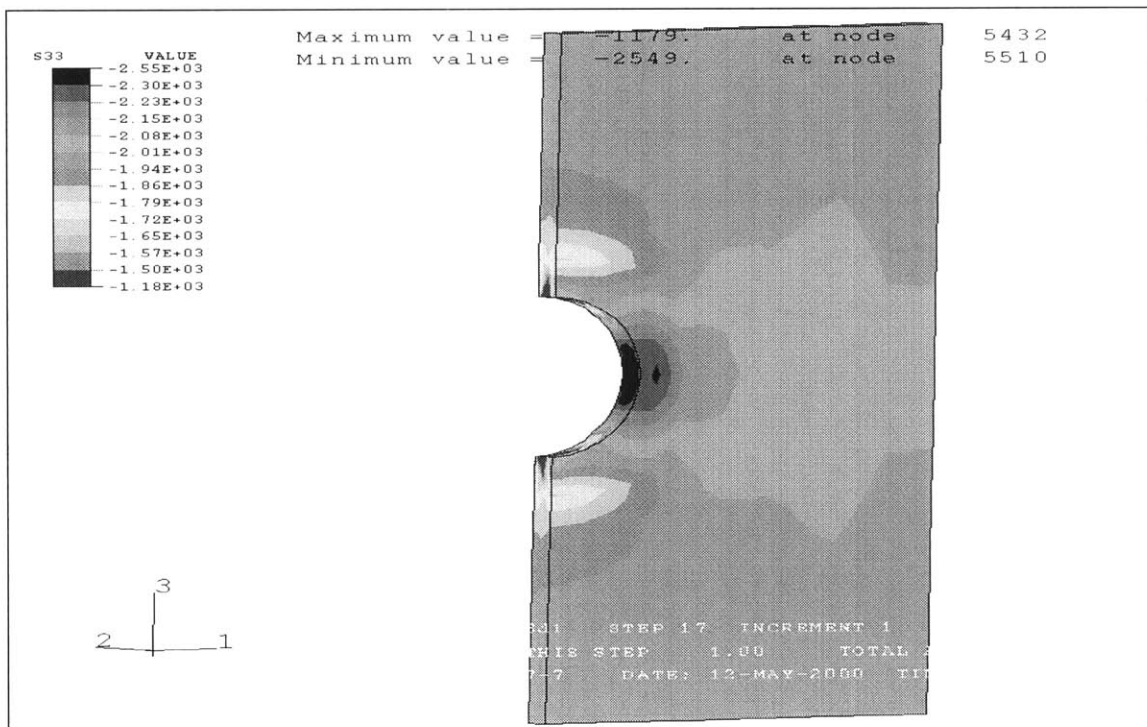


Figure 30. Stresses in the vertical direction at section 8-9
($K_x=K_y=1$ - dry conditions - $l_u=1\text{m}$ - excavation=8m)

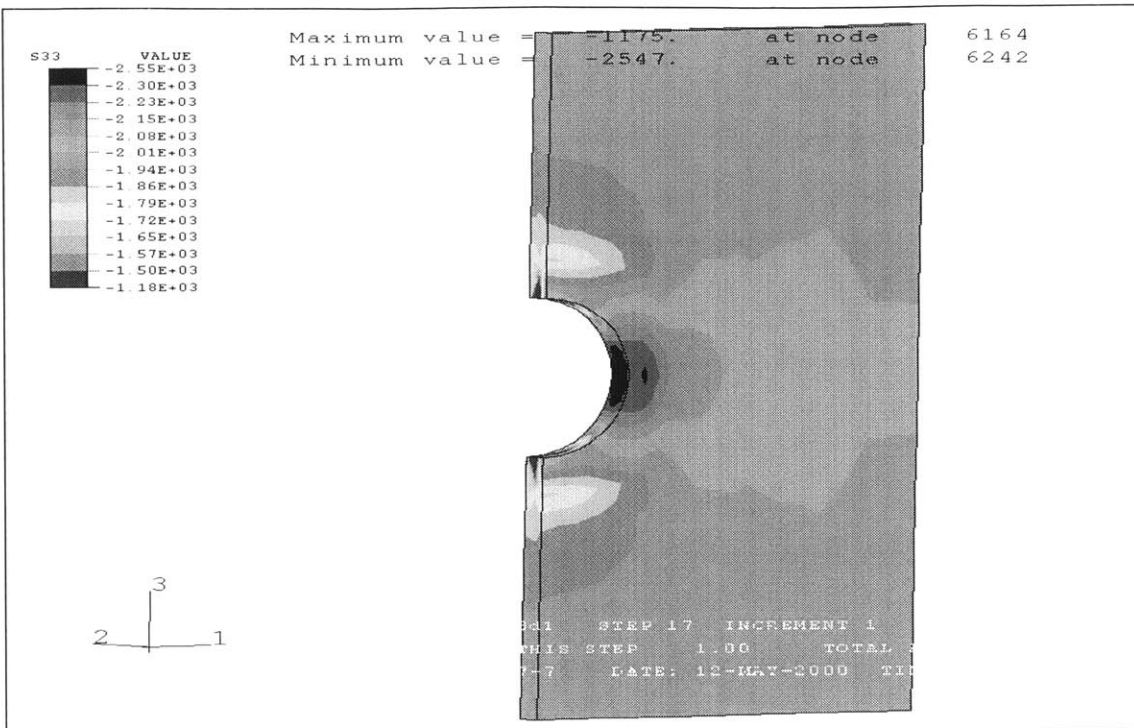


Figure 31. Stresses in the vertical direction at section 9-10
($K_x=K_y=1$ - dry conditions - $l_u=1\text{m}$ - excavation=9m)

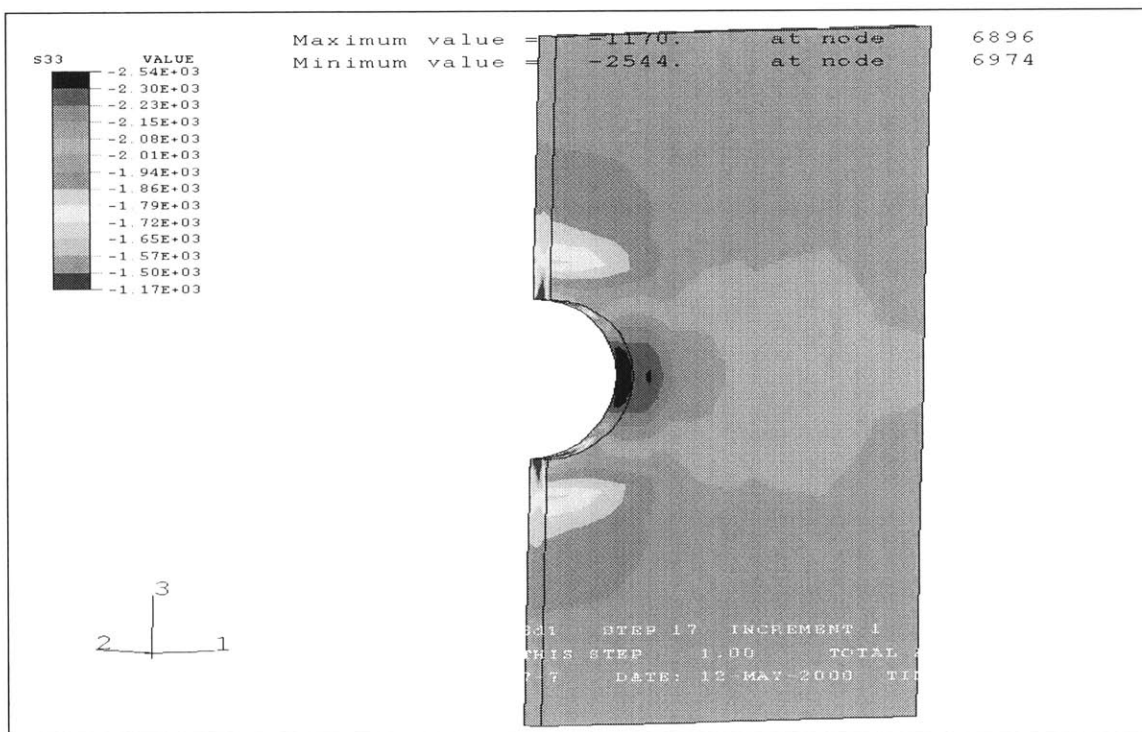


Figure 32. Stresses in the vertical direction at section 10-11
($K_x=K_y=1$ - dry conditions - $l_u=1\text{m}$ - excavation=10m)

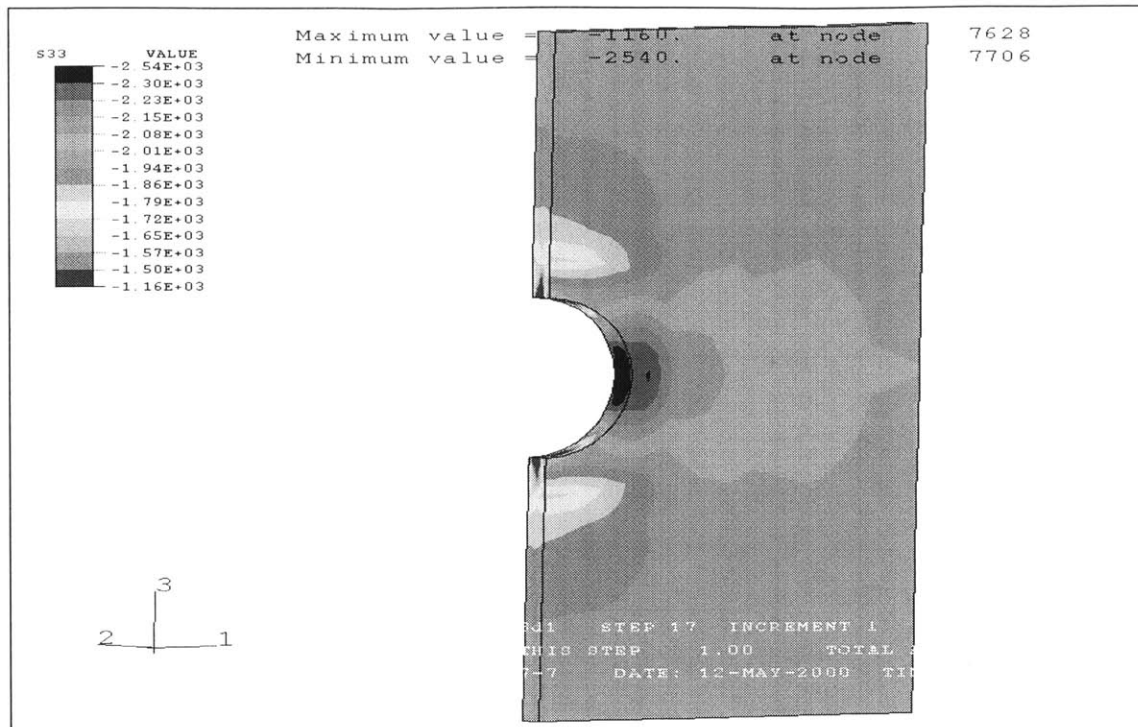


Figure 33. Stresses in the vertical direction at section 11-12
($K_x=K_y=1$ - dry conditions - $l_u=1\text{m}$ - excavation= 11m)

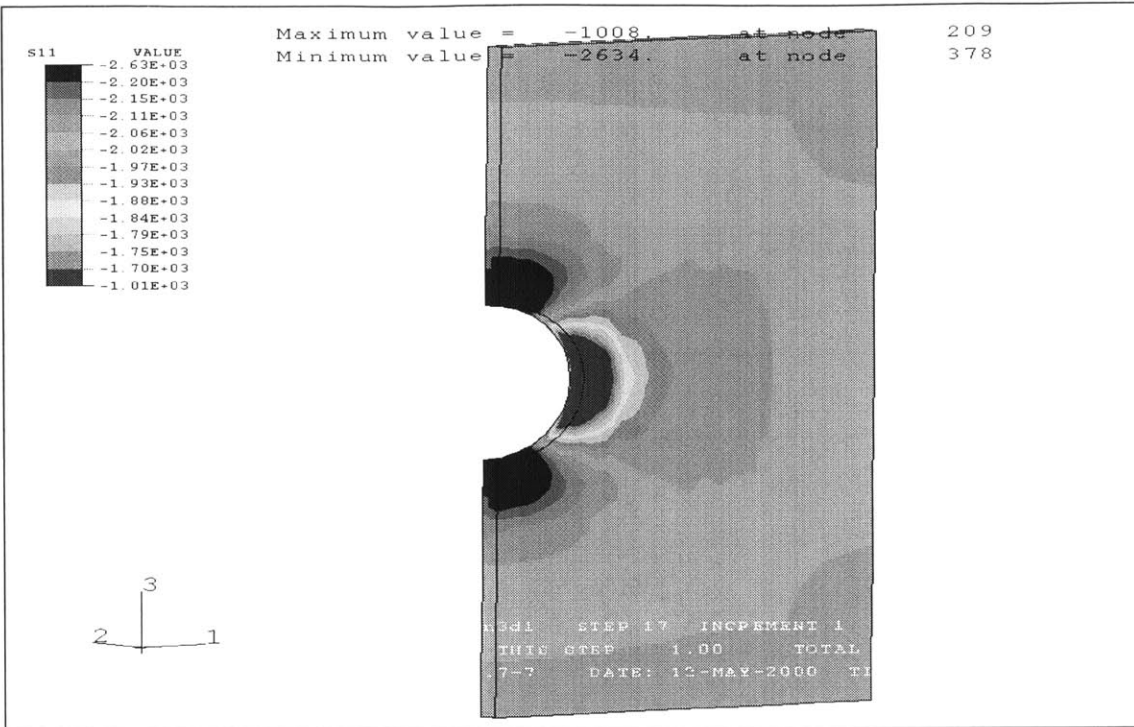


Figure 34. Stresses in the horizontal direction at section 1-2
($K_x=K_y=1$ - dry conditions - $l_u=1\text{m}$ - excavation= 1m)

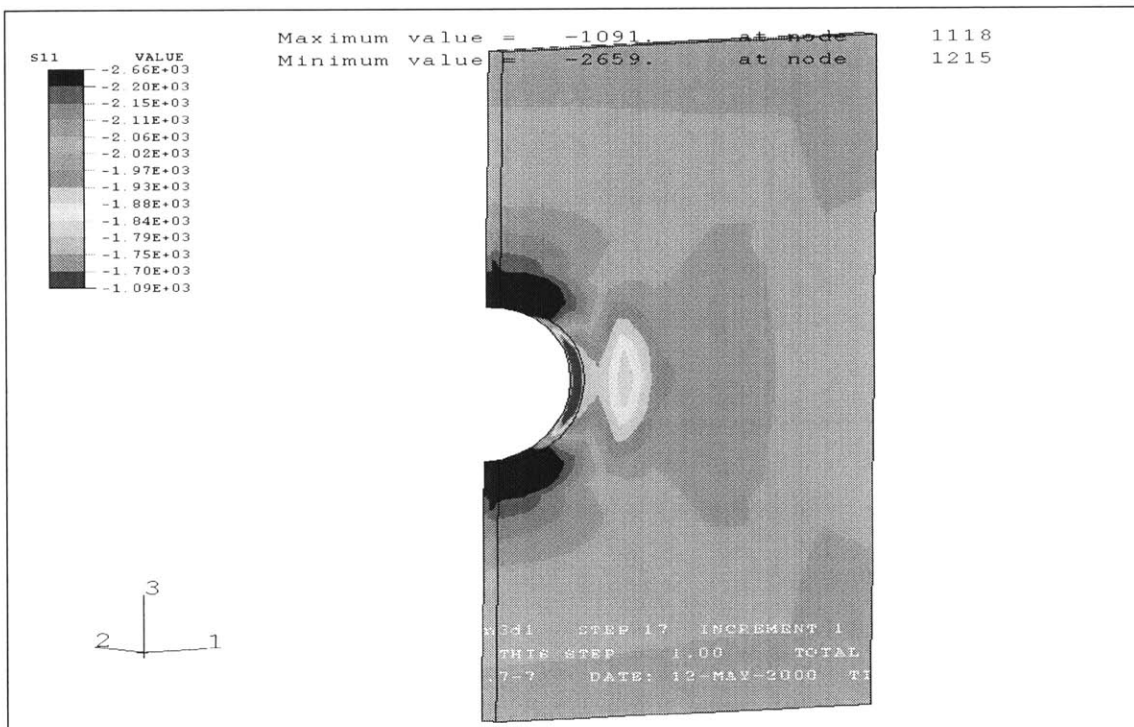


Figure 35. Stresses in the horizontal direction at section 2-3
($K_x=K_y=1$ - dry conditions - $l_u=1\text{m}$ - excavation= 2m)

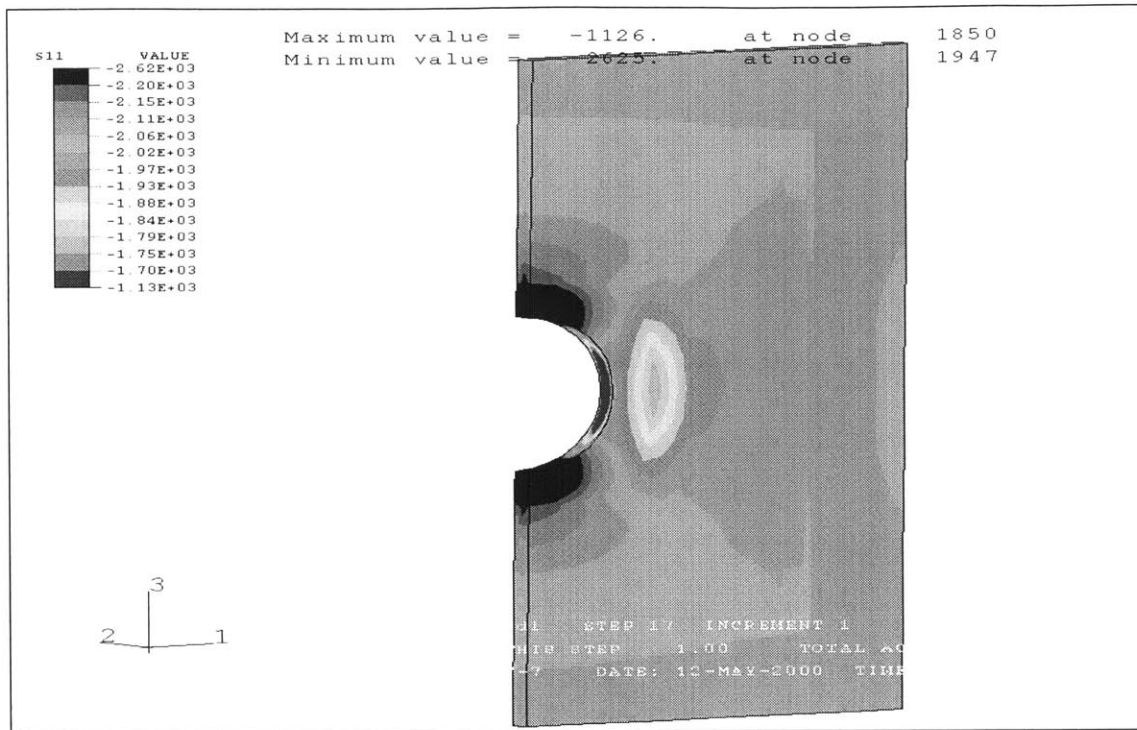


Figure 36. Stresses in the horizontal direction at section 3-4
($K_x=K_y=1$ - dry conditions - $I_u=1\text{m}$ - excavation=3m)

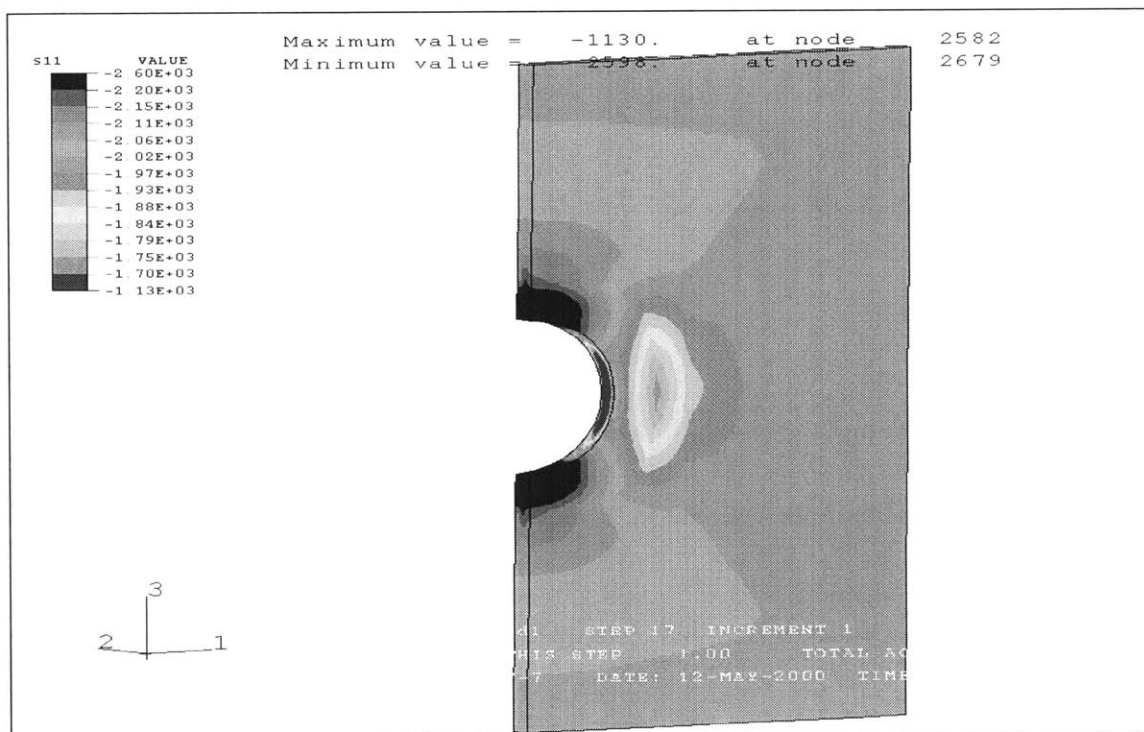


Figure 37. Stresses in the horizontal direction at section 4-5
($K_x=K_y=1$ - dry conditions - $I_u=1\text{m}$ - excavation=4m)

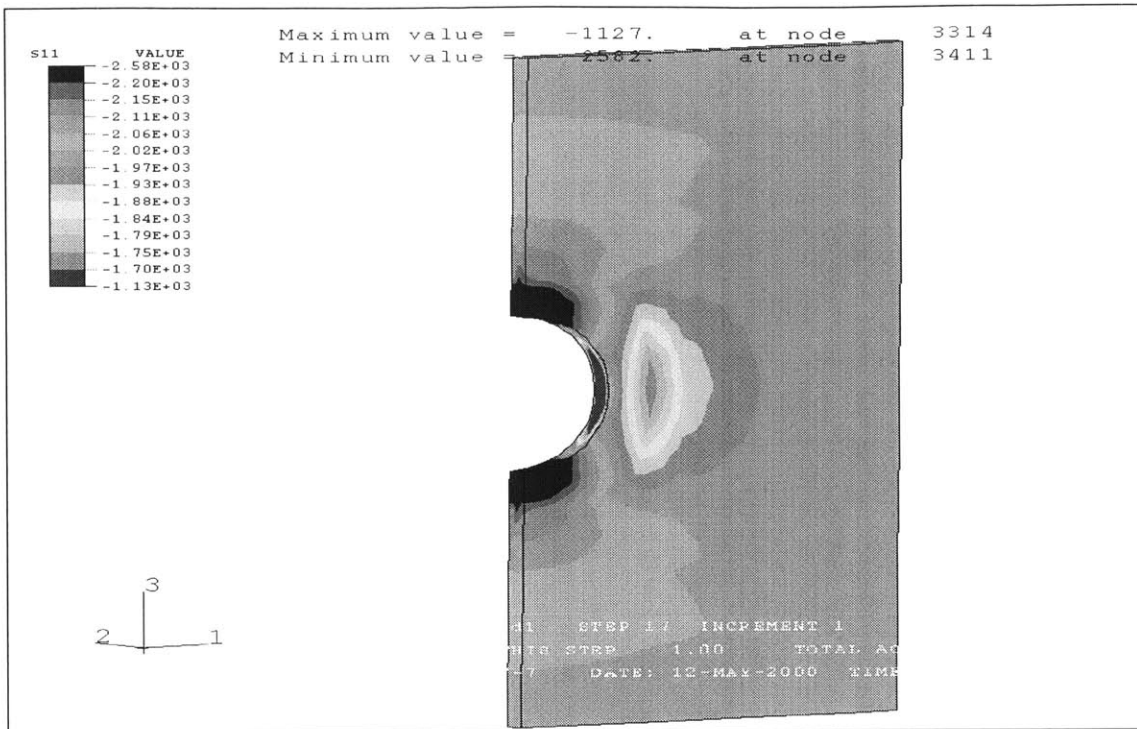


Figure 38. Stresses in the horizontal direction at section 5-6
($K_x=K_y=1$ - dry conditions - $I_u=1\text{m}$ - excavation=5m)

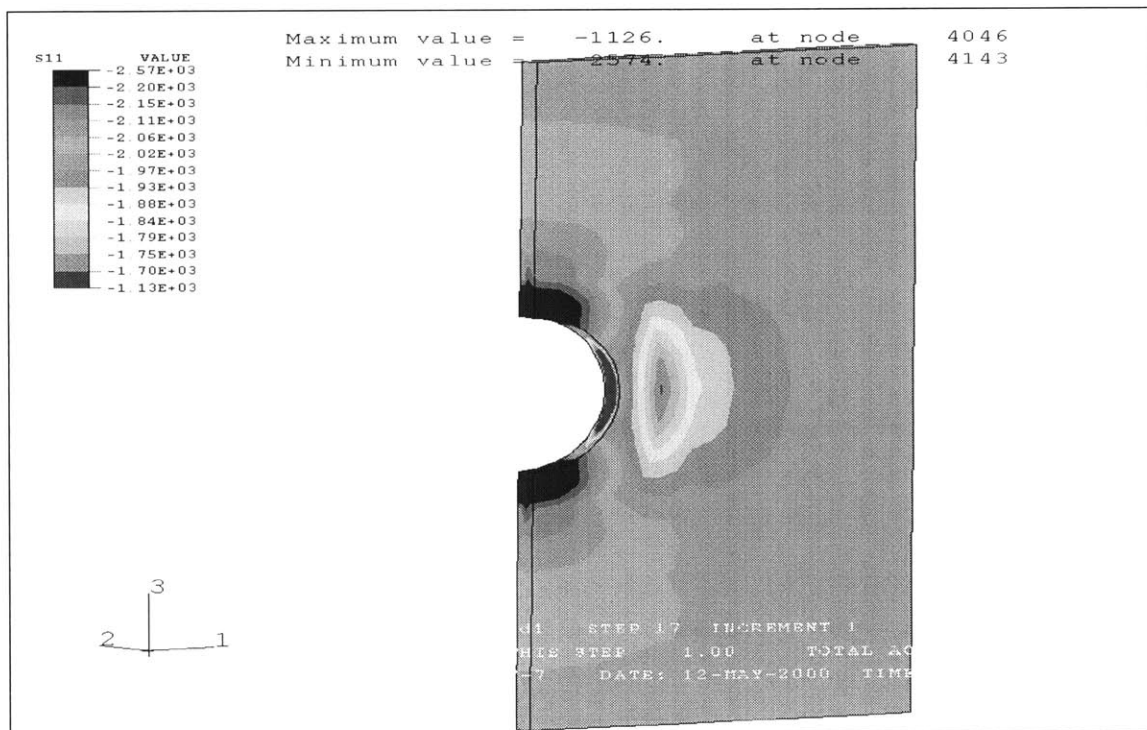


Figure 39. Stresses in the horizontal direction at section 6-7
($K_x=K_y=1$ - dry conditions - $I_u=1\text{m}$ - excavation=6m)

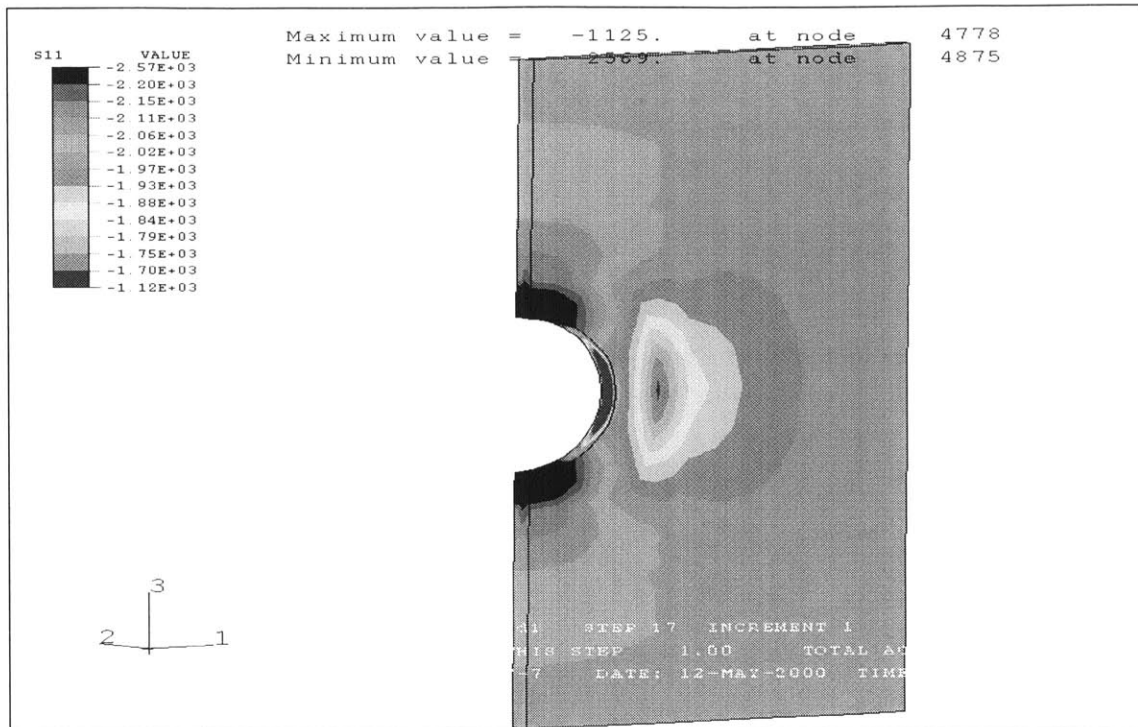


Figure 40. Stresses in the horizontal direction at section 7-8
($K_x=K_y=1$ - dry conditions - $l_u=1\text{m}$ - excavation=7m)

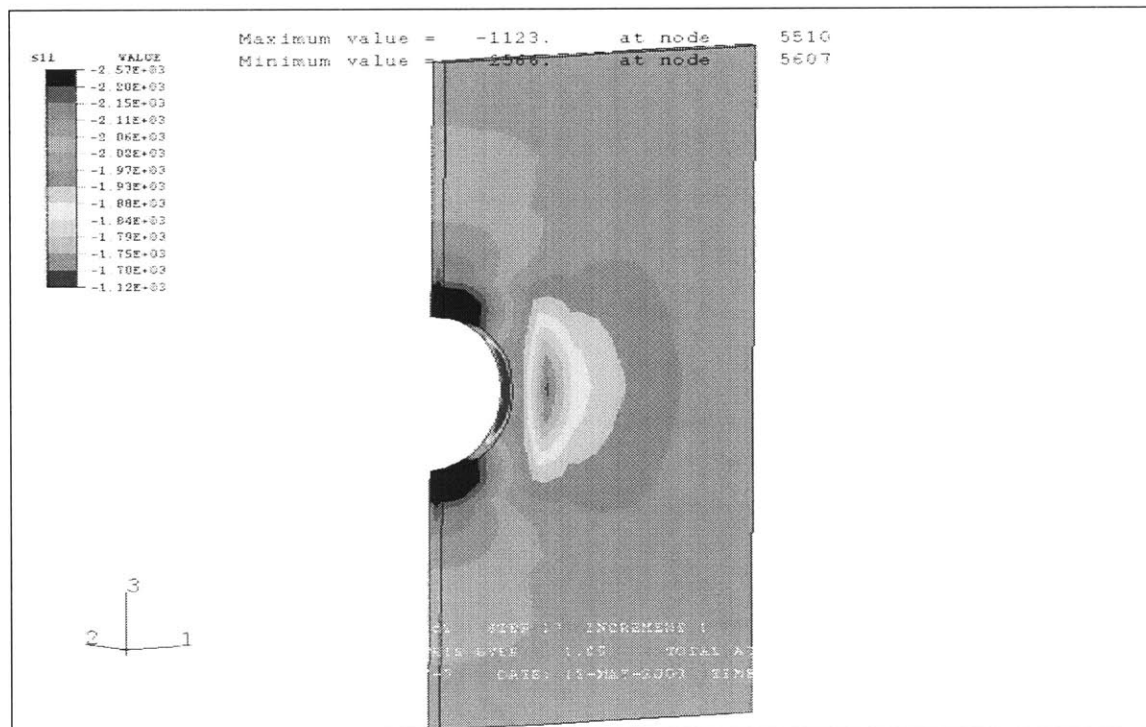


Figure 41. Stresses in the horizontal direction at section 8-9
($K_x=K_y=1$ - dry conditions - $l_u=1\text{m}$ - excavation=8m)

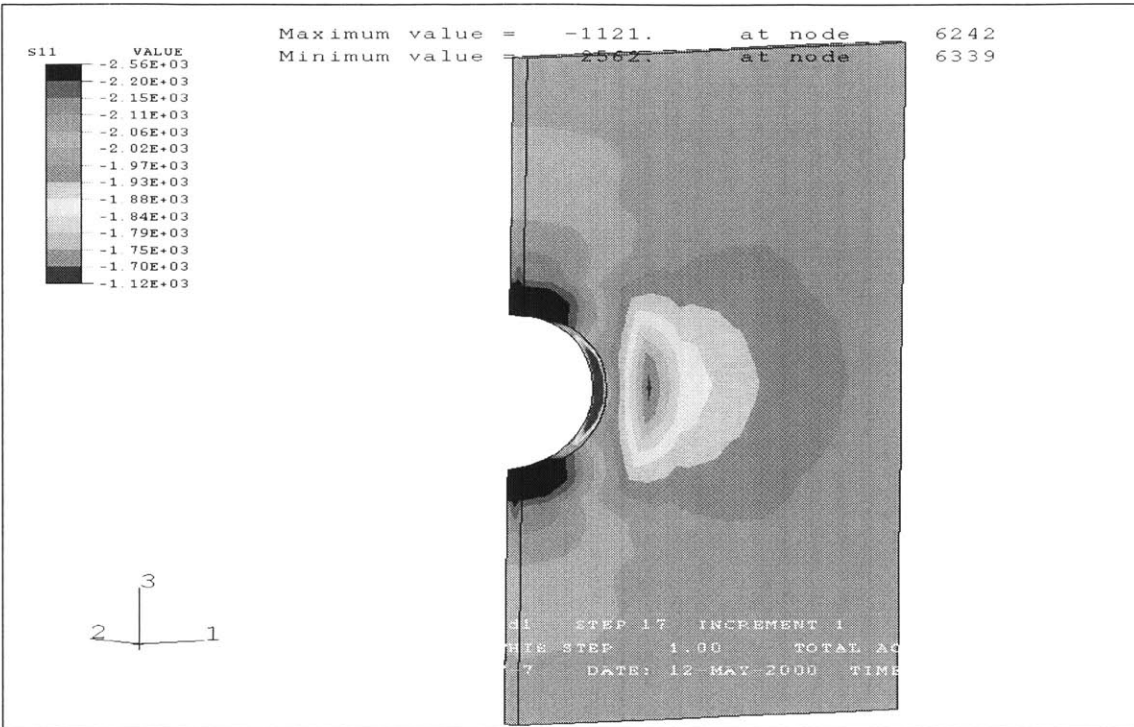


Figure 42. Stresses in the horizontal direction at section 9-10
($K_x=K_y=1$ - dry conditions - $l_0=1\text{m}$ - excavation=9m)

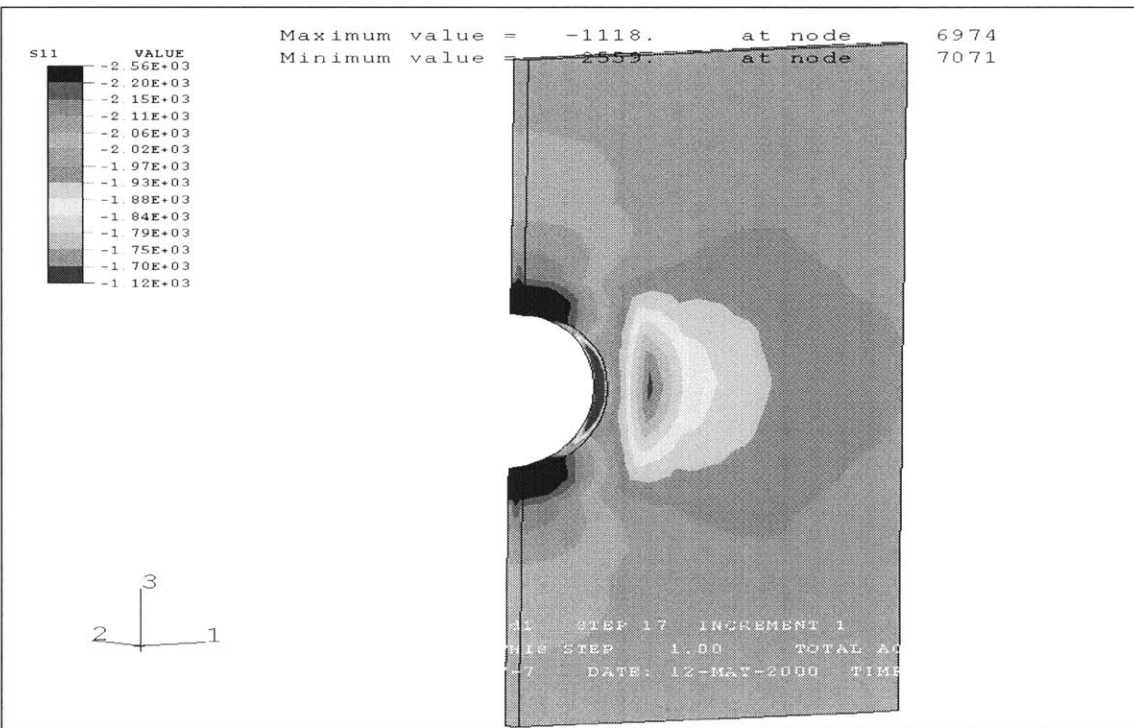


Figure 43. Stresses in the horizontal direction at section 10-11
($K_x=K_y=1$ - dry conditions - $l_0=1\text{m}$ - excavation=10m)

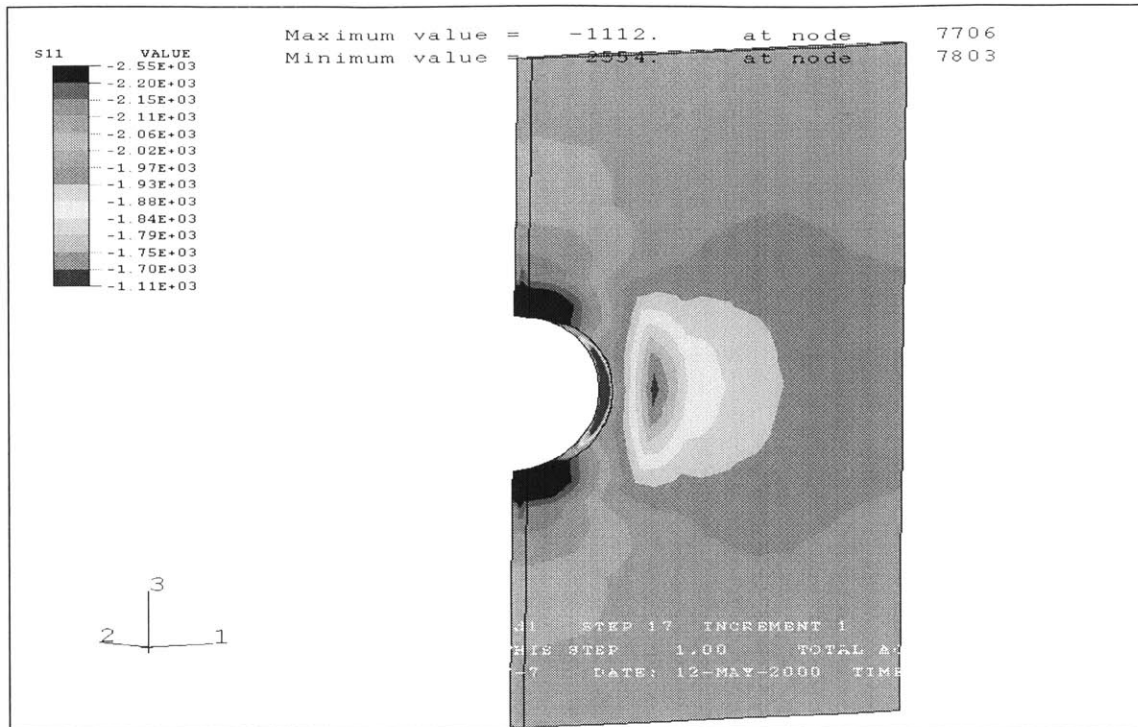


Figure 44. Stresses in the horizontal direction at section 11-12
($K_x=K_y=1$ - dry conditions - $l_u=1\text{m}$ - excavation=11m)

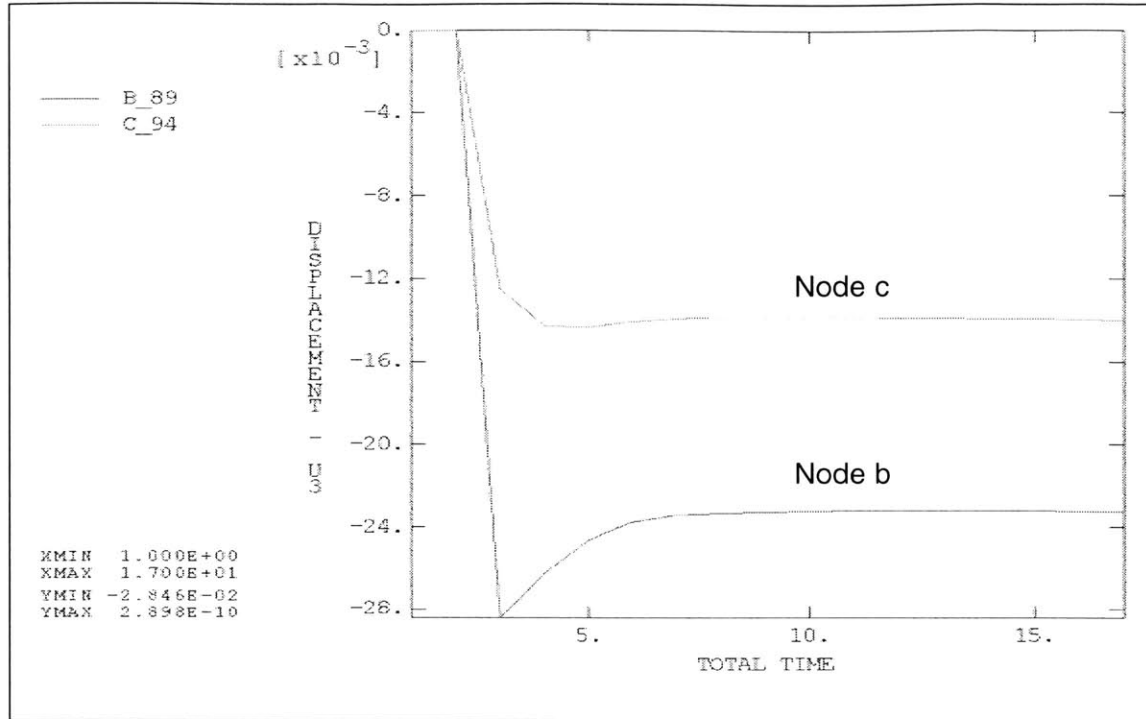


Figure 45. Variation of vertical displacement during the excavation ($K_x=K_y=1$ - dry conditions - $l_u=1\text{m}$ - nodes b,c)

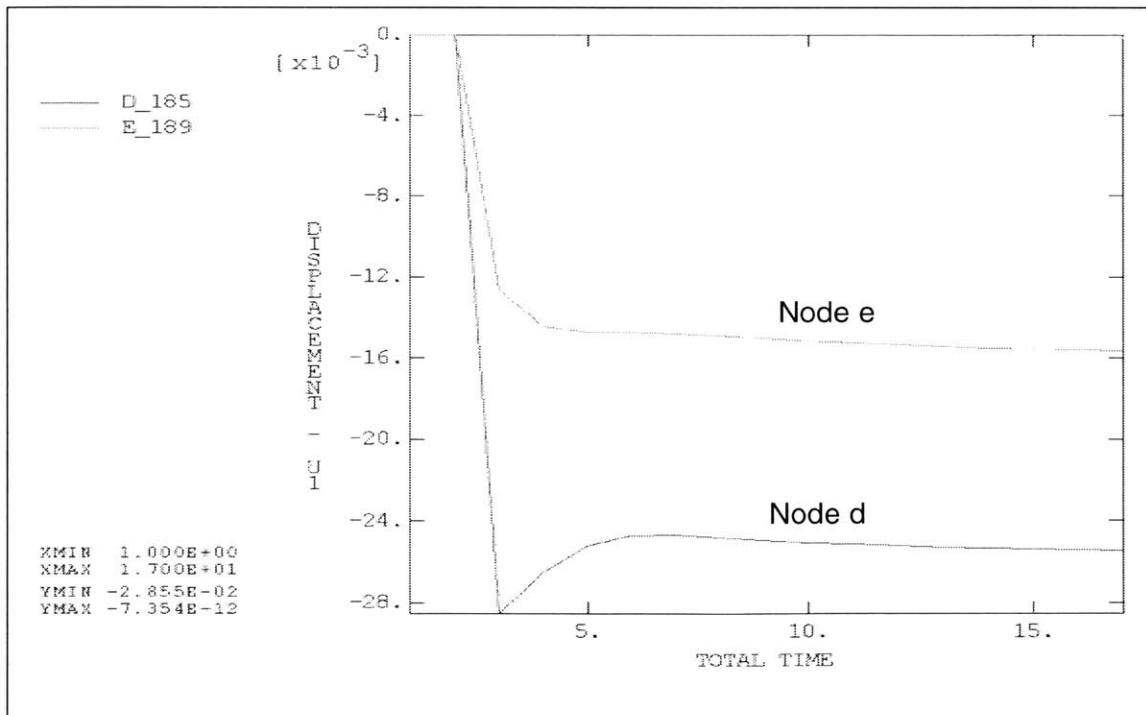


Figure 46. Variation of horizontal displacement during the excavation ($K_x=K_y=1$ - dry conditions - $l_u=1\text{m}$ - node d,e)

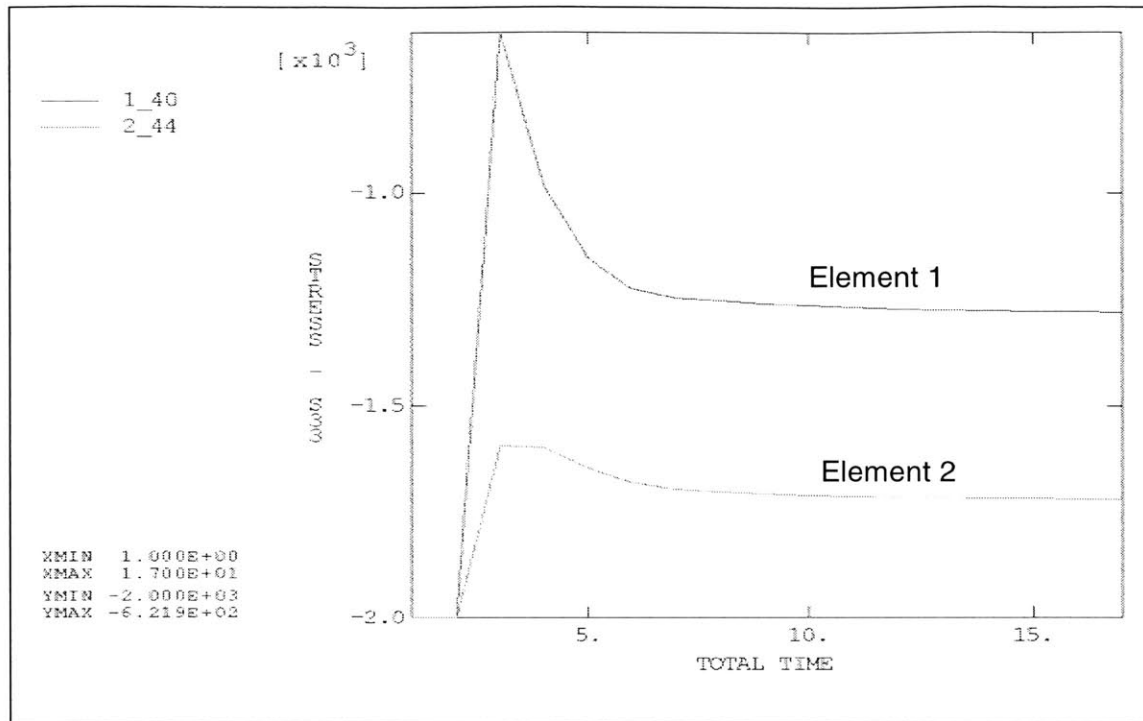


Figure 47. Variation of vertical stress during the excavation
($K_x=K_y=1$ - dry conditions - $l_u=1\text{m}$ - elements 1,2)

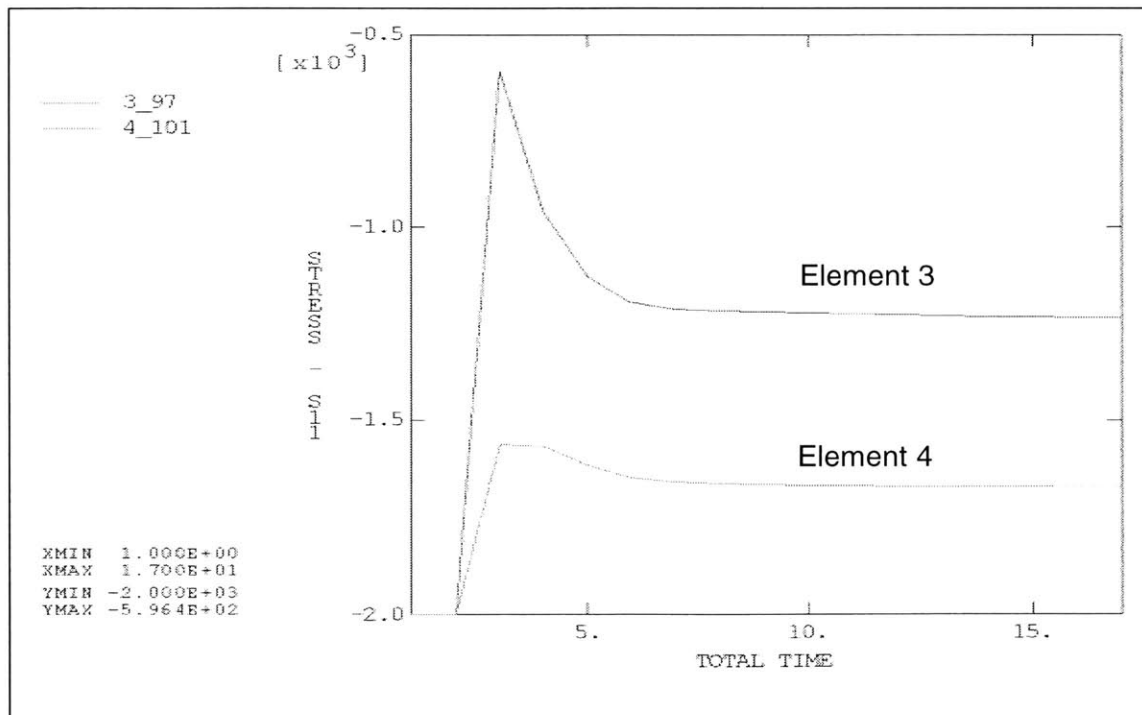


Figure 48. Variation of horizontal stress during the excavation
($K_x=K_y=1$ - dry conditions - $l_u=1\text{m}$ - elements 3,4)

APPENDIX IVb

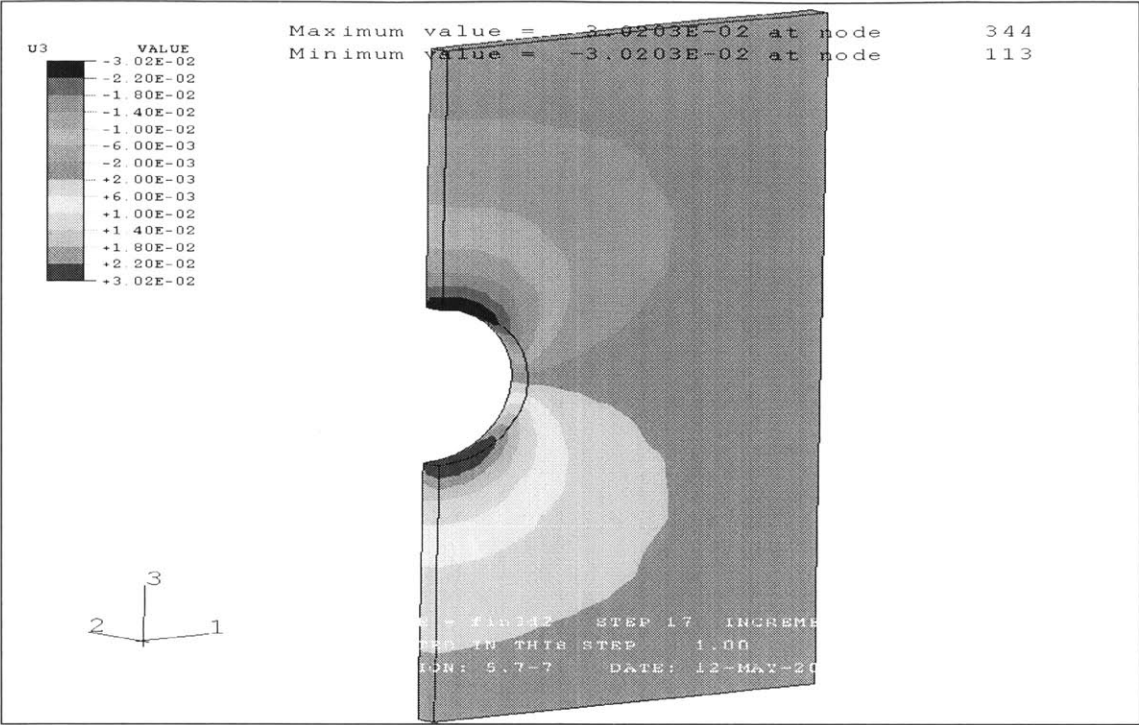


Figure 1. Displacement in the vertical direction at section 1-2
($K_x=K_y=0.5$ - dry conditions - $l_u=1\text{m}$ - excavation=1m)

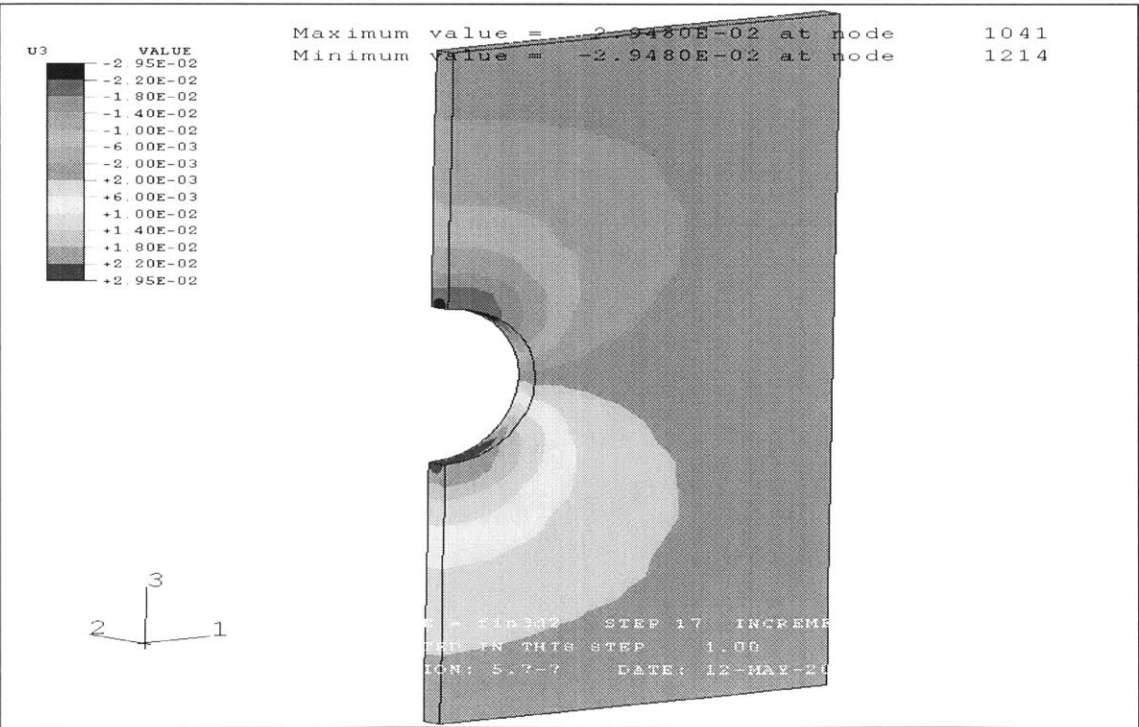


Figure 2. Displacement in the vertical direction at section 2-3
($K_x=K_y=0.5$ - dry conditions - $l_u=1\text{m}$ - excavation=2m)

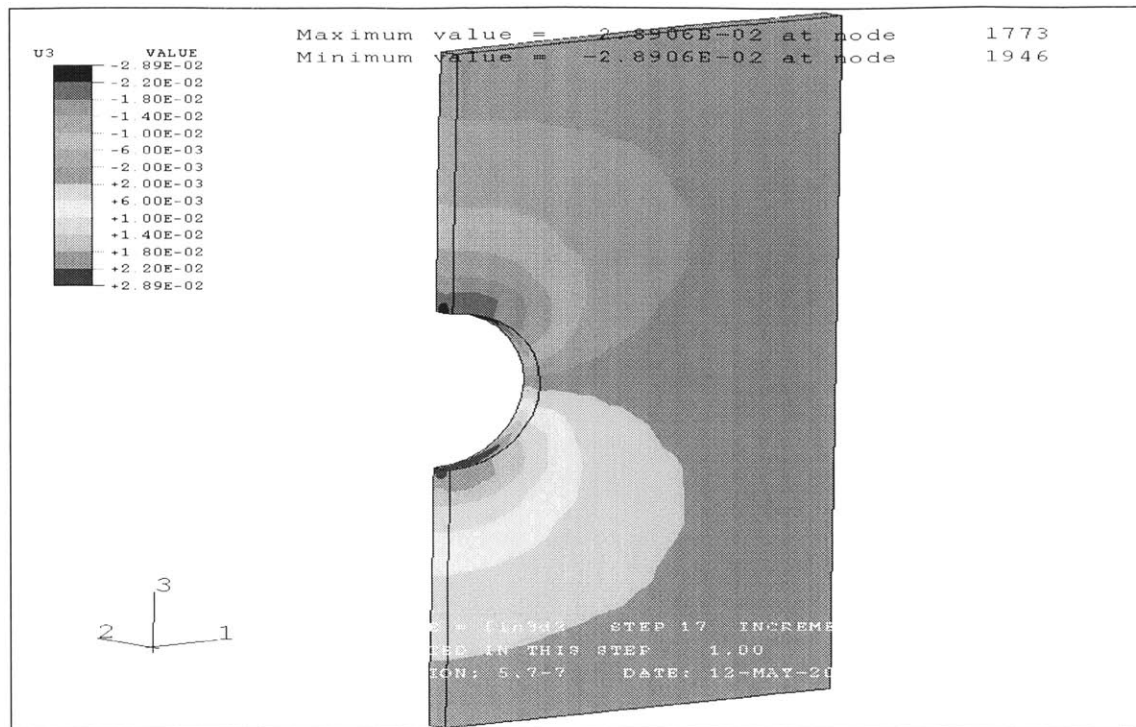


Figure 3. Displacement in the vertical direction at section 3-4
($K_x=K_y=0.5$ - dry conditions - $l_u=1\text{m}$ - excavation=3m)

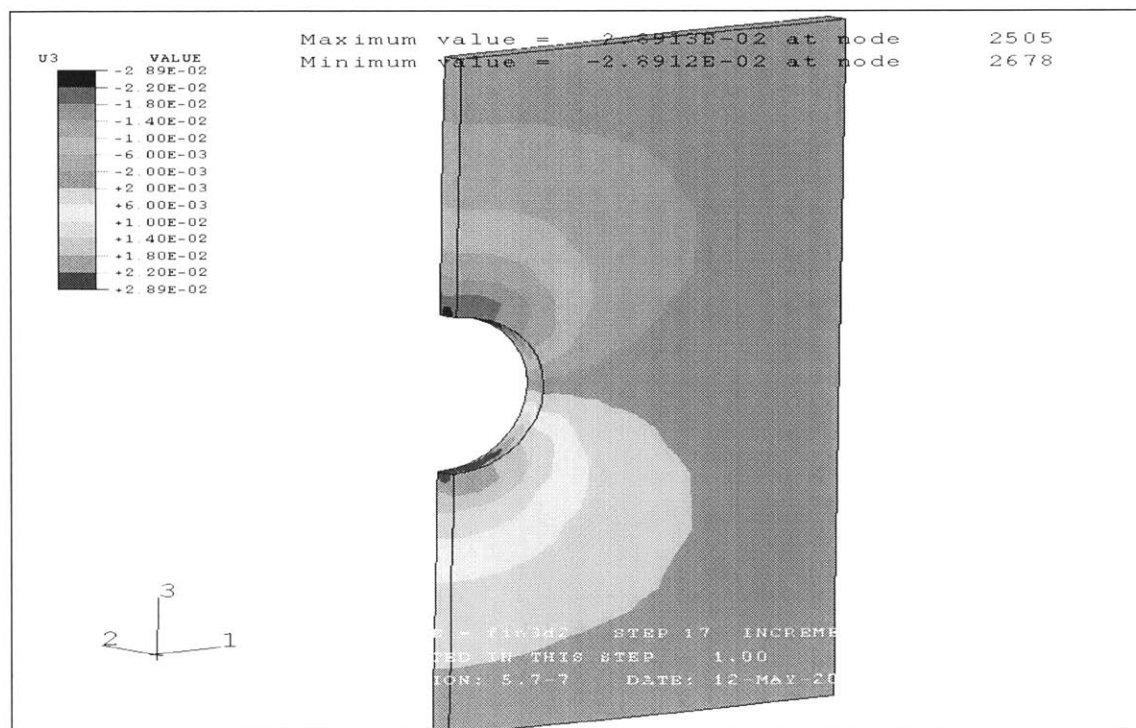


Figure 4. Displacement in the vertical direction at section 4-5
($K_x=K_y=0.5$ - dry conditions - $l_u=1\text{m}$ - excavation=4m)

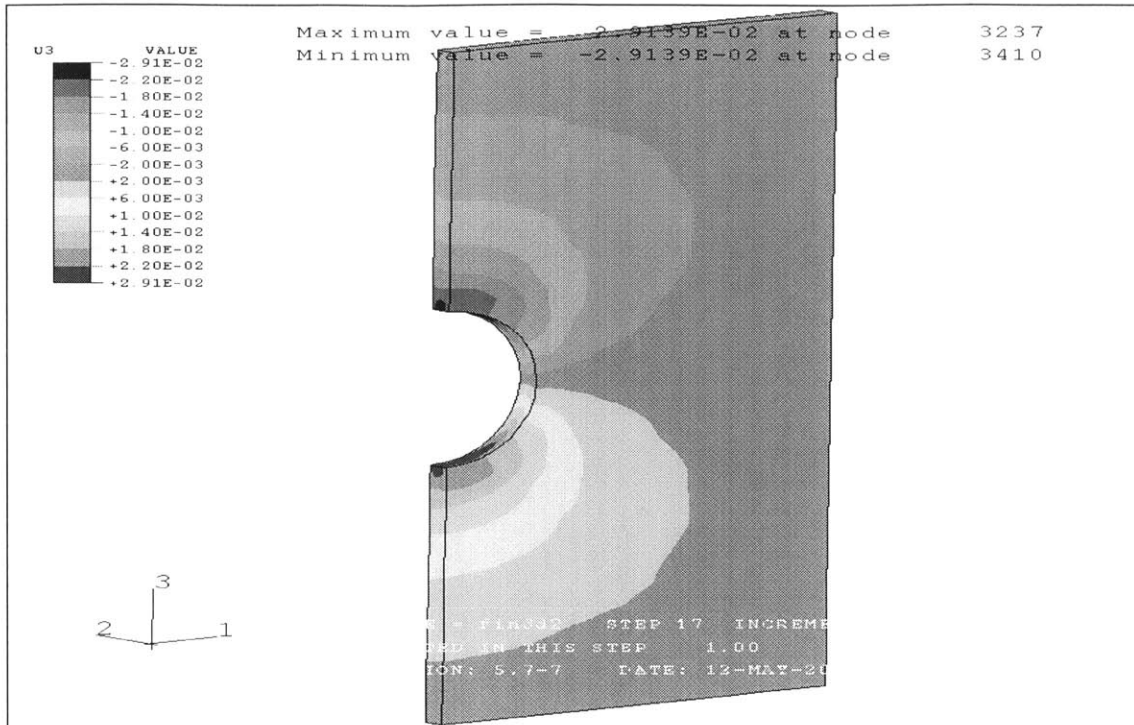


Figure 5. Displacement in the vertical direction at section 5-6
($K_x=K_y=0.5$ - dry conditions - $l_u=1\text{m}$ - excavation=5m)

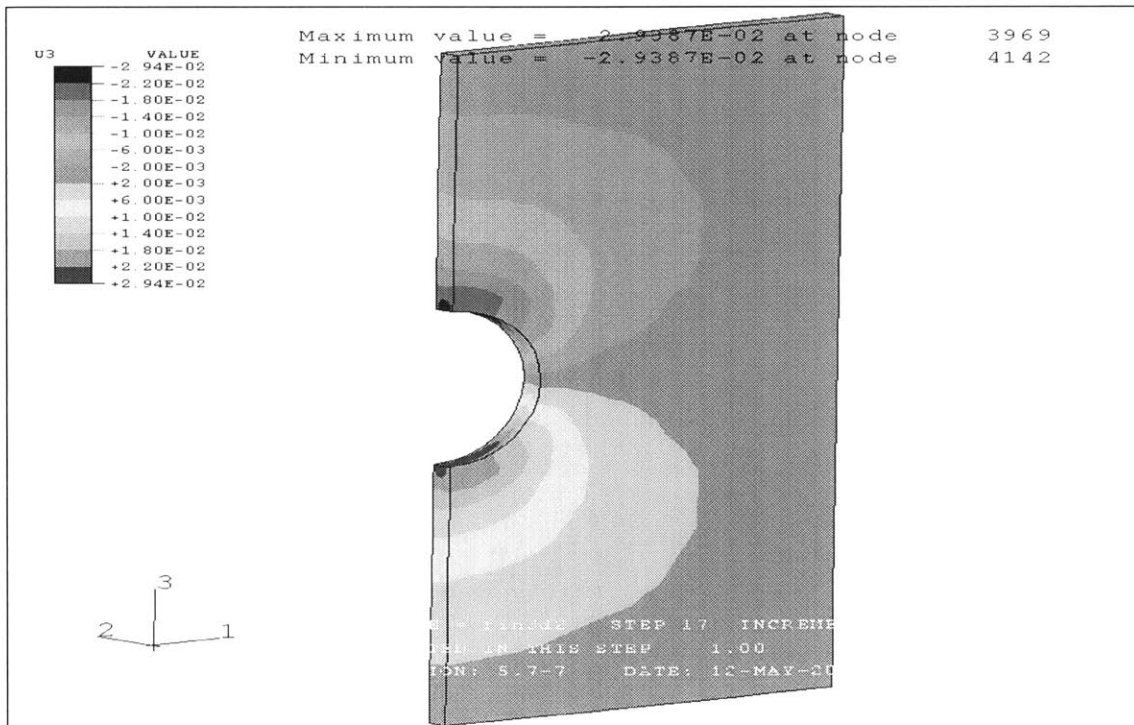


Figure 6. Displacement in the vertical direction at section 6-7
($K_x=K_y=0.5$ - dry conditions - $l_u=1\text{m}$ - excavation=6m)

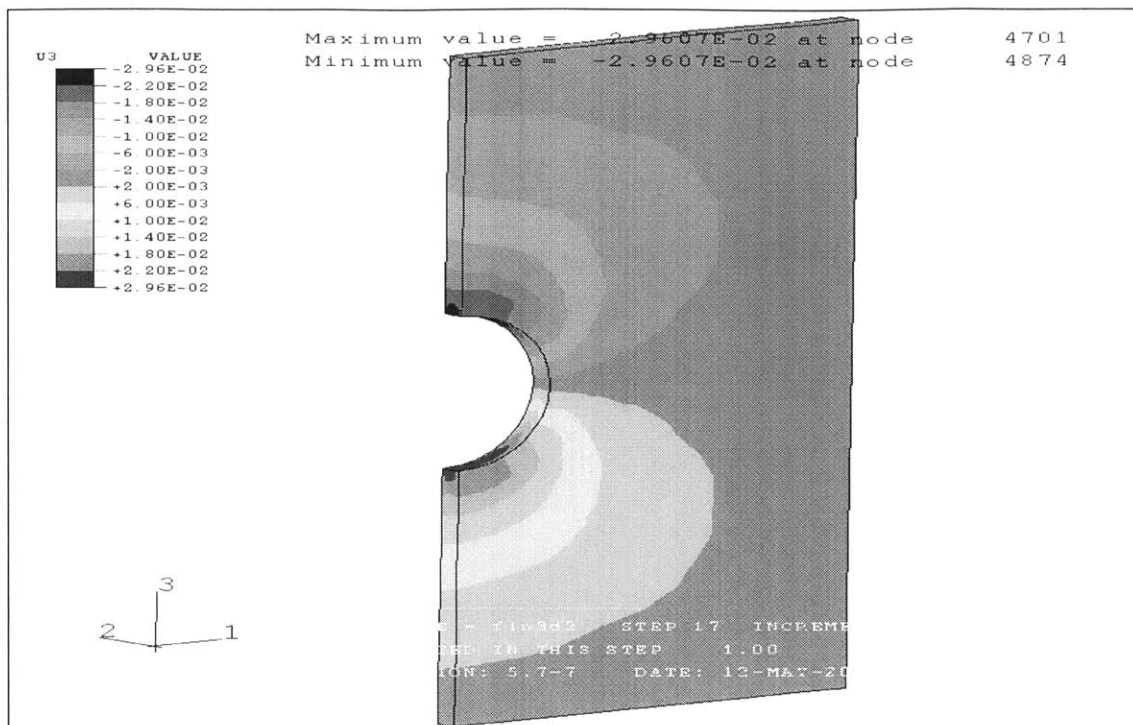


Figure 7. Displacement in the vertical direction at section 7-8
($K_x=K_y=0.5$ - dry conditions - $l_u=1\text{m}$ - excavation=7m)

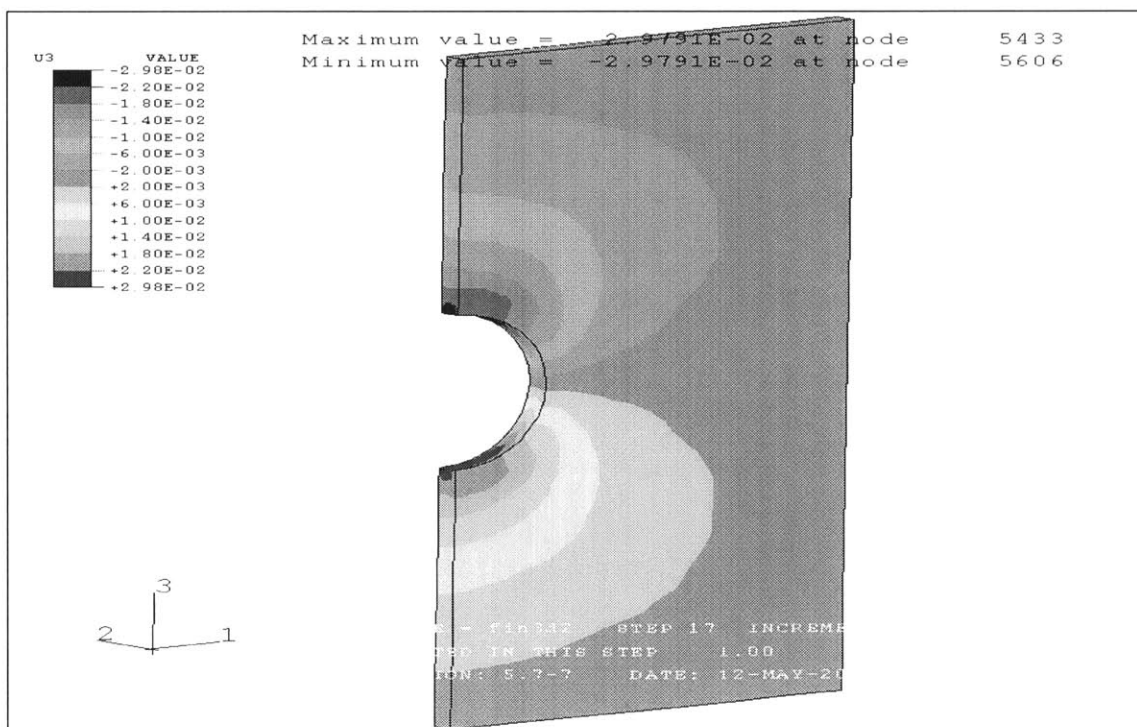


Figure 8. Displacement in the vertical direction at section 8-9
($K_x=K_y=0.5$ - dry conditions - $l_u=1\text{m}$ - excavation=8m)

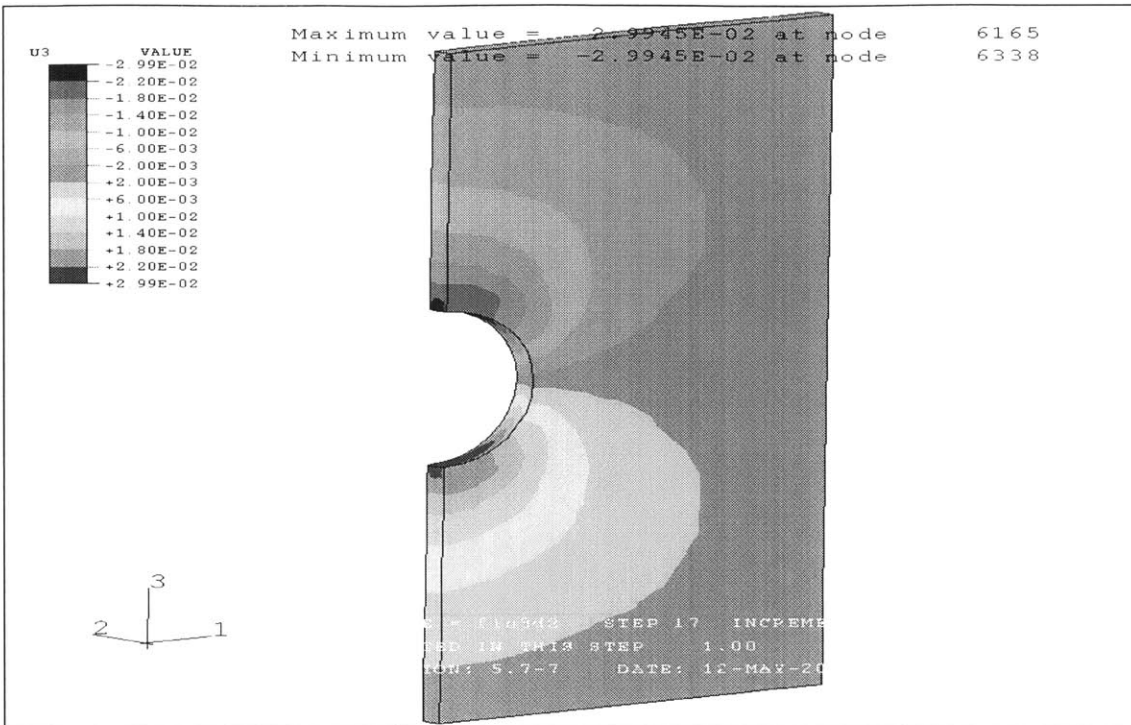


Figure 9. Displacement in the vertical direction at section 9-10
($K_x=K_y=0.5$ - dry conditions - $l_0=1\text{m}$ - excavation=9m)

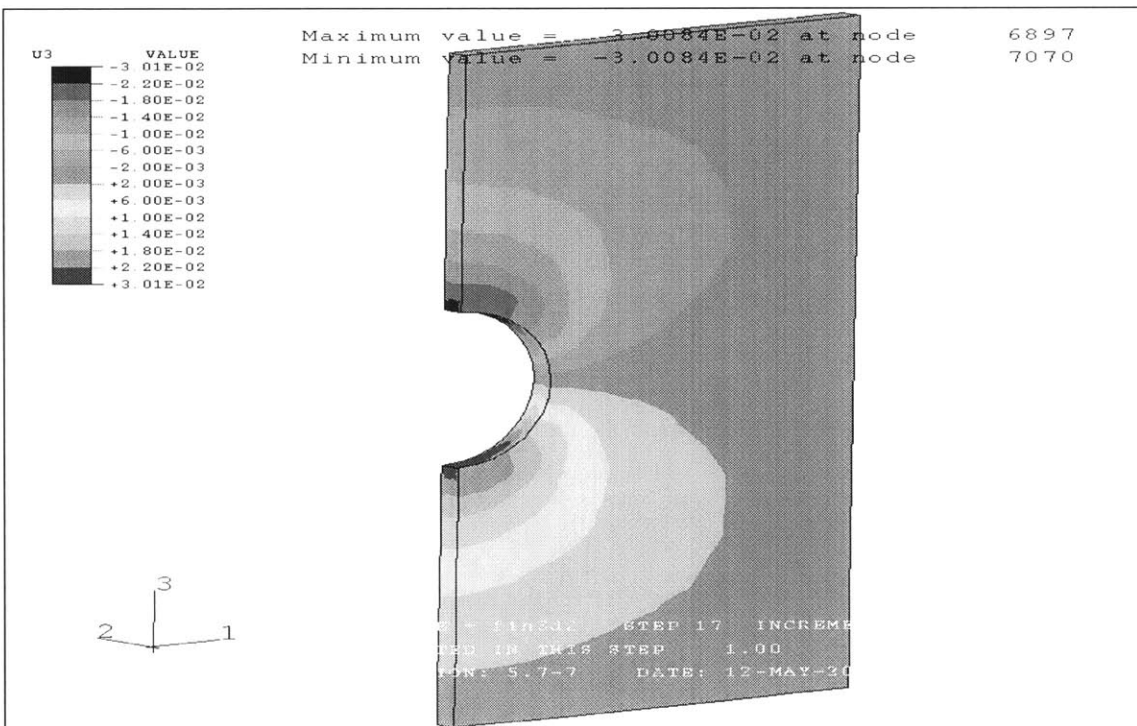


Figure 10. Displacement in the vertical direction at section 10-11
($K_x=K_y=0.5$ - dry conditions - $l_0=1\text{m}$ - excavation=10m)

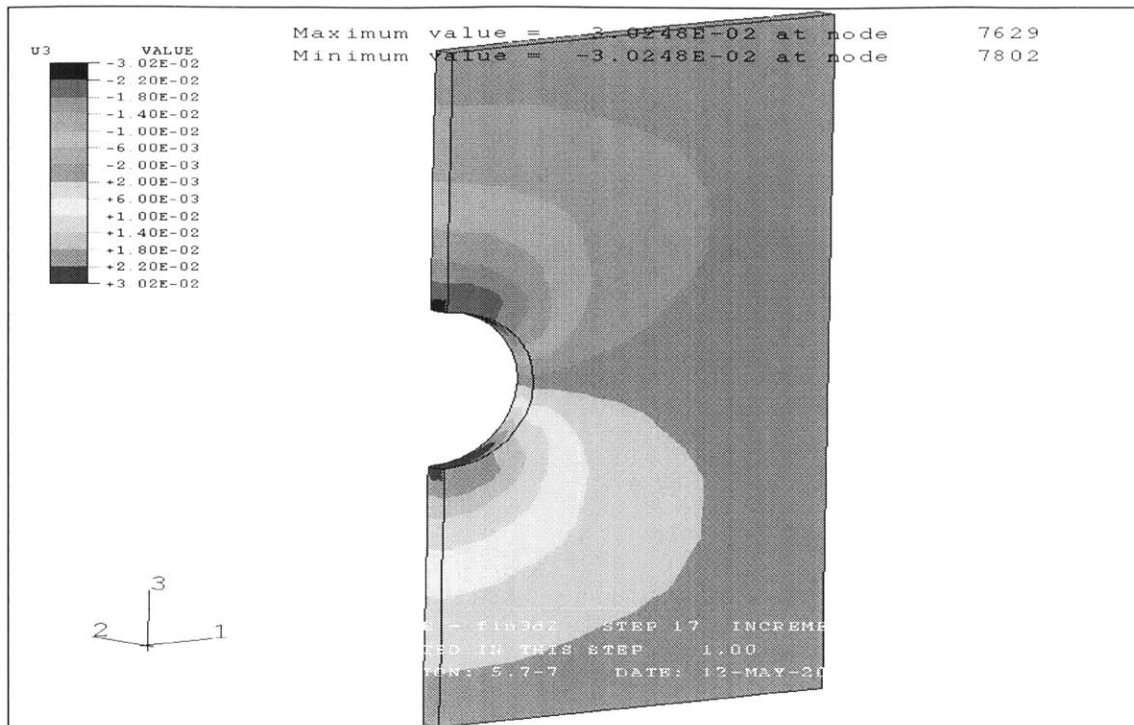


Figure 11. Displacement in the vertical direction at section 11-12
 ($K_x=K_y=0.5$ - dry conditions - $l_u=1\text{m}$ - excavation=11m)

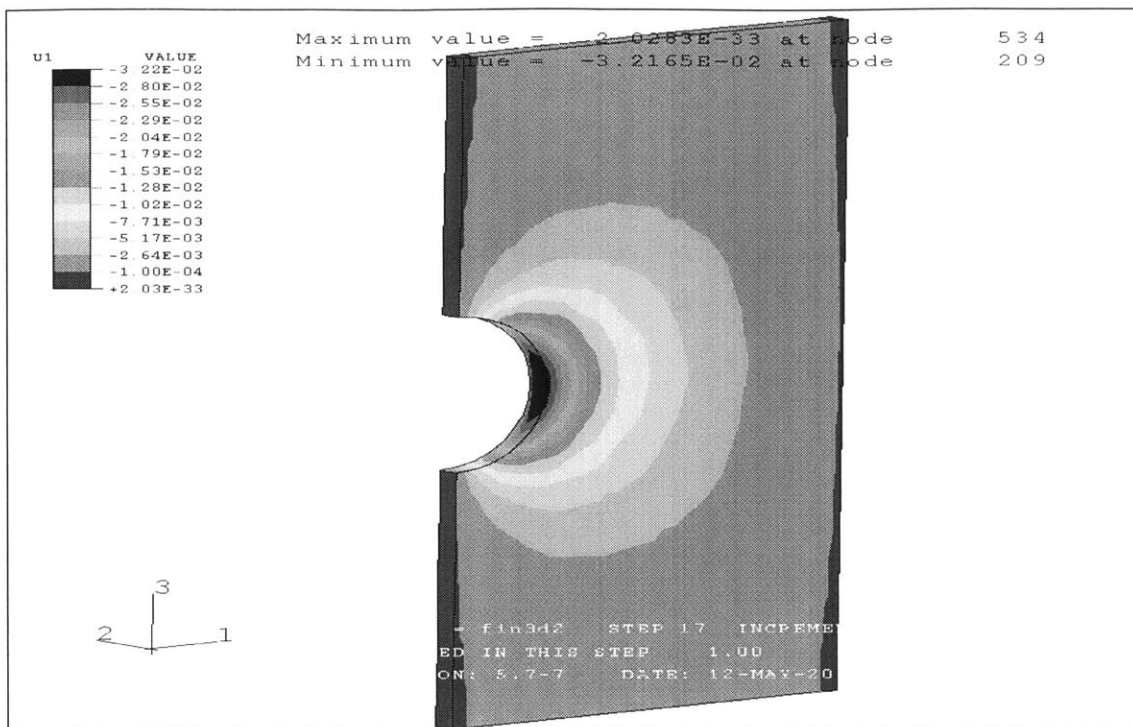


Figure 12. Displacement in the horizontal direction at section 1-2
($K_x=K_y=0.5$ - dry conditions - $l_u=1\text{m}$ - excavation=1m)

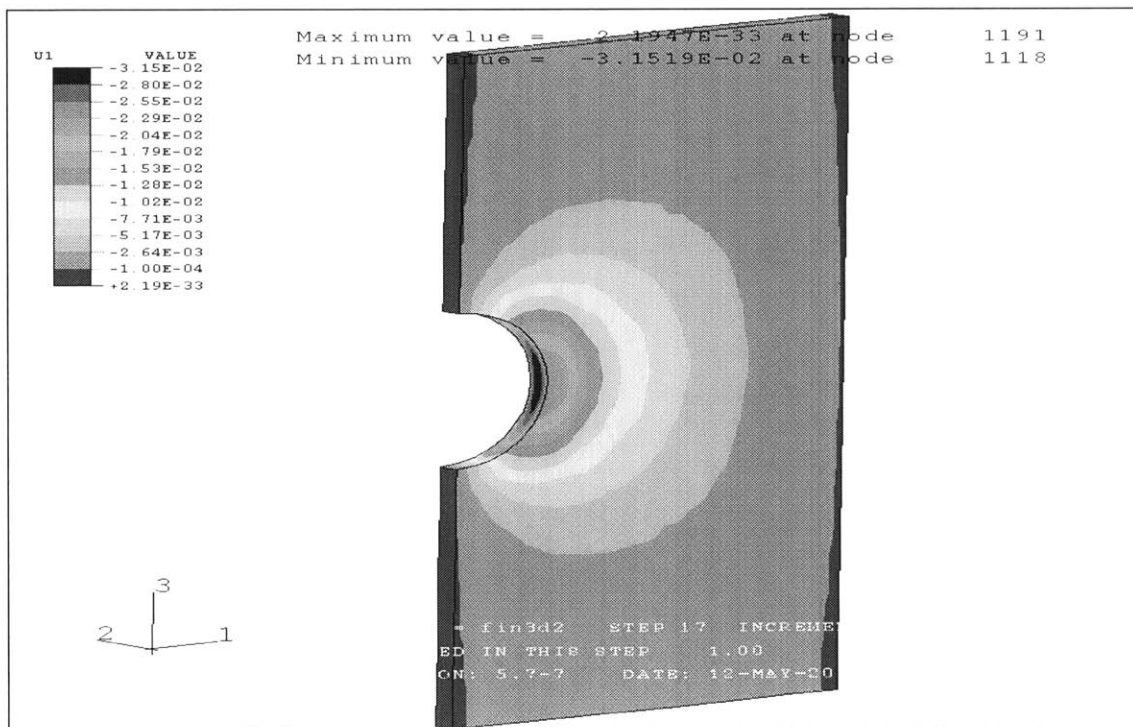


Figure 13. Displacement in the horizontal direction at section 2-3
($K_x=K_y=0.5$ - dry conditions - $l_u=1\text{m}$ - excavation=2m)

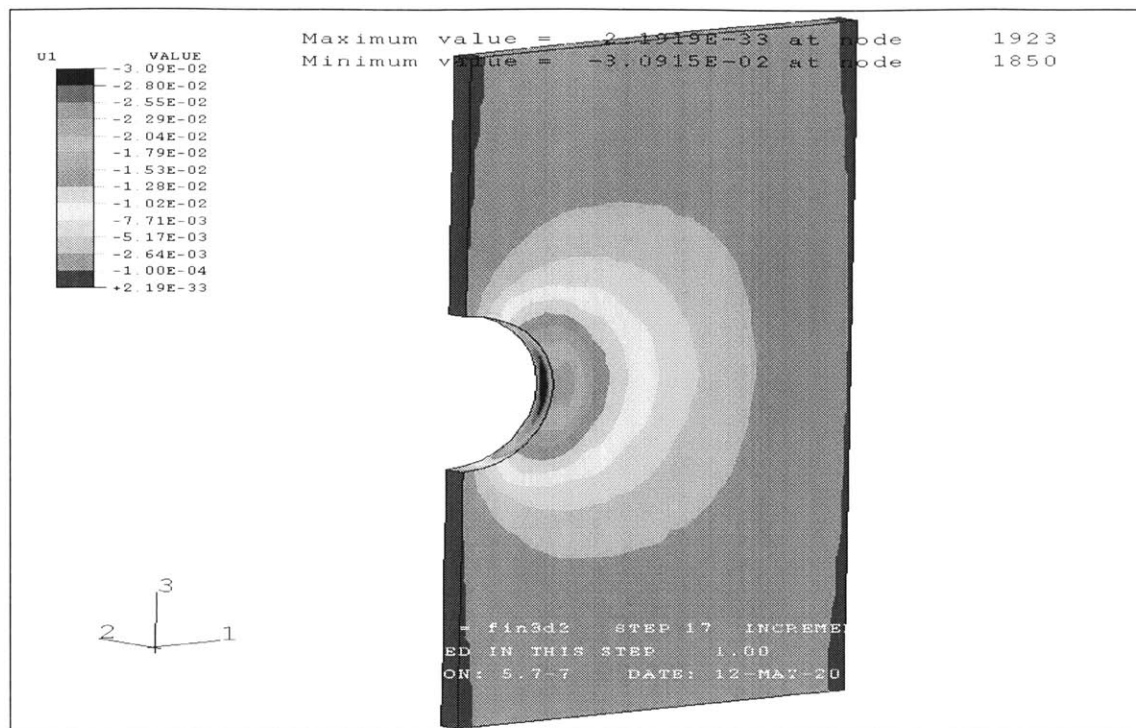


Figure 14. Displacement in the horizontal direction at section 3-4
($K_x=K_y=0.5$ - dry conditions - $l_u=1\text{m}$ - excavation=3m)

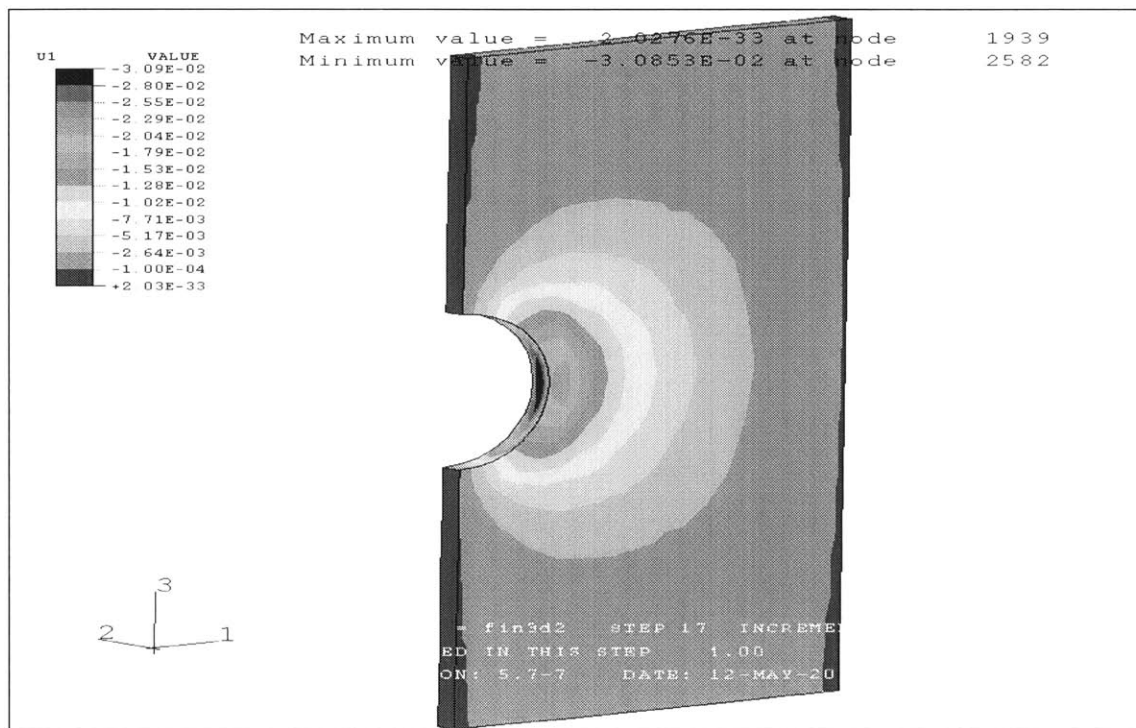


Figure 15. Displacement in the horizontal direction at section 4-5
($K_x=K_y=0.5$ - dry conditions - $l_u=1\text{m}$ - excavation=4m)

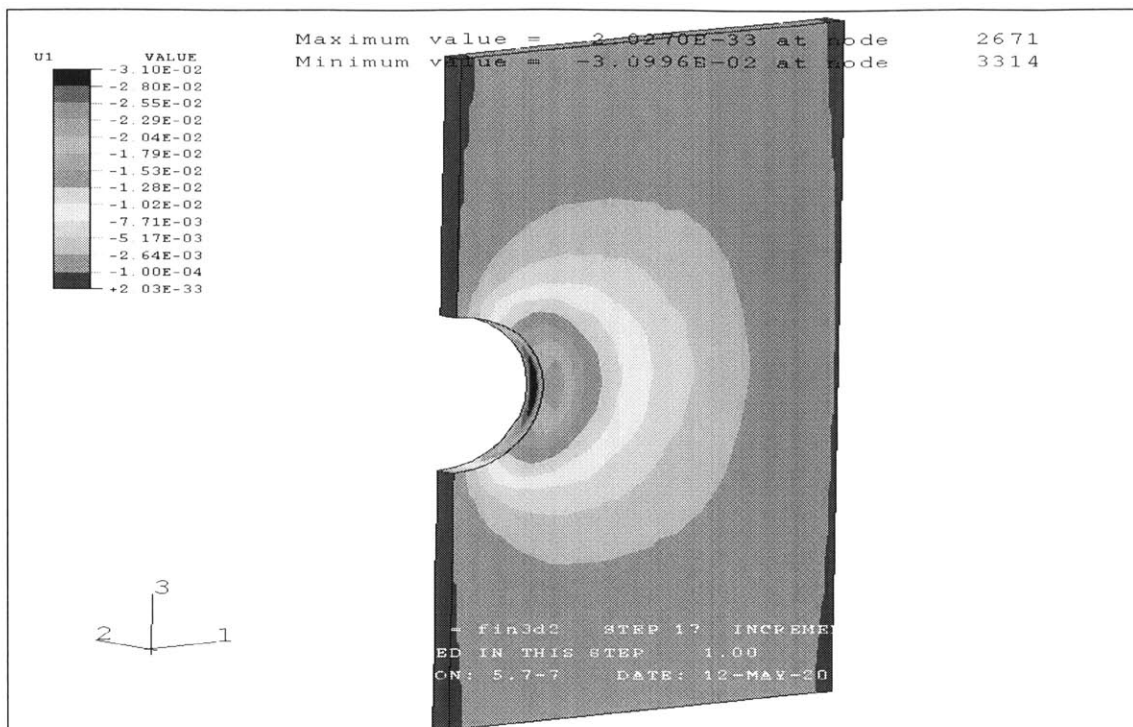


Figure 16. Displacement in the horizontal direction at section 5-6
($K_x=K_y=0.5$ - dry conditions - $l_u=1\text{m}$ - excavation=5m)

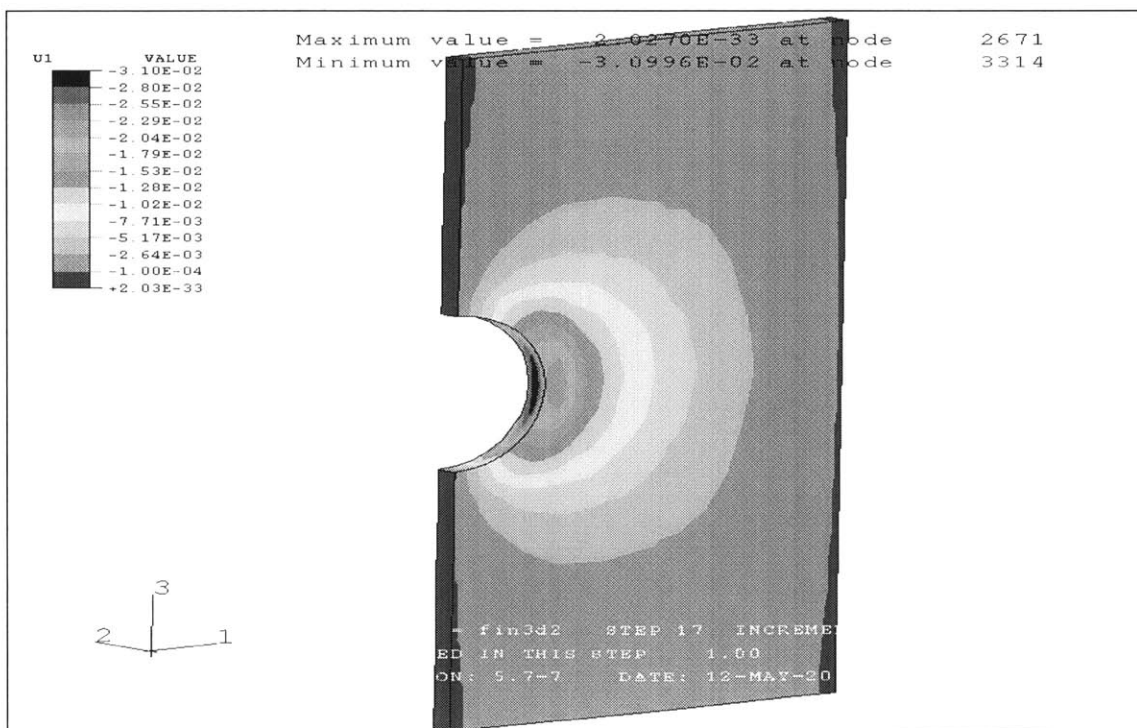


Figure 17. Displacement in the horizontal direction at section 6-7
($K_x=K_y=0.5$ - dry conditions - $l_u=1\text{m}$ - excavation=6m)

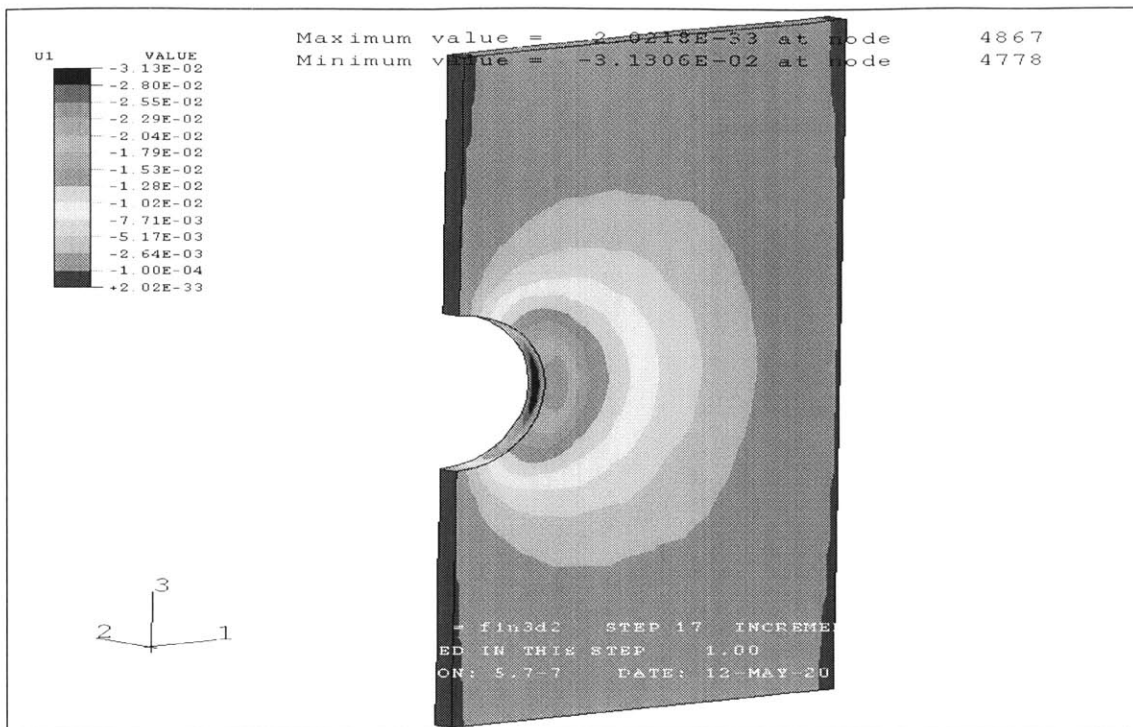


Figure 18. Displacement in the horizontal direction at section 7-8
 ($K_x=K_y=0.5$ - dry conditions - $l_u=1\text{m}$ - excavation=7m)

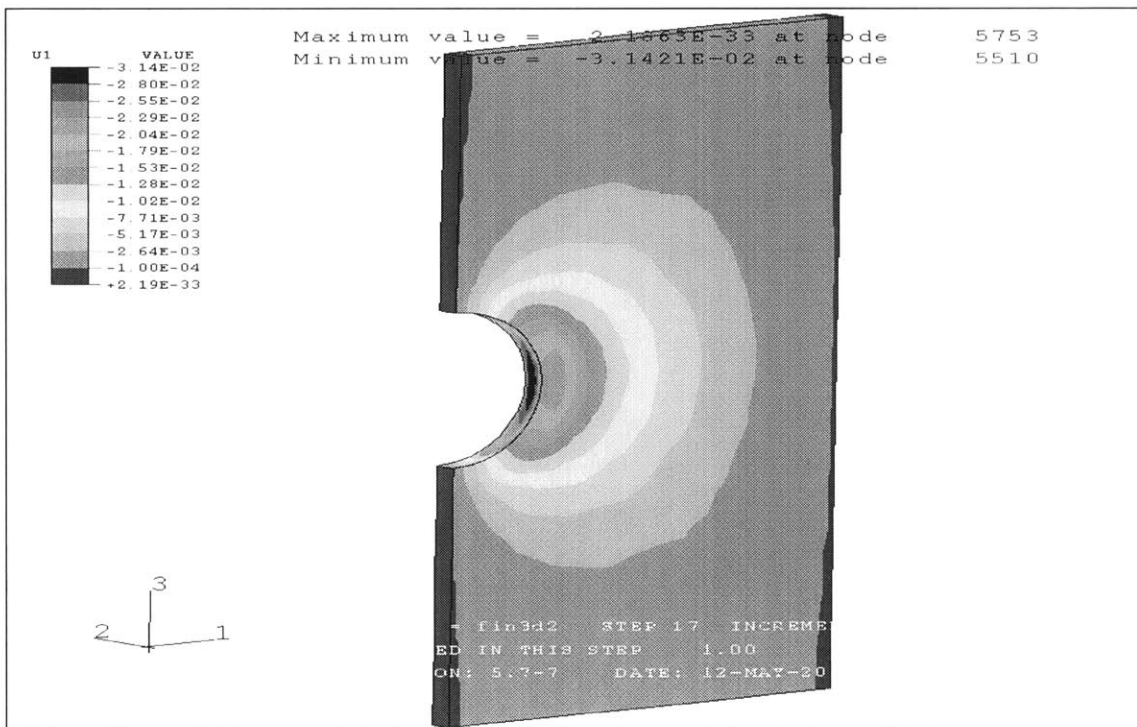


Figure 19. Displacement in the horizontal direction at section 8-9
 ($K_x=K_y=0.5$ - dry conditions - $l_u=1\text{m}$ - excavation=8m)

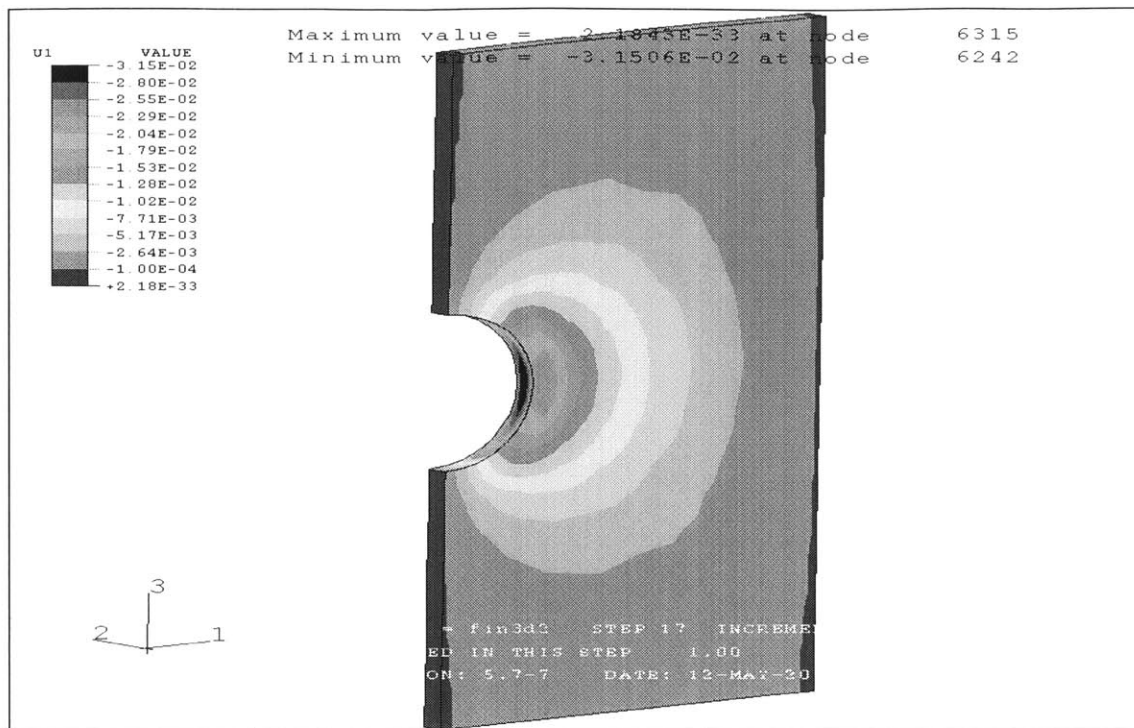


Figure 20. Displacement in the horizontal direction at section 9-10
($K_x=K_y=0.5$ - dry conditions - $l_u=1\text{m}$ - excavation=9m)

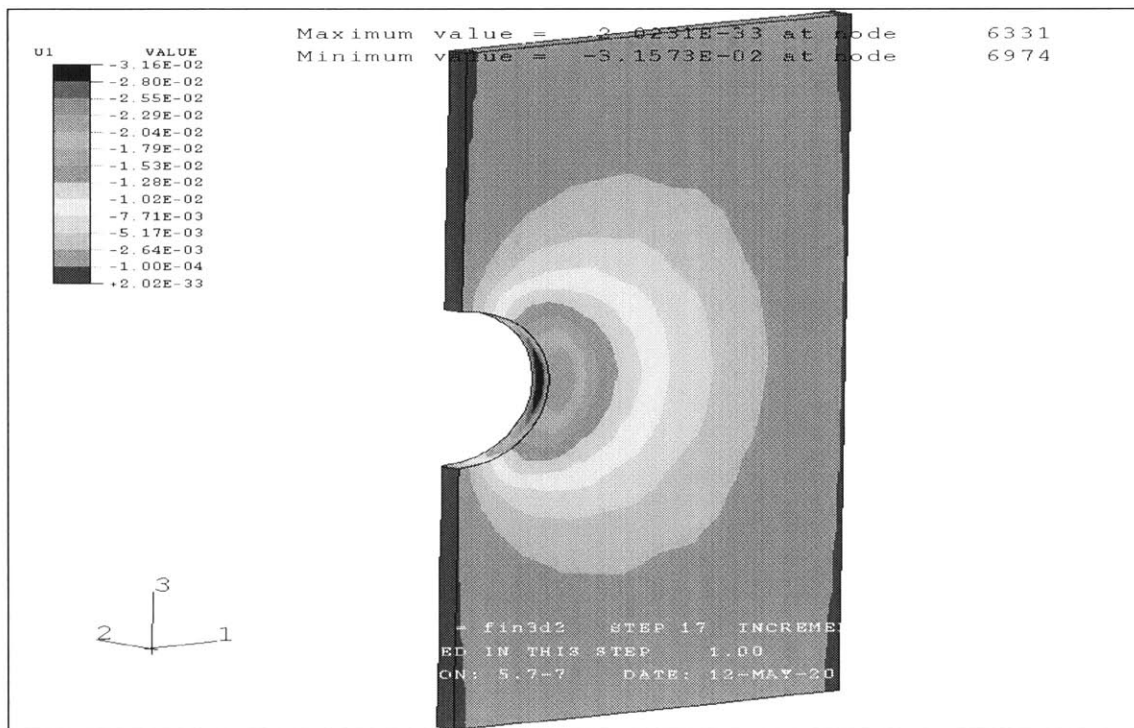


Figure 21. Displacement in the horizontal direction at section 10-11
($K_x=K_y=0.5$ - dry conditions - $l_u=1\text{m}$ - excavation=10m)

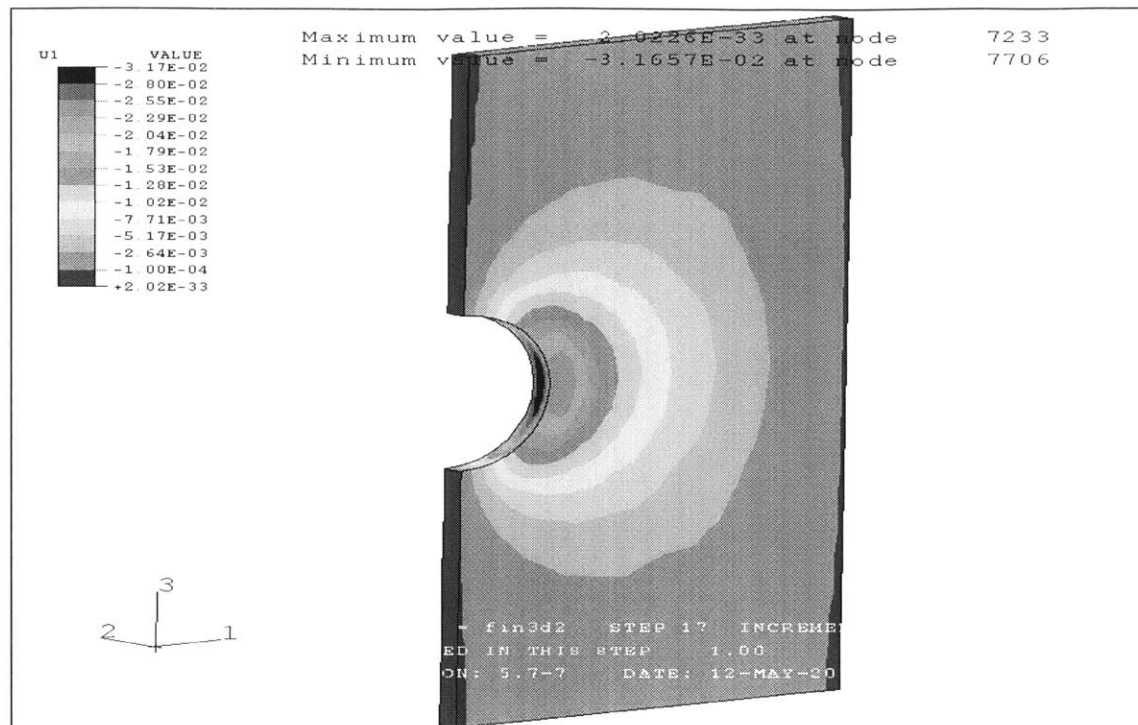


Figure 22. Displacement in the horizontal direction at section 11-12
 ($K_x=K_y=0.5$ - dry conditions - $I_u=1\text{m}$ - excavation=11m)

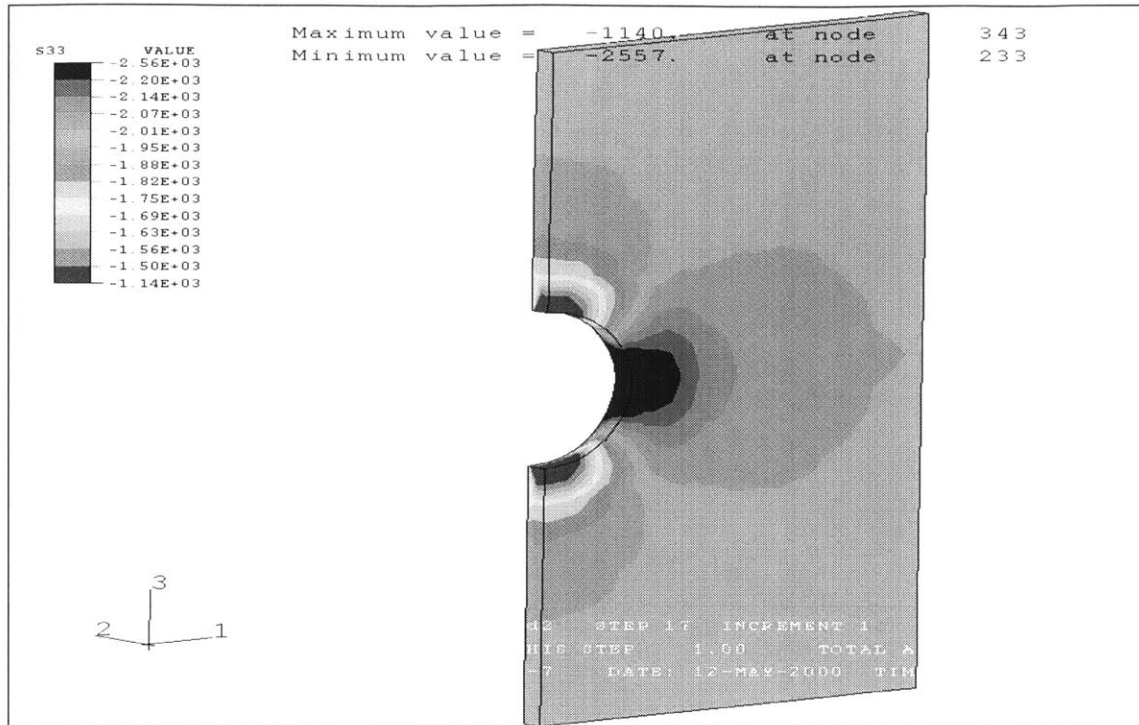


Figure 23. Stresses in the vertical direction at section 1-2
($K_x=K_y=0.5$ - dry conditions - $l_u=1\text{m}$ - excavation=1m)

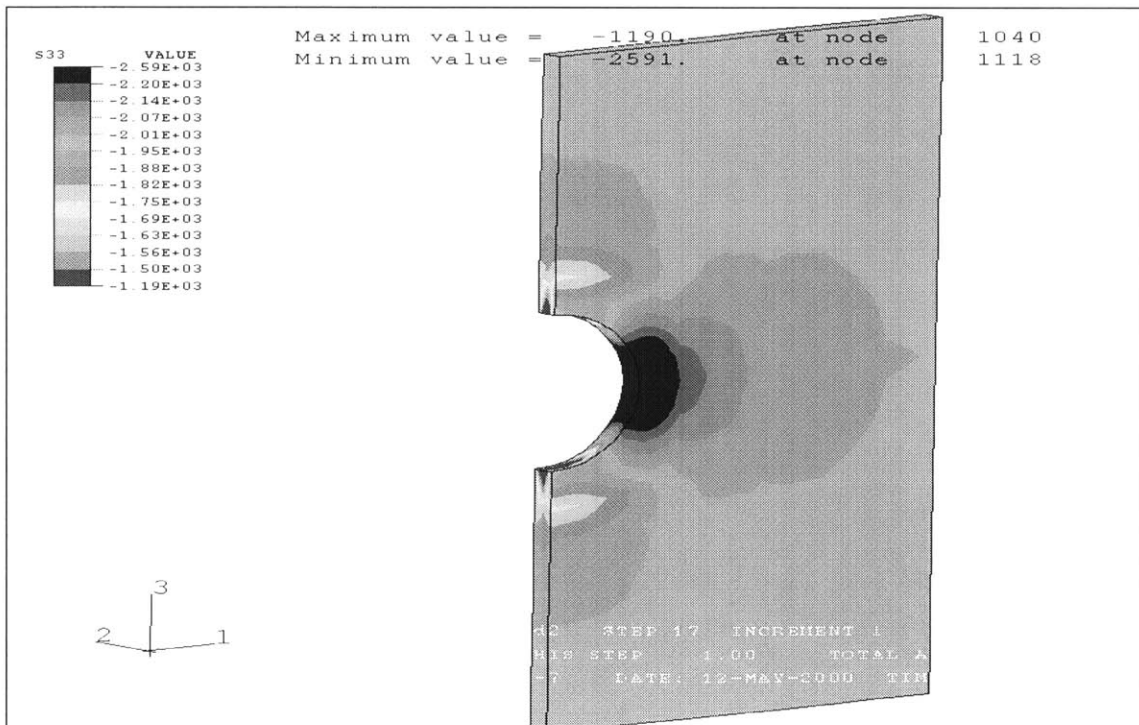


Figure 24. Stresses in the vertical direction at section 2-3
($K_x=K_y=0.5$ - dry conditions - $l_u=1\text{m}$ - excavation=2m)

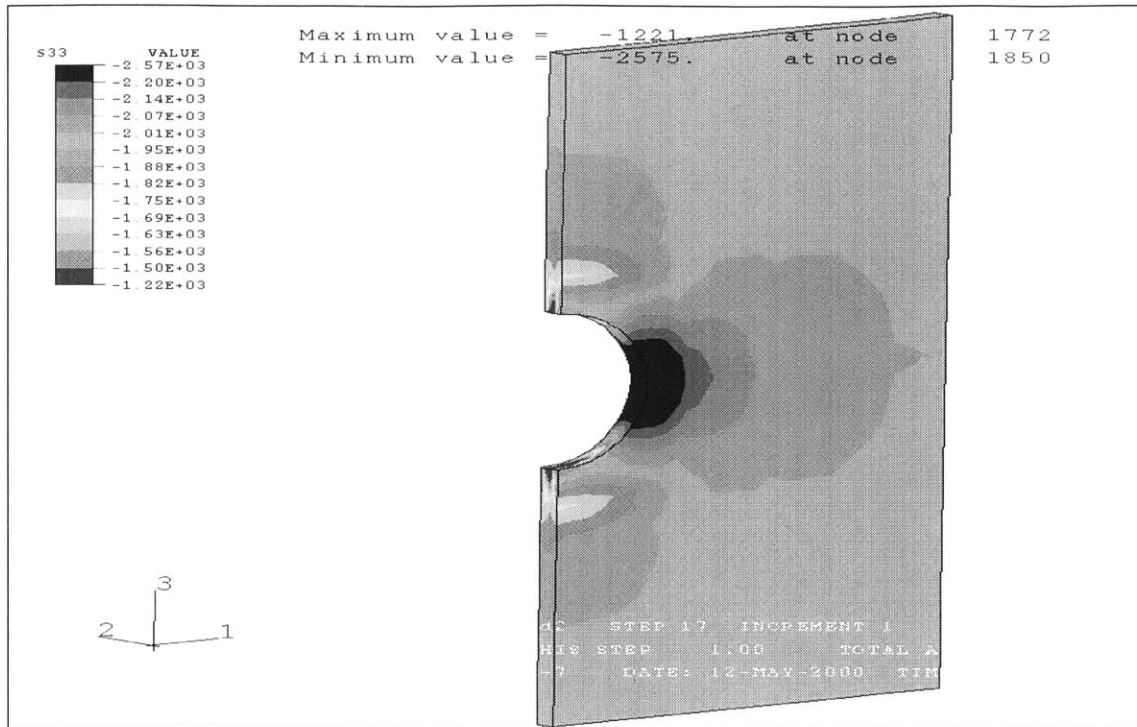


Figure 25. Stresses in the vertical direction at section 3-4
($K_x=K_y=0.5$ - dry conditions - $l_u=1\text{m}$ - excavation=3m)

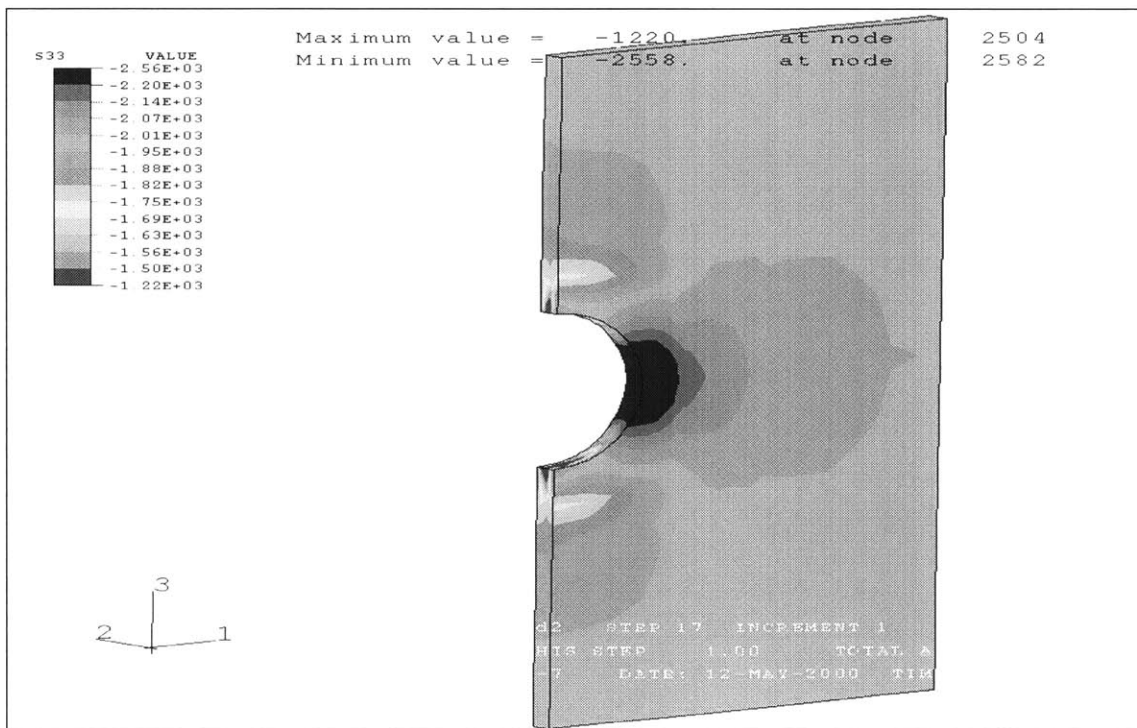


Figure 26. Stresses in the vertical direction at section 4-5
($K_x=K_y=0.5$ - dry conditions - $l_u=1\text{m}$ - excavation=4m)

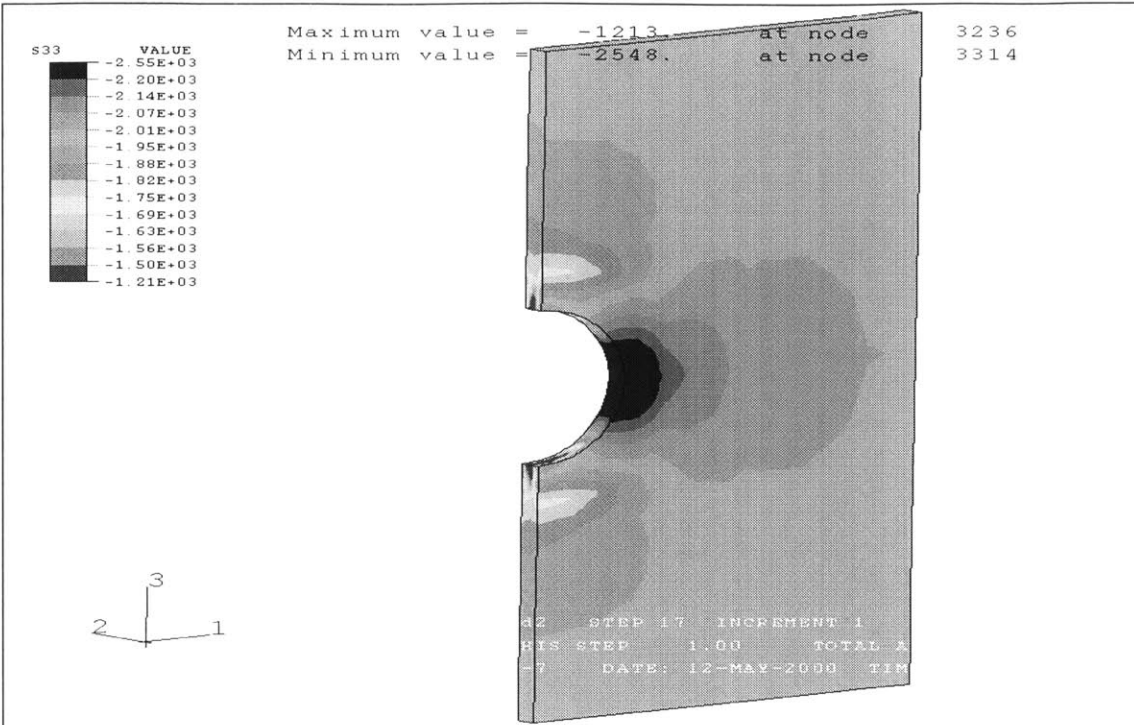


Figure 27. Stresses in the vertical direction at section 5-6
($K_x=K_y=0.5$ - dry conditions - $I_u=1\text{m}$ - excavation=5m)

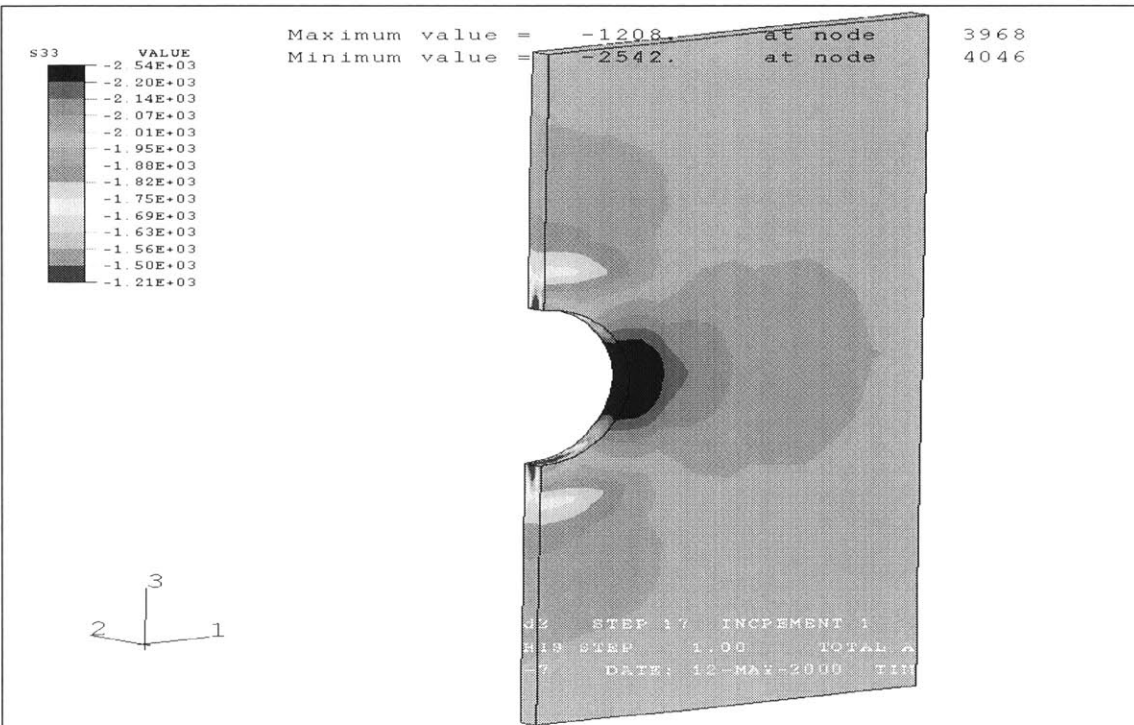


Figure 28. Stresses in the vertical direction at section 6-7
($K_x=K_y=0.5$ - dry conditions - $I_u=1\text{m}$ - excavation=6m)

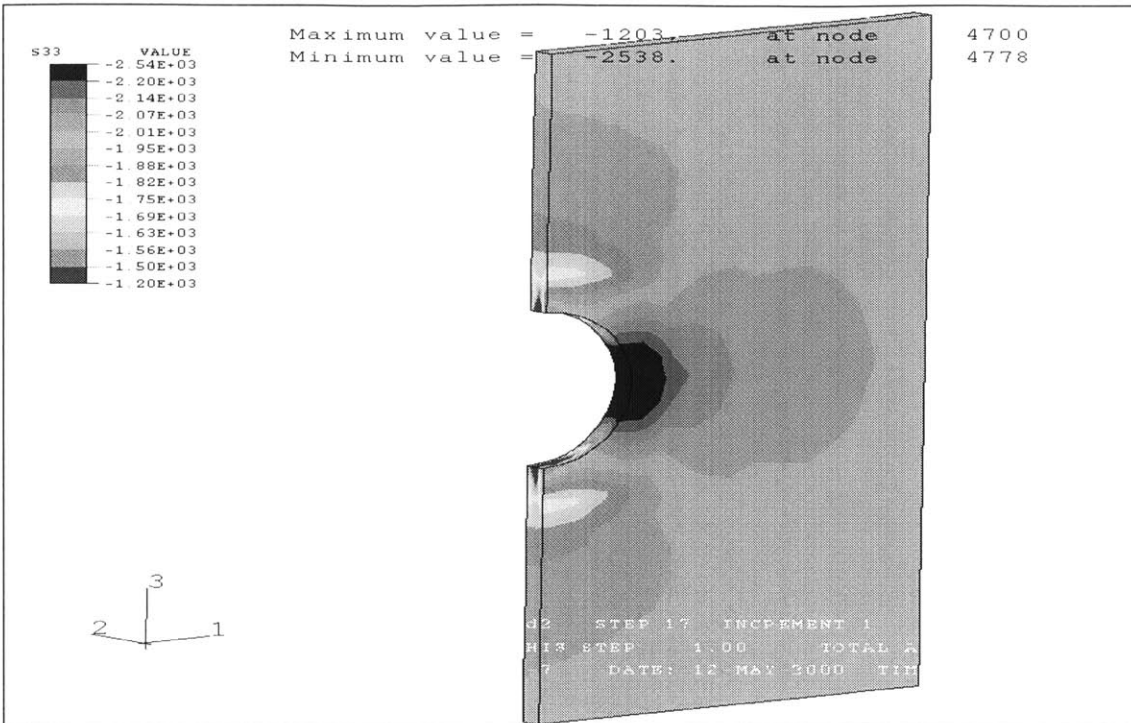


Figure 29. Stresses in the vertical direction at section 7-8
($K_x=K_y=0.5$ - dry conditions - $I_u=1\text{m}$ - excavation=7m)

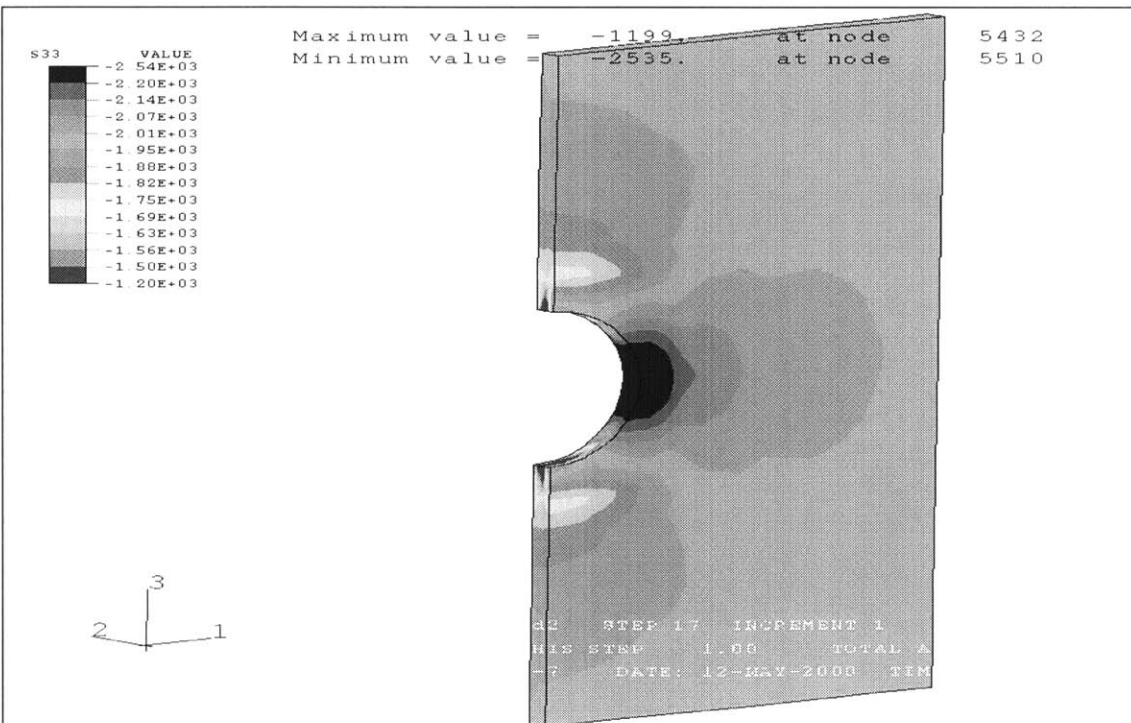


Figure 30. Stresses in the vertical direction at section 8-9
($K_x=K_y=0.5$ - dry conditions - $I_u=1\text{m}$ - excavation=8m)

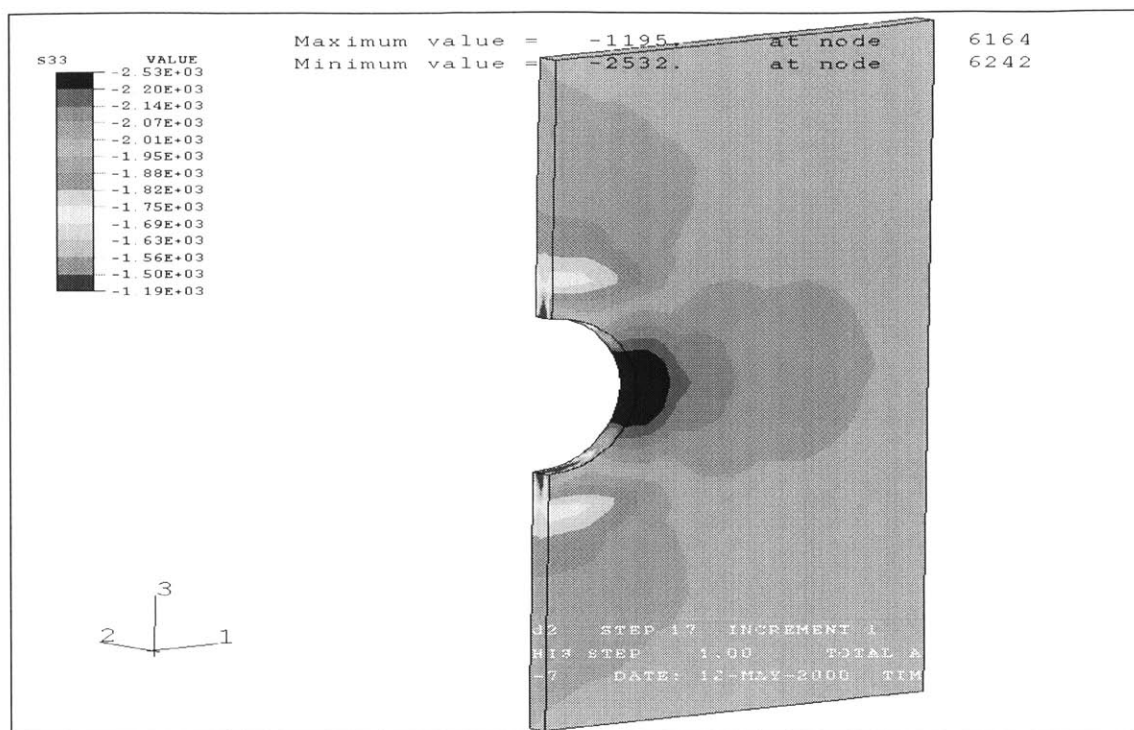


Figure 31. Stresses in the vertical direction at section 9-10
($K_x=K_y=0.5$ - dry conditions - $l_u=1\text{m}$ - excavation=9m)

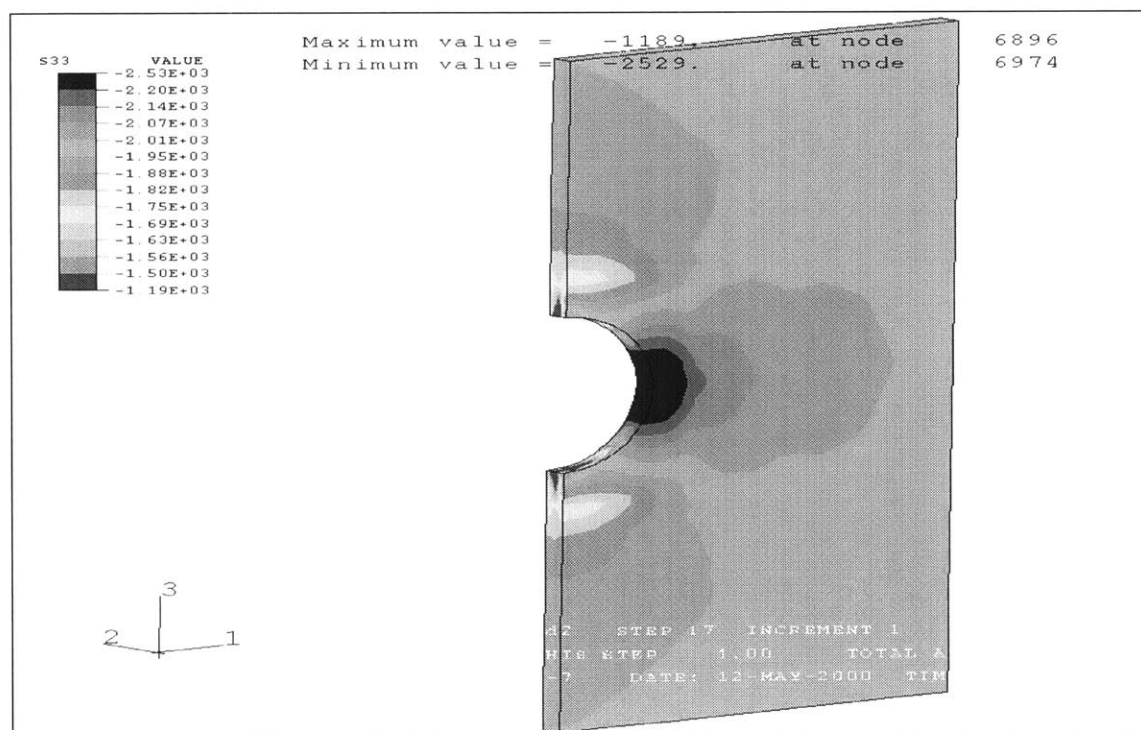


Figure 32. Stresses in the vertical direction at section 10-11
($K_x=K_y=0.5$ - dry conditions - $l_u=1\text{m}$ - excavation=10m)

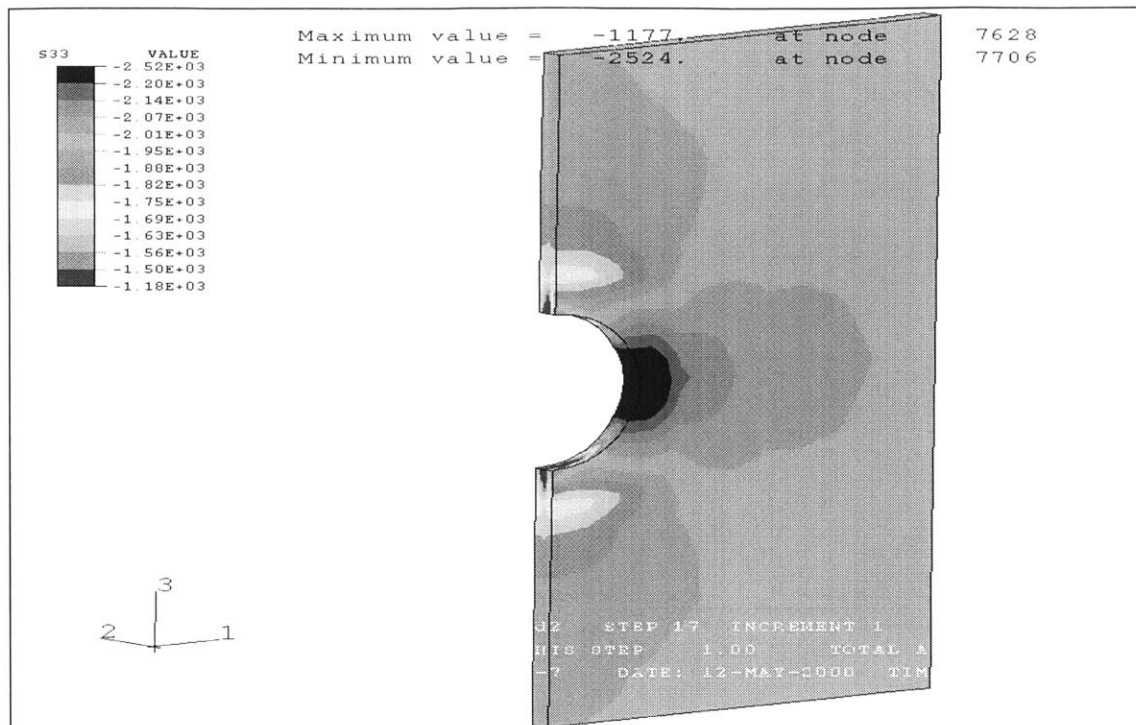


Figure 33. Stresses in the vertical direction at section 11-12
 ($K_x=K_y=0.5$ - dry conditions - $l_0=1\text{m}$ - excavation=11m)

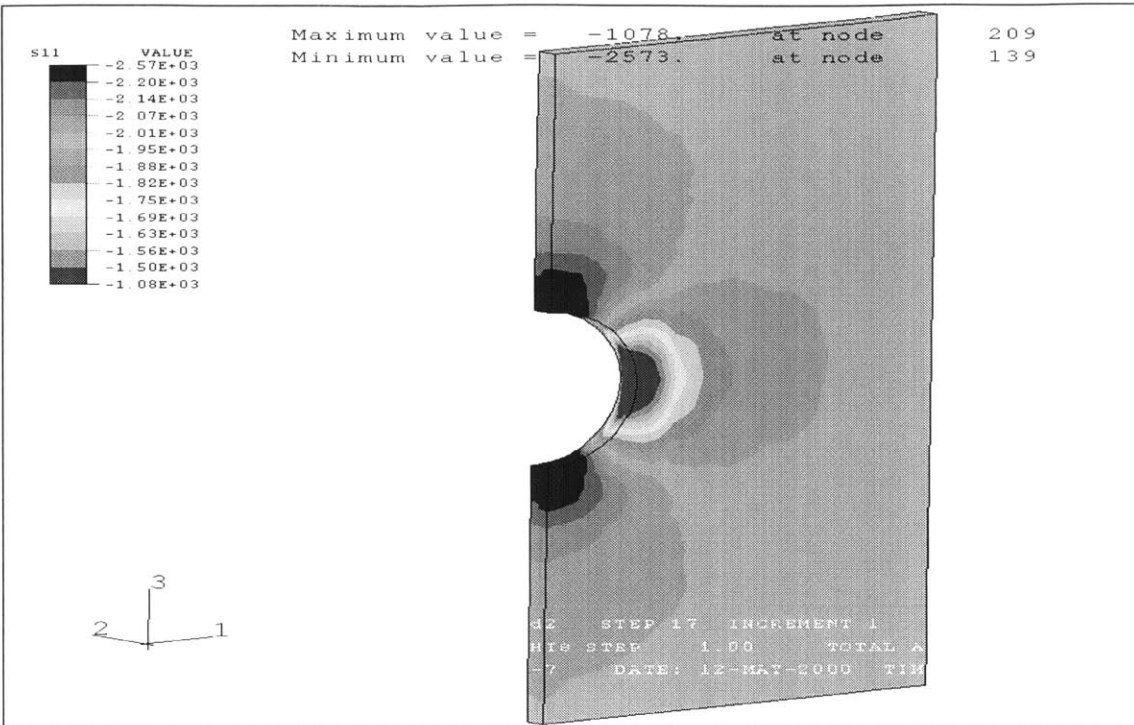


Figure 34. Stresses in the horizontal direction at section 1-2
($K_x=K_y=0.5$ - dry conditions - $l_u=1\text{m}$ - excavation=1m)

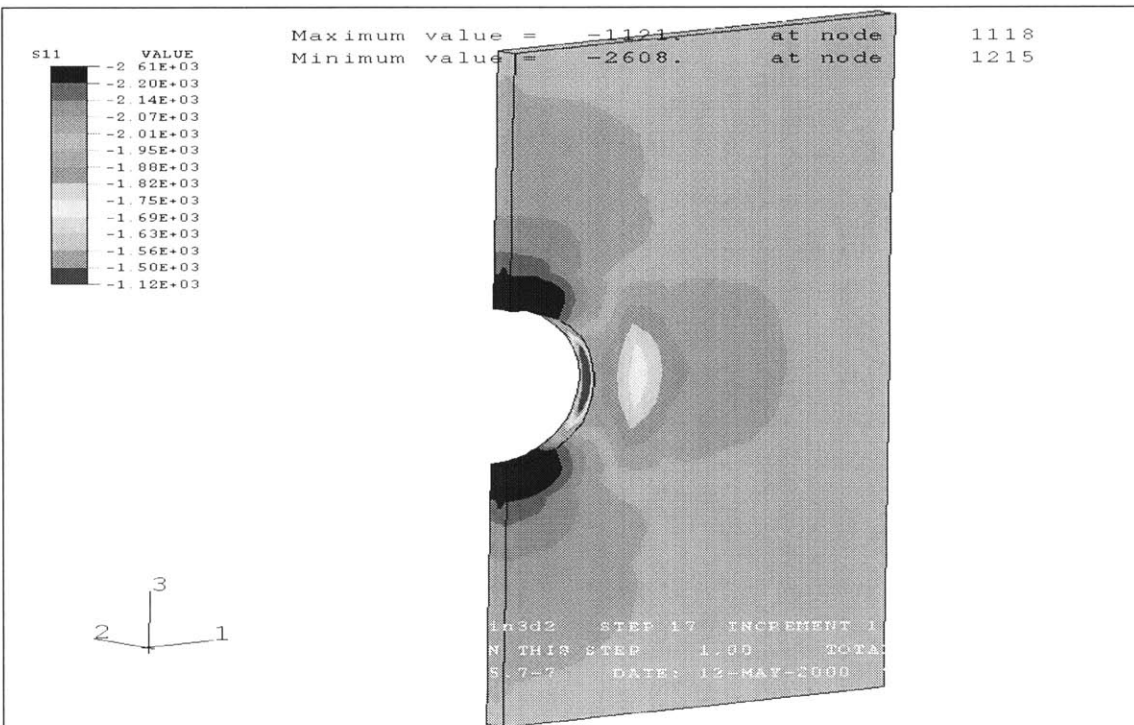


Figure 35. Stresses in the horizontal direction at section 2-3
($K_x=K_y=0.5$ - dry conditions - $l_u=1\text{m}$ - excavation=2m)

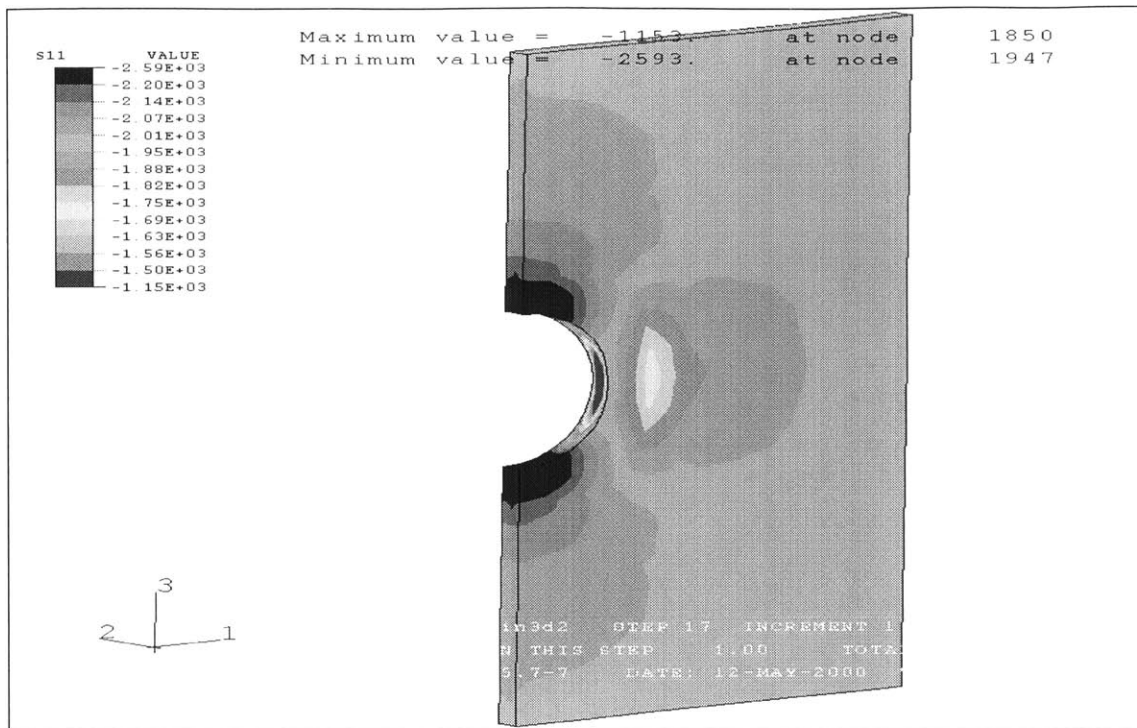


Figure 36. Stresses in the horizontal direction at section 3-4
($K_x=K_y=0.5$ - dry conditions - $l_u=1\text{m}$ - excavation=3m)

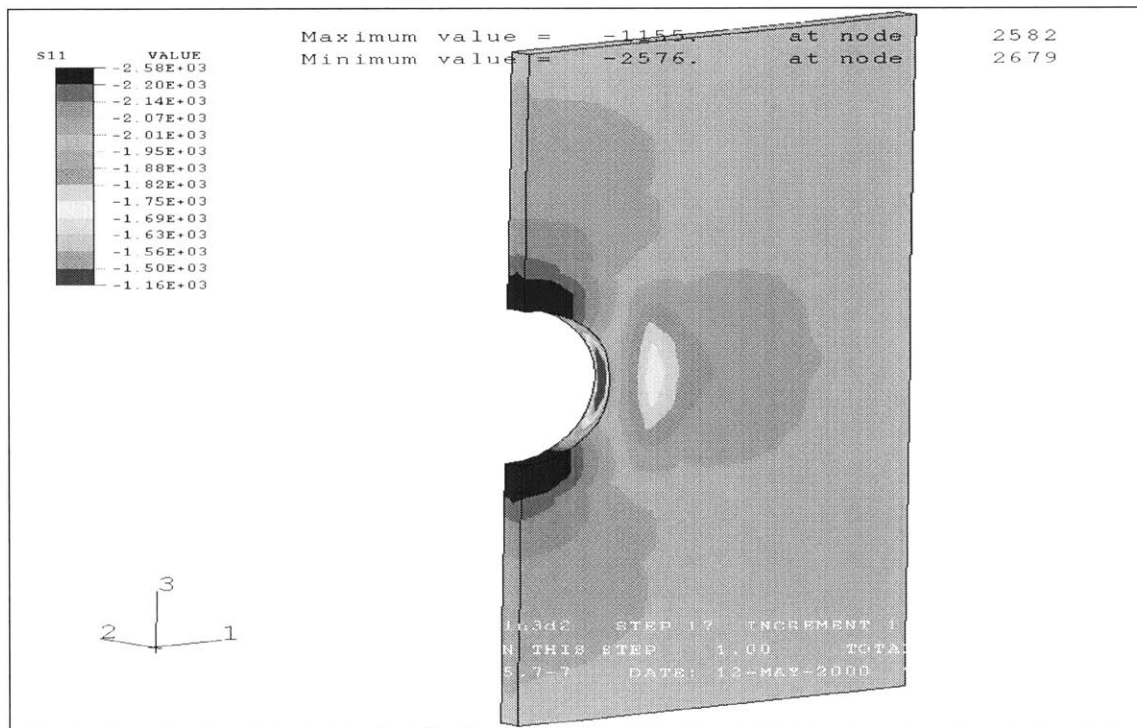


Figure 37. Stresses in the horizontal direction at section 4-5
($K_x=K_y=0.5$ - dry conditions - $l_u=1\text{m}$ - excavation=4m)

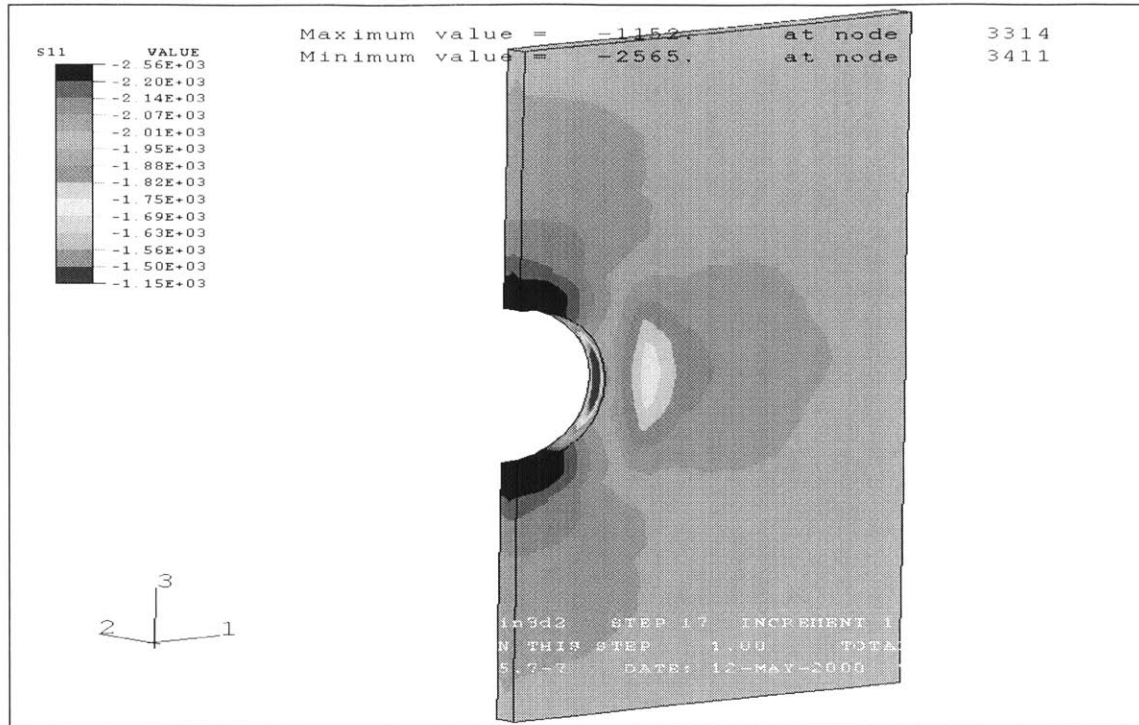


Figure 38. Stresses in the horizontal direction at section 5-6
($K_x=K_y=0.5$ - dry conditions - $I_u=1\text{m}$ - excavation=5m)

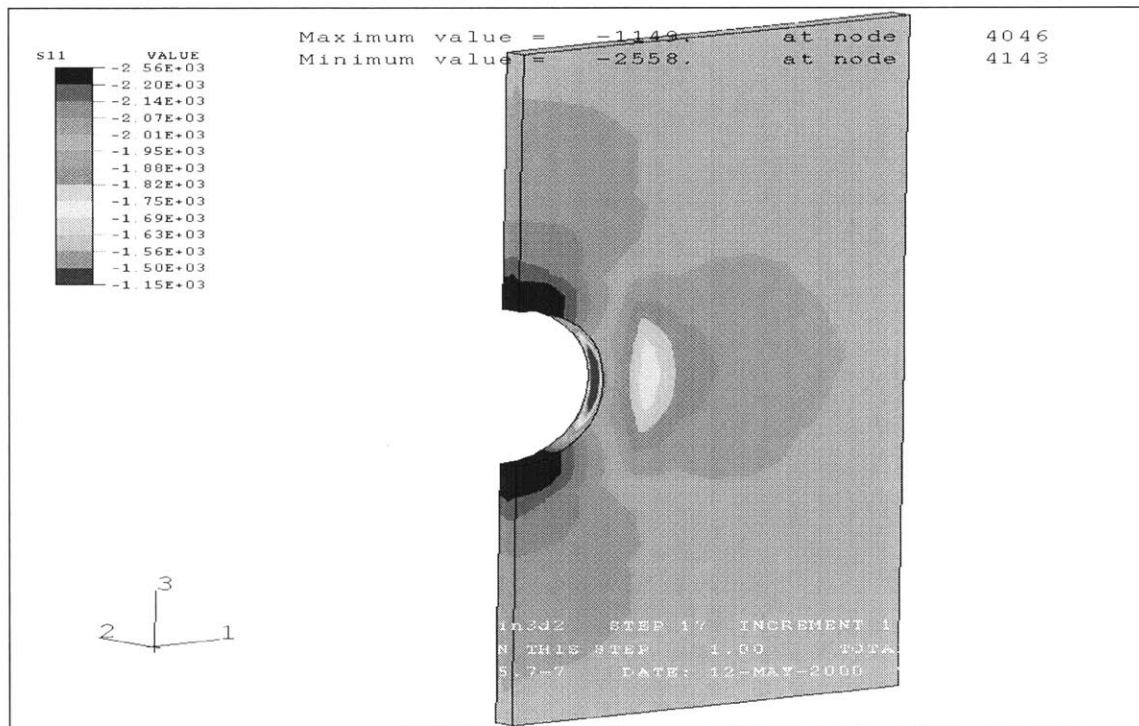


Figure 39. Stresses in the horizontal direction at section 6-7
($K_x=K_y=0.5$ - dry conditions - $I_u=1\text{m}$ - excavation=6m)

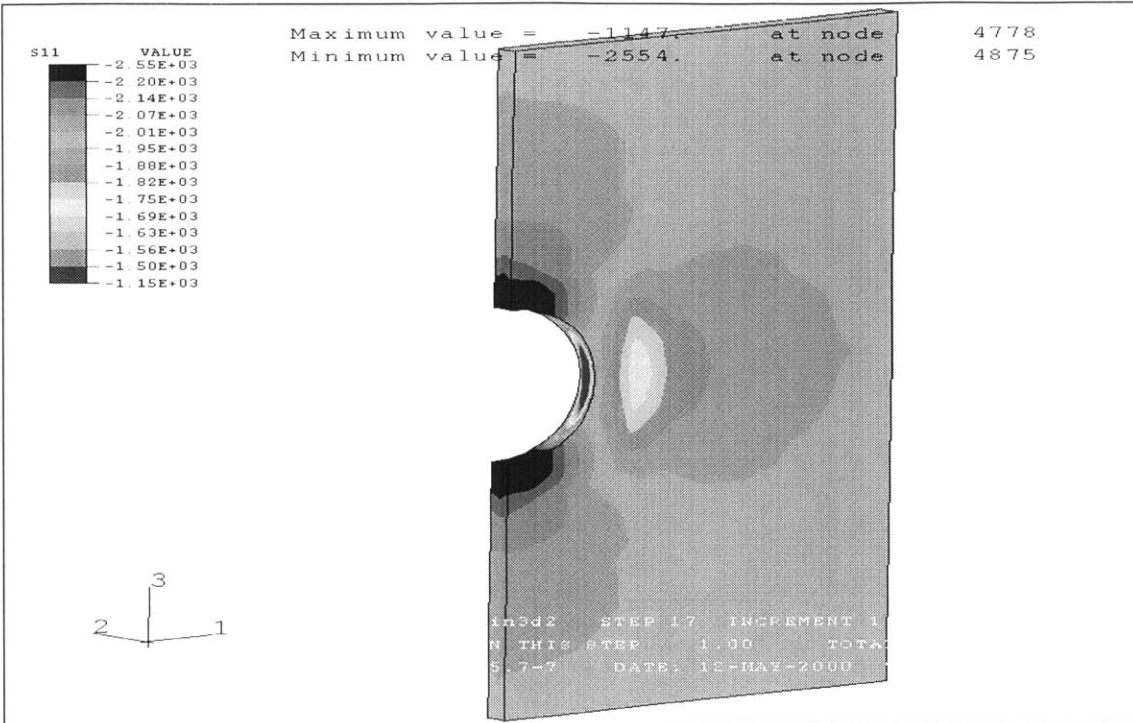


Figure 40. Stresses in the horizontal direction at section 7-8
($K_x=K_y=0.5$ - dry conditions - $l_u=1\text{m}$ - excavation=7m)

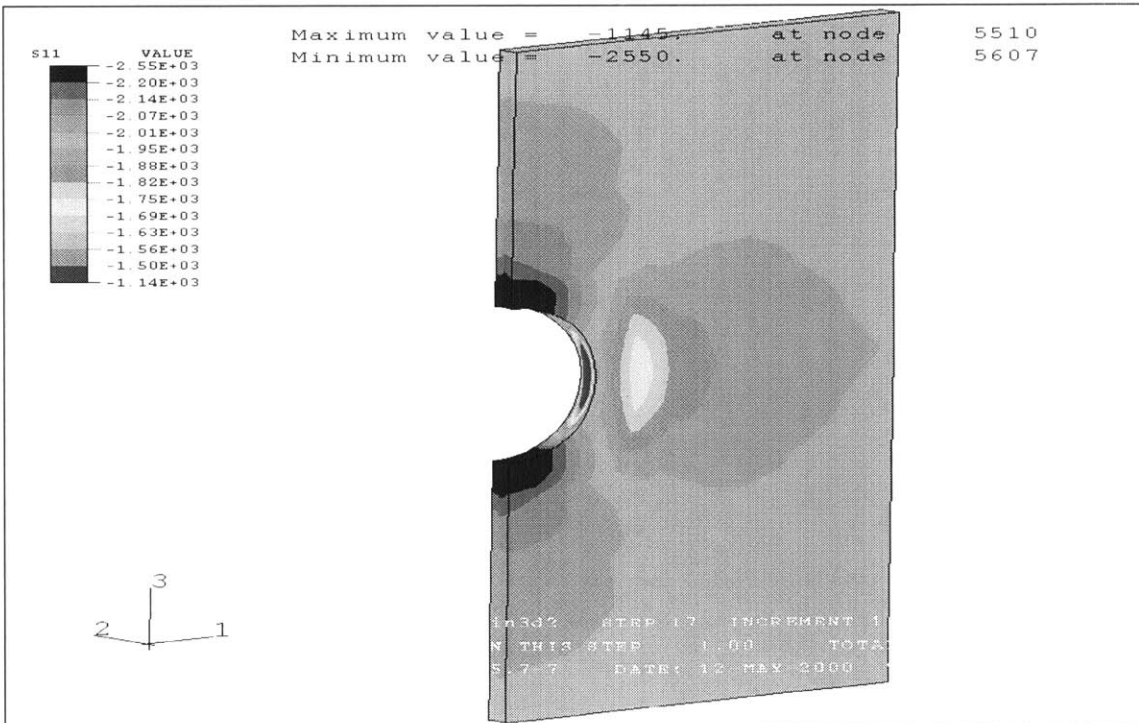


Figure 41. Stresses in the horizontal direction at section 8-9
($K_x=K_y=0.5$ - dry conditions - $l_u=1\text{m}$ - excavation=8m)

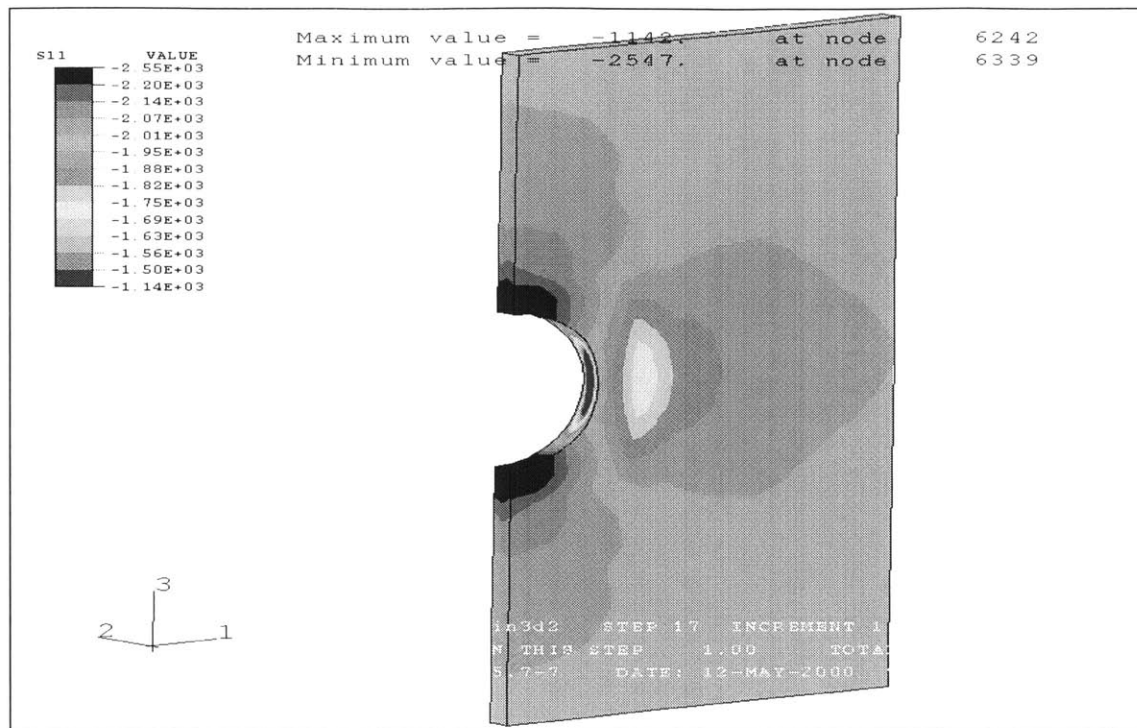


Figure 42. Stresses in the horizontal direction at section 9-10
($K_x=K_y=0.5$ - dry conditions - $l_u=1\text{m}$ - excavation=9m)

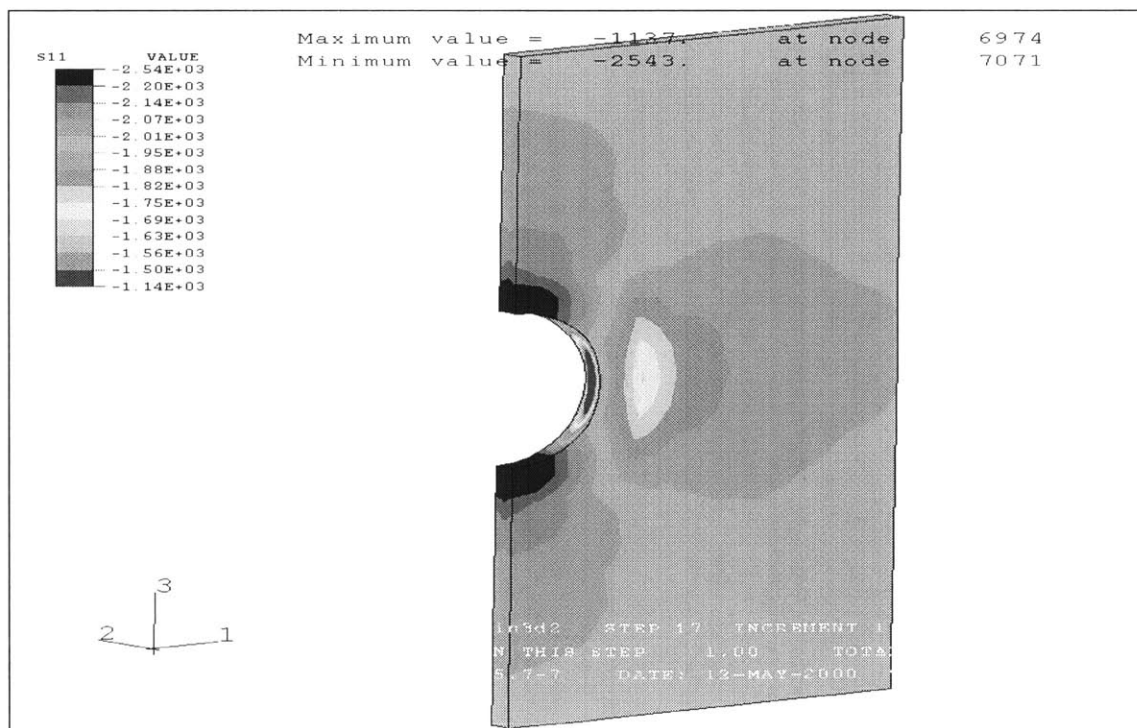


Figure 43. Stresses in the horizontal direction at section 10-11
($K_x=K_y=0.5$ - dry conditions - $l_u=1\text{m}$ - excavation=10m)

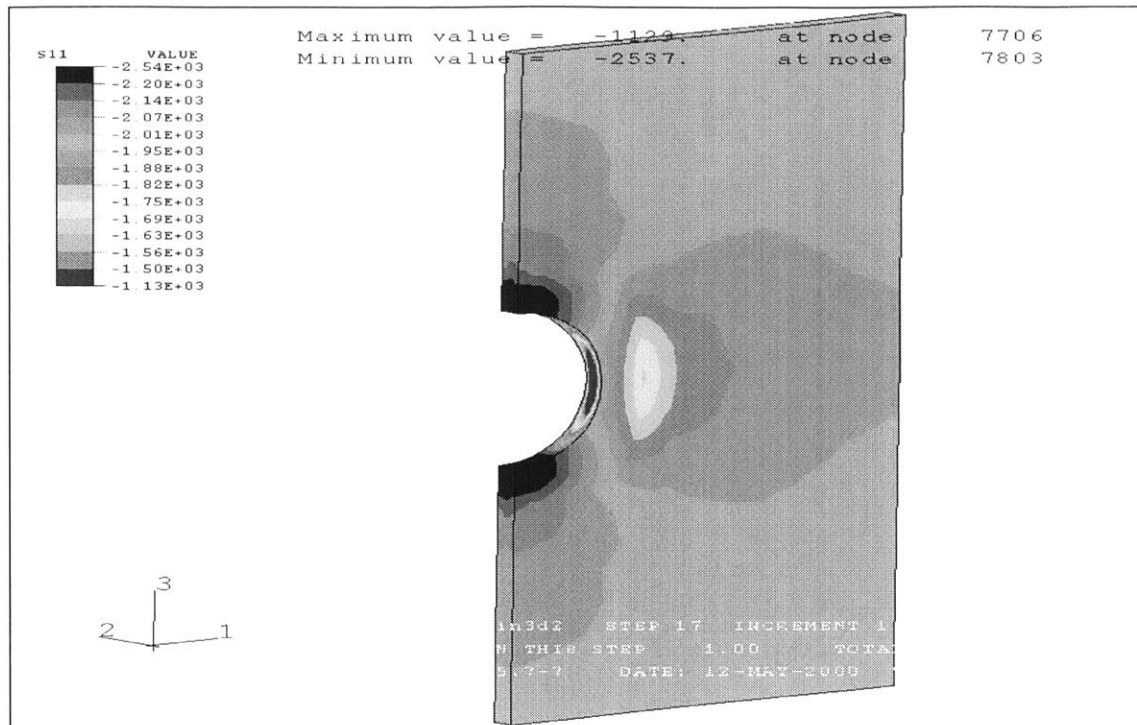


Figure 44. Stresses in the horizontal direction at section 11-12
 (Kx=Ky=0.5 - dry conditions – $I_u=1\text{m}$ – excavation=11m)

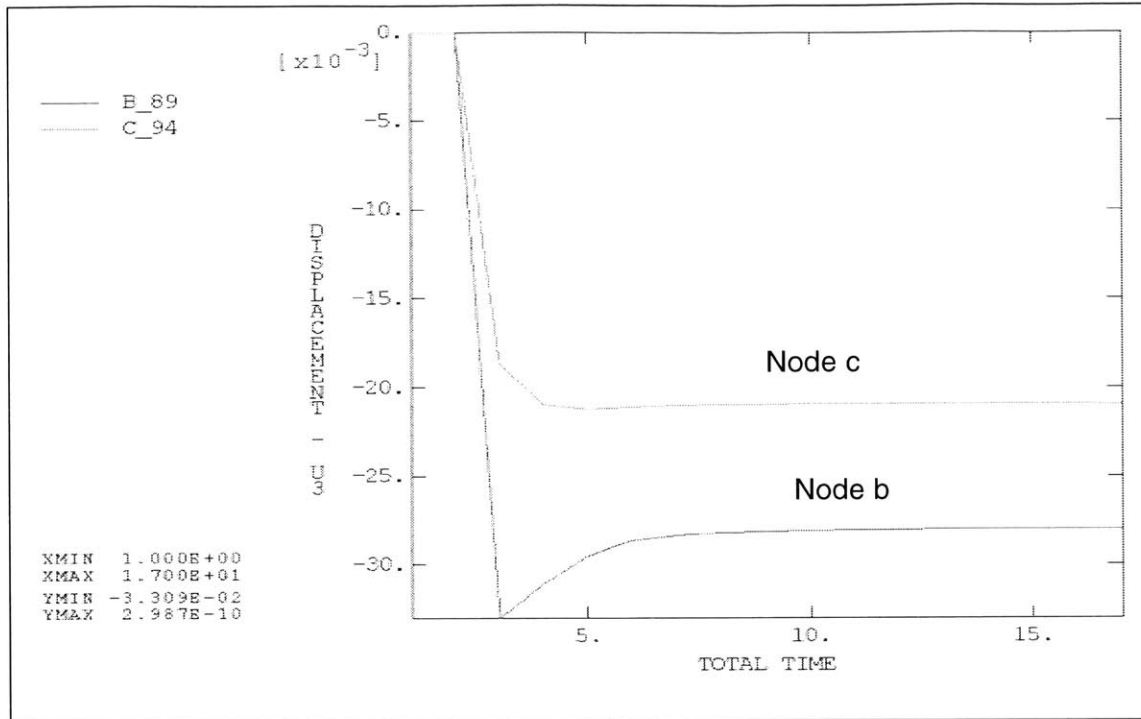


Figure 45. Variation of vertical displacement during the excavation (Kx=Ky=0.5 - dry conditions - $l_u=1\text{m}$ - nodes b,c)

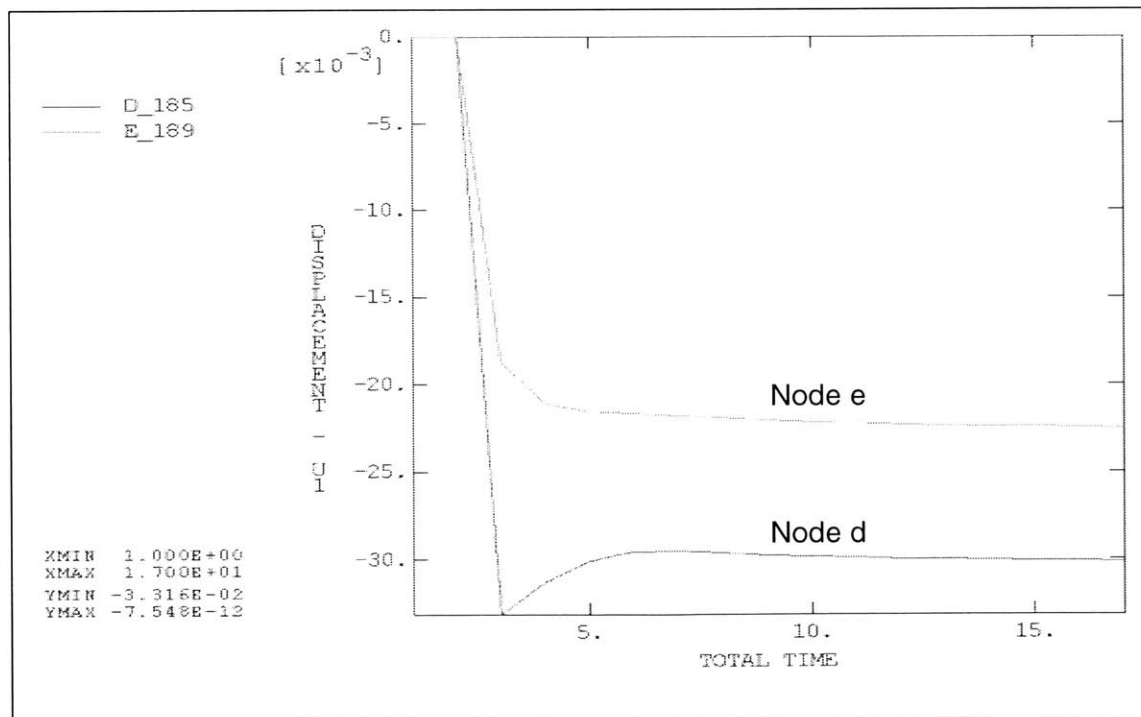


Figure 46. Variation of horizontal displacement during the excavation (Kx=Ky=0.5 - dry conditions - $l_u=1\text{m}$ - node d,e)

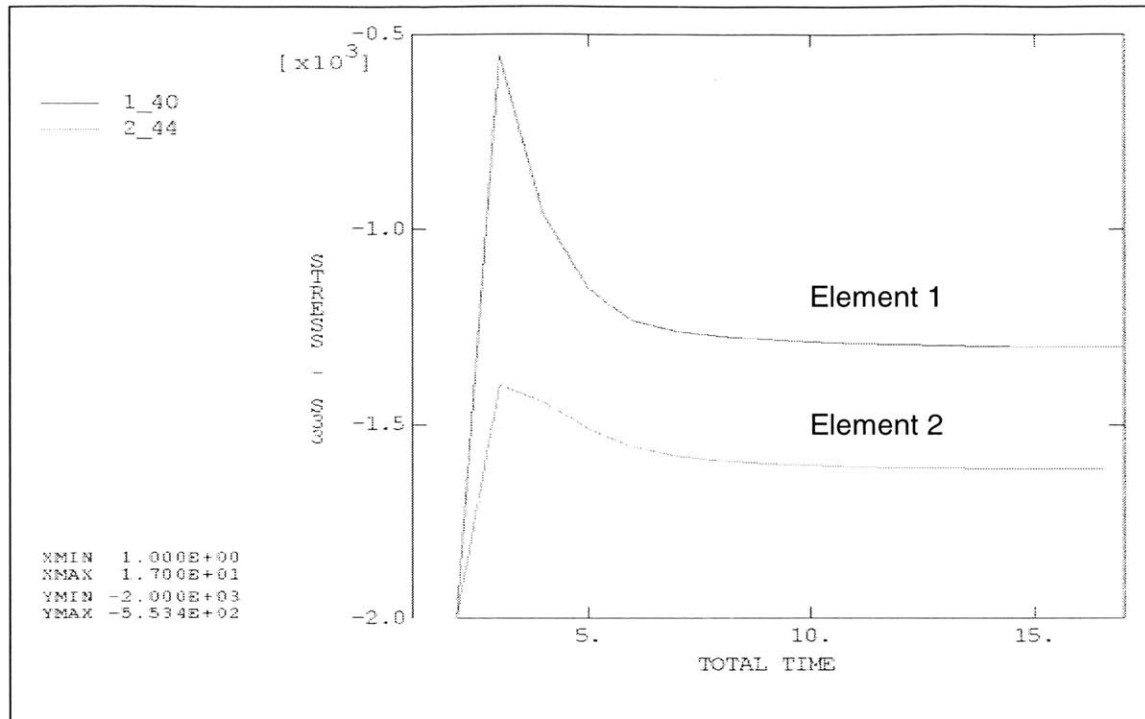


Figure 47. Variation of vertical stress during the excavation (Kx=Ky=0.5 - dry conditions – $l_u=1\text{m}$ – elements 1,2)

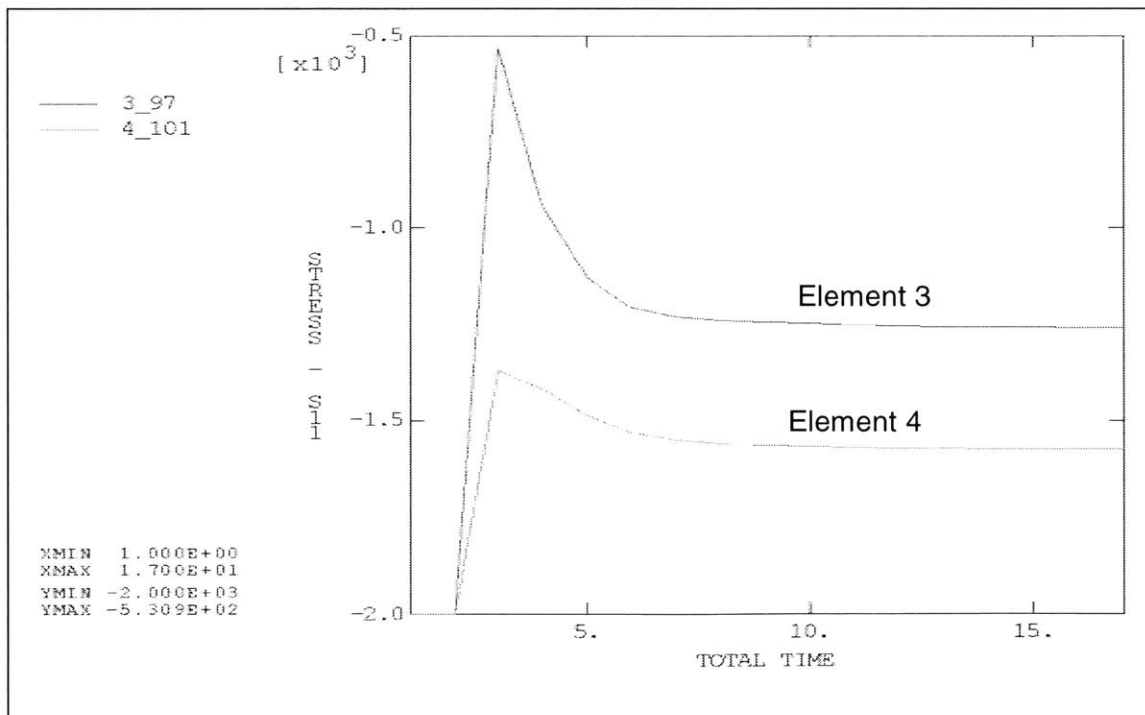


Figure 48. Variation of horizontal stress during the excavation (Kx=Ky=0.5 - dry conditions – $l_u=1\text{m}$ – elements 3,4)

APPENDIX IVc

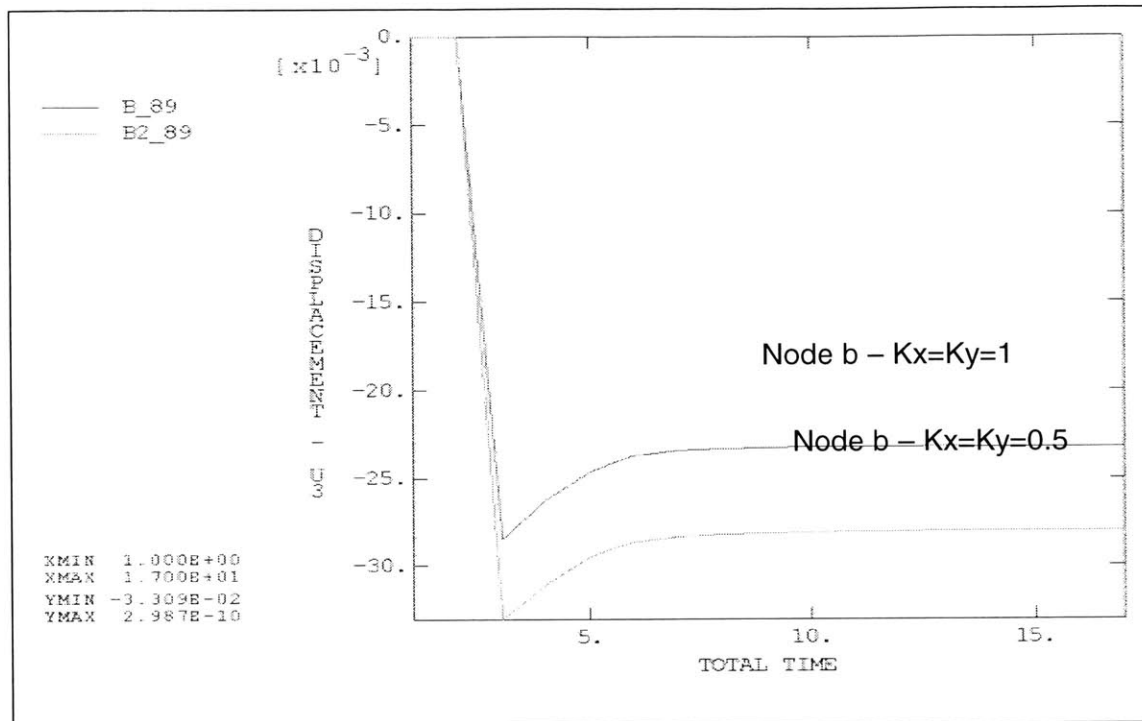


Figure 1. Variation of vertical displacement during the excavation (Kx=Ky=0.5 - Kx=Ky=1 - dry conditions - $l_u=1\text{m}$ - nodes b)

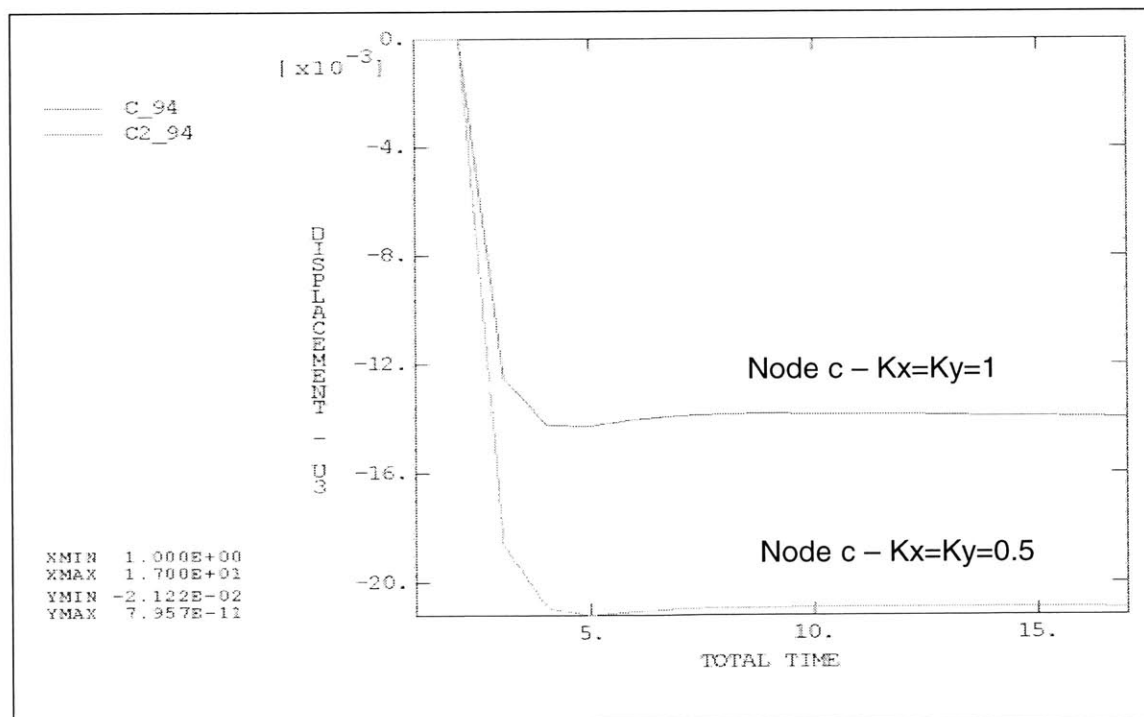


Figure 2. Variation of horizontal displacement during the excavation (Kx=Ky=0.5 - Kx=Ky=1 - dry conditions - $l_u=1\text{m}$ - node c)

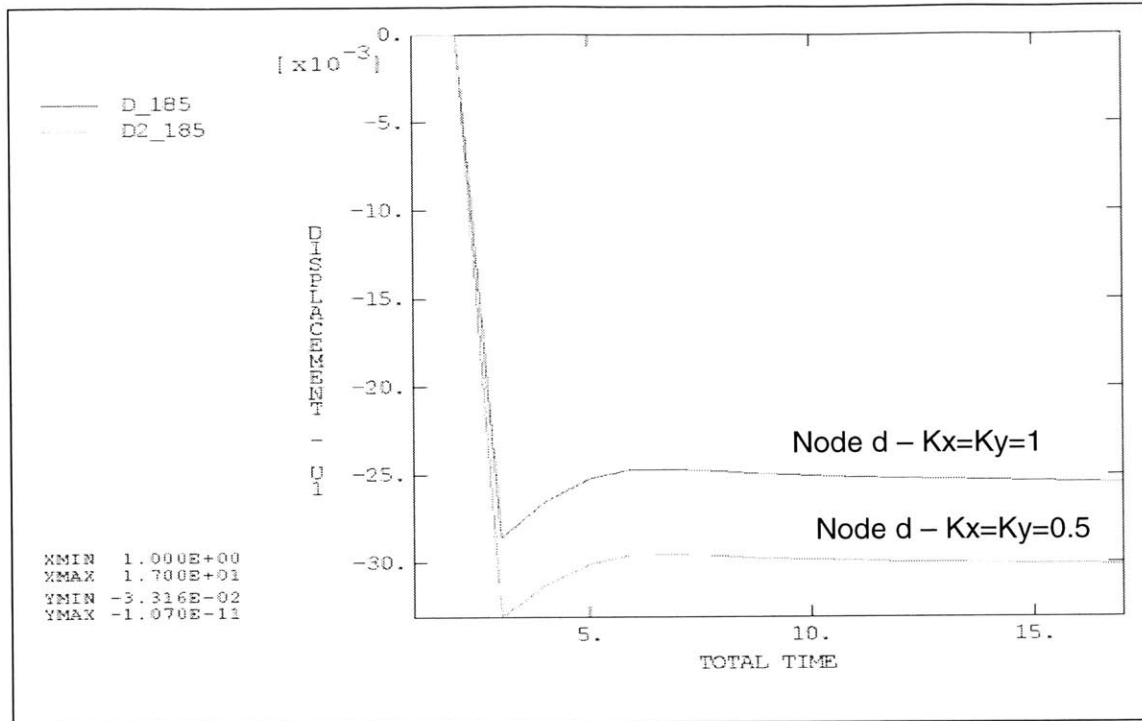


Figure 3. Variation of vertical stress during the excavation (Kx=Ky=0.5 - Kx=Ky=1 - dry conditions - $l_u=1\text{m}$ - node d)

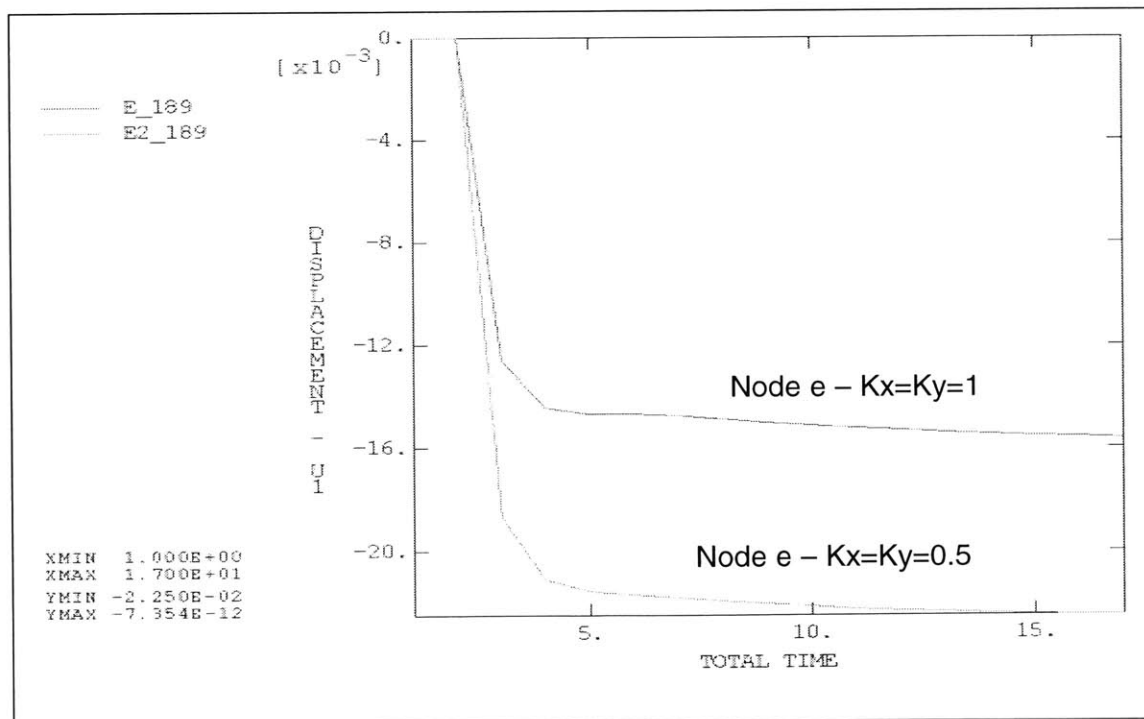


Figure 4. Variation of horizontal stress during the excavation (Kx=Ky=0.5 - Kx=Ky=1 - dry conditions - $l_u=1\text{m}$ - node e)

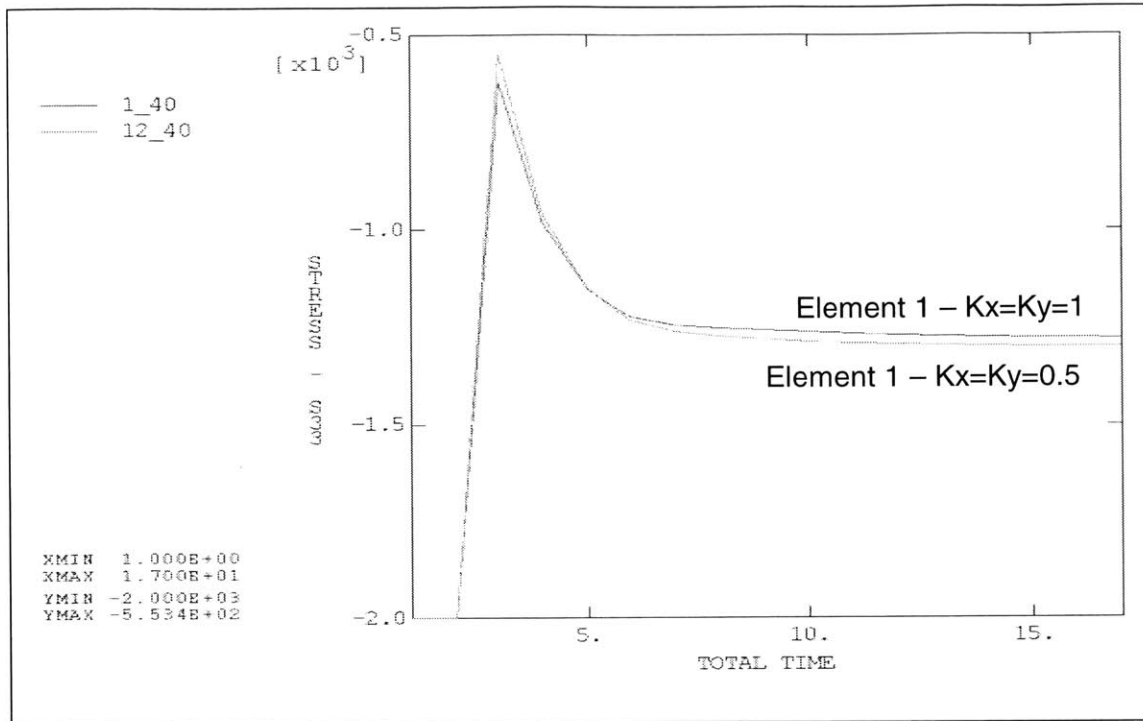


Figure 5. Variation of vertical displacement during the excavation ($K_x=K_y=0.5$ - $K_x=K_y=1$ - dry conditions - $l_u=1\text{m}$ - element 1)

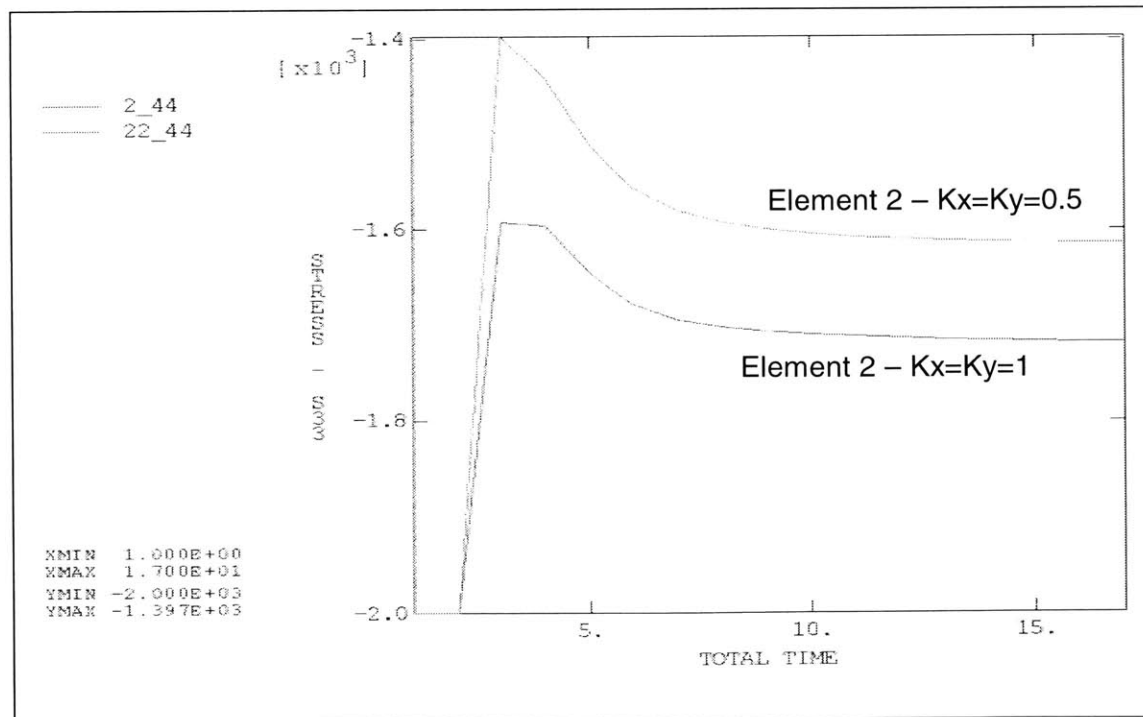


Figure 6. Variation of horizontal displacement during the excavation ($K_x=K_y=0.5$ - $K_x=K_y=1$ - dry conditions - $l_u=1\text{m}$ - element 2)

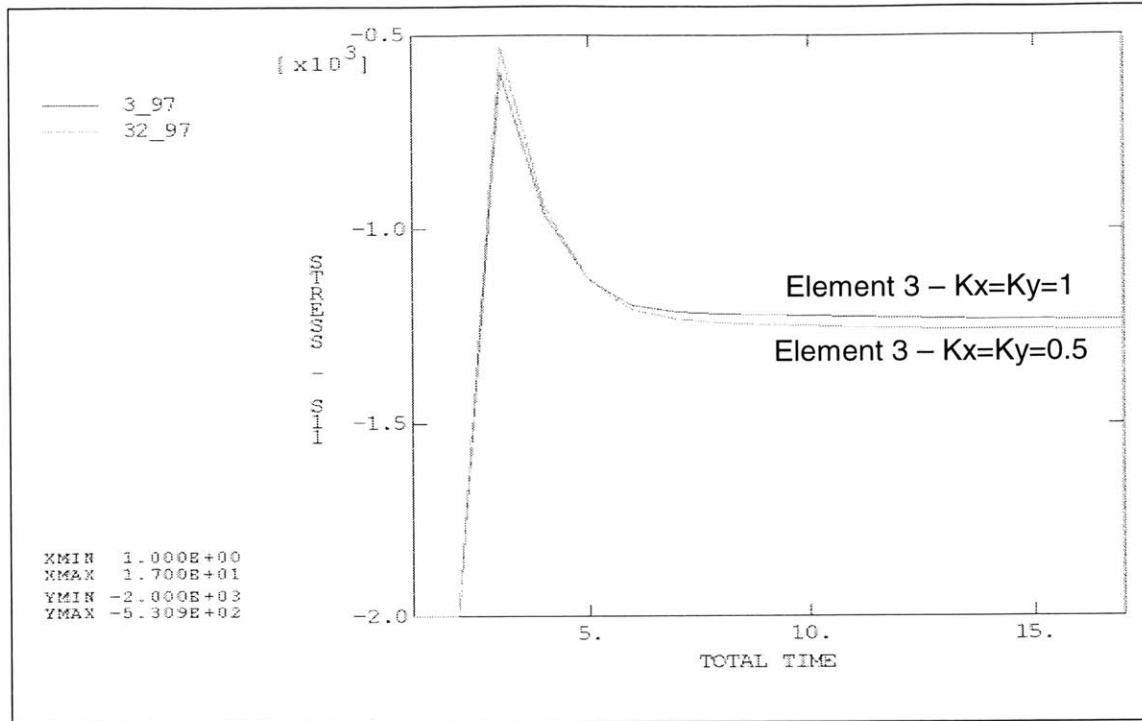


Figure 7. Variation of vertical stress during the excavation ($K_x=K_y=0.5$ - $K_x=K_y=1$ - dry conditions - $l_u=1\text{m}$ - elements 3)

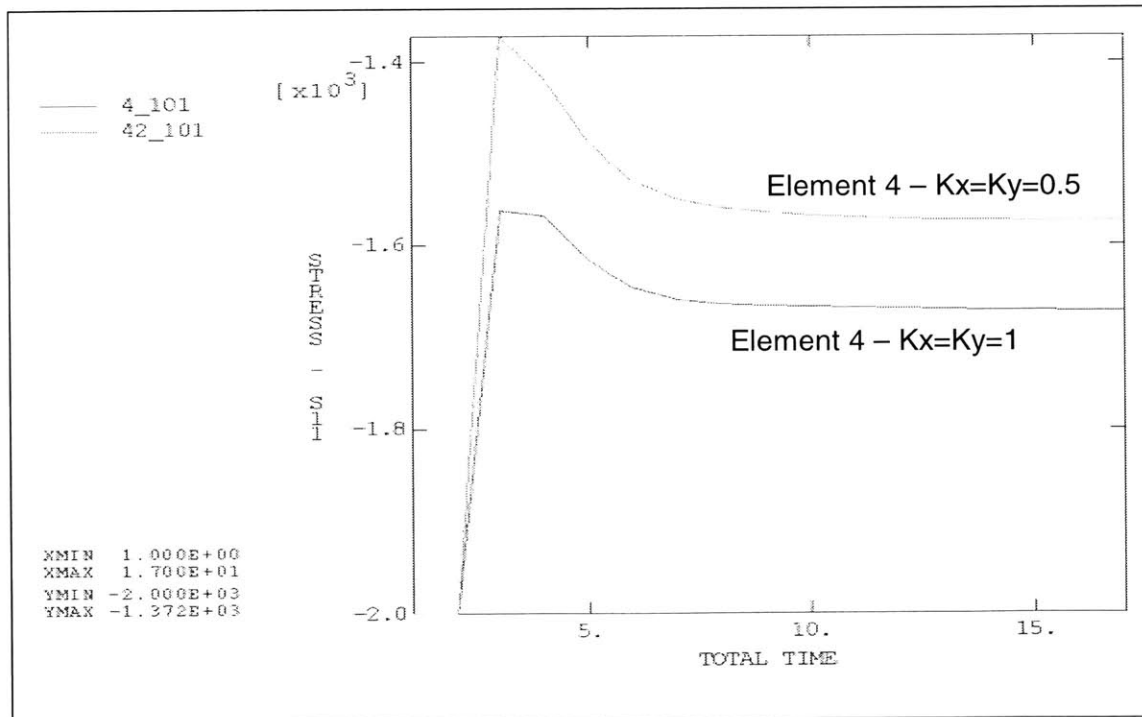


Figure 8. Variation of horizontal stress during the excavation ($K_x=K_y=0.5$ - $K_x=K_y=1$ - dry conditions - $l_u=1\text{m}$ - elements 4)

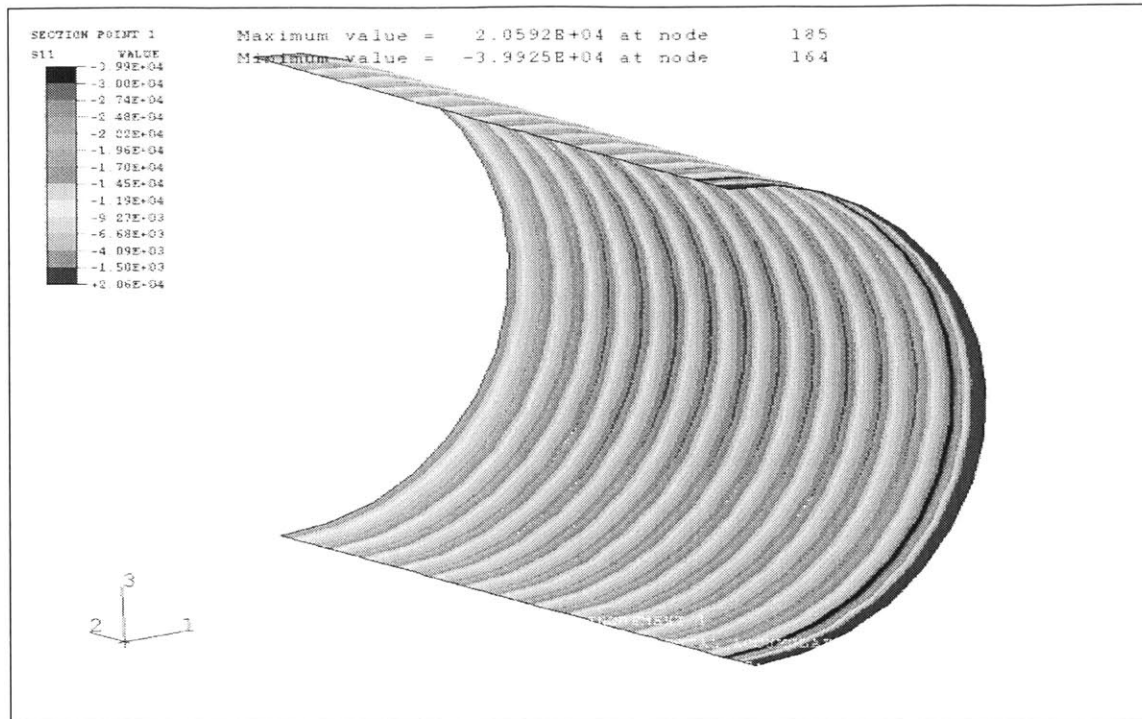


Figure 9. Variation of tangential stress in the liner
($K_x=K_y=0.5$ - dry conditions)

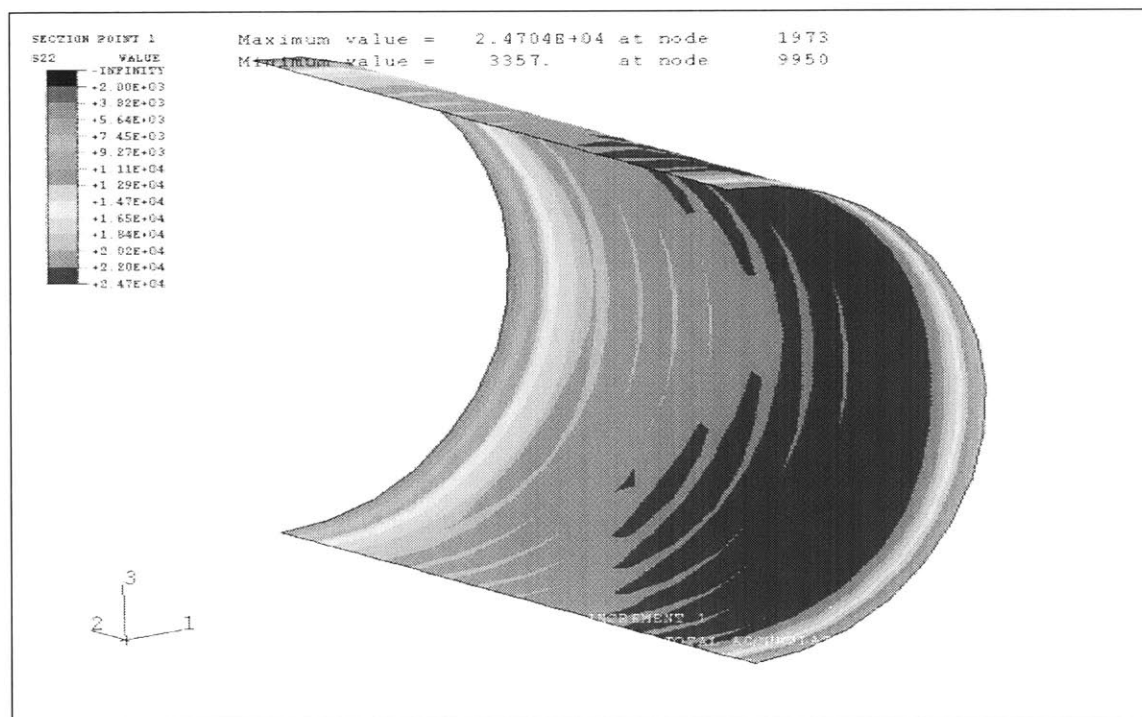


Figure 10. Variation of stress in the liner along its axis
($K_x=K_y=0.5$ - dry conditions)

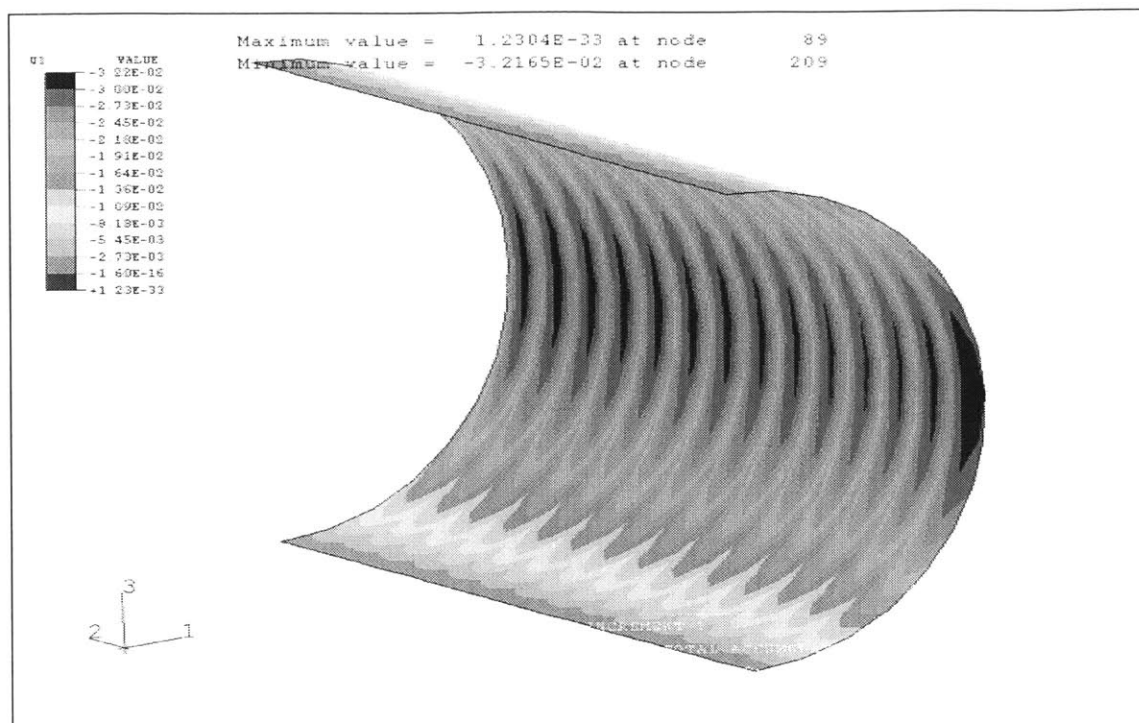


Figure 11. Variation of vertical horizontal during the excavation
($K_x=K_y=0.5$ - dry conditions)

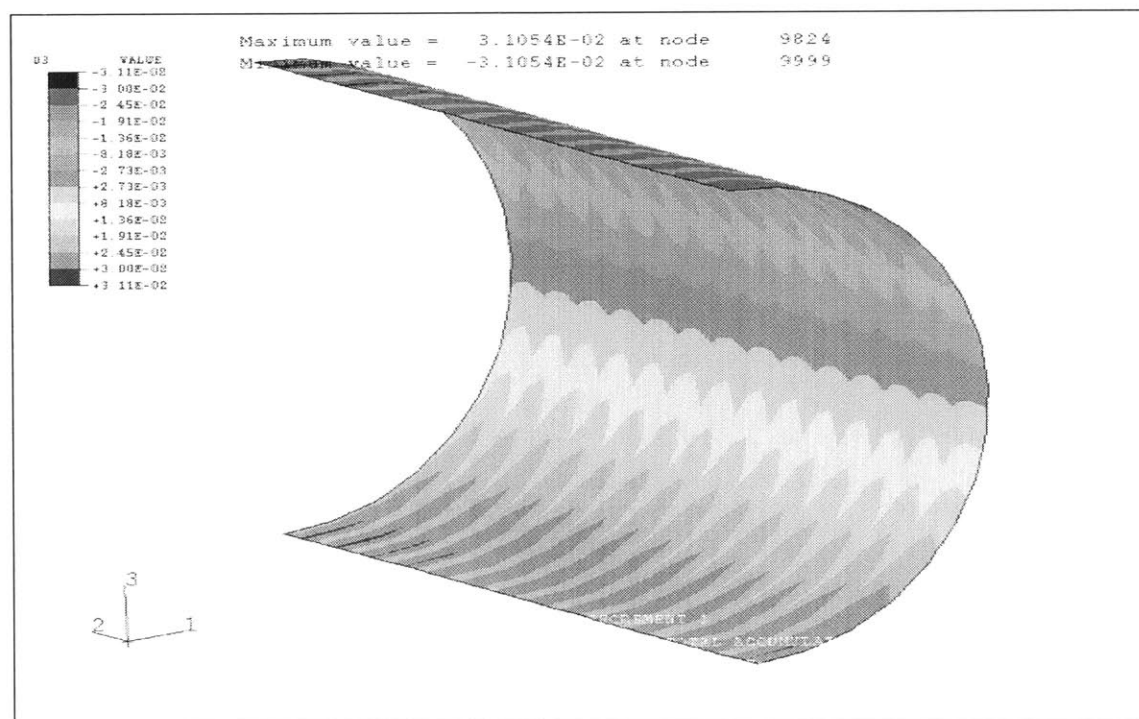


Figure 12. Variation of vertical displacement during the excavation
($K_x=K_y=0.5$ - dry conditions)

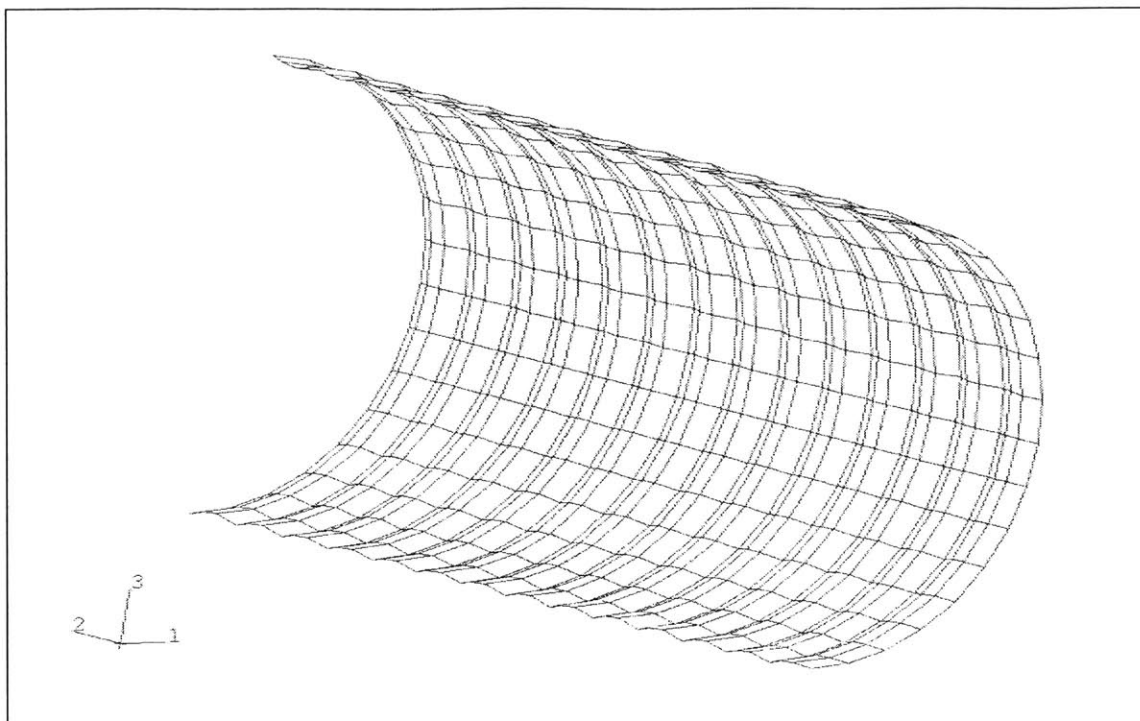


Figure 13. Deformed shape of the liner
($K_x=K_y=0.5$ - dry conditions)